Universidad de Guanajuato

División de Ciencias e Ingenierías
Campus León

Semiclassical statistical theory and computer simulations of confined quantum fluids

by

M.Sc. Víctor Manuel Trejos Montoya

Submitted to the Physical Engineering Department in partial fulfillment of the requirements for the degree of
Doctor in Physics

Thesis Supervisor
Dr. Alejandro Gil-Villegas Montiel

August 6th 2014

To My Brother
Cristian David Trejos

And to My Parents,
Víctor M. Trejos and Dolly Montoya J.
In Memory of My Grandfather Rafael Montoya

PREFACE

The thesis is submitted in partial fulfillment of the requirements for the Ph.D. degree at the Guanajuato University, at León, México. This work has been carried out from December 2010 to August 2014 at the Physical Engineering Department of the University of Guanajuato under the supervision of Dr. Alejandro Gil-Villegas. This work was supported by CONACYT through Grant Nos. 61418 and 151137, and a Ph.D. scholarship. Support from the University of Guanjuato was received through a Grant from Convocatoria Institucional 2013, DAIP.

Víctor Manuel Trejos Montoya
August 6th, 2014

ABSTRACT

Among various alternative fuels to gasoline an diesel, hydrogen remains to be a very attractive alternative. Nowadays, several types of porous materials have been extensively studied and tested as potential candidates for storage of hydrogen. On the other hand, the evaluation of an adsorptive process is commonly based in new adsorptive materials nanoporous technologies and predictive models based on equations of state. The great importance of hydrogen, thinking as a green combustible, have increased the searching for more accurate predicting models of thermodynamic properties. Molecular simulations and theoretical approaches are of key importance because the prediction of the adsorption properties over a wide range of temperatures and pressures would reduce the number of time consuming experiments required for performance evaluations. This thesis presents a theoretical analysis of the adsorption of mixtures containing quatum fluids at high pressures and low temperatures. Computer simulations under the Metropolis Monte Carlo scheme and molecular equation of state was the main methodology used in this work. The thesis is integrated in three items: The first step is the development of a semiclassical approach to model quantum fluids using the Statistical Associating Fluid Theory for Potential of Variable Range (SAFT-VR), that can be used to determine thermodynamic properties of quantum fluids. This theory is applied to the prediction of liquid-vapor properties of fluids like molecular hydrogen, neon, deuterium and helium-4. To understand the behaviour of these fluids under confinement and their adsorptive properties, in the second part of the thesis a MC simulation study of quantum fluids using semiclassical effective pair potentials is presented. The first and second parts are the basis for the development of a two-dimentional equation of state to predict adsorption isotherms of pure quantum fluids and mixtures of there onto different surface substrates. In all cases: theory, experimental data, and computer simulations were compared.

CONTENTS

LIST OF FIGURES

LIST OF TABLES

CHAPTER 1

INTRODUCTION

During the recent years, we have seen a recognition of a hydrogen based economy as a possible replacement for the current oil based economy. The initial interest in the use of hydrogen as a replacement for oil goes back to the late 1970s when the oil price increased dramatically.[1] The interests of using hydrogen as a fuel are environmental, due to a potential reduction in air pollution. On the other hand, hydrogen is widely used in the chemical industry, petroleum recovery and refining, electronic circuits and power generation.[2–5]

Due to its clean combustion and high heating value, hydrogen is under consideration as a replacement for fossil fuels in mobile applications.[6] The development of a suitable storage method is the major problem in order to change from petroleum to hydrogen as an energy carrier. The amount of hydrogen that can be safely stored in a vehicle is one of the more realistic problems of the storage of hydrogen. Physisorption is a promising method for storing hydrogen because the adsorbed hydrogen can be easily released at lower pressure.[7] Adsorbents such as dry activated carbon, nanoporous materials, zeolite-templated, graphene nanosheets and metal-organic frameworks (MOFs) have been intensively investigated.[8–15] Interesting methods to storage hydrogen as high pressure gas, liquid hydrogen, adsorption on porous materials at relatively low pressure, complex hydrides, among others, begin to be the best options. The successful development of new materials for hydrogen storage is the key to the success of hydrogen fuel cell technology.

Recently, major efforts to developing molecular simulations methods and molec-

ular theories have become become to be a necessity in the industry. All these efforts are made in order to characterize a storage material, measurements of the amount of hydrogen adsorbed at various temperatures and pressures. In addition, Monte Carlo simulation and SAFT-VR theories are appropriate and convenient methods in the case of gas adsorption onto different substrates. Prediction and calculation of thermodynamic properties, as well as the appropriate description of adsorption process with molecular equations of state as SAFT-VR, remains a crucial step in the development of the physico chemical process of adsorption. Therefore, the study on quantum effects on physical adsorption is now one of the attractive subjects in the field of adsorption.[16] The rigorous way to calculate thermodynamic properties of liquids using quantum contributions such as path-integral methods are necessary to understand the phenomenological behavior of hydrogen at low temperatures and high pressures under confinement. Such confinement can modify the localization of the gas-liquid transition.

The thesis is divided accordingly into the following chapters:

- **CHAPTER 2:** *Semiclassical theory for quantum fluids*
  This chapter introduces the reader with some concepts and definitions of the statistical mechanics and quantum mechanics. The classical and quantum partition function are discussed in order to explain how thermodynamic properties of the system; such as pressure, energies, chemical potential among others can be calculated. In this chapter we establish the difference between quantum and classical statistics.

- **CHAPTER 3:** *Semiclassical approach to model quantum fluids using the SAFT-VR theory*
  In this chapter, thermodynamic properties of quantum fluids are described using an extended version of the Statistical Associating Fluid Theory for Potentials of Variable Range (SAFT-VR), that takes into account quantum corrections to the Helmholtz free energy A, based on the Wentzel-Kramers-Brillouin (WKB) approximation.[17–19] A theoretical background of this approach (SAFT-VRQ) is presented, considering two different cases depending on the continuous or discontinuous nature of the particles pair interaction. On the other hand, an analytical expression for the first-order quantum perturbation term for a square-well potential, and the theory is applied to model thermodynamic properties of

hydrogen, deuterium, neon and helium. Vapor-liquid equilibrium (VLE), liquid and vapor densities, isochoric and isobaric heat capacities, Joule-Thomson coefficient and inversion curves are predicted accurately with respect to experimental data.

(Víctor M. Trejos and Alejandro Gil-Villegas, Semiclassical approach to model quantum fluids using the statistical associating fluid theory for systems with potentials of variable range. *Journal of Chemical Physics*, **136**, 184506, (2012).)

– **CHAPTER 4:** *Computer simulation of liquid -vapor coexistence of confined quantum fluids*

In this chapter, the liquid-vapor coexistence (LV) of bulk and confined quantum fluids has been studied by Monte Carlo computer simulation for particles interacting via a semiclassical effective pair potential $V_{eff}(r) = V_{LJ} + V_Q$, where V_{LJ} is the Lennard-Jones 12-6 potential (LJ) and V_Q is the first-order Wigner-Kirkwood (WK-1) quantum potential, that depends on $\beta = 1/kT$ and de Boer's quantumness parameter $\Lambda = h/\sigma\sqrt{m\epsilon}$, where k and h are the Boltzmann's and Planck's constants, respectively, m is the particle's mass, T is the temperature of the system, and σ and ϵ are the LJ potential parameters. Confinement effects were introduced using the Canonical Ensemble (NVT) to simulate quantum fluids contained within parallel hard walls separated by a distance L_p, within the range $2\sigma \leq L_p \leq 6\sigma$.

(Víctor M. Trejos and Alejandro Gil-Villegas and Alejandro Martinez, Computer simulation of liquid-vapor coexistence of confined quantum fluids. *Journal of Chemical Physics*, **139**, 184505, (2013).)

– **CHAPTER 5:** *Theoretical modeling of adsorption of classical and quantum fluids*

In this chapter is presented a summary of a semiclassical theoretical framework to model adsorption isotherms of quantum fluids based on the Statistical Associating Fluid Theory approach for classical and quantum bulk fluids (SAFT-VRQ), and its combination with (SAFT-VRQ-2D) to model quantum fluids. Adsorption of classical fluids as: methane, ethane, propane, butane, nitrogen and propylene are predicted onto different porous materials. On the other hand, adsorption of molecular hydrogen (H_2) onto graphene and other carbon-based

substrates is studied at low temperatures and high pressures. Results obtained for ϵ_w according to this procedure are consistent with experimental values of the isosteric heat and the prediction of adsorption isotherms is in very good agreement with experimental data.

(Víctor M. Trejos, Mario Becerra,Susana Figueroa-Gerstenmaier, and Alejandro Gil-Villegas, Theoretical modeling of adsorption of hydrogen onto graphene, MOFs and other carbon-based substrates. *Molecular Physics*, **1**, 1-9, (2014).)

– **CHAPTER 6:** *Semiclassical theory for adsorption of mixtures*

In this chapter a semiclassical theory for the adsorption of mixtures of fluids is presented. Adsorption of binary mixtures containing molecular hydrogen (H_2) onto different nanoporous materials are studied. A semiclassical theoretical framework to model adsorption based isotherms on the statistical associating fluid theory approach for classical and quantum bulk fluids (SAFT-VRQ), and its extension to described adsorbed systems (SAFT-VR-2D) is used. Additionally, the expression for the calculations of vapor-liquid equilibrium of binary mixtures is presented.

– **CHAPTER 7:** *Conclusions and perspectives*

In this chapter, the conclusions and perspectives exposed in previous chapters are summarized.

BIBLIOGRAPHY

[1] K. M. Thomas, *Dalton Trans.* 1487 (2009).

[2] V. M. Trejos, A. Gil-Villegas, *J. Chem. Phys.* **136**, 184506 (2012).

[3] P. Dagaut, G. Dayma, *Int. J. Hydrogen Energy* **31**, 505, (2006).

[4] K. Otsuka, Y. Shigeta, S. Takenaka, *Int. J. Hydrogen Energy* **27**, 11, (2002).

[5] E. Ch. Vagia, A. A. Lemonidou, *Int. J. Hydrogen Energy* **32**, 212, (2007).

[6] L. Schlapbach and A. Züttel, *Nature* **414**, 353 (2001).

[7] A. Züttel, *Naturwissenschaften* **91**, 157 (2004).

[8] P. Bénard and R. Chahine, *Langmuir* **17**, 1950 (2001).

[9] P. Bénard, R. Chahine, P.A. Chandonia, D. Cossement, G. Dorval-Douville, L. Lafia, P. Lachance, R. Paggiaro, E. Poirier, *J. of Alloys and Compounds* **446**, 380 (2007).

[10] P. Bénard and Richard Chahine, *Scripta Materialia* **56**, 803 (2007).

[11] G. Srinivas, Y. Zhu, R. Piner, N. Skipper, M. Ellerby, R. Ruoff, *Carbon* **48**, 630 (2010)

[12] A. G. Wong-Foy, A. J. Matzger, O. M. Yaghi, *J. Am. Chem. Soc.* **128**, 3494 (2006).

[13] N. P. Stadie, J. J. Vajo, R. W. Cumberland, A. A. Wilson, C. C. Ahn, B. Fultz *Langmuir* **28**, 10057 (2012).

[14] X-S. Wang, S. Ma, K. Rauch, J. M. Simmons, D. Yuan, X. Wang, T. Yildirim, W. C. Cole, J. J. López, A. de Meijere, H-C. Zhou, *Chem. Mater.* **20**, 3145 (2008).

[15] H. Furukawa, N. Ko, Y. B. Go, N. Aratani, S. B. Choi, E. Choi, A. O. Yazaydin, R. Q. Snurr, M. O'Keeffe, J. Kim, O. M. Yaghi, *Science* **329**, 424 (2010).

[16] H. Tanaka, J. Fan, H. Kanoh, M. Yudasaka, S. Iijima and K. Kaneko, *Mol. Phys.* **31**, 465 (2005).

[17] G. Wentzel, *Z. Phys.* **45**, 952, (1926).

[18] H. A. Kramers, *Z. Phys.* **39**, 828, (1926).

[19] L. Brillouin, *C. R. Acad. Sci. Paris* **183**, 24, (1926).

CHAPTER 2

SEMICLASSICAL THEORY FOR QUANTUM FLUIDS

This chapter introduces the reader with some concepts and definitions of the statistical mechanics and quantum mechanics. The classical and quantum partition function are discussed in order to explain how thermodynamic properties of the system as pressure, energies, chemical potential, radial distribution function among others can be calculated. This chapter will focus on definitions, for example as a ensembles, density matrix and others used to describe quantum fluids. The basic knowledge and terminology required for understand the following chapters will be introduced at an elementary level.

2.1 Classical Statistical Mechanics

A hundred of years ago, experimental studies of the macroscopic behavior of physical systems allowed thermodynamics to grow up, through the work of Carnot, Joule, Clausius and Kelvin. From the first and second laws of the thermodynamics theoretical conclusions were obtained.[1] At the same time, the kinetic theory of gases, began to emerge as a real mathematical theory; but it could not be made until about 1872 when Boltzmann developed his H-theorem and thereby established a direct connection between entropy and molecular dynamics. At the same time, the kinetic theory opened the door to understanding the ensemble theory. Here, in this point the classical thermodynamics was reduced to the status of an essential consequence of the get-together of the statistics and mechanics of the molecules constituting a

given physical system. It was then natural to give the resulting formalism the name *Statistical Mechanics*.[1]

2.1.1 Macroscopic and microscopic states

Considering a system composed of N identical particles confined to a space of volume V and the particles comprising the system could be regarded as noninteracting, the total energy of the system E, satisfy the following conditions

$$E = \sum_i n_i \epsilon_i \tag{2.1}$$

$$N = \sum_i n_i \tag{2.2}$$

where n_i is the number of particles with energy ϵ_i. According with the quantum mechanics, the single-particle energies ϵ_i are discrete and their values depend on the volume V to which the particles are confined. The possible values of the total energy E are also discrete. Therefore, the specification of the parameters N, V and E defines a *macrostate* of the system. At the molecular level, a large number of different ways in which the macrostate (N, V, E) of the system can be realized; so, there will be a large number of different ways in which the total energy E of the system can be distributed among the N-particles constituting it. Each of these different ways specifies a *microstate* of the system. The number of all microstates will be a function of N, V and E and may be denoted by the symbol $\Omega(N, V, E)$.

2.1.2 Classical partition function

Actually there are several different types of partition functions, each corresponding to different types of statistical ensemble (or, equivalently, different types of free energy). One of them is an ensemble whose members have fixed the number of particles of the system N, the volume V and the total energy E. This is called the *microcanonical ensemble* and is useful for theoretical discussions.[3] In the case of practical applications there are other ensembles most commonly used in statistical thermodynamics. The *canonical ensemble*, is one, in which the individual system have N, V and T are fixed.

Canonical Ensemble

In the limit of large quantum numbers and using a high-temperature approximation, the partition function in the canonical ensemble NVT can be written as[1]

$$Z = \sum_n e^{-\beta E_n} \tag{2.3}$$

where E_n is the energy of the n quantum state and $\beta = 1/kT$, being k the Boltzmann constant. In the 3N-dimensional phase space of spacial coordinates $\mathbf{r}$ and momenta $\mathbf{p}$ using an integral rather than a sum, the partition function is given by

$$Z(N,V,T) = \frac{1}{N!h^{3N}} \int e^{-\beta H(p_1 \cdots p_N, r_1 \cdots r_N)} d^3p_1 \cdots d^3p_N \, d^3r_1 \cdots d^3r_N \tag{2.4}$$

where h is the Planck's constant, p_i is the particle momenta, r_i is the particle position and H is the classical Hamiltonian. The factor $1/N!$ appears, in concordance with the rule of "correct Boltzmann counting".[2] Suppose, then, that the Hamiltonian can be written as $H = K(\mathbf{p}^N) + U(\mathbf{r}^N)$ where K and U are the kinetic and potential energy of the system respectively. Then the Eq. 2.4 can be written as

$$Z(N,V,T) = \frac{1}{N!\lambda_B^{3N}} \int e^{-\beta U(r_1 \cdots r_N)} d^3r_1 \cdots d^3r_N \tag{2.5}$$

where λ_B is the De Broglie wave length, due the integral of $\int d\mathbf{p}^N e^{-\beta K}$. The thermodynamic properties of the system can be obtained from the formula

$$Z(N,V,T) = e^{-\beta A(V,T)} \tag{2.6}$$

where A is the Helmholtz free energy. The Eq. (2.6) represents the connection between the canonical partition functions and the thermodynamic properties of the system. The chemical potential μ, pressure P and total energy E, can be obtained as follows

$$\mu = -kT \left(\frac{\partial \ln(Z)}{\partial N} \right)_{V,T} \tag{2.7}$$

$$P = kT \left(\frac{\partial \ln(Z)}{\partial V} \right)_{N,T} \tag{2.8}$$

$$E = kT^2 \left(\frac{\partial \ln(Z)}{\partial T} \right)_{N,V} \tag{2.9}$$

where T, V and N are the temperature, volume and number of particles of the system, respectively.

2.1.3 Radial distribution function

The radial distribution function, (or pair correlation function) $g(r)$ in a system of particles (atoms, molecules, colloids, etc.), describes how density varies as a function of distance from a reference particle. Consider a system of N particles in a volume V and a temperature T. The probability that molecule 1 is in dr_1 at r_1, and molecule 2 in dr_2 at r_2, etc., is given by[3]

$$P^{(N)}(r_1, \ldots, r_N) dr_1 \ldots dr_N = \frac{e^{-\beta U_N}}{Q_N} dr_1 \ldots dr_N \tag{2.10}$$

where Q_N is the configuration integral given as

$$Q_N = \int \ldots \int e^{-\beta U_N} dr_1 \ldots dr_N \tag{2.11}$$

where U_N is the potential energy due to interaction between particles. The probability that molecule 1 is in dr_1 at $r_1, \ldots$, molecule n in dr_n at r_n, irrespective of the configuration of the remaining $N - n$ molecules is obtained by integrating Eq. (2.10) over the remaining coordinates $r_{n+1} \ldots r_N$

$$P^{(n)}(r_1, \ldots, r_n) = \frac{1}{Q_N} \int \ldots \int e^{-\beta U_N} dr_{n+1} \ldots dr_N \tag{2.12}$$

The particles being identical, it is more relevant to consider the probability that any n of them occupy positions $r_1 \ldots, r_n$ in any permutation, thus defining the n-particle density

$$\rho^{(n)}(r_1, \ldots, r_n) = \frac{N!}{(N-n)!} P^{(n)}(r_1, \ldots, r_n) \tag{2.13}$$

In the specific case of $n = 1$, the quantity $\rho^{(1)}(r_1) dr_1$ is the probability that any one molecule will be found in dr_1. For a (homogeneous) liquid, it is independent of the

position r_1 and equal to the overall density of the system:

$$\frac{1}{V}\int \rho^{(1)}(r_1)dr_1 = \rho^{(1)} = \frac{N}{V} = \rho \tag{2.14}$$

It is now time to define a correlation function $g^{(n)}(r_1, \ldots r_n)$ by

$$\rho^{(n)}(r_1 \ \ldots r_n) = \rho^n g^{(n)}(r_1 \ldots r_n) \tag{2.15}$$

$g^{(n)}$ is called a correlation function, since if the atoms are independent from each other $\rho^{(n)}$ would simply equal ρ^n and therefore $g^{(n)}$ corrects for the correlation between atoms. From Eq. (2.13) and Eq. (2.15) it follows that

$$g^{(n)}(r_1 \ldots r_n) = \frac{V^n N!}{N^n (N-n)!} \cdot \frac{1}{Q_N} \cdots \int \mathrm{e}^{-\beta U_N} dr_{n+1} \cdots dr_N \tag{2.16}$$

The particle densities and the closely related, equilibrium particle distribution functions, defined below provide a complete description of the structure of a fluid, while knowledge of the low-order particle distribution functions, in particular of the pair density $\mathrm{g}^{(2)}(r_1, r_2)$, is often sufficient to calculate the equation of state and other thermodynamic properties of the system.[4] In the case where the system is also isotropic, the pair distribution function $\mathrm{g}^{(2)}(r_1, r_2)$ is a function only of the separation $r_{1,2} = |r_2 - r_1|$; it is then usually called the *radial distribution function* an written as $\mathrm{g}^{(2)}(r_1, r_2) = \mathrm{g}(r)$. This is a standard notation. The function $g(r)$ can also be thought of as the factor that multiplies the bulk density ρ to give a local density $\rho(r) = \rho \mathrm{g}(r)$ about some fixed molecule. There are two important features of the radial distribution function, a) $\mathrm{g}(r) \to 1$ as $r \to \infty$ and b) $\mathrm{g}(r) \to 0$ as $r \to 0$. The radial distribution fucntion has a remarkable importance because all the themodynamic properties of the system can be calculated using the $\mathrm{g}(r)$ function.

2.1.4 Thermodynamic properties in terms of g(r)

Several thermodynamic properties, such as total energy E, pressure P, among others can be calculated from the radial distribution function. The total energy E in terms of $\mathrm{g}(r)$, can be written as[3]

$$\frac{E}{NkT} = \frac{3}{2} + \frac{\rho}{2kT}\int_o^\infty u(r)\mathrm{g}(r, \rho, T)4\pi r^2 dr \tag{2.17}$$

where N is the number of particles in the system, ρ is the number density, $u(r)$ is the pair potential, k is the Boltzmann's constant and T is the temperature. The pressure of the system can also be calculated using $\mathrm{g}(r)$ as follows

$$P = \rho k_B T - \frac{2}{3}\pi\rho^2 \int_0^\infty \frac{du(r)}{dr} r^3 \mathrm{g}(r) dr \tag{2.18}$$

The chemical potential μ can be written in terms of a so-called coupling parameter ξ, wich varies from 0 to 1 and which has the effect of replacing the interaction of some central molecule, say 1, with the jth molecule of the system by $\xi u(r_{1j})$.

$$\frac{\mu}{kT} = \ln(\rho\lambda_B^3) + \frac{\rho}{kT} \int_0^1 \int_0^\infty u(r)\mathrm{g}(r;\xi) 4\pi r^2 dr d\xi \tag{2.19}$$

where λ_B is the Broglie wave length. From E, P and μ all the other thermodynamic properties can be obtained.

2.2 Semiclassical Statistical Mechanics

In previous sections we have treated the problem of systems composed of distinguible entities, in the case of quantum-mechanical systems composed of indistinguible entities the treatment and language is a little different. It's advisable to rewrite the ensemble theory in a language of the operators and the wave functions. Another interesting feature of the mechanical-quantum system is the behavior of interacting and noninteracting systems, where the patterns becomes even more complicated.[1] In the limit of high temperatures and low densities, the behavior of all physical systems tends asymptotically to classical behavior.

2.2.1 Quantum-mechanical: the density matrix

Considering an ensemble composed of N identical systems characterized by a Hamiltonian, which may be denoted by the operator H. At the time t, the physical states of the various systems in the ensemble can be characterized by the wave functions $\psi(r_i, t)$, where r_i denote the position coordinates relevant to the system under study. Let $\psi^k(r_i, t)$ denote the normalized wave function characterizing the physical state in which the kth system of the ensemble happens to be at time t. The time variation of

the function $\psi^k(t)$ will be determined by the Schrödinger equation

$$i\hbar\frac{d}{dt}\left|\psi(t)\right\rangle = H\left|\psi(t)\right\rangle \tag{2.20}$$

where $\hbar = h/2\pi$. A state of the system is a vector $|\psi>$. In the phase space of the positions, then the wave function can be denoted as $\psi(\mathbf{r}^N)$, and $|\psi>$ using the proyection as

$$\psi(\mathbf{r}^N) =< \mathbf{r}^N|\psi > \tag{2.21}$$

The probability of finding a system in the small configuration volume element $d\mathbf{r}^N$ at the time t, is given by

$$\psi^*\psi d\mathbf{r}^N \tag{2.22}$$

If, in particular we use the complete function base of the Hamiltonian H to represent the wavefuntion ψ, we obtain

$$\psi = \sum_n C_n u_n(\mathbf{r}^N)e^{-iE_nt/\hbar} \tag{2.23}$$

where E_n is the energy for an arbitrary state n, $u(\mathbf{r}^N)$ is the stationary wave function, and C_n is complex coefficient. From the Eqs. 2.22 and 2.24, we obtain

$$\psi^*\psi d\mathbf{r}^N = \sum_n\sum_m C_m^*C_n u_m^*u_n e^{-i(E_n-E_m)t/\hbar}d\mathbf{r}^N \tag{2.24}$$

In Eq. 2.24 the probability is a function of time; therefore, its necessary to calculate from the Eq. 2.24 the average on the time, as

$$\overline{\psi^*\psi}d\mathbf{r}^N = \sum_n |C_n|^2|u_n|^2 d\mathbf{r}^N \tag{2.25}$$

where the overline is a temporal average. The square modulus $|C_n|^2$ is the probability that a measurement performed on the system will find it to have the quantum numbers n. Using the corresponding principle,[5] we can obtain

$$|C_n|^2 = \frac{1}{N!}\frac{e^{-\beta E_n}}{Z_Q} \tag{2.26}$$

where Z_Q is the quantum partition function of the system. From Eqs. 2.25 and 2.26 we obtain

$$\overline{\psi^*\psi}d\mathbf{r}^N = \frac{1}{N!}\sum_n \frac{e^{-\beta E_n}}{Z_Q}|u_n|^2 d\mathbf{r}^N \tag{2.27}$$

Since the $\psi's$ are normalized, we have

$$\int \overline{\psi^*\psi}d\mathbf{r}^N = 1 \tag{2.28}$$

The Eq. 2.27 can be rewritten as

$$Z_Q = \frac{1}{N!}\int \sum_n e^{-\beta E_n}|u_n|^2 d\mathbf{r}^N \tag{2.29}$$

Using properties of state vectors in the Hilbert space, the above equation can be written in terms of the density matrix.[2,6] If $|n>$ is an state with a wave function $u_n(\mathbf{r}^N) =< \mathbf{r}^N|n >$, then $|n>$ is a complete base. Therefore

$$\sum_n |n >< n| = 1 \tag{2.30}$$

From the Eq. 2.29 we may take

$$\begin{aligned}\sum_n e^{-\beta E_n}|u_n|^2 &= \sum_n e^{-\beta E_n} < n|\mathbf{r}^N >< \mathbf{r}^N|n > \\ &=< \mathbf{r}^N|\sum_n e^{-\beta\hat{H}}|n >< n|\mathbf{r}^N > \\ &=< \mathbf{r}^N|e^{-\beta\hat{H}}|\mathbf{r}^N >\end{aligned} \tag{2.31}$$

where $\hat{H}$ is the Hamiltonian operator. Now the operator $\hat{H}|n >= E_n|n >$. Therefore the Eq. 2.29 can be written as

$$Z_Q = \frac{1}{N!}\int < \mathbf{r}^N|e^{-\beta\hat{H}}|\mathbf{r}^N > d\mathbf{r}^N \tag{2.32}$$

The partition function can be written in the form

$$Z_Q = \mathrm{Tr}e^{-\beta\hat{H}} \tag{2.33}$$

where the trace is to be taken over all states of the system that has N particles in the volume V. This form, which is explicitly independent of the representation, is sometimes convenient for calculations. The density operator $\hat{\rho_Q}$ is given by

$$\hat{\rho_Q} = \frac{1}{N!}\frac{e^{-\beta\hat{H}}}{Z_Q} \tag{2.34}$$

Furthermore, the density operator $\hat{\rho_Q}$ must satisfy the condition

$$\mathrm{Tr}(\hat{\rho_Q}) = 1 \tag{2.35}$$

An analogous expression to Eq. 2.5 is given by[2,7]

$$Z_Q = \frac{1}{N!\lambda_B^{3N}}\int W_N d\mathbf{r}^N \tag{2.36}$$

Using the sum of Slater determinants, we can obtain

$$\begin{aligned} W_N &= N!\lambda_B^{3N} < \mathbf{r}^N|e^{-\beta\hat{H}}|\mathbf{r}^N > \\ &= N!\lambda_B^{3N}\sum_n u_n^*(\mathbf{r}^N)e^{-\beta\hat{H}}u_n(\mathbf{r}^N) \end{aligned} \tag{2.37}$$

The sum of Slater determinants give the probability, $W_N d\mathbf{r}^N$, to find the system in a small volume $d\mathbf{r}^N$ centering over the point $\mathbf{r}^N$.[1] In the classical limit, we have

$$W_N = e^{-\beta U} \tag{2.38}$$

where U is the potential energy of the system. In the Wentzel- Kramers-Brillouin (WKB) approximation,

$$W_N = e^{-\beta U_{\text{eff}}} \tag{2.39}$$

where U_{eff} is the effective potential. The evaluation of W_N require to specify the Hamiltonian $\hat{H}$ and the wave function basis $u_n(\mathbf{r}^N)$. There are two formalisms used in this thesis:

- Wigner and Kirkwood formalism that uses free-particles as wave function basis.[8,9]
- Singh and Sinha formalism that uses hard-spheres as wave function basis.[7,10]

In the following chapters we will use these mentioned approaches.

BIBLIOGRAPHY

[1] R. K. Pathria & P. D. Beale, *Statistical Mechanics*, 3rd Edition, Elsevier, (2011).

[2] H. Huang, *Statistical Mechanics*, 2nd edition, John Wiley & Sons, (1987).

[3] D. A. McQuarrie, *Statistical Mechanics*, University Science Books, (2000).

[4] J.-P. Hansen and I.R. McDonald, *Theory of Simple Liquids*, 3rd Edition, (2006).

[5] I. C. Slater, *Physical Review* **38**, 237 (1931).

[6] L. Landau, E. Lifschitz, *Física Estadística*, Ed. Reverté, (2002).

[7] B. P. Singh, S. K. Sinha, *J. Chem. Phys.* **68**, 562 (1978).

[8] E. Wigner, *Phys. Rev.* **40**, 749 (1932).

[9] J. G. Kirkwood, *Phys. Rev.* **44**, 31 (1933).

[10] B. P. Singh, S. K. Sinha, *J. Chem. Phys.* **67**, 3645 (1977).

CHAPTER 3

SEMICLASSICAL APPROACH TO MODEL QUANTUM FLUIDS USING SAFT-VR

Thermodynamic properties of quantum fluids are described using an extended version of the Statistical Associating Fluid Theory for Potentials of Variable Range (SAFT-VR), that takes into account quantum corrections to the Helmholtz free energy A, based on the Wentzel-Kramers-Brillouin (WKB) approximation. We present the theoretical background of this approach (SAFT-VRQ), considering two different cases depending on the continuous or discontinuous nature of the particles pair interaction. For the case of continuous potentials, we demonstrate that the standard Wigner-Kirkwood theory for quantum fluids can be derived from the de Broglie-Bohm formalism for quantum mechanics, that can be incorporated within the Barker and Henderson perturbation theory for liquids in a straightforward way. When the particles interact via a discontinuous pair potential, the SAFT-VR method can be combined with the perturbation theory developed by Singh and Sinha (J. Chem. Phys. **67***, 3645, (1977); J. Chem. Phys.* **68***, 562, (1978)). We present an analytical expression for the first-order quantum perturbation term for a square-well potential, and the theory is applied to model thermodynamic properties of hydrogen, deuterium, neon and helium. Vapor-liquid equilibrium (VLE), liquid and vapor densities, isochoric and isobaric heat capacities, Joule-Thomson coefficient and inversion curves are predicted*

This chapter is based on a paper: Víctor M. Trejos and Alejandro Gil-Villegas, *J. Chem. Phys.*, 136, 184506, (2012).

accurately with respect to experimental data. We find that quantum corrections are important for the global behavior of properties of these fluids and not only for the low-temperature regime. In specific, predictions obtained for hydrogen compare very favorably with respect to cubic equations of state.

3.1 Introduction

Perturbation theories based on statistical mechanics have been developed and used extensively to model thermodynamic properties of classical fluids, characterized by a negligible de Broglie's wavelength, given by $\lambda_B = h/\sqrt{2\pi mkT}$, where h and k are the Planck's and Boltzmann's constants, respectively; m the mass of the particle and T the temperature. Since the triple point of most of the substances occurs at relative high temperatures, λ_B becomes very small compared to a characteristic size scale such as the mean distance between close particles, $\langle s \rangle$. Quantum fluids are typically substances of small molecular weight that exhibit a fluid phase at low temperatures, and their de Broglie's wavelength is of the same magnitude as $\langle s \rangle$, i.e, quantum effects are present; typical examples are hydrogen, deuterium, helium-4 and neon. The case of hydrogen is particularly relevant due to its technological application as an alternative energy resource in fuel cells, food industry, petroleum recovery and refining, pharmaceuticals, aerospace, electronic circuits and power generation.[1–3] Several equations of state have been proposed to describe thermodynamic properties of hydrogen, specifically cubic equations of state,[4] without considering quantum corrections.

On the other hand, quantum effects have been found to be important in the characterization of phase diagrams of fluids with more complex structures,[5–10] and in the last decade several experimental studies have shown the relevance of quantum entanglement in macroscopic systems, even at high temperatures.[11]

There have been a number of studies about quantum corrections in the prediction of thermodynamic and structural properties of fluids following different approaches,[5–34] being the Wigner-Kirkwood (WK) theory the first method used with this purpose.[12,13] In the WK theory, the partition function for a system of particles interacting via a pair-potential $u(r)$ is expanded in powers of h, using a complete set of wave functions for the evaluation of the expansion terms. In its original formalism, this expansion is obtained from non-interacting particles wave functions, and it is valid for continuous potentials;[18] a set of hard-spheres wave functions is required for

discontinuous interactions.[20] Other extensions and further analysis of this approach have been considered,[28,29] including its connection to the path-integral description,[35] which is a robust approach to model quantum fluids, particularly in computer simulations.[10,30–34]

In this chapter, we are interested in the modeling of thermodynamic properties of quantum fluids based on a Wentzel- Kramers-Brillouin (WKB) extension of the statistical associating fluid theory (SAFT).[36,37] Over the years, SAFT has been a very powerful method to describe a wide range of systems, most of them of industrial interest, and different versions have been derived. One of the versions of SAFT that has been useful in the task of understanding the correlation between molecular behavior and macroscopic properties is the SAFT for potentials of variable range (SAFT-VR) approach,[38,39] that models particles interacting via variable-ranged potentials. Quantum-mechanical calculations to determine size parameters in models using the SAFTVR approach was previously considered by Sheldon *et al.*[7] In this chapter, we study a different route, by modifying the SAFT-VR formalism with the introduction of quantum contributions to the Helmholtz free energy. In Sec. 3.2, we present the theoretical background behind the extension of SAFT-VR to include quantum effects. In Sec. 3.3, we focus our analysis in the case of a square-well potential. In Sec. 3.5, the SAFTVRQ method is applied to model phase behavior and thermodynamic properties of quantum fluids, studying two possible routes: (a) a high-temperature perturbation expansion where the quantum corrections are only taken at the level of the attractive part of the square-well (SW) potential and (b) the same as (a) but considering a quantum hard-spheres (QHS) free energy.

3.2 Quantum corrections for continuous and discontinuous potentials

3.2.1 Continuous potential

Green[14] developed a semiclassical theory for fluids applying the WK approach,[12,13] in order to obtain distribution functions satisfying a quantum version of the Liouville equation. Quantum corrections to distribution functions are given as a series expansion in powers of h^2, where the first term is the classical distribution function. A semiclassical distribution function was used to derive several thermodynamic proper-

ties for a fluid comprised of N particles interacting via a pair-potential $u(r)$. In the case of the Helmholtz free-energy, the corresponding quantum expression is given by

$$\begin{aligned} \frac{A}{NkT} &= \frac{A^c}{NkT} + \frac{\rho\beta^2h^2}{24\pi m}\int_0^\infty g^c\left(r\right)\nabla^2 u\left(r\right)r^2dr \\ &= \frac{A^c}{NkT} + 2\pi\rho\beta D\int_0^\infty g^c\left(r\right)\nabla^2 u\left(r\right)r^2dr, \end{aligned} \tag{3.1}$$

where ρ is the number density, $\beta = 1/kT$, $D = \lambda_B^2/24\pi$ and A^c and $g^c(r)$ are the Helmholtz free-energy and the radial distribution function for the *classical* system, respectively. Eq.(3.1) has a quantum correction proportional to λ_B^2 since the linear term must be null in order to guarantee a real value of the free energy (see Ref. [15]).

Kim *et al.*[16] used this approach to study the liquid-vapor equilibrium (VLE) for several quantum fluids assuming a Lennard-Jones pair potential (LJ), applying the Barker and Henderson perturbation theory (BH) for classical fluids,[40,41] deriving expressions for A^c and the quantum contribution A^Q given in the last term of Eq. (3.1). The high-temperature BH perturbation expansion for A^c was performed up to second order, in combination with the local compressibility approximation. The quantum energy A^Q was obtained using the hard-spheres (HS) radial distribution function $g_0(r)$ according to the procedure developed by Wertheim and Thiele,[42,43] with $g_0(r) = 1$ for $r > 5\sigma$, where σ is the LJ size parameter defined by $u(\sigma) = 0$, and the HS effective diameter was determined by the BH rule as in the classical theory. Very good descriptions were obtained for hydrogen, deuterium, helium-4 and neon, although some deviations were observed for neon with respect to the experimental data. It was assumed by the authors that the LJ potential was not a suitable pair interaction for neon.

A close-related approach was introduced by Jaen and Khan.[17] These authors applied the WKB method[44–46] in order to obtain the pair radial distribution function of a quantum fluid, using the statistical density matrix Δ. The WKB method deals with the approximate solution of the Schrödinger wave equation in the limit of short wavelengths, as in the case considered in optics when the geometric limit is obtained.[47] The properties of the classical system are used to calculate quantum corrections to the wave function or Δ. In the case considered by Jaen and Khan, the diagonal element of Δ of a system of interacting particles in the canonical ensemble was expanded in

a series of powers on $\alpha = \hbar^2/2m$, where the zeroth-order terms corresponds to the classical Δ. In this way, semiclassical expressions for the radial distribution function and the pair potential, u^e, were obtained as a power expansion on D,

$$g(r) = g^c(r) + D\nabla^2 g^c(r) + \frac{1}{2}D^2\nabla^2\nabla^2 g^c(r) + ..., \tag{3.2}$$

and

$$u^e(r) = u(r) + D\nabla^2 u(r) + \frac{9}{10}D^2\nabla^2\nabla^2 u(r) + ... \tag{3.3}$$

Particle-exchange contributions are not included in Eq.(3.3). By the nature of D, the effective quantum potential u^e depends on powers of β.

The statistical routes described previously are not independent, since Eq.(3.1) can be obtained directly from u^e considering the expansion up to first-order in D in Eq.(3.3). This connection, that apparently has not been noted before, allows us to apply the BH perturbation theory, obtaining the first-order perturbation term for a fluid interacting via the pair potential u^e and using the classical hard-spheres fluid as the reference system,

$$a_1 = 2\pi\rho \int_0^\infty g_0(r) u^e(r) r^2 dr, \tag{3.4}$$

where $g_0(r)$ is the classical HS radial distribution function that must be evaluated with a temperature-dependent BH diameter. It results that a_1 can be expressed as the sum of the classical and quantum contributions:

$$a_1 = a_1^c + a_1^Q, \tag{3.5}$$

with

$$a_1^c = 2\pi\rho \int_0^\infty g_0(r) u(r) r^2 dr, \tag{3.6}$$

and

$$a_1^Q = 2\pi\rho D \int_0^\infty g_0(r) \nabla^2 u(r) r^2 dr, \tag{3.7}$$

the last term being temperature dependent. In this way, Eq.(3.1) can be rewritten as a WKB Barker and Henderson perturbation expansion:

$$\frac{A}{NkT} = \frac{A^c}{NkT} + \beta a_1^Q. \tag{3.8}$$

It is interesting to note that the derivation of Eq.(3.8) and related expressions can be done using a different route to the statistical methods already described, using the de Broglie-Bohm formalism of quantum mechanics.[48–50] The wave function $\Psi(\mathbf{r},t)$ of a particle of mass m in a potential V (Ref. [51]) satisfies the Schrödinger equation,

$$-\frac{\hbar^2}{2m}\nabla^2\Psi(\mathbf{r},t)+V(\mathbf{r})\Psi(\mathbf{r},t)=-i\hbar\frac{\partial\Psi(\mathbf{r},t)}{\partial t}, \tag{3.9}$$

where $\mathbf{r}$ denotes the vector position of the particle at time t. Introducing the Madelung representation of the wavefunction,

$$\Psi(\mathbf{r},t)=R(\mathbf{r},t)e^{iS(\mathbf{r},t)/\hbar}, \tag{3.10}$$

where $R(\mathbf{r},t)$ and $S(\mathbf{r},t)$ are amplitude and phase functions of real variable, respectively, Eq.(3.9) is transformed into the following equations:

$$\frac{\partial S}{\partial t}+\frac{(\nabla S)^2}{2m}+V-\frac{\hbar^2}{2m}\frac{\nabla^2 R}{R}=0, \tag{3.11}$$

$$\frac{\partial R^2}{\partial t}+\nabla\cdot\left(R^2\frac{\nabla S}{m}\right)=0. \tag{3.12}$$

Following the de Broglie-Bohm approach, Eq.(3.11) can be reinterpreted as a Quantum version of the Hamilton-Jacobi equation of classical mechanics,

$$\frac{\partial S_c}{\partial t}+\frac{(\nabla S_c)^2}{2m}+V=0, \tag{3.13}$$

where S_c is the *action* of the particle. The motion equation of the particle can be obtained from the solution of Eq.(3.13), since the particle's momentum $\mathbf{p}$ is given by $\mathbf{p}=\nabla S_c$. The *quantum potential* is defined by

$$Q=-\frac{\hbar^2}{2m}\frac{\nabla^2 R}{R}, \tag{3.14}$$

in such a way that Eq.(3.11) is an extended version of Eq.(3.13), assuming that for quantum systems there is an effective potential energy defined by $u^e(r)=V(r)+Q$, and that $\mathbf{p}=\nabla S$. In the WKB approximation, once the phase function S of Ψ is expanded in powers of $\hbar$, the corresponding WKB quantum potential for a stationary

state of energy E is given by[50]

$$Q_{\mathrm{WKB}} = \frac{\hbar^2}{8m}\frac{\nabla^2 V}{V-E} - \frac{5\hbar^2}{32m}\left(\frac{\nabla V}{V-E}\right)^2, \tag{3.15}$$

This expression is valid in either case $E > V$ or $E < V$. By assuming that the kinetic energy $E - V \approx 3kT/2$, and considering the leading term in powers of β in Eq.(3.15), then the quantum potential reduces to

$$Q_{\mathrm{WKB}} = \pm D\nabla^2 V. \tag{3.16}$$

where the plus/minus sign corresponds to the $E < V$ or $E > V$ cases, respectively. Assuming that

$$V = \mp u(r), \tag{3.17}$$

where the selection of signs must be consistent with the respective cases in Eq.(3.16), we then recover Eq.(3.1) and Eq.(3.3). Consequently, we have demonstrated, within the semiclassical limit where the WKB approach is valid, that the statistical routes used to obtain the quantum free energy contribution for a system of particles interacting via a continuous potential are consistent with the assumption that the effective pair interaction to be taken into account in the evaluation of the perturbation terms is given by

$$u^e(r) = u(r) + Q_{\mathrm{WKB}}. \tag{3.18}$$

3.2.2 Discontinuous potentials

The h^2 expansion has several shortcomings when applied to discontinuous potentials, as has been reported by several authors.[18–29] Although most of these previous studies have been focused in low-density fluids and prediction of virial coefficients, a general framework, equivalent to Green's theory, has been developed for fluids by Singh and Sinha,[23,24] based in an alternative WK expansion that uses a hard-spheres wave function basis instead of the free-particle's one.[20] According to this approach, a high-temperature perturbation expansion can be performed for hard-core potential models given by

$$u(r) = u_{\mathrm{HS}}(r) + \phi(r), \tag{3.19}$$

where the discontinuous potential is divided into a hard spheres contribution, u_{HS}, and a perturbative potential, ϕ. The corresponding Helmholtz free energy can be expressed as

$$\frac{A}{NkT} = a^{ideal} + a^{Q}_{\mathrm{HS}} + \beta a_1 + \beta^2 a_2 - 24\pi\rho\beta D \int_0^\infty g_0^Q(r)\nabla^2\phi(r)\, r^2 dr, \tag{3.20}$$

where a^{ideal} is the ideal free energy, $a^{Q}_{\mathrm{HS}} = A^{Q}_{\mathrm{HS}}/NkT$ is the Helmholtz free energy of the QHS system, a_1 and a_2 are the first and second order perturbation terms defined in the same way as in the Barker and Henderson classical perturbation theory[40,41] but re-expressed in terms of correlation functions of the QHS fluid, being g_0^Q the corresponding radial distribution function. The perturbation expansion of the radial distribution function also follows the same formal expressions as in the the classical theory but in terms of the QHS correlation functions.[21]

The quantum behavior of the HS fluid introduces a significant difference with respect to its classical expression, since its contact value vanishes, i.e, $g_0^Q(\sigma) = 0$. Formally,

$$g_0^Q(r) = W(r) g_0(r), \tag{3.21}$$

where $W \to 1$ when $\lambda_B \to 0$ and $W \to 0$ when $r \to \sigma$; in the low-density limit W has been determined[22] and the leading term is given by

$$W(r) = 1 - exp\left[-\frac{2\pi}{\lambda_B^2}(r-\sigma)^2\right], \tag{3.22}$$

Quantum hard-sphere repel each other before they come into contact and an effective diameter can be defined,[19] given by

$$\sigma_{\mathrm{eff}} = \sigma + (1/2\sqrt{2})\lambda_B, \tag{3.23}$$

i.e., spheres "swell" in the quantum regime. Remarkably, Yoon and Sheraga[27] found that the classical formulas for the Helmholtz free energy and pressure given by the Carnahan Starling equation of state (CS EoS) (Ref. [52]) can reproduce Monte Carlo simulation values of the QHS system if this effective diameter is introduced in the CS EoS through the evaluation of a temperature dependent packing fraction given by $\eta_{\mathrm{eff}} = \eta\sigma^3_{\mathrm{eff}}$. In this way, a shifted contact value of the QHS radial distribution

function, $g_0(\sigma_{\text{eff}})$, is derived and the pressure is expressed according to the classical formula

$$Z = \frac{\beta P}{\rho} = 1 + 4\eta_{\text{eff}} g_0(\sigma_{\text{eff}}), \tag{3.24}$$

a result that will be important when we discuss the theory in the context of the SAFT-approach. A semiclassical limit of Eq.(3.20) can be obtained by considering the limit $g_0^Q \to g_0$ in the evaluation of the perturbation terms a_1 and a_2, obtaining

$$\frac{A}{NkT} = a^{ideal} + a^Q_{\text{HS}} + \beta(a^c_1 + a^Q_1) + \beta^2 a^c_2, \tag{3.25}$$

where a^Q_{HS} can be determined either by the CS EoS, $a^{\text{CS}}_{\text{HS}} = (4\eta - 3\eta^2)/(1-\eta)^3$, expressed in terms of η_{eff}, or by the approximated expression given by Jancovici,[19]

$$a^Q_{\text{HS}} = a^{\text{CS}}_{\text{HS}} + \frac{6\lambda_B}{\sqrt{2}\sigma}\eta g_0(\sigma), \tag{3.26}$$

The quantum mean attractive energy a^Q_1 is given in this case by

$$a^Q_1 = -24\pi\rho D \int_0^\infty g_0(r)\nabla^2\phi(r)\, r^2 dr. \tag{3.27}$$

Notice that the main difference between Eqs. (3.7) and (3.27) for a^Q_1 is the nature of the pair potential, that has also a repulsive contribution in Eq. (3.7).

3.3 SAFT-VRQ for square-well monomer fluid

In this section, we present an analytical evaluation of Eq.(3.27) when ϕ is considered as a square-well (SW) potential,

$$\phi(r;\sigma) = \begin{cases} -\epsilon & \text{if} \quad \sigma \le r \le \lambda\sigma \\ 0 & \text{if} \quad r > \lambda\sigma \end{cases} \tag{3.28}$$

where r is the distance between two segments, $-\epsilon$ is the depth energy, and λ is the range of the attractive forces. Introducing reduced variables, we have from Eq. (3.27)

$$a^Q_1 = -3\left[\frac{\Lambda}{\pi}\right]^2 \beta\epsilon\eta I^Q, \tag{3.29}$$

where $x = r/\sigma$, $\eta = \pi\rho\sigma^3/6$ is the packing fraction, $\Lambda = h/\sigma\sqrt{m\epsilon}$ is the de Boer's quantumness parameter, and

$$I^Q = \int_1^\infty g^c(x)\frac{d^2\phi}{dx^2}x^2dx. \tag{3.30}$$

Parameters D and Λ are related through the following expression

$$\frac{12D}{\sigma^2} = \left[\frac{\Lambda}{2\pi}\right]^2 \beta\epsilon. \tag{3.31}$$

According to Eq.(3.28),

$$\beta\frac{d\phi}{dx} = -e^{\beta\phi}\left(\frac{de^{-\beta\phi}}{dx}\right) \tag{3.32}$$

$$\beta\frac{d^2\phi}{dx^2} = \left(e^{\beta\phi}\frac{de^{-\beta\phi}}{dx}\right)^2 - e^{\beta\phi}\left(\frac{d^2e^{-\beta\phi}}{dx^2}\right), \tag{3.33}$$

where

$$\frac{de^{-\beta\phi}}{dx} = e^{\beta\epsilon}\delta(x-1) + (1-e^{\beta\epsilon})\delta(x-\lambda). \tag{3.34}$$

In order to obtain I^Q by Eqs.(3.30)-(3.34), the HS cavity function $y_0(x)$ is used instead of $g_0(x)$, since $y_0(x) = g_0(x)$ for $x \geq 1$ and it is a continuous function. Then we can apply the following result that is valid for an arbitrary continuous function $F(x)$:

$$\int_{-\infty}^{\infty} F(x)\frac{d\delta(x-x_0)}{dx}dx = -\left[\frac{dF}{dx}\right]_{x=x_0}. \tag{3.35}$$

Substituting Eqs. (3.33)-(3.35) in Eq. (3.30), we obtain

$$I^Q = I_1^Q + I_2^Q, \tag{3.36}$$

where

$$\beta I_1^Q = (1-e^{-\beta\epsilon})^2 y_0(\lambda)\lambda^2, \tag{3.37}$$

$$\beta I_2^Q = -(1-e^{-\beta\epsilon})\left[\frac{d}{dx}(y_0x^2)\right]_\lambda. \tag{3.38}$$

These expressions require to know $y_0(x)$ for a HS fluid. In this work we used the formula proposed by Boublik,[53]

$$y_0\left(x\right) = e^{f(\vartheta;x)} = e^{\vartheta_0+\vartheta_1 x+\vartheta_2 x^2+\vartheta_3 x^3}, \tag{3.39}$$

where ϑ_0, ϑ_1, ϑ_2 and ϑ_3 are functions of the packing fraction η given in Ref. [53]. Using this result in Eq.(3.38) gives

$$\left[\frac{d}{dx}(y_0 x^2)\right]_\lambda = \lambda y_0(\lambda)\left[2+\lambda\left(\frac{\partial f}{\partial x}\right)_\lambda\right], \tag{3.40}$$

with

$$\left(\frac{\partial f}{\partial x}\right)_\lambda = \vartheta_1 + 2\vartheta_2\lambda + 3\vartheta_3\lambda^2. \tag{3.41}$$

Eq. (3.40) can be evaluated using $y_0(\lambda)$ as given by Eq.(3.39). Instead of doing this, we used the compact expressions derived from the Carnahan-Starling theory[52] and the SAFT-VR approach,[38] respectively,

$$y_0(\lambda) = -\frac{1}{12\eta\epsilon\lambda^2}\left(\frac{\partial a_1^c}{\partial\lambda}\right). \tag{3.42}$$

Combining equations (3.29), (3.36)-(3.38) and (3.40)-(3.42), a final expression for a_1^Q is obtained, that is an explicit function on β, η, and λ, as in the case of the classic mean-attractive energy term a_1^c. It is important to note that the power expansion in β of Eqs. (3.37) and (3.38) introduces perturbation terms starting in β^2 in a_1^Q.

We now consider the more general case of a fluid composed of N chain molecules that could present more complex interactions, like associating anisotropic short-ranged attractive sites. In this case, the introduction of quantum corrections is more subtle and is not only given by the addition of a quantum free-energy contribution like in Eqs.(3.1) and (3.20). Following the statistical associating fluid theory,[36,37] the Helmholtz free energy is given by

$$\frac{A}{NkT} = \frac{A^{ideal}}{NkT} + \frac{A^{mono}}{NkT} + \frac{A^{chain}}{NkT} + \frac{A^{Assoc}}{NkT}, \tag{3.43}$$

where A^{ideal}, A^{mono}, A^{chain} and A^{assoc} are the ideal, monomer, bonding and associating energy contributions, respectively; arising from the different structural elements involved in this case, and obtained following the SAFT-VR approach where

the monomers forming the chain molecules interact via potentials of variable repulsive or/and attractive ranges.[38,39,54,55] In the case of the energy contribution due to monomers, we have that

$$\frac{A^{mono}}{NkT} = m_s a, \tag{3.44}$$

where m_s is the number of segments of the chain molecule, and a is the free energy of a monomeric fluid whose properties are given by Eq.(3.25). The second-order term can be derived from the local compressibility approximation,[40,41]

$$a_2 = \frac{1}{2} K_0 \eta \frac{\partial a_1}{\partial \eta}, \tag{3.45}$$

with

$$K_0 = \frac{(1-\eta)^4}{1+4\eta+4\eta^2}. \tag{3.46}$$

Then it is clear that a_2 follows a similar expression as a_1,

$$a_2 = a_2^c + a_2^Q, \tag{3.47}$$

where

$$a_2^c = \frac{1}{2} K_0 \eta \frac{\partial a_1^c}{\partial \eta}, \tag{3.48}$$

and

$$a_2^Q = \frac{1}{2} K_0 \eta \frac{\partial a_1^Q}{\partial \eta}. \tag{3.49}$$

In this work, we have used $a_2 = a_2^c$. The consideration of the other SAFT-VR terms, A^{chain} and A^{assoc}, is more subtle; since in the classical theory, they are functions of the contact value of the SW radial distribution function $g(\sigma)$, which is obtained by a first-order perturbation expansion.[38] This term arises in the evaluation of the bonding volume, whose expression is formally the same for a quantum fluid. However, quantum mechanically $g(\sigma) = 0$ when we consider fluids whose particles interact via a hard-core potential.[56] This effect is consequence of the extinction of the wave functions when the particles come into contact, i.e, pressure is not given by collisions, as in the classical case, but by repulsions. However, since we know that QHS behave as a fluid formed by spheres with a larger diameter,[19,27] we can use an effective contact distance σ_{eff} defined by Eq. (3.23), that is taken into account to reproduce the QHS pressure, according to Eq. (3.24). In this way, an effective contact value can be

obtained from the self-consistency between Eqs.(3.24) and (3.26):

$$g_0(\sigma_{\text{eff}}) = \left[1 + \frac{3\lambda_B}{2\sqrt{2}\sigma}\right] g_0(\sigma) + \frac{3\lambda_B}{2\sqrt{2}\sigma}\eta\frac{dg_0(\sigma)}{d\eta}, \tag{3.50}$$

that can be substituted in the SAFT-VR expression for $g_{SW}(\sigma)$,[38]

$$g_{SW}(\sigma) = g_0(\sigma_{\text{eff}}) + \frac{1}{4}\beta\left[\frac{\partial a_1}{\partial\eta} - \frac{\lambda}{3\eta}\frac{\partial a_1}{\partial\lambda}\right]. \tag{3.51}$$

Notice that $g_0(\sigma_{\text{eff}}) \to g_0(\sigma)$ when $\lambda_B \to 0$, and Eq. (3.51) reduces to the standard SAFT-VR expression for classical fluids. Eqs. (3.50) and (3.51) imply that the energy terms A^{chain} and A^{assoc} contain quantum contributions that are not additive, as in the case of A^{mono}. This is particularly significant in the case of the associating term, that describes hydrogen-bonding thermodynamics. The relevance of quantum effects in the formation of hydrogen bonds has been discussed by several authors,[8–10] and the SAFT-VRQ approach presented here gives a theoretical route to model some of these effects.

3.4 Discrete perturbation theory (DPT)

According to the DPT theory,[57] a system of N spherical particles contained in a volume V, interacting via a pair potential $u(r)$, can be approximated by a discrete pair potential $u_d(r)$, given as a sequence of SW and square-shoulders (SS). The resulting pair potential is given by

$$u_d(r) = u^{\text{HS}}(r) + \sum_{i=1}^{n}\phi_i(r) \tag{3.52}$$

where $u^{\text{HS}}(r)$ is the hard-sphere contribution and $\phi_i(r)$ a perturbative pair potential given by

$$\phi_i(r) = \begin{cases} \epsilon_i & \lambda_{i-1}\sigma \le r < \lambda_i\sigma \\ 0 & \text{otherwise} \end{cases} \tag{3.53}$$

where ϵ is the well-depth potential and its value could be: i) positive in the case of a SW interaction, ($\epsilon < 0$), ii) negative in the case of a SS interaction, ($\epsilon > 0$). A schematic representation of the discrete pair potential $u_d(r)$ is displayed in Fig. 3-1

The Helmholtz free energy, $a = A/NkT$, for a system of particles interacting via a discrete pair potential can be written as[57]

$$\frac{A}{NkT} = \frac{A^{\mathrm{HS}}}{NkT} + \beta \sum_{i=1}^{n} \left[a_1^{\mathrm{C}} (\lambda_i, \epsilon_i; \eta) - a_1^{\mathrm{C}} (\lambda_{i-1}, \epsilon_i; \eta) \right] \tag{3.54}$$
$$+ \beta \sum_{i=1}^{n} \left[a_1^{\mathrm{Q}} (\lambda_i, \epsilon_i; \eta) - a_1^{\mathrm{Q}} (\lambda_{i-1}, \epsilon_i; \eta) \right] + \beta^2 \sum_{i=1}^{n} \left[a_2^{\mathrm{C}} (\lambda_i, \epsilon_i; \eta) - a_2^{\mathrm{C}} (\lambda_{i-1}, \epsilon_i; \eta) \right]$$

where N is the number of particles, η is the packing fraction, λ_i is the parameter of the variable range in each step, and A^{HS} is the hard-sphere contribution.

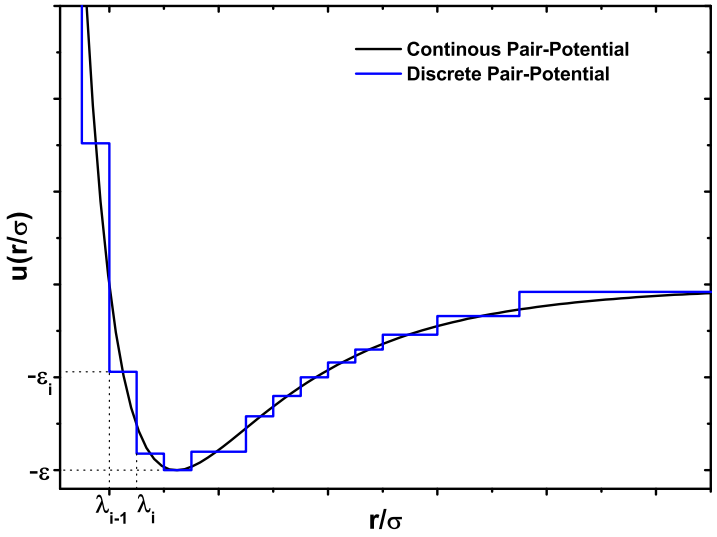

Figure 3-1: Schematic representation of a hard-core attractive potential (solid line). It can be approximated by a sequence of square-wells and square-shoulders. The details of the discretization are discussed explicitly in the text.

The quantum contribution a_1^{Q} given by Eq. 3.29, can be rewritten via a discrete pair potential as

$$a_1^{\mathrm{Q}} (\lambda_i, \epsilon_i; \eta) = \frac{1}{4} \eta \left[\frac{\Lambda}{\pi} \right]^2 (1 - e^{-\beta\epsilon})^2 y_0(\lambda_i) \lambda_i^2 - (1 - e^{-\beta\epsilon}) \left[\frac{d}{dx} (y_0 x^2) \right]_{\lambda_i} \tag{3.55}$$

In order to discretize the Lennard-Jones pair potential, we construct a succession of steps i and truncate the potential at a distance of $r < 1.95\sigma$.

3.5 Results and Discussion

Quantum corrections are required at low temperatures and high pressures. We analyzed these effects for hydrogen, deuterium, neon and helium-4, comparing the prediction obtained using a classical EoS, as given by SAFT-VR, and two variations of the semiclassical approach, according to Eq.(3.25): using a classical hard-spheres fluid, i.e., $a^{Q}_{\mathrm{HS}} \approx a^{CS}_{\mathrm{HS}}$, and the QHS free energy given by Eq.(3.26), that has a quantum correction with a linear term on λ_B. We will denote these equations as SAFT-VRQ and SAFT-VRQL, respectively. As detailed bellow, we found that both quantum EoS give very accurate results, although in overall SAFT-VRQ performs better, particularly when we consider the case of helium-4. We also tested the Yoon and Sheraga QHS free energy,[27] although it is not very accurate in comparison with SAFT-VRQ and SAFT-VRQL, and the corresponding results are not presented here.

In Table 3.1, we report the model parameters for the studied substances that were obtained by fitting experimental data of vapor pressure and saturated liquid density, as reported in Ref. [58], and assuming monomeric fluids, i.e., $m_s = 1$. The optimal parameters were determined by using a Levenberg-Marquartd minimization algorithm,[75] based on previous work on the VLE of asymmetric mixtures at high pressures,[60–62] using the following objective function:

$$f_{ob} = \sum_{i=1}^{M} \left(\frac{P_i^{cal} - P_i^{\exp}}{P_i^{\exp}} \right)^2 + \sum_{i=1}^{M} \left(\frac{\rho_i^{L,cal} - \rho_i^{L,\exp}}{\rho_i^{L,\exp}} \right)^2 , \tag{3.56}$$

where M is the number of experimental data points, and P and ρ are the pressure and density, respectively. The superscripts *exp* and *cal* denote experimental and calculated values, respectively. The set of optimized parameters are segment diameter (σ), SW depth energy (ϵ/k) and SW attractive range (λ). As can be observed in Table 3.1 by comparing with the classical values, in all the cases the inclusion of quantum effects systematically reduces the diameter σ and range λ and increases the depth energy ϵ when SAFT-VRQ is used. For SAFT-VRQL the effects are similar, with exception of the range λ that is always higher. The variation of these parameters has a global effect on the phase diagram. It is important to bear in mind that SW fluids of different attractive ranges are non-conformal fluids, i.e., they do not follow corresponding states, as in the case of fluids described by the LJ potential. Although the SW parameters reported in Table 3.1 are close to the corresponding LJ values

(see Ref. [16], for example), their differences are also determined by the change in the shape of the SW potential as λ varies.

Using the molecular parameters given in Table 3.1, the VLE coexistence curves were obtained by finding the liquid and vapor densities satisfying thermal equilibrium, $T^L = T^V$, mechanic equilibrium, $P^L = P^V$ and chemical equilibrium $g^L = g^V$, where P and g are the pressure and chemical potential, respectively. A standard Newton-Raphson method[75] was used to solve the system of non-linear equations.

Table 3.1: Optimized SAFT-VR, SAFT-VRQ and SAFT-VRQL parameters for hydrogen (H_2), deuterium (D_2), neon (Ne) and helium-4 (He) fluids obtained by fitting to experimental data of vapor pressure and saturated liquid density.[58] Monomeric fluids are considered ($m_s = 1$). Molecular parameters are: the range of the square-well interaction (λ), the hard-spheres diameter (σ), the attractive square-well energy (ϵ) and the scaled de Broglie wavelength ($\Lambda = h/\sigma\sqrt{m\epsilon}$). The values for every substance correspond to the classical (SAFT-VR, first row) and quantum versions (SAFT-VRQ and SAFT-VRQL, second and third rows, respectively).

Substance	λ	$\sigma/\text{Å}$	$(\epsilon/k)/K$	Λ
H_2	1.7184	3.0232	18.0805	0
	1.7114	2.8983	19.9291	2.3921
	1.7170	2.8690	26.4096	2.0992
D_2	1.7374	2.9150	20.4311	0
	1.6006	2.9066	25.9657	1.4723
	1.5990	2.8906	34.6549	1.2815
He	1.7260	2.9860	2.6943	0
	1.6799	2.7595	3.4973	4.2409
	1.6852	2.7461	5.6091	3.3650
Ne	1.5442	2.6914	32.8498	0
	1.5328	2.6949	33.4450	0.6252
	1.5823	2.6463	34.0730	0.6308

Results are shown in Fig. (3-2). For all the substances, the addition of quantum corrections clearly improves the classical prediction for the whole phase diagram. The SAFT-VRQL approach, that considers a λ_B linear term contribution to the QHS free energy, improves the SAFT-VRQ prediction of the critical temperature and pressure for hydrogen, deuterium and neon; however, in the case of helium-4, SAFT-VRQ is more accurate. Notice that for this last substance, the VLE occurs at very low temperatures (2.5 K - 5.3 K) and we can expect that the QHS free energy must include higher terms on λ_B, since helium-4 has the largest value of the reduced de Broglie wavelength Λ (see Table 3.1).

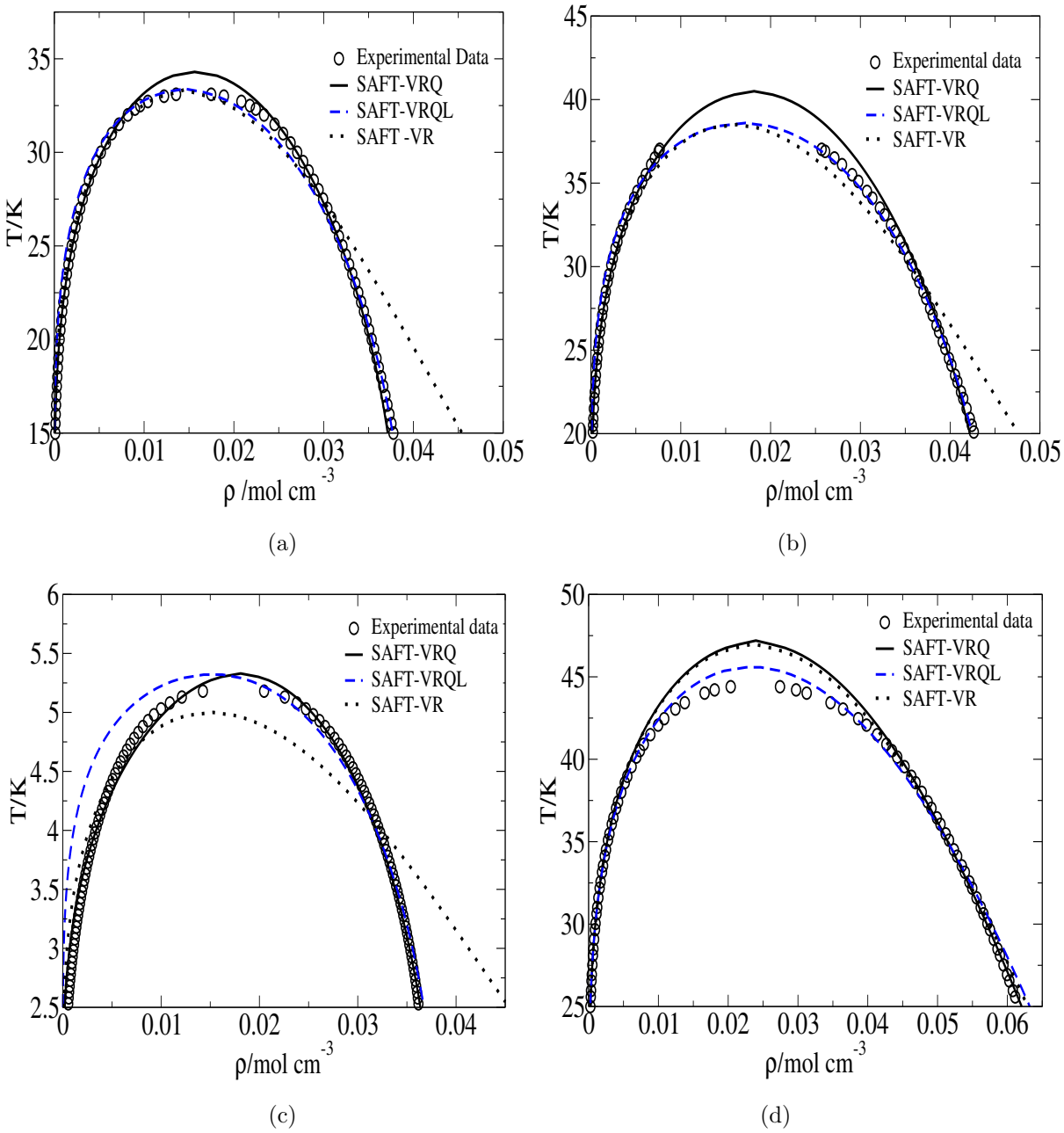

Figure 3-2: Vapor-liquid coexistence as predicted by the SAFT-VR, SAFT-VRQ and SAFT-VRQL approaches. Experimental data were taken from NIST Chemistry WebBook.[58] Substances presented are: a) hydrogen, b) deuterium, c) helium-4 and d) neon.

The predicted VLE and pressure-volume P-V super critical isotherms for the same substances using the SAFT-VRQ approach are shown in Fig. (3-3). Results are very accurate compared to experimental data, with the well-known overestimation of the

critical pressure.[38] These results validate the application of the SAFT-VRQ approach for high values of temperature and pressure, where most of the use of these fluids is required. Another important thermodynamic property to consider is the specific heat capacity. The following relationship between the isochoric heat capacity (C_V) and the isobaric heat capacity (C_p) can be established:[63]

$$C_p = C_p^{id} + C_V^{res} + R\frac{\left[Z + T\left(\frac{\partial Z}{\partial T}\right)_V\right]^2}{\left[Z + \rho\left(\frac{\partial Z}{\partial \rho}\right)_T\right]} - R, \tag{3.57}$$

where the superscripts id and res denote ideal and residual heat capacity contributions, respectively, Z is the compressibility factor defined by $Z = \eta(\partial a/\partial\eta)$, and R is the gas constant. The ideal isobaric heat capacity (C_p^{id}) can be expressed as a power series on temperature,[64] and C_V^{res} is given by:

$$\frac{C_V^{res}}{RT} = -2\left(\frac{\partial a^{res}}{\partial T}\right) - T\left(\frac{\partial^2 a^{res}}{\partial T^2}\right) \tag{3.58}$$

or

$$\frac{C_V^{res}}{R} = -\beta^2\left[2a_2^c + 2\left(\frac{\partial a_1^Q}{\partial \beta}\right) + \beta\left(\frac{\partial^2 a_1^Q}{\partial \beta^2}\right)\right]. \tag{3.59}$$

where a^{res} is the residual free Helmholtz energy contribution defined as,

$$a^{res} = a^{\mathrm{HS}} + \beta a_1 + \beta^2 a_2 + \beta a^Q \tag{3.60}$$

In Fig. (3-4), the accuracy in the predictions of C_p is given for (a) hydrogen, (b) deuterium, (c) helium-4, and (d) neon reported as the percentage deviation error. Deviations are below 6% for a wide range of temperatures and pressures.

In Fig. (3-5), we present predictions for the Joule-Thomson coefficient μ for (a) hydrogen, (b) deuterium, (c) helium-4, and (d) neon. This coefficient is defined by

$$\mu = \left(\frac{\partial T}{\partial P}\right)_H, \tag{3.61}$$

where H is the enthalpy. Depending of state conditions of μ, the fluid is cooled ($\mu > 0$) or heated ($\mu < 0$) for a small change in pressure at constant enthalpy H. The sign of the Joule-Thomson coefficient, μ, depending on: i) hte identity of gas, ii) pressure and temperature, iii) the relatives magnitudes of the attractive and repulsive

forces.

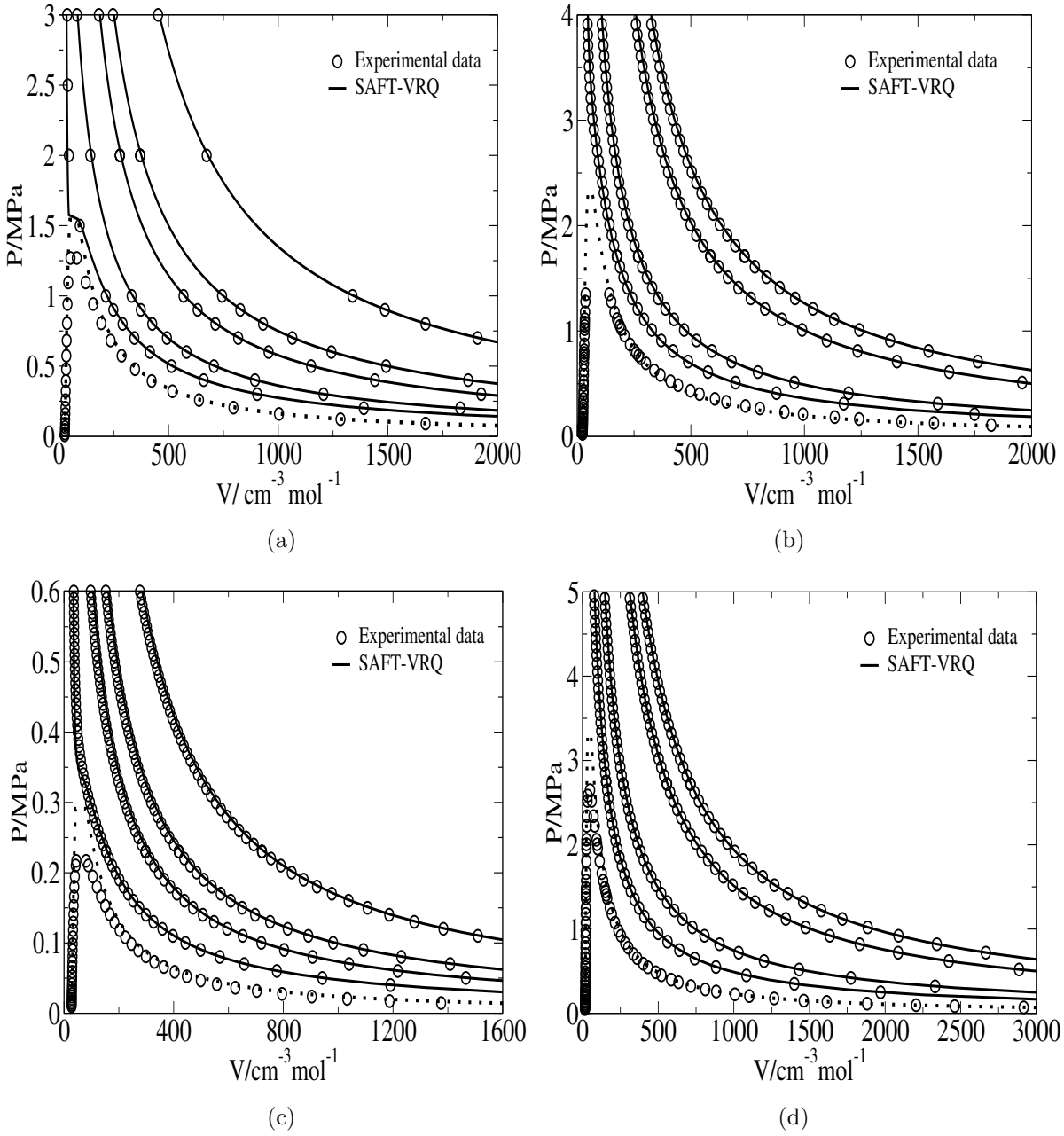

Figure 3-3: Pressure-volume isotherms as predicted by SAFT-VRQ and compared with experimental data in the vapor-liquid coexistence and supercritical regions. Experimental data were taken from NIST Chemistry WebBook.[58] The supercritical temperatures are given in solid lines for each substance, from top to bottom: a) hydrogen, 160K, 90K, 70K, 45K and 35K; b) deuterium, 150K, 120K, 60K and 45K; c) helium-4, 20K, 12K, 9K and 6K; d) neon, 230K, 180K, 90K and 60K. The envelope of the coexistence curve is denoted by a dotted line.

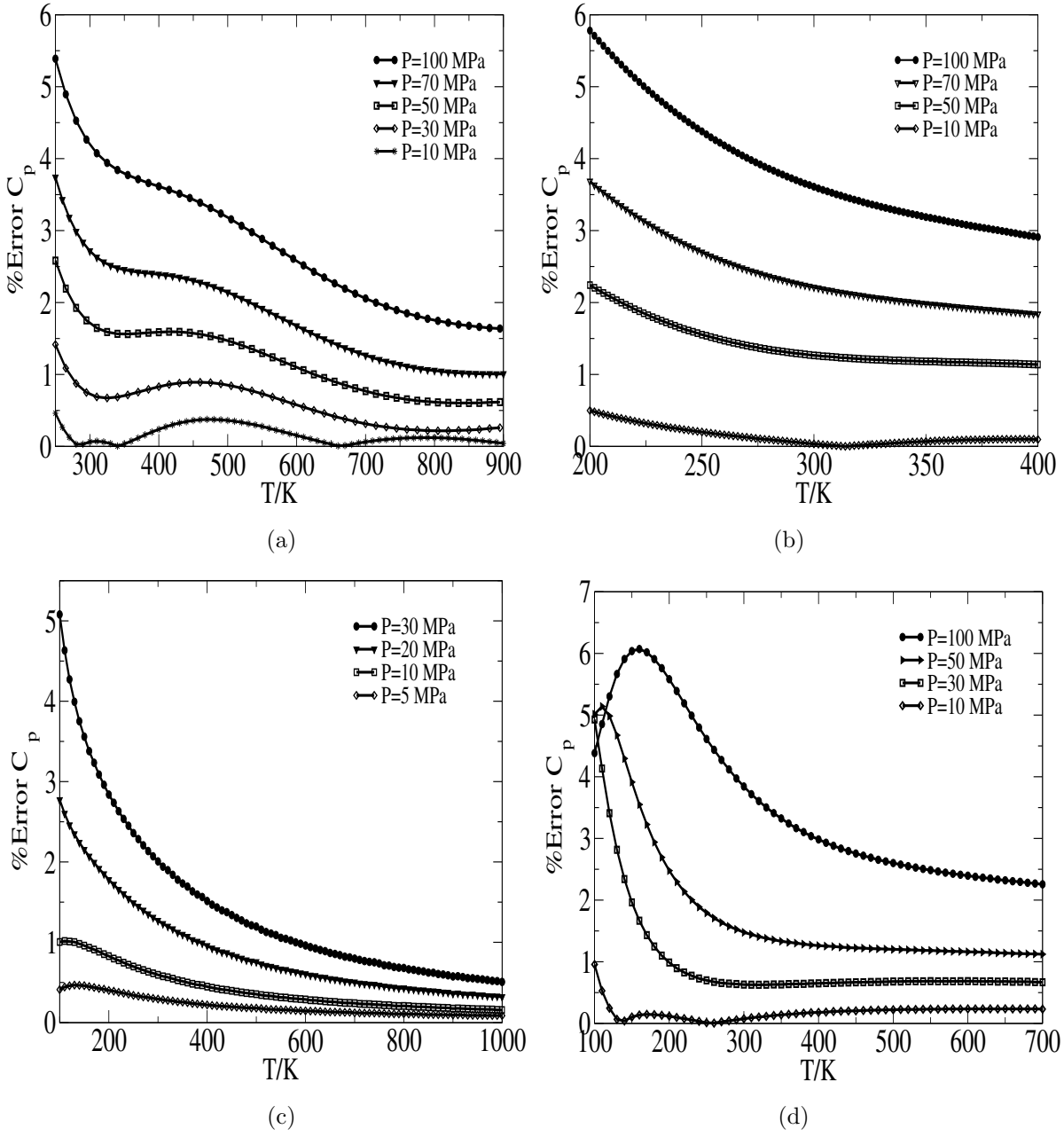

Figure 3-4: Percentage error deviation for the isobaric heat capacity as predicted by the SAFT-VRQ approach. Experimental data were taken from NIST Chemistry WebBook.[58] Substances presented are: a) hydrogen, b) deuterium, c) helium-4 and d) neon.

The cooling effect is observed when attractive interactions are dominant *i.e.* ($Z < 1$), and the warming effect is observed under conditions when repulsive interactions are dominant *i.e.* ($Z > 1$).[65] From standard thermodynamics relationships is known

that

$$\mu = -\frac{1}{C_p}\left[V - T\left(\frac{\partial V}{\partial T}\right)_p\right] = -\frac{1}{C_p}\left[V + T\frac{(\partial P/\partial T)_V}{(\partial P/\partial V)_T}\right], \tag{3.62}$$

or equivalently,

$$\mu = -\frac{1}{\rho C_p}\left[1 - \frac{T^*}{\eta}\frac{(\partial P^*/\partial T^*)_\eta}{(\partial P^*/\partial \eta)_{T^*}}\right], \tag{3.63}$$

where $P^* = P\sigma^3/\epsilon$ and $T^* = kT/\epsilon$, and

$$\left(\frac{\partial P^*}{\partial T^*}\right)_\eta = \eta^2\left(\frac{6}{\pi}\right)\left[\left(\frac{\partial a}{\partial \eta}\right) + T^*\frac{\partial}{\partial T^*}\left(\frac{\partial a}{\partial \eta}\right)\right], \tag{3.64}$$

$$\left(\frac{\partial P^*}{\partial \eta}\right)_{T^*} = T^*\left(\frac{6}{\pi}\right)\eta\left[2\left(\frac{\partial a}{\partial \eta}\right) + \eta\left(\frac{\partial^2 a}{\partial \eta^2}\right)\right]. \tag{3.65}$$

Equations (3.64)-(3.65) can be used to derive the predicted values of μ according to the SAFT-VRQ approach. The behavior of μ as a function of the pressure is observed in Fig. (3-5) for three isotherms corresponding to: (a) hydrogen, T = 160 K, 200 K, and 300 K; (b) deuterium, T = 150 K, 250 K, and 300 K; (c) helium-4, T = 10 K, 15 K, and 20 K; and (d) neon, T = 150 K, 250 K, and 300 K SAFT-VRQ predictions deviate systematically from experimental values, an effect basically due to the magnification of the inaccuracy on C_p. However, the accuracy obtained for helium-4 is remarkable.

The constant enthalpy lines on the T-P diagram pass through a point where $\mu = 0$, and the inversion curve corresponds to the set of all these points, that has an inflection point, characterized by the *Inversion Temperature*, T_{inv}. Gases that show a heating effect at one temperature also present a cooling effect when the temperature is below their upper T_{inv}. The inversion curve is obtained by solving the following equation at every thermodynamic point:

$$T^*\left(\frac{\partial P^*}{\partial T^*}\right)_\eta - \eta\left(\frac{\partial P^*}{\partial \eta}\right)_{T^*} = 0, \tag{3.66}$$

that combined with Eqs. (3.64–3.65) is used for the prediction of T_{inv} for hydrogen, Fig. (3-6). The Eq. (3.66) can be rewritten in terms of the compresibility factor (Z), as

$$1 + Z^{HS} - \beta^2\left[Z_2 + \left(\frac{\partial Z^Q}{\partial \beta}\right)\right] - 2Z - \eta^2\left(\frac{\partial^2 a}{\partial \eta^2}\right) = 0 \tag{3.67}$$

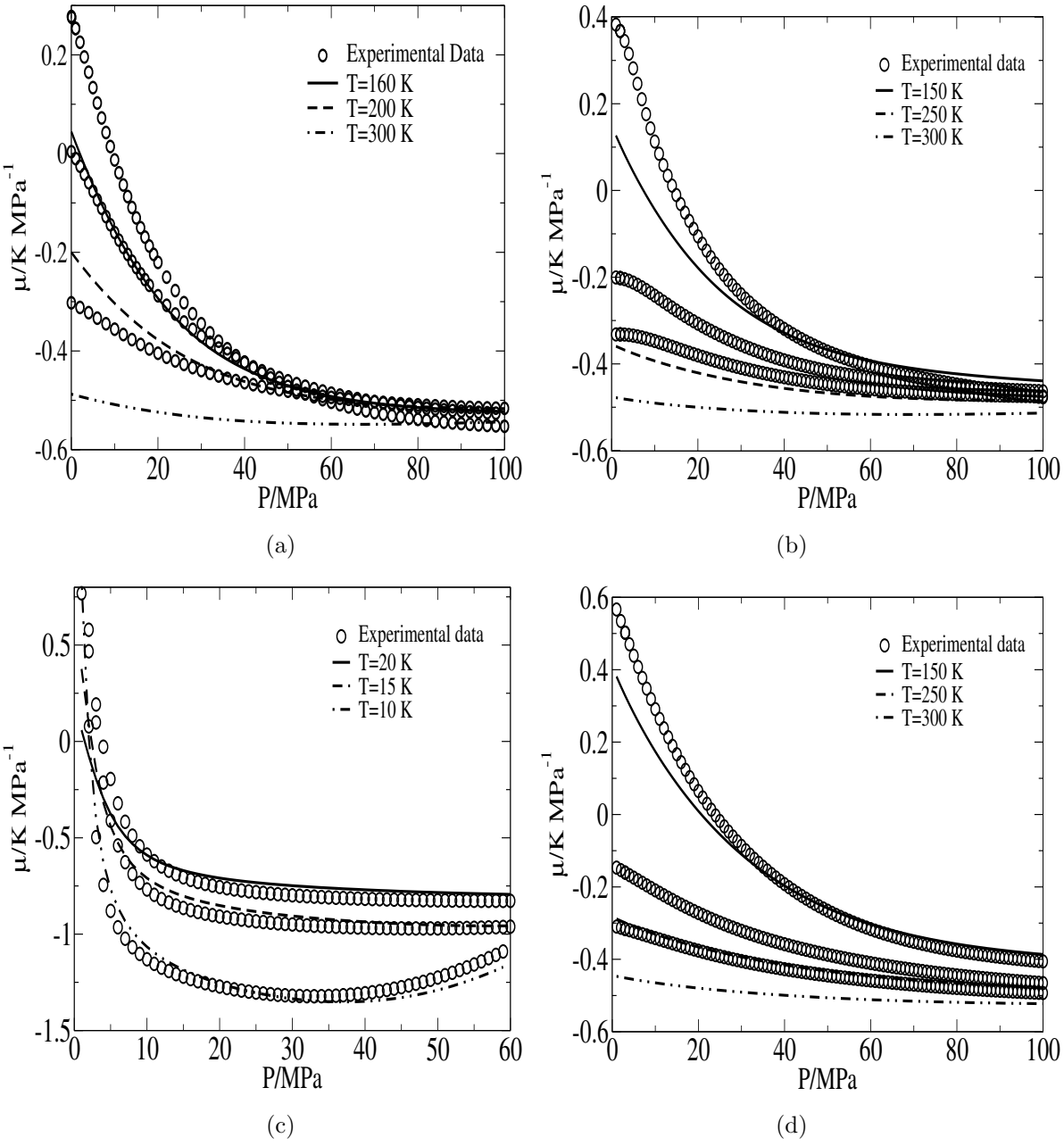

Figure 3-5: Joule-Thomson coefficient as predicted by the SAFT-VRQ approach. Experimental data were taken from NIST Chemistry WebBook.[58] Substances presented are: a) hydrogen, b) deuterium, c) helium-4 and d) neon.

with

$$Z = 1 + Z^{HS} + \beta Z_1 + \beta^2 Z_2 + \beta Z^Q \tag{3.68}$$

Four different results are given: the SAFT-VR predictions where A^{mono} is obtained by a first or second-order perturbation expansion (denoted by SAFT-VR(1) and SAFT-VR(2), respectively), the SAFT-VRQ results, and the Predicting-Soave-Redlich-Kwong (PSRK);[66] the last EoS being the best cubic equations of state used for this substance.[4]

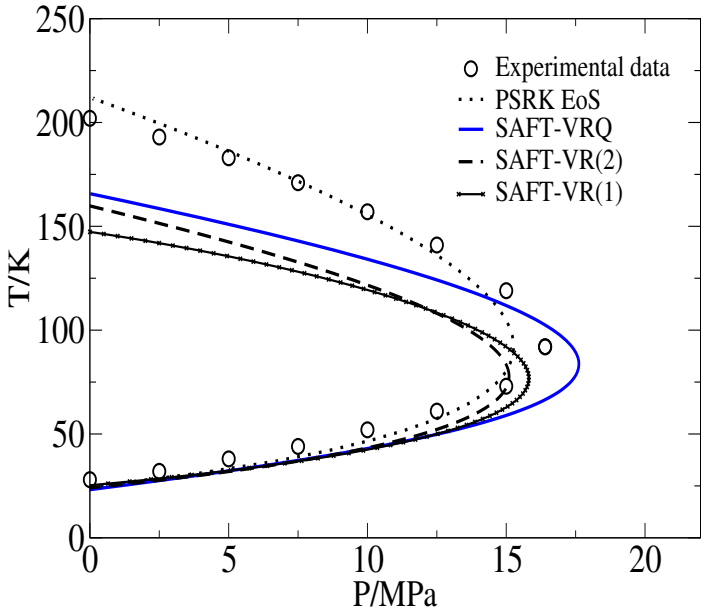

Figure 3-6: Joule-Thomson inversion curves for hydrogen as predicted by the first and second-order perturbation SAFT-VR expressions (denoted as SAFT-VR(1) and SAFT-VR(2), respectively), the SAFT-VRQ approach and Predicting-Soave-Redlich-Kwong (PSRK).[66] Experimental data taken from Perry's Chemical Engineers' Handbook.[64] The fitted parameters for the cubic equation was taken from Ref. [4].

The lower branch of the inversion curve is predicted accurately by all the EoS. However, for the upper branch the introduction of the quantum correction improves the classical prediction given by SAFT-VR. It is interesting to see that the SAFT-VRQ prediction works better even at high temperatures where is not expected that quantum effects should be important. We found here again that the introduction of quantum corrections has an important global effect on the thermodynamic property. The PSRK EoS has a very good performance at low and high temperatures. The results obtained here by using cubic equations of state were extended for the study of

refrigerants.[67] Finally, SAFT-VR + DPT, is an original form to built different kinds of continuous pair potential via a sequence of SW and SS interactions. In Fig. 3-7, we present predictions for the VLE for methane using a discrete Lennard-Jones pair potential. Experimental data are compared with the calculations with SAFT-VR + DPT approach. The predictions were accurate in both density and temperature.

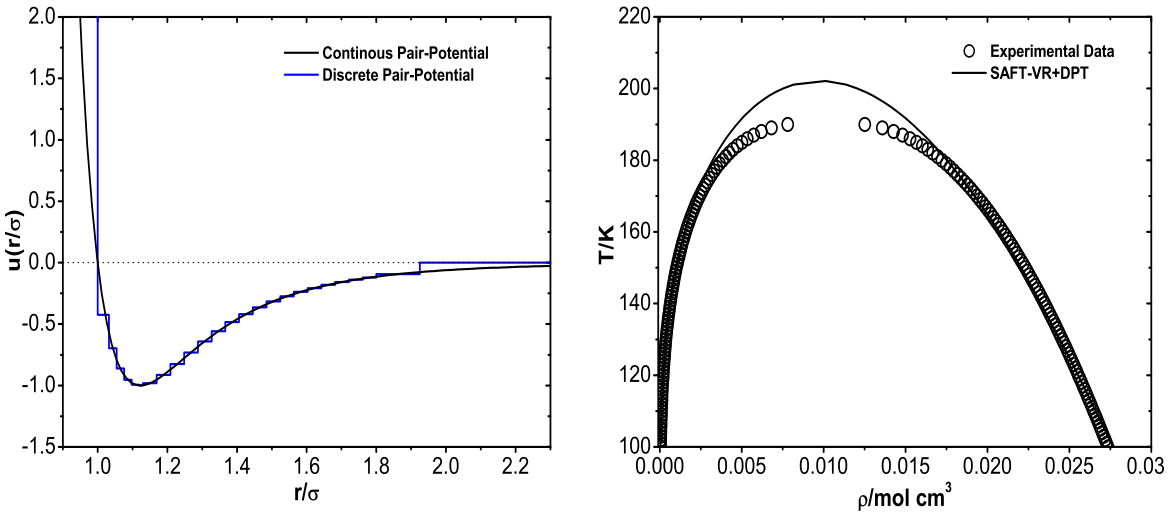

(a) (b)

Figure 3-7: Vapor-liquid coexistence as predicted by the SAFT-VR using a discrete pair potential. Experimental data were taken from NIST Chemistry WebBook.[58] Substances presented are: a) Schematic representation of a discrete Lennard-Jones pair potential (solid line), b) VLE predictions for methane.

All the results obtained in this chapter can be approximated by SAFT-VR + DPT for quantum fluids. This methodology is a more realistic description for the shape of the potential of real fluids.

Conclusions

This chapter has been concerned with the development of a semiclassical theory to model quantum effects in fluids within the framework of the SAFT-VR approach. Depending on the nature of the pair potential between particles, two different routes can be established. In the first one, valid for continuous potentials, the WKB approximation can be used following the standard statistical mechanics method derived

previously by several authors[14,16,17] based on the Wigner-Kirkwood expansion.[12,13] We have shown that the de Broglie-Bohm approach for quantum mechanics can be used within the Barker and Henderson perturbation theory when the WK expansion is applied for continuous potentials. In the second approach, valid for discontinuous potentials, we have applied the theory developed by Singh and Sinha[23–25] and evaluated analytically the first quantum perturbation term arising from the attractive potential of a square-well interaction. By considering different expressions of the QHS Helmholtz free energy, we have studied quantum fluids such as hydrogen, deuterium, helium-4 and neon, finding that the VLE properties can be accurately described by SAFT-VRQ, and other thermodynamic properties like isobaric heath capacity, Joule-Thomson coefficient and related inversion curves are also satisfactorily predicted. Although results have been presented for the most simple cases where only the ideal and monomeric contributions are required, we have considered semiclassical expressions for contributions to the free energy due to chain formation and association that are used in the SAFT formalism, where the evaluation of the bonding volume depends on the radial distribution function. This feature is particularly relevant in the modeling of hydrogen-bonded fluids, such as water, where there is a whole evidence that quantum effects are very important to understand its phase diagram at low temperatures.[10] Computer simulations studies would be desirable in order to confirm and validate the extension of SAFT-VRQ for continuous model interactions such as the Mie potential, taking advantage that a robust SAFT-γ approach has been proposed recently for this potential,[55] whose quantum potential is given by

$$Q_{WKB} = \frac{CD\epsilon}{r^2}\left[\lambda_r(\lambda_r-1)\left(\frac{\sigma}{r}\right)^{\lambda_r} - \lambda_a(\lambda_a-1)\left(\frac{\sigma}{r}\right)^{\lambda_a}\right], \tag{3.69}$$

where ϵ and σ are the energy and size potential parameters of the Mie potential,

$$C = \frac{\lambda_r}{\lambda_r-\lambda_a}\left(\frac{\lambda_r}{\lambda_a}\right)^{\frac{\lambda_a}{\lambda_r-\lambda_a}}, \tag{3.70}$$

and λ_r and λ_a are exponents that determine the range of the repulsive and attractive interactions. Computer simulations using the Feynman's pathintegrals method provides very accurate results for quantum fluids;[30–32] since the de Broglie-Bohm theory can be related to this method (see Sec. 6.9 of Ref. [50]) and the WK expansion can be expressed in terms of action functions used either in the Feynman's or

de Broglie-Bohm's theories,[29] it would be desirable to develop a further analysis of the approach used here. Finally, the results obtained for the SW fluid can also be applied to model other discrete potentials based on classical perturbation theory,[57] whose WKB extension can be obtained using the semiclassical approach followed in this study.

BIBLIOGRAPHY

[1] P. Dagaut, G. Dayma, *Int. J. Hydrogen Energy* **31**, 505, (2006).

[2] K. Otsuka, Y. Shigeta, S. Takenaka, *Int. J. Hydrogen Energy* **27**, 11, (2002).

[3] E. Ch. Vagia, A. A. Lemonidou, *Int. J. Hydrogen Energy* **32**, 212, (2007).

[4] K. Nasrifar, *Int. J. Hydrogen Energy* **35**, 3802, (2010).

[5] J. P. Wolbach, S. I. Sandler, *Ind. Eng. Chem. Res.* **36**, 4041, (1997).

[6] E. García, A. Martínez-Richa, A. Villegas, L. Mendoza-Huízar, A. Gil-Villegas, *J. Phys. Chem. A* **106**, 10342, (2002).

[7] T. J. Sheldon, B. Giner, C. S. Adjiman, A. Galindo, G. Jackson, D. Jacquemin, V. Wathelet, E. A. Perpète, *Comp. Aid. Chem. Eng.* **22**, 143, (2006).

[8] M. E. Tuckerman, D. Marx, M. L. Klein, M. Parrinello, *Science* **275**, 817, (1997).

[9] X-Z. Li, B. Walker, A. Michaelides, *PNAS* **108**, 6369, (2011).

[10] E. G. Noya, L. M. Sesé, R. Ramírez, C. McBride, M. M. Conde, C. Vega, *Mol. Phys.* **109**, 149, (2011).

[11] L. Amico, R. Fazio, A. Osterloh, V. Vedral, *Rev. Mod. Phys.* **80**, 517 (2008).

[12] E. Wigner, *Phys. Rev.* **40**, 749, (1932).

[13] J. G. Kirkwood, *Phys. Rev.* **44**, 31, (1933).

[14] H. S. Green, *J. Chem. Phys.* **19**, 955, (1951).

[15] L. D. Landau and E. M. Lifschitz, *Statistical Physics*, Part 1, 3rd ed. (Butherworth-Heinemann, Oxford, 1980).

[16] S. Kim, D. Henderson, J. A. Barker, *Can. J. Phys.* **47**, 99, (1969).

[17] J. K. Jaen, A. Khan, *J. Chem. Phys.* **46**, 260, (1967).

[18] M. E. Boyd, S. Y. Larsen, J. E. Kilpatrick, *J. Chem. Phys.* **50**, 4034, (1969).

[19] B. Jancovici, *Phys. Rev.* **178**, 178, (1969).

[20] E. J. Derderian, W. A. Steele, *J. Chem. Phys.* **55**, 5795, (1971).

[21] Y. Singh, *Mol. Phys.* **27**, 1687, (1974).

[22] W. G. Gibson, *Phys.Rev. A* **11**, 270, (1975).

[23] B. P. Singh, S. K. Sinha, *J. Chem. Phys.* **67**, 3645, (1977).

[24] B. P. Singh, S. K. Sinha, *J. Chem. Phys.* **68**, 562, (1978).

[25] N. Singh, S. K. Sinha, *J. Chem. Phys.* **69**, 2709, (1978).

[26] J. A. Barker, *J. Chem. Phys.* **70**, 2914, (1979).

[27] B.-J. Yoon, H. A. Scheraga, *J. Chem. Phys.* **88**, 3923, (1988).

[28] Fujiwara, T. A. Osborn, and S. F. J. Wilk, *Phys. Rev. A* **25**, 14 (1982).

[29] C. Pisani, B. H. J. McKellar, *Phys. Rev. A* **44**, 1061, (1991).

[30] L. M. Sesé, R. Ledesma, *J. Chem. Phys.* **102**, 3776, (1995).

[31] M. Sesé, *Mol. Phys.* **85**, 931 (1995).

[32] M. Sesé and R. L. E. Bailey,**119**, 10256 (2003).

[33] D. M. Ceperley, *Rev. Mod. Phys.* **67**, 279, (1995).

[34] Q. Wang, J. K. Johnson, *Fluid Phase Equil.* **132**, 93, (1997).

[35] R. P. Feynman, *Statistical Mechanics*, (Benjamin, New York, 1972).

[36] W. G. Chapman, K. E. Gubbins, G. Jackson, M. Radosz, *Fluid Phase Equil.* **52**, 31, (1989).

[37] W. G. Chapman, K. E. Gubbins, G. Jackson, M. Radosz, *Ind. Eng. Chem. Res.* **29**, 1709, (1990).

[38] A. Gil-Villegas, A. Galindo, P. J. Whitehead, S. J. Mills, G. Jackson, A. N. Burgess, *J. Chem. Phys.* **106**, 4168, (1997).

[39] A. Galindo, L. A. Davies, A. Gil-Villegas, G. Jackson, *Mol. Phys.* **93**, 241, (1998).

[40] J. A. Barker, D. Henderson, *J. Chem. Phys.* **47**, 2856, (1967).

[41] J. A. Barker, D. Henderson, *J. Chem. Phys.* **47**, 4714, (1967).

[42] M. S. Wertheim, *Phys. Rev. Lett.* **10**, 321, (1963).

[43] E. Thiele, *J. Chem. Phys.* **39**, 474, (1963).

[44] G. Wentzel, *Z. Phys.* **45**, 952, (1926).

[45] H. A. Kramers, *Z. Phys.* **39**, 828, (1926).

[46] L. Brillouin, *C. R. Acad. Sci. Paris* **183**, 24, (1926).

[47] M. Born, E. Wolf, *Principles of Optics* (Cambridge University Press, Cambridge, 2005).

[48] D. Bohm, *Phys. Rev.* **85**, 166, (1952).

[49] D. Bohm, *Phys. Rev.* **85**, 180, (1952).

[50] P. R. Holland, *The Quantum Theory of Motion* (Cambridge University Press, Cambridge, 1993).

[51] S. Gasiorowicz, *Quantum Physics* (John Wiley & Sons, New York, 1996).

[52] N. F. Carnahan, K. E. Starling, *J. Chem. Phys.* **51**, 635, (1969).

[53] T. Boublik, *Mol. Phys.* **59**, 371, (1986).

[54] L. A. Davies, A. Gil-Villegas, G. Jackson, *Int. J. Thermophys.* **19**, 675, (1998).

[55] C. Avendaño, T. Lafitte, A. Galindo, C. S. Adjiman, G. Jackson, E. Müller, *J. Phys. Chem. B* **115**, 11154, (2011).

[56] B. P. Singh, S. K. Sinha, *Phys. Rev. A* **18**, 2701, (1978).

[57] A. L. Benavides, A. Gil-Villegas, *Mol. Phys.* **97**, 1225, (1999).

[58] NIST Chemistry Webbook, *webbook.nist.gov/chemistry/.*

[59] W. H. Press, S. A. Teukolsky, W. T. Vetterling, B. P. Flannery,*Numerical Recipes:The art of the scientific computing* (Cambridge University Press, 3rd ed., New York, 2007).

[60] J.A. López, V.M. Trejos, C.A. Cardona, *Fluid Phase Equil.* **248**, 147, (2006).

[61] J.A. López, V.M. Trejos, C.A. Cardona, *Fluid Phase Equil.* **275**, 1, (2008).

[62] V.M. Trejos, J.A. López, C.A. Cardona, *Fluid Phase Equil.* **293**, 1, (2010).

[63] F. A. Perdomo, A. Gil-Villegas, *Fluid Phase Equil.* **306**, 124, (2011).

[64] R. H. Perry, D. W. Green, J.O. Maloney, *Perrys chemical engineers handbook* (McGraw Hill, 7th ed., New York, 1997).

[65] P. Atkins and J. de Paula, *Physical chemistry* (W. H. Freeman, 9th ed., New York, 2010).

[66] T. Holderbaum, J. Gmehling, *Fluid Phase Equil.*, **70**, 251, (1991).

[67] Susana Figueroa-Gerstenmaier, Martin Lísal, Ivo Nezbeda, William R. Smith and Víctor M. Trejos, *Fluid Phase Equilibria* **375**, 143, (2014).

CHAPTER 4

COMPUTER SIMULATION OF LIQUID-VAPOR COEXISTENCE OF CONFINED QUANTUM FLUIDS

The liquid-vapor coexistence (LV) of bulk and confined quantum fluids has been studied by Monte Carlo computer simulation for particles interacting via a semiclassical effective pair potential $V_{eff}(r) = V_{LJ} + V_Q$, where V_{LJ} is the Lennard-Jones 12-6 potential (LJ) and V_Q is the first-order Wigner-Kirkwood (WK-1) quantum potential, that depends on $\beta = 1/kT$ and de Boer's quantumness parameter $\Lambda = h/\sigma\sqrt{m\epsilon}$, where k and h are the Boltzmann's and Planck's constants, respectively, m is the particle's mass, T is the temperature of the system, and σ and ϵ are the LJ potential parameters. The non-conformal properties of the system of particles interacting via the effective pair potential $V_{eff}(r)$ are due to Λ, since the LV phase diagram is modified by varying Λ. We found that the WK-1 system gives an accurate description of the LV coexistence for bulk phases of several quantum fluids, obtained by the Gibbs Ensemble Monte Carlo method (GEMC). Confinement effects were introduced using the Canonical Ensemble (NVT) to simulate quantum fluids contained within parallel hard walls separated by a distance L_p, within the range $2\sigma \leq L_p \leq 6\sigma$. The critical temperature of the system is reduced by decreasing L_p and increasing Λ, and the liquid-vapor transition is not longer observed for $L_p/\sigma < 2$, in contrast to what has been observed for the classical system.

This chapter is based on a paper: Víctor M. Trejos and Alejandro Gil-Villegas and Alejandro Martinez, *J. Chem. Phys.*, 136, 184506, (2013).

4.1 Introduction

Confined systems is a major area of basic and applied research with diverse applications in nanotechnology.[1] Properties of fluids are strongly modified when they are confined, since atoms and molecules adsorbed onto a surface display a different potential energy between themselves as compared to their energy when they are in a bulk phase;[2] in consequence, the phase diagram of the confined fluid is modified and the critical temperature is reduced; experimental values of the ratio of the critical temperatures (adsorbed fluid/bulk fluid) vary around 0.4 for a wide range of molecular fluids.[3–5] In this way, surfaces work as energy reservoirs that allow different conditions for the realization of phase transitions as well as the appearance of novel phases.

Another application of confined fluids are sieving process, where components of a fluid mixture are separated by the size and shape of molecules, achieved and engineered through molecular-scale filters and pores.[6] In the case of quantum fluids, such as hydrogen and deuterium, i.e, substances of small molecular weight m whose de Broglie's wavelength ($\lambda_B = h/\sqrt{2\pi mkT}$, where T, h and k are the temperature, Planck's and Boltzmann's constants, respectively) has a magnitude comparable to the mean distance between particles, quantum sieving is a novel separation method based on isotopes distinction performed in nanopores that have a size comparable to λ_B.[7–13] Quantum sieving is a promising low-cost method for recycling fuel from a nuclear reaction; as cryogenic filters, separate mixture components via equilibrium condensation at low temperatures.[14]

Prediction of thermodynamic properties of quantum fluids is of particular relevance in physics, astronomy and chemical engineering,[15–18] and specifically hydrogen has deserved great attention due to their technological applications in aerospace, electronics and petrochemical industry.[19–21] The possibility of developing an economy based on hydrogen[22] that could attend energy and environmental problems is based on optimal methods for hydrogen storaging in cells, that requires a better understanding of the properties of quantum fluids under confinement.[23,24] On the other hand, in the last decade several studies have shown the possibility of observing quantum effects with molecules of increasing size, like matter wave interferometry of buckyballs[25,26] and organic molecules with 430 atoms,[27] as well as measuring entanglement effects in macroscopical systems.[28]

Over the years, different models and methods have been proposed to study quantum effects in fluids.[29–61] The Wigner-Kirkwood (WK) theory[29–32] was the first approach developed for the prediction of thermodynamic and structural properties of fluids at a semiclassical level, where quantum corrections are given by h^2-power terms that are functionals of second and higher-order derivatives of a continuous pair potential $V(r)$. This approach has been applied for the Lennard-Jones model[33,34] and also for other molecular systems.[35] Close-related semiclassical methods to the WK theory have also been used[36,37] and demonstrated the relevance of quantum corrections at high pressures.[38] However, the WK method does not converge for discontinuous potentials and alternative approaches are required, where the quantum corrections include odd powers of h.[39,40] Quantum hard-spheres (HS) and square-well (SW) fluids have been studied in this way, either for the calculation of virial coefficients[41,42] or by perturbation theories.[43–47] Based on the seminal work by Feynman on path integrals[62] and on robust molecular-simulation methods developed for classical fluids,[63–67] several authors have studied quantum fluids with computer simulations,[49–61] including the reproduction of a metallic phase for hydrogen[61] as predicted by Wigner and Huntington.[68]

In chapter 3 we presented a semiclassical equation of state valid for quantum fluids[60] based on the Statistical Associating Fluid Theory for potentials of variable range (SAFT-VR)[69] and a perturbation theory for quantum fluids;[43–46] this approach could give very good predictions of the liquid-vapor phases of hydrogen (H_2), deuterium (D_2), neon (Ne) and helium-4 (He). In this chapter, we review the application of effective potentials in computer simulations of quantum fluids, and we address the effect of confinement studying the quantum corrections to a Lennard-Jones fluid contained between hard-parallel walls, that has been studied classically by Liu *et al.*[70] using histogram-reweighting grand canonical Monte Carlo simulations. The information obtained is a previous step in the development of a molecular-based equation of state for confined hydrogen, based on the SAFT-VR extensions to confined[71–73] and quantum fluids.[60]

4.2 Mathematical Model

We consider a system of N particles interacting via a semiclassical pair potential V_{eff} that consists in a pair potential $V(r)$ with a quantum correction $V_Q(r)$,

$$V_{\text{eff}}(r) = V(r) + V_Q(r) \tag{4.1}$$

In this work $V(r)$ is given by the Lennard-Jones potential (LJ),

$$V_{LJ}(r) = 4\epsilon \left[\left(\frac{\sigma}{r}\right)^{12} - \left(\frac{\sigma}{r}\right)^{6} \right] \tag{4.2}$$

where r is the relative distance between particles, σ is a characteristic length parameter defined by $V_{LJ}(\sigma) = 0$ and ϵ is the depth of the attractive well. Although Eq.(4.1) can be applied to other potential models besides the LJ interaction, there is an extensive list of studies performed with this potential that allowed us to compare our results. The standard theory for V_Q is the Wigner-Kirkwood potential,[29–32] that at first-order in β is given by

$$V_Q(r) = D\nabla^2 V_{LJ}(r) = \frac{4\epsilon D}{\sigma^2} \left[11 \cdot 12 \left(\frac{\sigma}{r}\right)^{14} - 5 \cdot 6 \left(\frac{\sigma}{r}\right)^{8} \right], \tag{4.3}$$

where $D = \lambda_B^2/24\pi$; we will refer to Eq.(4.3) as the WK-1 model. Eq.(4.3) agrees with the first-order expressions for V_Q from Feynman-Hibbs,[62] Bohm's[60] and Jaen-Khan theories.[36]

In order to assess the effect of considering a second order contribution in β in V_Q to describe the low temperature regime, we studied the WK-2 and Jaen-Khan potentials (JK), finding that WK-2 gives non-physical results and, consequently, restricting our study to the the JK model, given by

$$\begin{aligned} V_Q(r) &= D\nabla^2 V_{LJ}(r) + \frac{9}{10} D^2 \nabla^2 \nabla^2 V_{LJ}(r) \\ &= -\frac{9}{10} 4\epsilon \left(\frac{D}{\sigma^2}\right)^2 \left[11 \cdot 12 \cdot 13 \cdot 14 \left(\frac{\sigma}{r}\right)^{16} - 5 \cdot 6 \cdot 7 \cdot 8 \left(\frac{\sigma}{r}\right)^{10} \right], \end{aligned} \tag{4.4}$$

The Eq. (4.2)-(4.4) provides physical and realistic information about the mechanism that leads to the phase separation of matter.

4.2.1 Bulk phases

The Gibbs Ensemble Monte Carlo method (GEMC)[66,67] was used to simulate the vapor-liquid phase equilibrium of quantum fluids. Results were obtained for $N = 1000$ particles uniformly distributed in a cubic simulation cell divided into two boxes of equal volumes $N = N_1 + N_2 = 1000$. A random distribution of particles was set up as initial configuration in both boxes, and periodic boundary conditions (PBC) were used during the simulations. Standard GEMC particles movements were considered: displacements of particles within each box, trial changes of volumes and trial interchanges of particles between the two boxes. The total number of particles N and the total volume $V = V_1 + V_2$ were fixed constant whereas the volumes $V_{1,2}$ and the number of particles $N_{1,2}$ per box were varied during the simulations. The number of cycles used to reach equilibrium and for averaging was 1-2x10^7 cycles in each case, where a cycle was defined by 90 attempts of displacements of particles, 900 attempts of volume changes and 1 attempt of interchange of particles. Maximum displacement and maximum volume changes were adjusted to give 30-40% and approximately 50% of accepted moves for subsystem, respectively. We used the random walk method developed by Frenkel and Smit[65] to generate a new configuration in the volume step. Finally, particles interchange between the boxes were adjusted to 9-11% of the number of particles interchanged per cycle. The mean numbers of particles N_1 and N_2, volumes V_1, V_2, and energies for the two coexisting phases were obtained as configurational averages over the accumulated stage of the simulation. The errors in the average properties of interest were estimated by calculating the standard deviations. For the estimation of the critical point, we used a scaling law and the rectilinear diameters recipe[74] as a first estimate for the Wegner expansion, i.e, the critical parameters ρ_c and T_c are given by

$$\rho_{\pm} = \rho_c + C_2|t| \pm \frac{1}{2}B_o|t|^{\beta} \tag{4.5}$$

where ρ_- and ρ_+ denote the vapor and liquid densities, respectively, and $t = 1-T/T_c$. This expression allowed us to fit the coexistence data and to obtain estimates for ρ_c, T_c, β and the amplitude terms C_2 and B_o. We used the apparent critical exponent obtained in this way in order to describe the overall shape of the coexistence curves. The critical constants were estimated by fitting the GEMC data to Eq. (4.5), using a non-linear squares procedure.[75] Simulations were performed with a cut-off radius r_c for the total potential and a tail contribution U^{tail} was used to correct the systematic

error induced by the truncation,[65]

$$\frac{U^{tail}}{N\rho} = \frac{1}{2}\int_{r_c}^{\infty} V_{LJ}(r)\, 4\pi r^2 dr + \frac{D}{2}\int_{r_c}^{\infty} \nabla^2 V_{LJ}(r)\, 4\pi r^2 dr \tag{4.6}$$

where ρ is the average number density. We have truncated the pair potential at cut-off ratios 2.5σ and 4σ. We found that the size and cut-off effects are less than 1%.

4.2.2 Confined phases

Liu *et al.*[70] presented the phase behavior of a classical LJ fluid confined between parallel hard walls, using histogram-reweighting grand canonical Monte Carlo simulations. In order to study the modification that quantum effects introduce with respect to a classical system, we selected the same model. The canonical ensemble method[76,77] was applied for a WK-1 fluid with a particle-wall interaction given by

$$u(r) = \begin{cases} \infty & \text{if} \quad z < \sigma/2 \\ 0 & \text{if} \quad \sigma/2 \leq z \end{cases} \tag{4.7}$$

where z is the distance between the fluid particles and the wall, and periodic boundary conditions were applied in the x and y coordinates. The effective quantum potential was truncated at $r_c = 2.5\sigma$ and no long-tail corrections were considered.

In order to perform computer simulations with this method, we followed the same procedures and technical details described in our previous studies with classical discontinuous potential systems.[78,79] The simulation box consisted of a rectangular parallelepiped with fixed lengths $L_y \geq 10\sigma$, $L_x = 10L_y$ and $2\sigma \leq L_p \leq 6\sigma$, where L_p is the wall separation. The density of the system is defined by $\rho^* = N\sigma^3/V$, where N is the total number of particles and V is the total volume of the confined system defined by $V = L_x L_y L_p$. We selected $L_z = L_p$ as the distance between the hard walls. A dense phase formed by $N = 1372$ with an initial random distribution was placed at the center of the rectangular parallelepiped, obtaining two vapor phases with a liquid phase in between. The acceptance ratio of particle's displacement was fixed to 40%.

The equilibration process consisted of 1-8x10^7 MC cycles and 1-8x10^7 cycles for accumulated averages. The density profile, $\rho^*(x)$, was obtained every two cycles, using the data values corresponding to $0 < x < L_x/2$, since the profile is symmetrical

in the x coordinate. The LV coexistence densities were obtained as a function of the x coordinate of the simulation box, and parametrized using an hyperbolic tangent function,[80]

$$\rho^*(x) = \frac{1}{2}(\rho_L^* + \rho_V^*) - \frac{1}{2}(\rho_L^* - \rho_V^*)\tanh\left(\frac{x - x_o}{d}\right) \tag{4.8}$$

where ρ_L^* and ρ_V^* are the bulk densities corresponding to the liquid and vapor phase, respectively, d is the interface width and x_o is the position in the transition layer.

4.3 Results

4.3.1 Bulk phases

The semiclassical effective potentials WK-1 and JK for hydrogen (H_2) are depicted in Fig. 4-1, using $\Lambda = 1.7378$ as reported by Kim *et al.*,[33] and for temperatures $T^* = kT/\epsilon = 0.1, 0.6, 1.0, 5.0$. Due to the semiclassical approximation used along this work, no nuclear spin effects are taken into account and there is not a distinction between the hydrogen isomers (orthohydrogen and parahydrogen) and we can assume that the description obtained corresponds to a mixture of these isomers.

As expected, the effect of V_Q is more important at low temperatures and the potentials have strong variations between them. These differences reduce as temperature is increased, although quantum effects are still observed at $T^* = 5$. In all the cases, the net effect of V_Q is to increase the effective size of the particles with respect to the Lennard-Jones fluid parameter σ. We found that the JK model overestimates the effective size of the particles due to the second-order correction term.

The quantum parameter Λ modifies the scaling behavior of the LJ potential, as observed in Fig. 4-1, since there is not a universal potential written as a function of r/σ and u/ϵ as in the case of V_{LJ}, i.e., the WK-1 system does not follow a corresponding states behavior. This non-conformal property has as major effect that the phase diagram is modified by varying Λ, in similar way to what happens with the range λ for a SW fluid; in Fig. 4-2, we present the WK-1 pair potentials at $T^* = 0.60$ for $\Lambda = 0.5991, 1.2249, 1.7378$, and 2.6783, that corresponds to the cases of neon (Ne), deuterium (D_2), hydrogen (H_2) and helium-4 (He), respectively.[33] The corresponding LV phase diagrams were obtained by the GEMC method; the case of the classical LJ fluid ($\Lambda = 0.0$) is also reported for comparison.

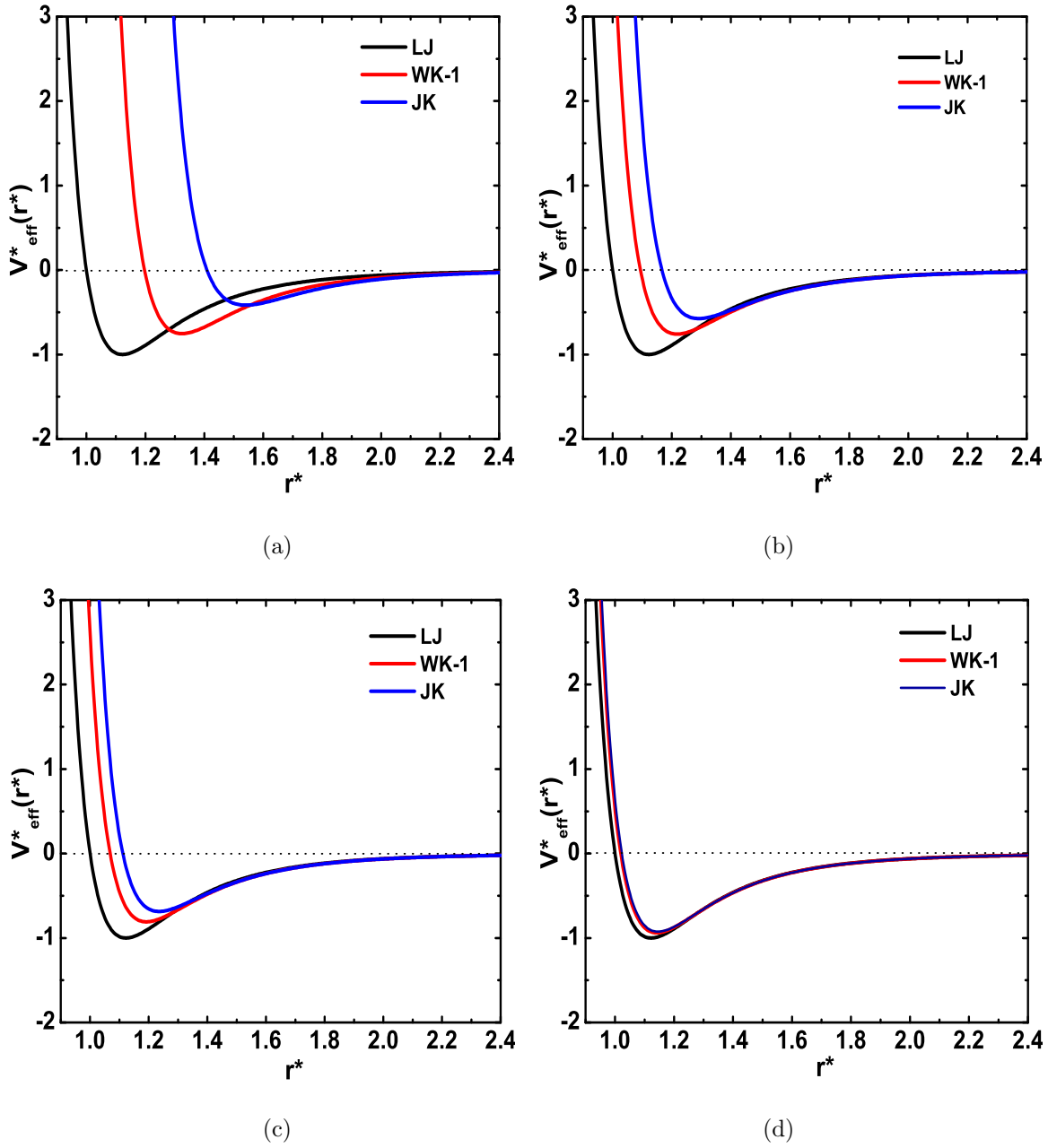

Figure 4-1: Comparison between pair potentials: Lennard-Jones (LJ), Wigner-Kirkwood (WK-1), and Jaen-Kahn (JK). The quantum systems were obtained for hydrogen ($\Lambda = 1.7378$ reported by Kim *et al.*,[33]) and temperatures a) $T^* = 0.10$, b) $T^* = 0.60$, c) $T^* = 1.0$ and d) $T^* = 5.0$. Each potential is given scaled by the LJ energy parameter, i. e., $V^*_{\text{eff}} = V_{\text{eff}}/\epsilon$.

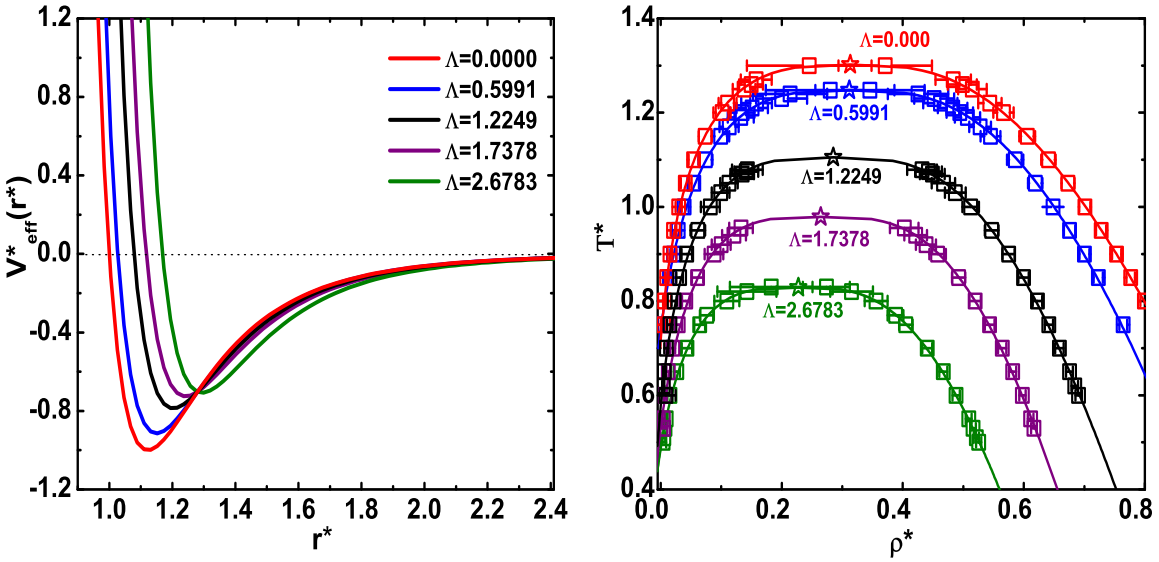

(a) (b)

Figure 4-2: (a) WK-1 pair potential, $V^*_{\rm eff} = V_{\rm eff}/\epsilon$, for hydrogen, deuterium, neon and helium-4 at $T^* = 0.60$. The LJ parameters σ and ϵ were taken from Kim *et al.*,[33] and given in Table 4.2. (b) GEMC LV coexistence curves for the previous WK-1 systems (squares), solid curves were obtained using Eq (4.5). The critical points obtained by a Wegner expansion,[74] as explained in the text, are denoted by stars.

The Λ dependence of the critical values of temperature and density, and the corresponding critical exponent, are given in Table 4.1. By increasing Λ, the critical temperature decreases.

Table 4.1: Critical temperature T^*_c, critical density ρ^*_c, and critical exponent β estimated from GEMC data for the WK-1 potential used in this work. Fitted values of Bo and C_2 are also given. The errors are estimated from the respective errors in the densities of the coexisting vapor and liquid phases. Results were obtained with a cut-off radius $r_c = 4\sigma$.

Λ	ρ^*_c	T^*_c	β	Bo	C_2
0.0000	0.3134±0.0008	1.3019±0.0002	0.3297±0.0026	1.0856±0.0045	0.2307±0.0036
0.5991	0.3118±0.0013	1.2478±0.0001	0.3220±0.0040	1.0220±0.0085	0.1741±0.0075
1.2249	0.2850±0.0008	1.1051±0.0020	0.2963±0.0060	0.8708±0.0055	0.1358±0.0031
1.7378	0.2645±0.0011	0.9787±0.0026	0.2895±0.0079	0.7757±0.0064	0.0979±0.0038
2.6783	0.2273±0.0006	0.8289±0.0001	0.3048±0.0024	0.6957±0.0028	0.0929±0.0026

Table 4.2: Optimized GEMC parameters for hydrogen (H_2), deuterium (D_2), neon (Ne), and helium-4 (He) fluids obtained by fitting to LV coexistence experimental data. The Lennard-Jones parameters are σ and ϵ, obtained from Kim *et al.*,[33] and de Boer's quantumness parameter is $\Lambda = h/\sigma\sqrt{m\epsilon}$.

Substance	LJ parameters[33]			GEMC parameters		
	$(\epsilon/k)\,/K$	$\sigma/$Å	Λ	$(\epsilon/k)\,/K$	$\sigma/$Å	Λ
Ne	37.10	2.670	0.5991	35.283	2.7661	0.5930
D_2	37.00	2.928	1.2249	34.118	3.0067	1.2417
H_2	37.00	2.928	1.7378	33.434	3.0450	1.7579
He	10.22	2.556	2.6783	6.3141	2.8927	3.0109

Table 4.3: Critical temperature T_c and critical density ρ_c estimated from GEMC data for the WK-1 fluid studied in this work. Experimental data (T_c^{exp} and ρ_c^{exp}) were taken from the NIST Chemistry WebBook.[81] Results were obtained with a cut-off radius $r_c = 4\sigma$.

Substance	ρ_c^{exp}/mol L^{-1}	ρ_c/mol L^{-1}	T_c^{exp}/K	T_c/K
Ne	23.882	24.465±0.0318	44.491	44.026±0.0035
D_2	17.327	17.412±0.0139	38.340	37.704±0.0682
H_2	15.508	15.557±0.0171	33.145	32.722±0.0869
He	17.399	15.594±0.0094	5.195	5.2338±0.0006

A comparison between the molecular parameters reported by Kim *et al.*,[33] and the parameters recalculated from the GEMC simulation data are given in Table 4.2. The optimal parameters were determined by fitting to experimental data of vapor pressure and vapor-liquid density for every system, obtained from the NIST Chemistry WebBook.[81]

A damped least-squares method[75] was used, based on previous work on the LV coexistence of asymmetric mixtures at high pressures.[82–84] The objective function required for this calculation was given by

$$f_{ob} = \sum_{i=1}^{M} \left(\frac{\rho_i^{V,cal} - \rho_i^{V,\mathrm{exp}}}{\rho_i^{V,\mathrm{exp}}} \right)^2 + \sum_{i=1}^{M} \left(\frac{\rho_i^{L,cal} - \rho_i^{L,\mathrm{exp}}}{\rho_i^{L,\mathrm{exp}}} \right)^2, \tag{4.9}$$

where M is the number of experimental data points, and ρ is the density. The superscripts *exp*, *cal*, L and V denote the experimental and calculated values, and

the liquid and vapor phases, respectively.

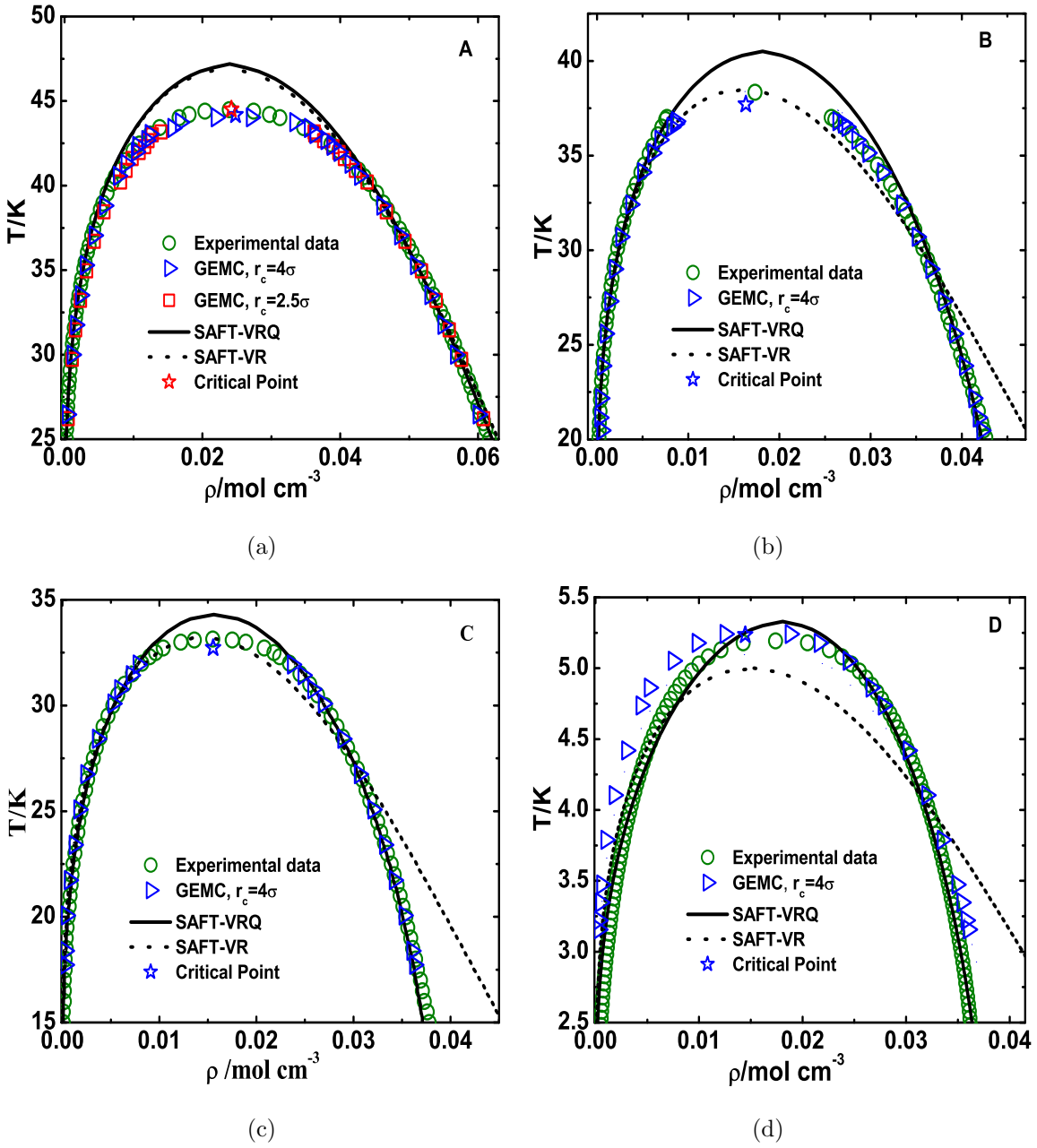

Figure 4-3: GEMC liquid-vapor coexistence of quantum fluids (triangles) compared to experimental data (circles),[81] using a cut-off radius $r_c = 4\sigma$ and $r_c = 2.5\sigma$. The critical points obtained by a Wegner expansion,[74] as explained in the text, are denoted by stars. The continuous and dotted lines corresponds to SAFT-VRQ and SAFT-VR results respectively. Results correspond to: a) neon, b) deuterium, c) hydrogen and d) helium, using the optimized molecular parameters reported in Table 4.2.

The values of the diameter (σ) and the energy parameter (ϵ/k) were optimized according to Eq. (4.9). As observed in Table 4.2, the GEMC diameter σ is greater than Kim *et al.* values,[33] whereas the energies ϵ have lower values.

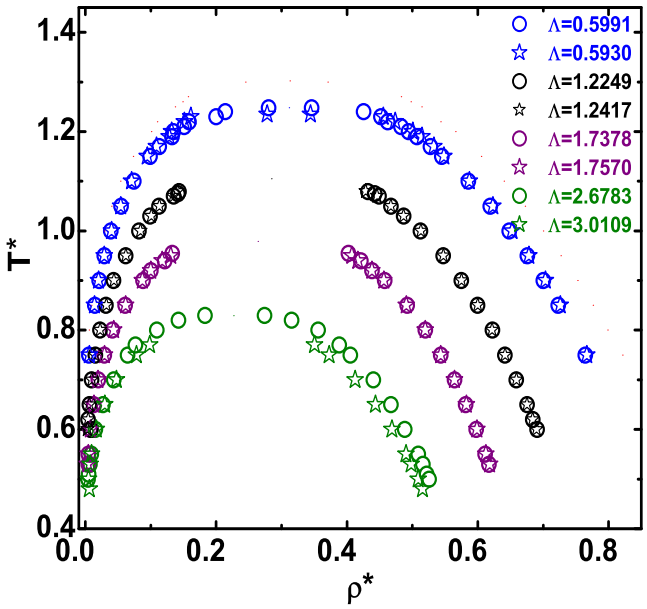

Figure 4-4: GEMC LV coexistence curves for optimized values of the LJ parameters σ and ϵ; circles and stars correspond to Λ values taken from Kim *et al.*,[33] and for the optimized LJ parameters, respectively.

The reparametrized GEMC LV equilibrium data is compared with the corresponding experimental values in Fig. 4-3. GEMC results were obtained using as a cut-off distance $r_c = 4\sigma$. For Ne, D_2 and H_2 we can observe that the GEMC and experimental data are in very good agreement. For helium-4, the simulations results are moderately satisfactory, taking into account the range of the experimental data (2.5K - 5.3K), although we could expect a worse performance of a semiclassical approach in this case. The corresponding critical values for densities and temperatures for all the systems are given in Table 4.3. The JK system does not show a liquid-vapor coexistence, that can be explained in terms of the increase of the repulsive potential as observed in Fig. 4-1.

Notice that the GEMC fitted parameters values (σ,ϵ) modifies the parameter Λ originally calculated with the values reported in ref. [33]. In order to assure a consistent set of molecular parameters (σ, ϵ, Λ), an iterative procedure can be used

to improve the representation of the experimental data, that consists in repeating the GEMC simulations using the recalculated Λ parameter, and then to obtain σ and ϵ by the same fitting procedure used before. The procedure is repeated until a convergence criteria for the determination of Λ is satisfied. We found that this method converges very fast after two iterations; the results for the convergence are presented in Fig. 4-4.

A robust version of SAFT-VR for Mie potentials has recently been developed,[85] being the LJ interaction a particular case. This new approach, which has given very accurate predictions for a wide range of substances, can be extended to quantum fluids using the method presented in Ref. [60], and specific equations of state could be obtained for the WK-1 potentials studied here.

4.3.2 Confined phases

A first step in the computer simulation of confined quantum fluids consisted in the study of the classical fluid with $\Lambda = 0$. The bulk phase was obtained using the NVT ensemble for 1372 and 2048 particles with a cut-off radius $r_c = 2.5\sigma$, contained into a cell box with dimensions $L_y = L_z = 13.41\sigma$ and $L_x = 39.81\sigma$. Density profiles for the LV coexistence for temperatures $T^* = 0.70$ and $T^* = 0.92$ are presented in Fig. 4-5(a). A clear formation of two phases can be observed. To confirm these predictions, results were also obtained using the GEMC method with $N = 1000$ particles and a cut-off radius $r_c = 2.5\sigma$, without long tail-corrections. Results obtained from both methods are summarized in Table 4.4, where we observe that are in very good agreement.

Table 4.4: Liquid-Vapor coexistence densities ρ_L^* and ρ_V^* at temperatures $T^* = 0.70$ and $T^* = 0.92$ obtained from computer simulation for the WK-1 fluid with a cut-off radius $r_c = 2.5\sigma$.

T^*	Method	ρ_L^*	ρ_V^*	N	Reference
0.70	NVT-MC	0.812288	0.00284807	1372	This work
0.70	NVT-MC	0.813583	0.00263298	2048	This work
0.70	GEMC	0.815991	0.00390470	1000	This work
0.70	NVT-MC	0.812000	0.00290000	2048	Trokhymchuk *et al.*,[77]
0.92	NVT-MC	0.700541	0.03094120	1372	This work
0.92	NVT-MC	0.701654	0.02815890	2048	This work
0.92	GEMC	0.703820	0.02936230	1000	This work
0.92	NVT-MC	0.706500	0.02940000	1000	Trokhymchuk *et al.*,[77]

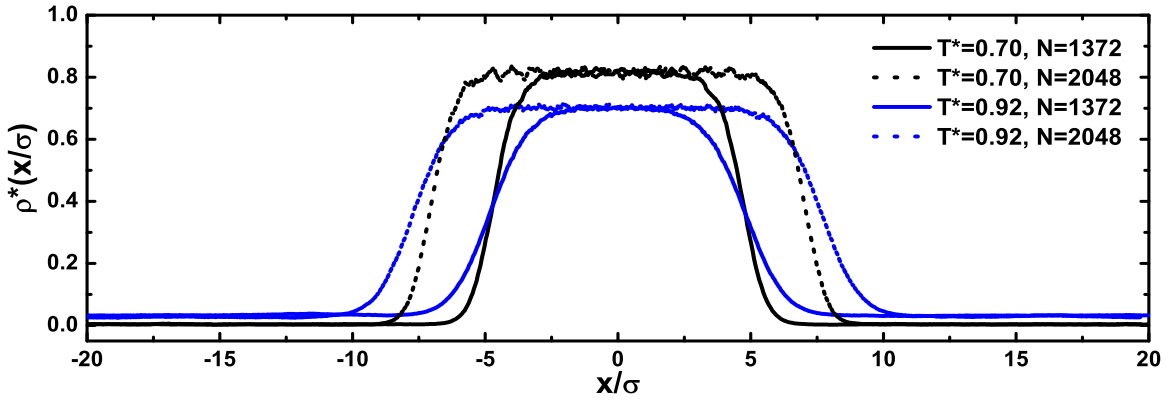

(a)

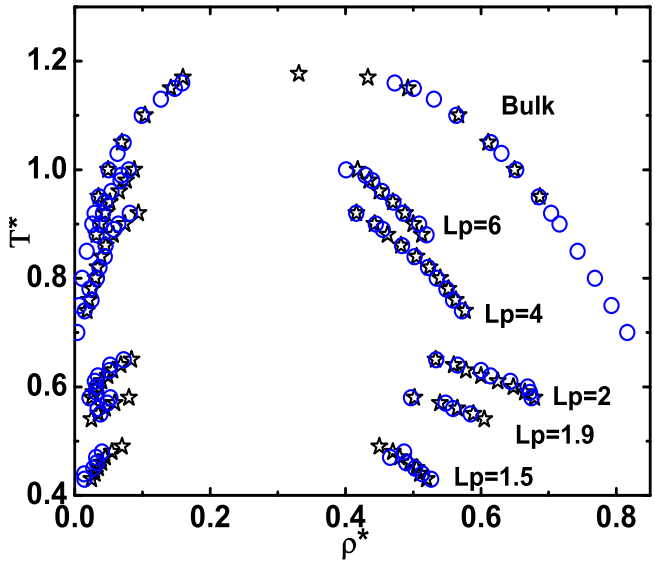

(b)

Figure 4-5: (a) Density profiles for a LJ fluid obtained by NVT-MC simulations, for temperature and density $T^* = 0.70$ and $\rho^* = 0.92$, respectively. Two sets of results are shown corresponding to simulations using different number of particles ($N = 1372$ and $N = 2048$), and a cut-off radius $r_c = 2.5\sigma$ without tail corrections. (b) LV coexistence curves obtained for bulk and confined LJ fluids w ith $L_p/\sigma = 1.5, 1.9, 2, 4, 6$ (circles) compared with results reported in ref. [70] (stars). Results were obtained with a cut-off radius $r_c = 2.5\sigma$, $N = 1372$ particles and without tail corrections.

The LV phase diagram is presented in Fig. 4-5(b) where the case corresponding to the bulk system was simulated with GEMC and the confined diagrams at different values of wall separations L_p were calculated with NVT-MC. The confined systems were obtained for five different wall separations, $L_p/\sigma = 1.5, 1.9, 2, 4, 6$.

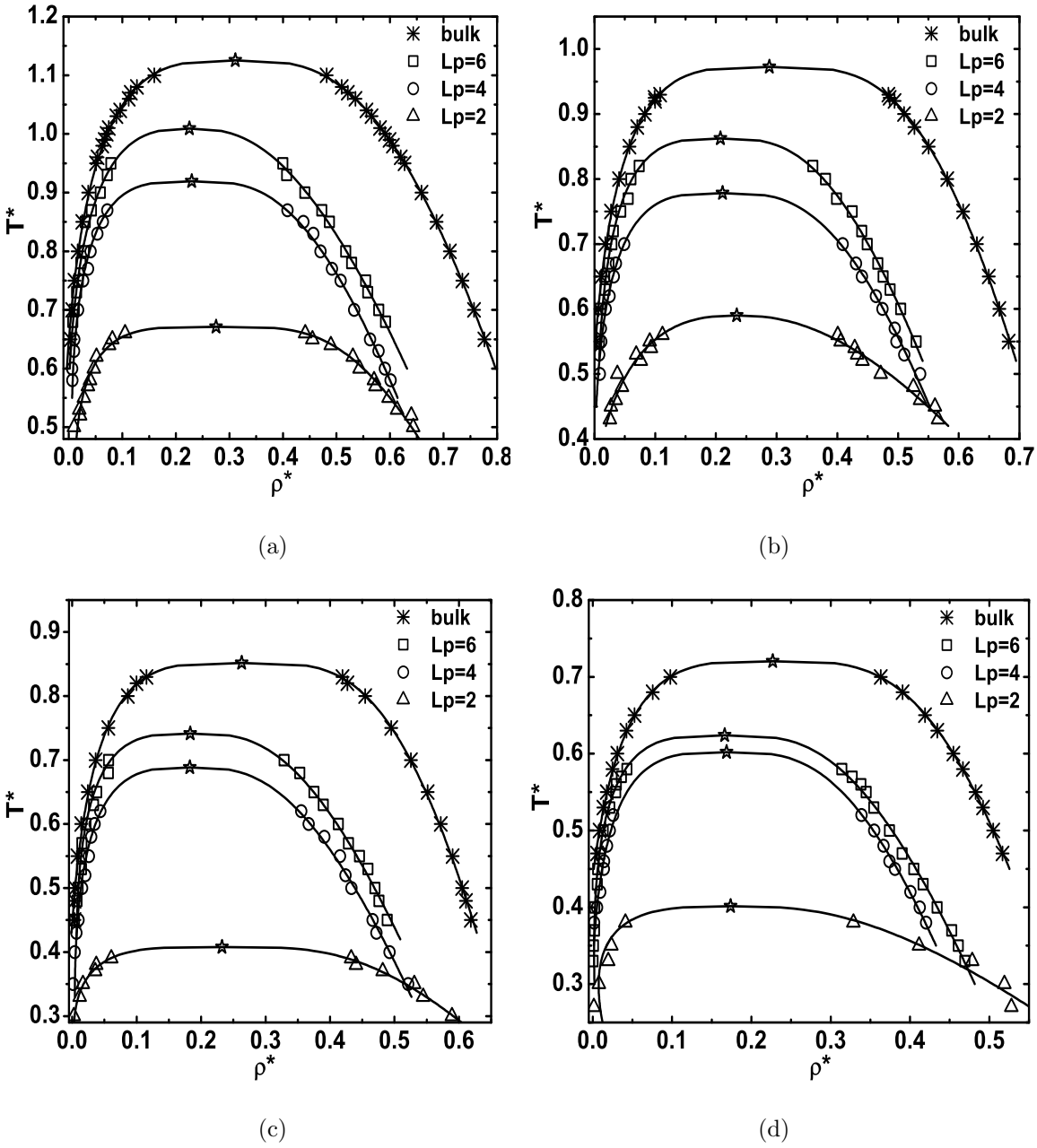

Figure 4-6: LV coexistence of confined WK-1 fluids obtained with the NVT-MC method, using a cut-off radius $r_c = 2.5\sigma$, $N = 1372$ particles and without tail corrections. Results correspond to (a) neon, (b) deuterium, (c) hydrogen and (d) helium-4, using the LJ parameters reported by Kim *et al.*[33] Three wall separations were considered, $L_p/\sigma = 2, 4, 6$, and GEMC results for the bulk system are also included. Solid curves were obtained using Eq (4.5), with an estimation of the critical points denoted by stars, using the Wegner expansion.[74]

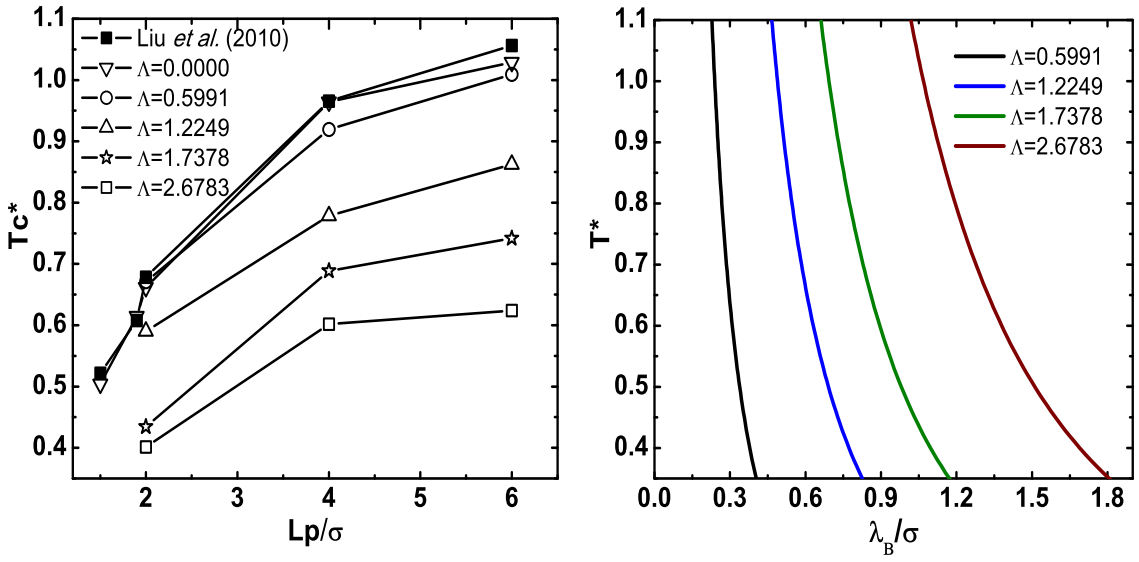

(a) (b)

Figure 4-7: (a) Critical temperature T_c^* as a function of the wall separation L_p for confined WK-1 fluids. Results correspond to neon, deuterium, hydrogen and helium-4, using the LJ parameters reported in .[33] Three wall separations were considered, $L_p/\sigma = 2, 4, 6$. Results for the classical LJ system are included, obtained in this work and from Liu *et al.*[70] (b) Thermal de Broglie wavelength as a function of temperature for the systems considered in (a).

Very good agreement was found between the results obtained here with the data reported by Liu *et al.*,[70] even for $L_p < 2$. However, it is important to bear in mind that the method followed by these authors consisted in histogram-reweighting grand canonical MC simulations, which is more appropiate for the detailed study of the critical region.

The LV coexistence curves for WK-1 fluids under confinement were obtained for three wall separations $L_p/\sigma = 2, 4, 6$, see Fig. 4-6. Results correspond to (a) neon, (b) deuterium, (c) hydrogen and (d) helium-4. The phase diagrams are modified in similar way by reducing L_p or increasing Λ, i.e., confinement and quantumness tend to reduce the LV phase region.

The trend of the critical temperature T_c versus the wall separation L_p is shown in Fig. 4-7(a), and compared with the classical behavior obtained by Liu *et al.*[70] Since the LV coexistence could be preempted by a solid phase, it is clear that the determination of the triple point is necessary in order to have a proper determination of the phase diagram; however, we can conclude that the introduction of quantum

effects substantially modifies the phase diagram of a confined fluid with a Λ value of a typical substance like H_2. On the other hand, the de Broglie wavelengths for all the substances reported here are of the same order of magnitude than the confinement distance L_p, as observed in Fig. 4-7(b). This is a clear indication that the presence of a liquid phase for a confined fluid requires the introduction of the quantum potential in order to describe its properties when $L_p < 6\sigma$, since quantum diffraction becomes very relevant.

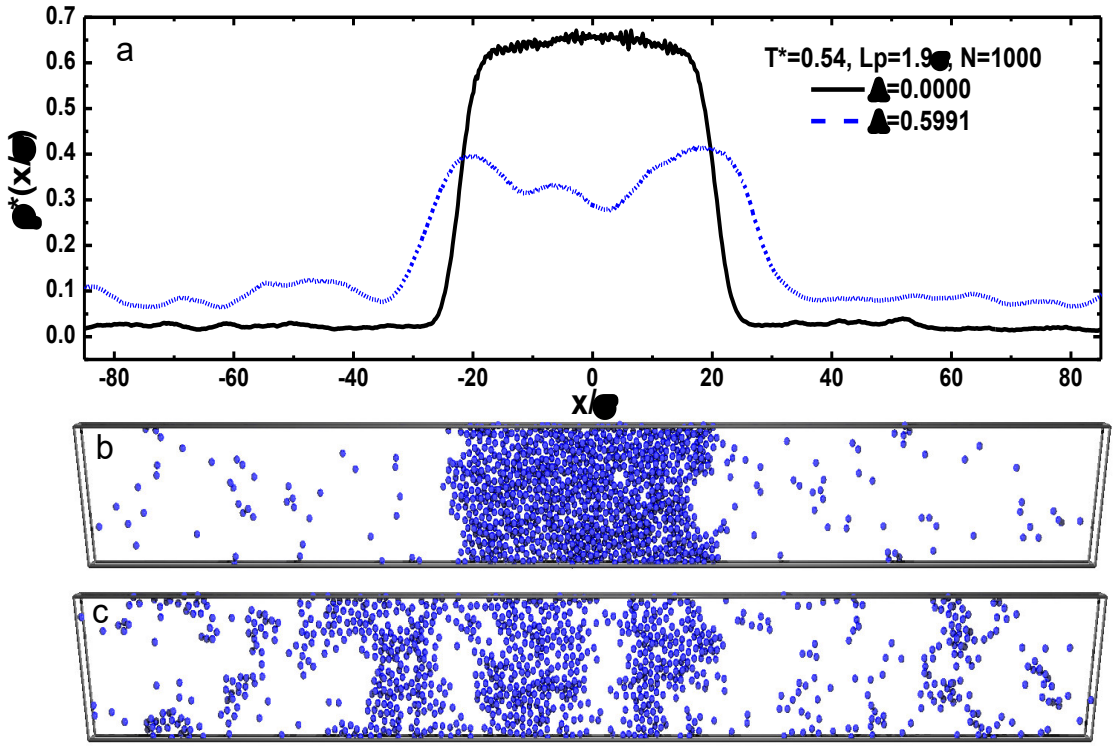

Figure 4-8: (a) Comparison between density profiles of confined LJ and WK-1 systems (black and blue lines, respectively), obtained by NVT-MC simulations with 1000 particles for temperature $T^* = 0.54$ and $L_p/\sigma = 1.9$. (b) and (c) are the corresponding snapshots of configurations for both systems.

For $L_p/\sigma < 2$ we found that the density profiles have strong variations not observed in the classical system. In Fig. 4-8(a) we present a comparison of the density profiles observed for the LJ and WK-1 systems, for $\Lambda = 0.5991$, $T^* = 0.54$ and $L_p/\sigma = 1.9$, as well as the corresponding snapshots of configurations in Figs. 4-8(b) and 4-8(c) for the LJ and WK-1 systems, respectively. Whereas the classical system

clearly shows a liquid-vapor transition, the quantum system presents a modulated phase with the presence of voids, similar to the phases observed for 2D disks systems.[86,87] The trend observed for the classical LJ fluid is that just for $L_p = 2\sigma$ there is evidence of a 3D-2D crossover in the behavior of the critical temperature T_c^*.[70] Although in the quantum case was not possible to determine T_c^* when $L_p/\sigma < 2$, the similarity between phases with 2D-systems suggest a dimensional crossover although the liquid-vapor transition could be already lost.

Semiclassical expressions for a effective radial distribution $g_{\text{eff}}(r)$ were obtained by Jaen and Khan, using the statistical density matrix Δ. The effective radial distribution function $g_{\text{eff}}(r)$, were obtained as a power expansion on D:

$$g_{\text{eff}}(r) = g^c(r) + D\nabla^2 g^c(r) + \frac{1}{2}D^2\nabla^2\nabla^2 g^c(r) \tag{4.10}$$

The Eq. (4.10) is a powerful tool in the calculation of the radial distribution function when analytical expressions for $g^c(r)$ are available. Other suitable way to obtain the radial distribution function is usually by calculating the distance between all particle pairs and binning them into a histogram. Given the interaction pair potential, the radial distribution function can be computed via computer Monte Carlo simulation method.

In this work, we obtain the effective radial distribution function and the energy profiles using the Wigner-Kirkwood potential[29–32] WK-1 model. The JK approximation for the quantum radial distribution function were not taking into account in this work. In the case of the semiclassical approximation the radial distribution functions were obtained by using Monte Carlo simulation in the canonical NVT ensemble for a system of $N = 1000$ particles and a cut-off radius $r_c = 4.0\sigma$, without long tail-corrections. The semiclassical effective potential WK-1 were used in the both cases, radial distribution function and energy profiles. On the other hand, quantum simulations using path integrals were developed using a system of $N = 125$ particules interacting via LJ pair potential given by the Eq. (4.2).

A comparison between semiclassical approximation (using WK-1 pair potential system) and quantum approximation (using path integrals) for the radial distribution function and internal energy are shown in Figs. (4-9)-(4-10), respectively. Results correspond to neon, deuterium, hydrogen and helium-4 using the LJ parameters reported in ref. [33].

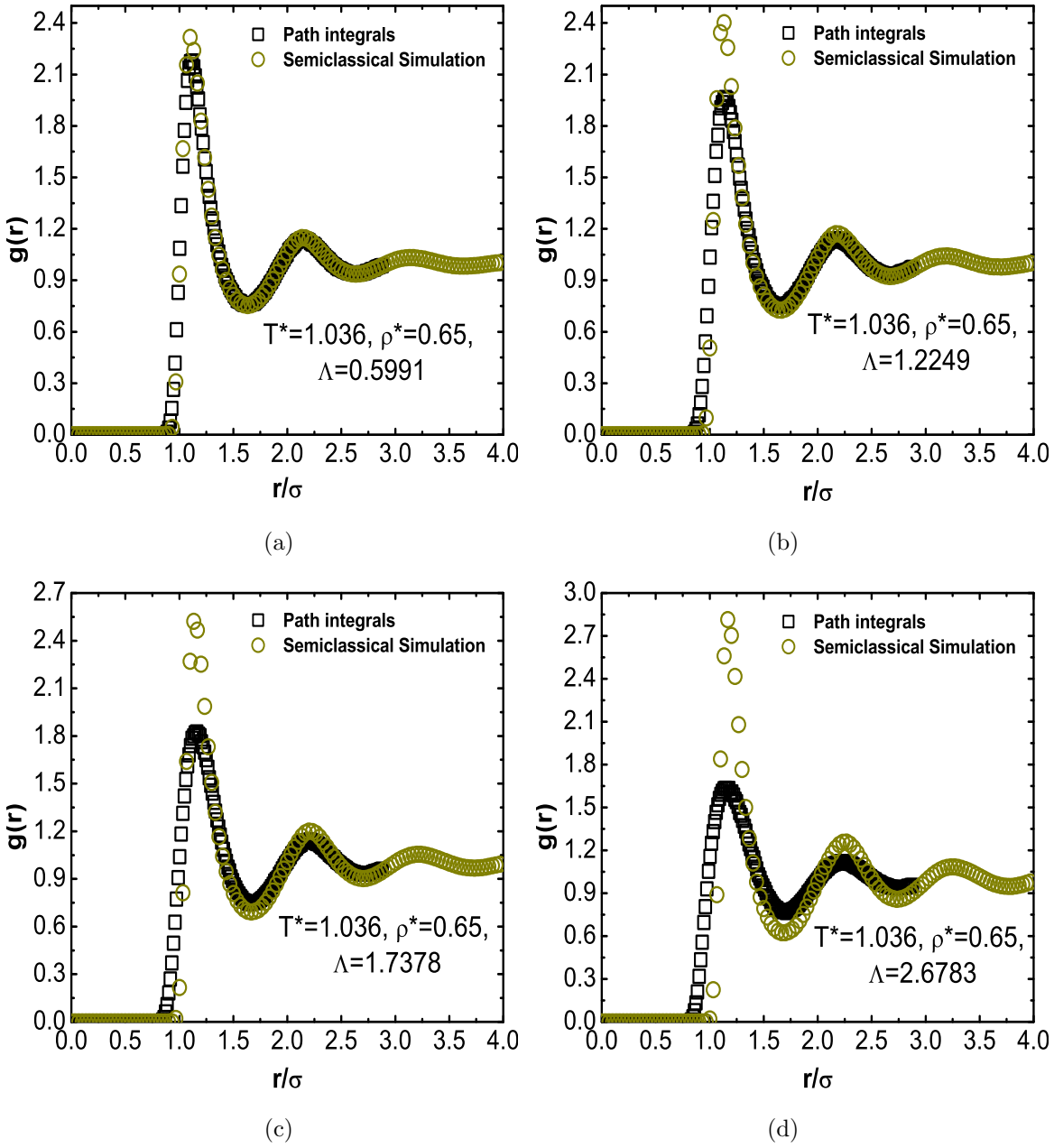

Figure 4-9: Predictions for the radial distribution function $g(r)$, for a system of particles interacting via: a) semiclassical aproximation using a WK-1 pair potential. b) quantum aproximation using path-integrals.[88,89] Results correspond to (a) neon, (b) deuterium, (c) hydrogen and (d) helium-4, using the LJ parameters reported by Kim *et al.*[33] The simulations were obtained at temperature $T^* = kT/\epsilon = 1.036$ and density $\rho^* = \rho\sigma^3 = 0.65$.

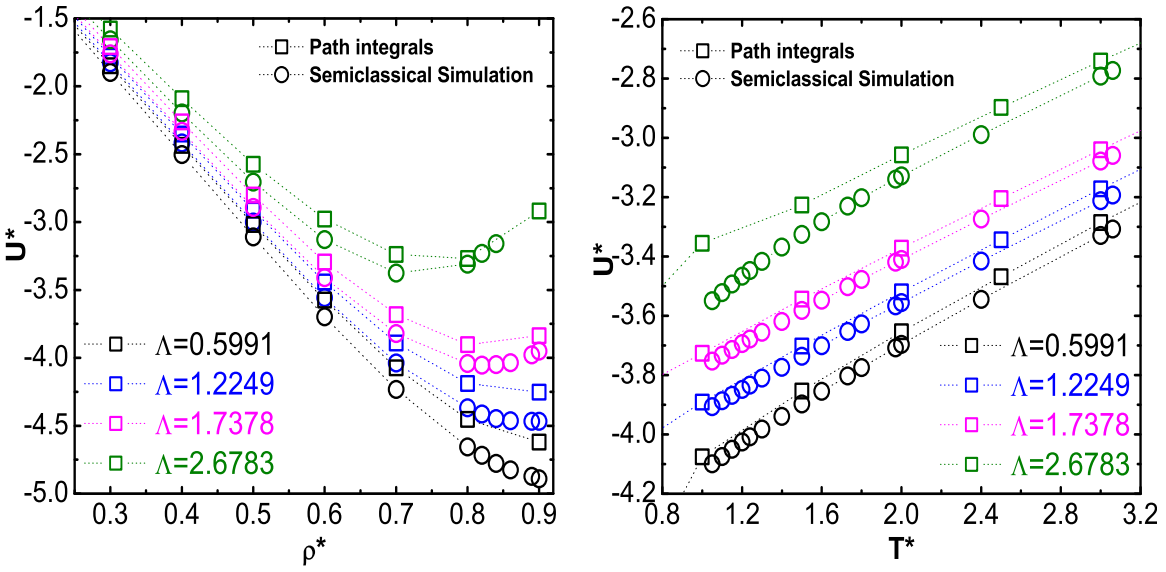

Figure 4-10: Predictions for the internal energy $U^* = U/N\epsilon$, for a system of particles interacting via: a) semiclassical aproximation using a WK-1 pair potential b) quantum aproximation using path-integrals.[88,89] Results correspond to (a) temperature constant $T^* = 2.0$, (b) density constant $\rho^* = 0.60$.

As can be observed in Fig. 4-9 when the de Boer's parameter increase, the first peak of the radial distribution function using the semiclassical approximation, increased significantly compared with the path integrals results. At low values of the Boer's parameter (*i.e.* Neon), the concordance between the semiclassical approximation and path integrals is remarkable. In the case of neon, deuterium and hydrogen the results are very close between the two approximations when $r/\sigma > 1.5$, *i.e.* after the value of the second peak in the $g(r)$.

In Fig. 4-10 the reduced internal energy $U^* = U/N\epsilon$, as a function of the density $\rho^* = \rho\sigma^3$, and the reduced temperature $T^* = kT/\epsilon$, for the WK-1 pair potential are given. Semiclassical approximation is compared with path-integrals[88,89] for several values of the the Boer's quantumness parameter, that measure the strength of the quantum contribution. From Fig. 4-10(a), it is clear that semiclassical and quantum approximations are identical at low densities; the behavior differs considerably at densities nearly to 0.9, when the quantum effects becomes to be remarkable. Finally, internal reduced energy profiles as a funtion of the reduced temperature at density constant of $\rho^* = 0.60$, are presented in Fig. 4-10(b). Here the concordance between

the semiclassical and path integrals is not good in all temperature ranges.

Conclusions

We have presented semiclassical simulations for thermodynamic properties of quantum fluids using GEMC and NVT-MC methods, either for bulk or for a specific confinement geometry-parallel hard walls. Several effective potentials were considered, based on semiclassical approaches.[29,30,36] As a model system we considered molecules interacting via a Lennard-Jones pair potential complemented by a temperature-dependent quantum potential. This effective potential determines non-conformal properties to the fluid system. Very good agreement has been obtained for the prediction of bulk phases where experimental data is available, and a simple approach to obtain optimized parameters of the LJ potential from GEMC data has been provided. For the case of confined fluids, we have compared their LV phase diagram with respect to the classical model studied in ref. [70], and the effect of the reduction of the critical temperature by reducing L_p is now enhanced by increasing the quantumness of the system, measured by Λ. For $L_p/\sigma < 2$ the liquid-vapor transition seems to be lost, and this could be as a consequence of the preempting of a solid phase; however, a dimensionality crossover could be present as in the case of the classical LJ fluid, since the configurations observed have strong similarities with classical 2D-systems at low temperatures.

Although robust methods based on the path-integral formalism are well known, we have shown that an accurate description of the liquid and vapor phases can be obtained using semiclassical potentials. The information presented here is a valuable tool to be used in combination with thermodynamic theoretical approaches developed previously for classical confined fluids,[71–73] that require equations of state for three- and two-dimensional fluids, as well as a semiclassical version of the SAFT-VR approach.[60]

BIBLIOGRAPHY

[1] L. D. Gelb, K.E. Gubbins, R. Radhakrishnan, M. Sliwinska-Bartkowiak, *Rep.Prog.Phys.* **62**, 1573 (1999).

[2] O. Sinanoglu, K. S. Pitzer, *J. Chem. Phys.* **32**, 1279 (1960).

[3] F. A. Putnam, T. Fort, *J. Phys. Chem.* **81**, 2171 (1977).

[4] Bhethanabotla, W. Steele, *J. Phys. Chem.* **92**, 3285 (1988).

[5] F. del Río, A. Gil-Villegas, *J. Phys. Chem.* **95**, 787 (1991).

[6] J. Han, J. Fu, R. B. Schoch, *Lab Chip.* **8**, 23 (2008).

[7] J. J. Breenakker, V. D. Borman, S. Y. Krylov, *Chem. Phys. Lett.* **232**, 379 (1995).

[8] G. Garberoglio, M. M. Deklavon, J. K. Johnson, *J. Phys. Chem. B* **110**, 1733 (2006).

[9] Y.Wang, S.K. Bhatia, *J. Phys. Chem. C* **113**, 14953 (2009).

[10] J. Cai, Y. Xing, X. Zhao, *RSC Adv.* **2**, 8579 (2012).

[11] A. Gotzias, Th. Steriotis, *Mol. Phys.* **110**, 1179 (2012).

[12] D. Liu, W. Wang, J. Mi, C. Zhong, Q. Yang, D. Wu, *Ind. Eng. Chem. Res.* **51**, 434 (2012).

[13] J. Teufel, H. Oh, M. Hirscher, M. Wahiduzzaman, L. Zhechkov, A. Kuc, T. Heine, D. Denysenko, D. Volkmer, *Adv. Mater.* **25**, 635 (2013).

[14] P. Kowalczyk, P. A. Gauden, A. P. Terzyk, *J. Phys. Chem. B* **114**, 5047 (2010).

[15] K. Nasrifar, *Int. J. Hydrogen Energy* **35**, 3802 (2010).

[16] C. Honggang, Z. Jinyang, X. Ping, L. Lei, L. Yanlei, B. Haiyan,*Int. J. Hydrogen Energy* **35**, 3100 (2010).

[17] H. F. Wilson and B. Militzer, *Phys. Rev. Lett.* **104**, 121101 (2010).

[18] S. Xu, M. Jura, D. Koester, B. Klein, B. Zuckerman, *Ap. J.* **766**, L18 (2013).

[19] P. Dagaut, G. Dayma, *Int. J. Hydrogen Energy* **31**, 505 (2006).

[20] K. Otsuka, Y. Shigeta, S. Takenaka, *Int. J. Hydrogen Energy* **27**, 11 (2002).

[21] E. Ch. Vagia, A. A. Lemonidou, *Int. J. Hydrogen Energy* **32**, 212 (2007).

[22] V. A. Goltsov, T. N. Veziroglu, *Int. J. Hydrogen Energy* **26**, 909 (2001).

[23] J. Yang, A. Sudik, C. Wolverthon, D. J. Siegel, *Chem. Soc. Rev.* **39**, 656 (2010).

[24] V. Tozzini, V. Pellegrini, *Phys. Chem. Chem. Phys.* **15**, 80 (2013).

[25] M. Arndt, O. Nairz, J. Vos-Andreae, C. Keller, G. van der Zouw, A. Zeilinger, *Nature* **401**, 680 (1999)

[26] L. Hackermüller, S. Uttenthaler, K. Hornberger, E. Reiger, B. Brezger, A. Zeilinger, M. Arndt, *Phys. Rev. Lett.* **91**, 090408 (2003).

[27] S. Gerlich, S. Eibenberger, M. Tomandl, S. Nimmrichter, K. Hornberger, P. J. Fagan, J. Tüxen, M. Mayor, M. Arndt, *Nat. Commun.* **2:263** doi:10.1038/ncomms1263 (2011).

[28] L. Amico, R. Fazio, A. Osterloh, V. Vedral, *Rev. Mod. Phys.* **80**, 517 (2008).

[29] E.Wigner, *Phys. Rev.* **40**, 749 (1932).

[30] J. G. Kirkwood, *Phys. Rev.* **44**, 31 (1933).

[31] H. S. Green, *J. Chem. Phys.* **19**, 955 (1951).

[32] L. D. Landau and E. M. Lifschitz, *Statistical Physics,* Part 1, 3rd ed. (Butherworth-Heinemann, Oxford, 1980).

[33] S. Kim, D. Henderson, J. A. Barker, *Can. J. Phys.* **47**, 99 (1969).

[34] J.-P. Hansen and J.-J. Weis, *Phys. Rev.* **188**, 314 (1969).

[35] J. G. Powles and G. Rickayzen, *Mol. Phys.* **38**, 1875 (1979).

[36] J. K. Jaen, A. Khan, *J. Chem. Phys.* **46**, 260 (1967).

[37] M. A. Hooper, S. Nordholm, *Aust. J. Chem.* **33**, 2029 (1980).

[38] R. J. Sadus, *J. Phys. Chem.* **96**, 3855 (1992).

[39] B. Jancovici, *Phys. Rev.* **178**, 178 (1969).

[40] W. G. Gibson, *Phys.Rev. A* **11**, 270 (1975).

[41] M. E. Boyd, S. Y. Larsen, J. E. Kilpatrick, *J. Chem. Phys.* **50**, 4034 (1969).

[42] E. J. Derderian, W. A. Steele, *J. Chem. Phys.* **55**, 5795 (1971).

[43] Y. Singh, *Mol. Phys.* **27**, 1687 (1974).

[44] B. P. Singh, S. K. Sinha, *J. Chem. Phys.* **67**, 3645 (1977).

[45] B. P. Singh, S. K. Sinha, *J. Chem. Phys.* **68**, 562 (1978).

[46] N. Singh, S. K. Sinha, *J. Chem. Phys.* **69**, 2709 (1978).

[47] B.-J. Yoon, H. A. Scheraga, *J. Chem. Phys.* **88**, 3923 (1988).

[48] T. J. Sheldon, B. Giner, C. S. Adjiman, A. Galindo, G. Jackson, D. Jacquemin, V. Wathelet, E. A. Perpète, *Comp. Aid. Chem. Eng.* **22**, 143 (2006).

[49] J. A. Barker, *J. Chem. Phys.* **70**, 2914 (1979).

[50] D. Thirumalai, R. W. Hall, and B. J. Berne, *J. Chem. Phys.* **81**, 2523 (1984).

[51] L. M. Sesé, R. Ledesma, *J. Chem. Phys.* **102**, 3776 (1995).

[52] L. M. Sesé,*Mol. Phys.* **85**, 931 (1995).

[53] Q. Wang, J.K. Johnson, J.Q. Broughton *Mol. Phys.* **89**, 1105 (1996).

[54] Q. Wang, J.K. Johnson, J.Q. Broughton *J. Chem. Phys.* **107**, 5108 (1997).

[55] Q. Wang, J. K. Johnson, *Fluid Phase Equil.* **132**, 93 (1997).

[56] Q. Wang, J.K. Johnson, *Mol. Phys.* **95**, 299 (1998).

[57] L. M. Sesé, R. L. E. Bailey, *J. Chem. Phys.* **119**, 10256 (2003).

[58] X-Z. Li, B. Walker, A. Michaelides, *PNAS* **108**, 6369 (2011).

[59] E. G. Noya, L. M. Sesé, R. Ramírez, C. McBride, M. M. Conde, C. Vega, *Mol. Phys.* **109**, 149 (2011).

[60] V. M. Trejos, A. Gil-Villegas, *J. Chem. Phys.* **136**, 184506 (2012).

[61] J. Chen, X.-Z. Li, W. Zhang, M. Probert, C. Pickard, R. Needs, A. Michaelides, E. Wang, *Nat. Commun.* **4**, 2064 (2013).

[62] R. P. Feynman, *Statistical Mechanics* (Benjamin, New York, 1972).

[63] K.E. Gubbins, *Rev. Inst. Fr. Pet.* **51**, 59 (1996).

[64] D. Frenkel, in M. Meyer and V. Pontikis, *Computer Simulation in Materials Science* (Kluwer, Dordrecht, 1991).

[65] D. Frenkel and B. Smit, *Understanding Molecular Simulation: From Algorithms to Applications,* 2nd ed. (Academic, New York, 2002).

[66] A. Z. Panagiotopoulos, *Mol. Phys.* **61**, 813 (1987).

[67] A. Z. Panagiotopoulos, N. Quirke, M. Stapleton, and D. J. Tildesley, *Mol. Phys.* **63**, 527 (1988).

[68] E. Wigner, H. B. Huntington,*J. Chem. Phys.* **3**, 764 (1935).

[69] A. Gil-Villegas, A. Galindo, P. J. Whitehead, S. J. Mills, G. Jackson, A. N. Burgess, *J. Chem. Phys.* **106**, 4168 (1997).

[70] Y. Liu, A. Z. Panagiotopoulos, and P. Debenedetti, *J. Chem. Phys.* **132**, 144107 (2010).

[71] A. Martínez, M. Castro, C. McCabe, A. Gil-Villegas, *J. Chem. Phys.* **126**, 074707 (2007).

[72] G. Jiménez-Serratos, S. Santillán, C. Avendaño, M. Castro, A. Gil-Villegas, *Oil & Gas Sci. Tech.* **63**, 329 (2008).

[73] M. Castro, A. Martínez, A. Gil-Villegas, *AST* **29**, 59 (2011).

[74] F. Wegner, *Phys. Rev. B* **5**, 4529 (1972).

[75] W. H. Press, S. A. Teukolsky, W. T. Vetterling, B. P. Flannery, *Numerical Recipes: The Art of the Scientific Computing,* 3rd ed. (Cambridge University Press, New York, 2007).

[76] G. A. Chapela, S. E. Martínez-Casas and C. Varea, *J. Chem. Phys.* **86**, 5683 (1987).

[77] A. Trokhymchuk, J. Alejandre, *J. Chem. Phys.* **111**, 8510 (1999).

[78] M. G. Jiménez-Serratos, C. Vega, A. Gil-Villegas, *J. Chem. Phys.* **137**, 204104 (2012).

[79] M. G. Jiménez-Serratos, A. Gil-Villegas, C. Vega, F. J. Blas, *J. Chem. Phys.* **139**, 114901 (2013).

[80] J. W. Cahn and J. E. Hilliard, *J. Chem. Phys.* **28**, 258 (1958).

[81] See *webbook.nist.gov/chemistry/* for NIST Chemistry Webbook.

[82] J.A. López, V.M. Trejos, C.A. Cardona, *Fluid Phase Equil.* **248**, 147 (2006).

[83] J.A. López, V.M. Trejos, C.A. Cardona, *Fluid Phase Equil.* **275**, 1 (2009).

[84] V.M. Trejos, J.A. López, C.A. Cardona, *Fluid Phase Equil.* **293**, 1 (2010).

[85] T. Lafitte, A. Apostolakou, C. Avendaño, A. Galindo, C. S. Adjiman, E. Müller, G. Jackson *J. Chem. Phys.* **139**, 154504 (2013).

[86] S. Mejía-Rosales, A. Gil-Villegas, B. Ivlev, J. Ruíz-García, *J. Phys. Cond. Matt.* **14**, 4795 (2002).

[87] S. Mejía, A. Gil-Villegas, B. Ivlev y J. Ruíz-García, *J. Phys. Chem. B*, **110**, 22230 (2006).

[88] The path integral computer simulation results were taken from the study in development by Cesar Hernández Serna, Ph.D. thesis in process.

[89] C. Serna Hernández, V. M. Trejos, A. Gil-Villegas, *J. Chem. Phys. In process.*

CHAPTER 5

THEORETICAL MODELING OF ADSORPTION OF CLASSICAL AND QUANTUM FLUIDS

Adsorption of molecular hydrogen (H_2) onto graphene and other carbon-based substrates is currently a research area of interest, where molecular-based approaches are required to describe thermodynamic properties of this and other related systems. We present a semiclassical theoretical framework to model adsorption isotherms of quantum fluids such as H_2, based on the Statistical Associating Fluid Theory approach for classical and quantum bulk fluids (SAFT-VRQ), and its extension to describe adsorbed systems (SAFT-VR-2D). Although the application of the theory relies on the determination of eight molecular parameters, seven of them can be obtained from bulk thermodynamic properties, the ratio of the critical temperatures of the adsorbed and bulk phases, and theoretical estimations about the range of the surface-particles potential and the energy-depth of the particle-particle potential of the adsorbed fluid. The energy-depth of the surface-particle potential, ϵ_w, is the free molecular parameter that can be obtained by fitting to experimental data of adsorption isotherms. Results obtained for ϵ_w according to this procedure are consistent with experimental values of the isosteric heat and the prediction of adsorption isotherms is in very good agreement with experimental data.

This chapter is based on a paper: Víctor M. Trejos, Mario Becerra, Susana Figueroa-Gerstenmaier, and Alejandro Gil-Villegas, *Mol. Phys.*, 1, 1-9, (2014).

5.1 Introduction

Recently, the interest in green fuels as hydrogen is due to a number of factors such as security of supply issues, increased of global demand, oil price rises and concerns that world oil production is close to reaching a peak. Therefore, the benefits of using hydrogen as a fuel are strategic, arising from potential decreased reliance on oil, and environmental, due to a potential reduction in air pollution

For this century, hydrogen plays a major role as an energy resource with great potential to transform our economy.[1] One of the fundamental problems to solve is the suitable storage of hydrogen in cells, that requires a better understanding of the properties of quantum fluids under confinement.[2,3] Hydrogen and its isotopes, deuterium and tritium, are substances of small molecular weight, m, whose de Broglie's wavelength ($\lambda_B = h/\sqrt{2\pi mkT}$, where T and k are the temperature and Boltzmann's constants, respectively) has a magnitude comparable to the mean distance between particles. It is also possible that λ_B is comparable to a typical nanopore size and then to perform a process of separation between isotopes, known as quantum sieving.[4,5] Quantum sieving is a promising low-cost method for recycling fuel from a nuclear reaction and as cryogenic filters that separate mixture components via equilibrium condensation at low temperatures.[6]

Hydrogen storage methods currently under consideration include high pressure gas, liquid hydrogen, adsorption on porous materials at relatively low pressure, complex hydrides and hydrogen intercalation in metals. Nanoporous materials have been the focus of attention for solving the challenge of hydrogen storage in an efficient, cheap, and safe way. At the same time, the discovery of graphene has made possible to get advances in this area, and is one of the most intense areas of development in recent years. Among the most common materials considered to adsorb hydrogen are porous carbons, nanotubes, zeolites, porous polymers, and metal-organic frameworks.[7–9] Microporous carbons are, among all these possible choices, the most popular ones due their very high surface area, particularly microporous activated carbons, activated carbon fibers and carbon nanotubes. Unfortunately, both experimental data and theoretical predictions are, in general, not in a good agreement, and there is free room to improvements using statistical mechanics methods and molecular thermodynamic theories. For example, density functional theories (DFT) and molecular simulations are very successful methods in this direction, since they are able to pre-

dict adsorption isotherms and capillary condensation. A recent review devoted to present the current state and capabilities of DFT family of methods and the role of molecular modeling in confined systems.[10,11]

The interest to describe the thermodynamic properties of confined fluids requires the possibility of generating molecular based theories with the same level of accuracy as the most recent theories used to model a wide range of substances and their thermodynamic phases in bulk conditions.[12,13] Since the pioneering work by Hill[14] and de Boer,[15] thermodynamic properties of adsorbed phases can be explained in terms of two-dimensional (2D) systems. A 2D van der Waals model for pure fluids and their mixtures can describe adsorption in homogeneous substrates,[16–19] and 3D equations of state like Peng-Robinson, Soave-Redlich-Kwong and Eyring can be adapted to their 2D versions for binary mixtures of molecular fluids adsorbed on zeolite.[20] Accurate 2D equations of state based on perturbation theories for Lennard-Jones[21] and square-well fluids[22–25] have been used to model adsorption of monolayers, based on a now well-established 2D behavior of these systems, as evidenced by experiments, including the case of colloidal particles at the air-water interface.[26] Nevertheless, results from computer simulations suggest that the 2D approach is not restricted to model monolayer adsorption,[24] since once the first adsorbed layer reaches a high packing value in its density, then a second layer starts to form following a 2D arrangement. This mechanism also explains the formation of quantum fluid films on substrates and its quasi two-dimensional behavior.[27]

Recent advances on the modeling of adsorption have been made extending the Statistical Associating Fluid Theory for chain molecules interacting with potentials of variable range (SAFT-VR)[28,29] in order to include a two-dimensional approximation for adsorbed phases (SAFT-VR-2D).[23,24] This approach has been successfully applied to the prediction of adsorption isotherms of substances like nitrogen, carbon-dioxide and methane and their mixtures, adsorbed onto activated carbon,[25,30] and for more complex systems like asphaltenes in porous rocks,[31] using a previous theory developed for bulk asphaltenes.[32] In the chapter 3, a SAFT-VR approach was extended to describe quantum fluids in bulk phases[33] and used to describe the liquid-vapor phase equilibria of substances like molecular hydrogen (H_2), molecular deuterium (D_2), helium-4 (He^4) and neon (Ne). This new theory (SAFT-VRQ) combines the SAFT-VR method with perturbation theories for quantum square-well (SW) fluids in two and three dimensions (3D).[22,34–37]

In this chapter, we present a semiclassical theory of adsorption based on the SAFT-VRQ approach, presenting a modeling of classical fluids (e.g. methane, ethane, propane) and quantum fluids (e.g. hydrogen) adsorbed onto different materials such as activated carbon, silica gel and others materials, *i.e.,* graphene, activated carbon, metallic organic frameworks.

5.2 Classical adsorption model

In this study, we consider a model of a single-component fluid composed of N spherical particles of diameter σ in the presence of a uniform wall. Due to the wall, the behavior of the particles is different depending upon their distance to the wall. The interaction potential exerted by the wall on a particle is denoted as u_{pw}, and we can assume the potential u_{pw} as a function of the perpendicular distance of the wall (see Fig. 5-1). In this case, the particle-wall potential is given by

$$u_{pw}(z,\sigma,\lambda_w) = \begin{cases} \infty & \text{if } \ z \leq 0 \\ -\epsilon_w & \text{if } \ 0 < z \leq \lambda_w\sigma \\ 0 & \text{if } \ z > \lambda_w\sigma \end{cases} \tag{5.1}$$

where z is the perpendicular distance of the particles from the wall, ϵ_w is the depth, and $\lambda_w\sigma$ is the range of the attractive potential. In our approximation, we describe the system as being composed of two subsystems: a fluid whose particles are near to the wall, i.e., when $z \leq \lambda_w\sigma$, which we shall refer to as the "adsorbed fluid", and a fluid whose particles are far from the wall, i.e, when $z > \lambda_w\sigma$, i.e., the "bulk fluid". In this way, the length scale that characterizes the adsorbed fluid is given by $\lambda_w\sigma$. This approach is formally valid if we do not take into account the interface between the adsorbed and bulk fluids.

The adsorbed and bulk fluids have different properties due to the wall; it is well known that the interaction between molecules is modified by the presence of the wall and therefore the pair interaction between particles is different for the adsorbed and bulk phases. In the adsorption model, we denote $u_{pp}(r,\epsilon,\lambda)$ and $u_{pp}^{ads}(r,\epsilon_{ads},\lambda_{ads})$ as the pair potential for particles in the bulk and adsorbed phases, respectively (see Fig. 5-1). where ϵ, λ and ϵ_{ads}, λ_{ads} are parameters that describe the energy depth and the range of the potential for the bulk and adsorbed particles, respectively.[38]

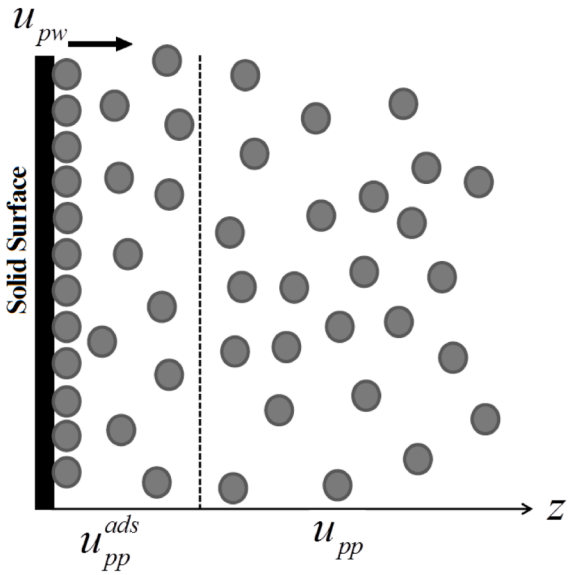

Figure 5-1: Illustration of surface area of adsorption. Adsorbed particles of the adsorptive gas a function of distance from the adsorbent surface. The u_{pp}, u_{pp}^{ads} and u_{pw} are the pair potentials for the bulk, adsorbed phase and wall-particle, respectively.

In the case of the adsorbed fluid, the pair potential interaction can be described as a decoupling of the x,y coordinates from the coordinate z for each adsorbed particle, as follows

$$\phi(x,y) = \int u_{pp}^{ads}(x,y,z)dz. \tag{5.2}$$

According with Eq. (5.2), the pair potential of the adsorbed particles u_{pp}^{ads}, only depends of the coordinates in parallel directions to the wall. Therefore, the adsorbed fluid can be approximated by a quasi-two dimensional system. The canonical partition function of the adsorbed fluid is given by

$$Q_{ads}(N,V,T) = \frac{V_{ads}^N}{N!\lambda_B^{3N}} Z_{ads}, \tag{5.3}$$

where V_{ads} is the adsorbed volume, λ_B, is the de Broglie wavelength, and Z_{ads} is the configurational partition function defined by

$$Z_{ads} = \frac{1}{V_{ads}^N} \int d^N\vec{r} e^{-\beta U}, \tag{5.4}$$

where $\beta = 1/kT$, and U is the total interaction potential, expressed as the sum of

two terms as

$$U = U_{pw} + U_{pp}^{ads}. \tag{5.5}$$

where U_{pw} is the total particle-wall interaction potential ($U_{pw} = Nu_{pw}(z)$), and U_{pp}^{ads} is the total particles pair potential ($U_{pp}^{ads} = (1/2)N(N-1)\phi(x,y)$), where the factor $(1/2)N(N-1)$ corresponds to distinct pairs in the system. In this way, Eq. (5.4) can be rewritten as

$$Z_{ads} = \frac{1}{V_{ads}^N} \int d^N z e^{-\beta N u_{pw}(z)} \int d^N x d^N y e^{-\beta \frac{N(N-1)}{2} \phi(x,y)}. \tag{5.6}$$

The adsorbed fluid can be characterized by a volume V_{ads}, that corresponds to an adsorption area (S), and perpendicular distance between the wall and the fluid affected by the wall (z_o). Therefore, the Eq. (5.6) can be rewritten as

$$Z_{ads} = Z_{1D} Z_{2D}, \tag{5.7}$$

where

$$Z_{1D} = \frac{1}{z_0^N} \int_0^{z_0} d^N z e^{-\beta N u_{pw}(z)}, \tag{5.8}$$

$$Z_{2D} = \frac{1}{S^N} \int d^N x d^N y e^{-\beta \frac{N(N-1)}{2} \phi(x,y)}, \tag{5.9}$$

where Z_{1D} and Z_{2D} are the one and two-dimensional configurational partition functions, respectively. The distance z_o can be written as a function of the range of the attractive potential of the wall and the diameter of the particles ($z_o = \lambda_w \sigma$). In this way, the Eq. (5.8) can be expressed as

$$Z_{1D} = \frac{1}{(\lambda_w \sigma)^N} \int_0^{\lambda_w \sigma} d^N z e^{-\beta N u_{pw}(z)} = \left[\frac{1}{\lambda_w \sigma} \int_0^{\lambda_w \sigma} dz e^{-\beta u_{pw}(z)} \right]^N, \tag{5.10}$$

The configurational partition function Z_{1D} in Eq. (5.10) can be evaluated using the mean-value theorem, *i.e.*,

$$Z_{1D} = e^{-\beta N u_{pw}(z^*)}. \tag{5.11}$$

where z^* is the value of the coordinate z that guarantees the mean value of the Boltzmann factor. The canonical partition function of the adsorbed fluid is given by

$$Q_{ads} = Q_{ads}^{1D} Q_{ads}^{2D} \tag{5.12}$$

where

$$Q_{ads}^{1D} = \frac{z_o^N}{\lambda_B^N} e^{-\beta N u_{pw}(z^*)} \tag{5.13}$$

$$Q_{ads}^{2D} = \frac{S^N}{N!\lambda_B^{2N}} \int d^N x d^N y e^{-\beta \frac{N(N-1)}{2} \phi(x,y)}, \tag{5.14}$$

Rearranging the Eqs. (5.12-5.14) we can obtain

$$Q_{ads} = Q_{ads}^{2D} \left(\frac{\lambda_w \sigma}{\lambda_B} \right)^N e^{-\beta N u_{pw}(z^*)}, \tag{5.15}$$

Applying the standard relation $A_{ads} = -kT\ln(Q_{ads})$, the Helmholtz free energy of the absorbed fluid is given by

$$\frac{A_{ads}}{NkT} = \frac{A_{2D}}{NkT} - \ln\left(\frac{\lambda_w \sigma}{\lambda_B} \right) + \beta u_{pw}(z^*). \tag{5.16}$$

where A_{2D} is the Helmholtz free energy of a two-dimensional fluid interacting via the potential $\phi(x, y)$, which can be described by perturbation theory using hard-disks as a reference fluid,

$$\frac{A_{2D}}{NKT} = \frac{A_{2D}^{ideal}}{NkT} + \frac{A_{2D}^{mono}}{NkT} + \frac{A_{2D}^{chain}}{NkT} \tag{5.17}$$

where A^{ideal} is the ideal free energy, A^{mono} is the excess free energy due to monomer segments, A^{chain} is the contribution due to the formation of the chains of monomers and the subscript $2D$ correspond to the 2D-fluid. In this study, the free energy due to intermolecular association is not considered. In the case of 2D-fluids the Eq. (5.17) can be rewritten as

$$\frac{A_{2D}}{NkT} = \ln\left(\rho_{ads}\lambda_B^2\right) - 1 + m\left(a_{HD} + \beta a_1^{2D} + \beta^2 a_2^{2D}\right) + a_{2D}^{chain}, \tag{5.18}$$

where m is the number of monomer segments of chain, a_{HD} is the excess Helmholtz free energy for a fluid of hard-disks, a_1^{2D} and a_2^{2D} are the first two terms of the perturbation theory and a_{2D}^{chain} is the term of the free energy of chains for for a 2D-fluid. In the particular case of the wall-particle interaction is given by a square-well interaction of range $\lambda_w\sigma$ and energy depth ϵ_w, we have that $u_{pw}(z*) = -m\epsilon_w$. On the other hand, we consider an analogous perturbation expression for the bulk fluid,

$$\frac{A_{3D}}{NKT} = \frac{A_{3D}^{ideal}}{NkT} + \frac{A_{3D}^{mono}}{NkT} + \frac{A_{3D}^{chain}}{NkT} \tag{5.19}$$

where the Helmholtz free energy is defined similarly as a 2D-fluid but the subscript $3D$ makes reference to a 3D-fluid. The Eq. (5.19) can be rewritten as

$$\frac{A_{3D}}{NkT} = \ln\left(\rho_b \lambda_B^3\right) - 1 + m\left(a_{HS} + \beta a_1^{3D} + \beta^2 a_2^{3D}\right) + a_{3D}^{chain}, \tag{5.20}$$

where a_{HS} is the hard-sphere free energy, a_1^{3D} and a_2^{3D} are the first two terms of the perturbation theory and a_{3D}^{chain} is the term of the free energy of chains for for a 3D-fluid. Detailed information about the 3D expressions for the Helmholtz free energy was presented in the references [28, 33].

5.3 Semiclassical approximation

The semiclassical approximation include terms containing quantum information of the system, assuming that the quantum corrections are relatively small compared with the classical result. The semi-classical approximation must be included in the classical theory; for example, at relatively high temperatures when the de Brogliés wavelength becomes very small compared to a characteristic scale such as the mean distance between close particles. The adsorption model is a function of a pair potential that describe the interaction between particles. Therefore, two routes arise to describe the behavior of the quantum fluids (use continuous or discrete pair potentials). The semiclassical expression for the Helmholtz free energy can be written as

$$\frac{A}{NkT} = \frac{A^{ideal}}{NkT} + \frac{A^{mono}}{NkT} + \frac{A^{chain}}{NkT} + \beta a_1^Q, \tag{5.21}$$

where a_1^Q is a first-order of quantum corrections. The Eq.(5.21) is particularly valid two-dimensional[24] and three-dimensional[28,33] fluids. In the following section, we are interested in the modeling of thermodynamic properties of the 2D quantum fluids using a semiclassical approach by the quantum expressions proposed by Mishra and Sinha.[22] Therefore, the Eq. (5.21) can be rewritten for fluids in two and tree dimensions, including the quantum expressions as

$$\frac{A_{2D}}{NkT} = \ln\left(\rho_{ads} \lambda_B^2\right) - 1 + m\left(a_{HD} + \beta(a_1^{2D} + a_1^{Q2D}) + \beta^2 a_2^{2D}\right) + a_{2D}^{chain}, \tag{5.22}$$

and

$$\frac{A_{3D}}{NkT} = \ln\left(\rho_b \lambda_B^3\right) - 1 + m\left(a_{HS} + \beta(a_1^{3D} + a_1^{Q3D}) + \beta^2 a_2^{3D}\right) + a_{3D}^{chain}, \tag{5.23}$$

where the superscript Q is refered to quantum expresion in $2D$ and $3D$ dimensions. Notice that in the above equations the terms a_1 in $2D$ and $3D$ can be expressed as the sum of the classical and quantum contributions.

5.3.1 Semiclassical 2D SAFT-VR approach

The SAFT-VR approach for 3D-fluids was explained in the last chapters. In the case of the SAFT-VR-2D, it follows the same structure used to describe a 3D-fluid. We calculated the a^{HD}, a_1^{2D}, a_2^{2D}, a_{2D}^{chain} for the classical Helmholtz free energy of a two dimensional fluid. On the other hand, the quantum contribution term a_1^{Q2D} is calculated using the semiclassical expressions proposed by Mishra and Sinha.[22] The Helmholtz free energy A for a pure 2D-component of chain molecules can be written into the various contributions as

$$\frac{A_{2D}}{NkT} = \frac{A_{2D}^{\mathrm{ideal}}}{NkT} + \frac{A_{2D}^{\mathrm{mono}}}{NkT} + \frac{A_{2D}^{\mathrm{chain}}}{NkT} \tag{5.24}$$

where N is the total number of molecules, T is the temperature, and k is the Boltzmann constant.

Ideal contribution: The free energy of an ideal gas in two dimensions is given by

$$\frac{A_{2D}^{\mathrm{ideal}}}{NkT} = \ln\left(\rho_{2D}\lambda_B^2\right) - 1 \tag{5.25}$$

where λ_B is the thermal de Broglie wavelength.

Monomer Contribution: The contribution due to the monomers is given by

$$\frac{A_{2D}^{\mathrm{mono}}}{NkT} = m\frac{A_{2D}^{\mathrm{M}}}{N_s kT} = m\left(a^{\mathrm{HD}} + \beta(a_1^{\mathrm{2D}} + a_1^{\mathrm{Q2D}}) + \beta^2 a_2^{\mathrm{2D}}\right) \tag{5.26}$$

The Helmholtz free energy for a hard-disk fluid is obtained from the Henderson equation,[39]

$$a^{\mathrm{HD}} = \frac{9\gamma}{8(1-\gamma)} - \frac{7}{8}\ln(1-\gamma), \tag{5.27}$$

where $\gamma = (\pi/4)\rho_{2D}\sigma^2$, is the packing molar fraction of a two-dimensional fluid, ρ_{ads} is the density of the adsorbed fluid and σ is the diameter of the particle. The first order perturbation term of the Helmholtz free energy can be written as

$$a_1^{\mathrm{2D}} = -2\gamma\epsilon_{ads}(\lambda_{ads}^2 - 1)\mathrm{g}^{\mathrm{HD}}(\sigma, \gamma_{\mathrm{eff}}), \tag{5.28}$$

where g^{HD} is the hard disk radial distribution function in the contact value and γ_{eff} is the effective molar packing fraction, given by

$$\mathrm{g}^{\mathrm{HD}}(\sigma, \gamma_{\mathrm{eff}}) = \frac{1 - 7/16\gamma_{\mathrm{eff}}}{(1 - \gamma_{\mathrm{eff}})^2}, \tag{5.29}$$

where

$$\gamma_{\mathrm{eff}} = d_1\gamma + d_2\gamma^2 \tag{5.30}$$

$$d_1 = 1.4215 - 0.405625\lambda - 0.0386981\lambda^2 \tag{5.31}$$

$$d_2 = 1.5582 - 1.89768\lambda + 0.405215\lambda^2 \tag{5.32}$$

The second-order term is given by the local compressibility approximation result

$$a_2^{2D} = \frac{1}{2}\epsilon_{ads}K^{\mathrm{HD}}\gamma\left(\frac{\partial a_1^{2D}}{\partial\gamma}\right), \tag{5.33}$$

where K^{HD} is the isothermal compressibility given by

$$K^{\mathrm{HD}} = \frac{(1-\gamma)^3}{1 + \gamma + 3/8\gamma^2 - 1/8\gamma^3}.$$

According with Mishra and Sinha,[22] the semiclassical quantum 2D-expression a_1^{Q2D} is given by

$$a_1^{\mathrm{Q2D}} = \sqrt{2}\gamma\left(\frac{\lambda_B}{\sigma}\right)\mathrm{g}_{2D}^{\mathrm{SW}}(\sigma) = \left(\frac{\Lambda\gamma}{\sqrt{\pi T^*}}\right)\mathrm{g}_{2D}^{\mathrm{SW}}(\sigma) \tag{5.34}$$

where

$$\left(\frac{\lambda_B}{\sigma}\right) = \frac{\Lambda}{\sqrt{2\pi T^*}} \tag{5.35}$$

where $\mathrm{g}_{2D}^{\mathrm{SW}}(\sigma)$ is the contact value of the square-well radial distribution function and can be obtained as a high-temperature expansion as

$$\mathrm{g}_{2D}^{\mathrm{SW}}(\sigma) = \mathrm{g}^{\mathrm{HD}}(\sigma) + (\beta\epsilon)\mathrm{g}_1^{2D}(\sigma), \tag{5.36}$$

Applying the Leibnitz theorem we obtain

$$\mathrm{g}_1^{2D}(\sigma) = \frac{1}{2\epsilon}\left[\frac{\partial a_1^{2D}}{\partial \gamma} - \frac{\lambda}{2\gamma}\frac{\partial a_1^{2D}}{\partial \lambda}\right] \tag{5.37}$$

Chain Contribution: The contribution due to the formation of chains, is given by

$$a_{2D}^{\text{chain}} = -(m-1)\ln\left(y_{2D}^{\text{M}}(\sigma)\right) \tag{5.38}$$

where y_{2D}^{M} is the contact value of the background function of the monomeric 2D-fluid, defined by

$$y_{2D}^{\text{M}}(\sigma) = \mathrm{g}_{2D}^{\text{SW}}(\sigma)e^{-\beta\epsilon} \tag{5.39}$$

The 2D-dimensional SAFT-VR formalism have the many advantages in the description of real quantum fluids in terms of a few thermodynamic variables.

5.3.2 Results for 2D SAFT-VR approach

The vapor-liquid equilibria (VLE) for a pure 2D-fluid, can be calculated using the physical conditions of equilibria, the equality of temperature (T), pressure (P) and chemical potential (μ). We solve the conditions for phase equilibria of the square-well 2D system that take into account quantum corrections, using the Levenberg-Marquartd minimization algorithm.[40] In Fig 5-2(a) we show the VLE results given by SAFT-VR 2D for a monomeric segment $m = 1$. The SAFT-VR 2D EoS provides an accurate representation of the simulation data for several values of the range λ.

Results obtained from the Eq. 5.21 for the VLE of flexible chains of $m = 1; 2; 4; 8$ and 16, square-well segments with range of $\lambda = 1.5$ are presented in Fig. 5-2(b). The critical temperatures as a function of the monomeric segment ($m = 1; 2; 4; 8$ and 16), and the variable range parameter are showed in Fig. 5-2(c). Here, for the specific case of $m = 1$, we fitted the results obtained by using a second order polynomial expression given by

$$\lambda_{2D} = 7.7927T_c^{*3} - 19.6364T_c^{*2} + 17.6721T_c^{*} - 3.9919 \tag{5.40}$$

where λ_{2D} is the range variable parameter and T_c^* is the reduced critical temperature, both for a fluid in 2D.

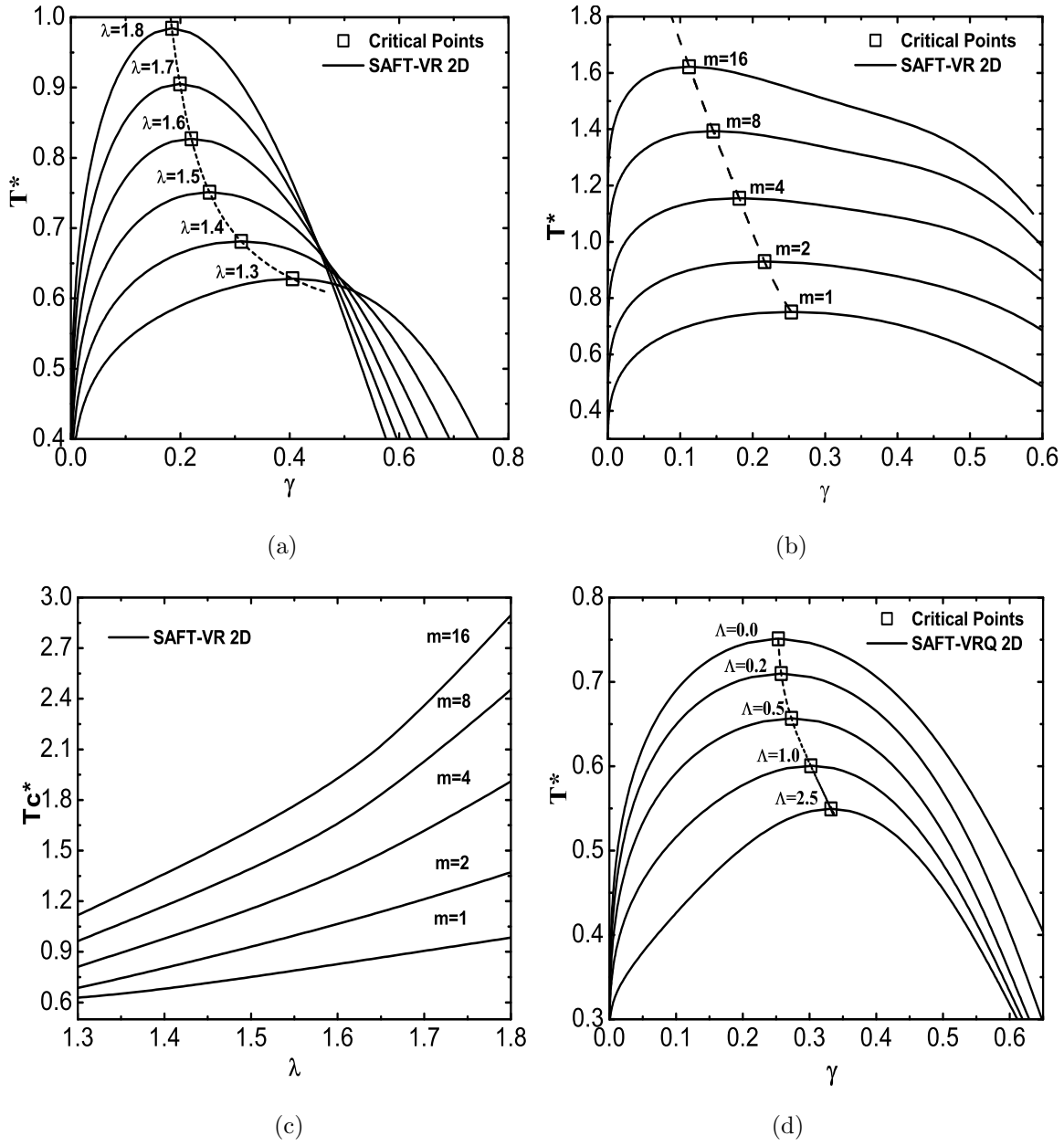

Figure 5-2: Vapor-liquid coexistence by SAFT-VR and SAFT-VRQ approaches for a 2D square-well. Cases presented: (a) monomeric fluids with $m = 1$, (b) monomeric chains of m segments, (c) critical temperatures as function of the variable range parameter, (d) quantum contributions at differents values of the de Boer's parameter (Λ). In all the cases, $T^* = kT/\epsilon$ is the reduced temperature, $\gamma = \pi\rho_{\text{ads}}\sigma^2$ is the 2D packing-fraction and m is the monomeric segments.

Similar expressions can be obtained for fluids in 3D.

$$T_c^{*3D} = 0.6845\lambda_{3D}^2 + 0.1233\lambda_{3D} - 0.3963 \tag{5.41}$$

where T_c^{*3D} is the reduced critical temperature and λ_{3D} is the range variable parameter, both for a fluid in 3D. Eqs. 5.40 and 5.41 will be a powerful tool in the following sections.

Table 5.1: Critical parameters obtained for a 2D-Square-Well fluid. T_c^*, P_c^* are the predicted SAFT-VR-2D critical temperature and pressure points in reduced units, $T_c^* = kT_c/\epsilon$ and $P_c^* = P_c\sigma^3/\epsilon$. These values are obtained by solving the pair of equations generated by the conditions $(\partial P/\partial\rho)_{T_c,P_c} = 0$ and $(\partial^2 P/\partial\rho^2)_{T_c,P_c} = 0$. m is the number of monomeric segment, λ is the SW range parameter, γ_c is the critical molar packing fraction.

m	λ	T_c^*	γ_c	P_c^*
1.0	1.250	0.6099	0.4632	0.1907
1.0	1.375	0.6659	0.3314	0.1053
1.0	1.750	0.9446	0.1915	0.0807
1.0	1.500	0.7510	0.2533	0.0859
2.0	1.250	0.6352	0.3727	0.0502
4.0	1.375	0.9361	0.1801	0.0181
8.0	1.500	1.3936	0.1457	0.0107
16.0	1.750	2.6218	0.2087	0.0166

Table 5.2: Critical parameters obtained for a 2D-Square-Well fluid. T_c^*, P_c^* are the predicted SAFT-VRQ-2D critical temperature and pressure points in reduced units, $T_c^* = kT_c/\epsilon$ and $P_c^* = P_c\sigma^3/\epsilon$. These values are obtained by solving the pair of equations generated by the conditions $(\partial P/\partial\rho)_{T_c,P_c} = 0$ and $(\partial^2 P/\partial\rho^2)_{T_c,P_c} = 0$. m is the number of monomeric segment, λ is the SW range parameter, γ_c is the critical molar packing fraction and Λ is the the de Boer's quantumness parameter.

m	λ	Λ	T_c^*	γ_c	P_c^*
1.0	1.50	0.0000	0.7510	0.2533	0.0859
1.0	1.50	0.5991	0.6423	0.2793	0.0871
1.0	1.50	1.2249	0.5860	0.3106	0.1279
1.0	1.50	1.7378	0.5652	0.3228	0.1798
1.0	1.50	2.6783	0.5470	0.3333	0.2903

In Table 5.1, critical temperatures T_c, critical pressures P_c and critical molar packing fractions η_c for different values of number of monomeric segments m are presented. The values reported in the Table 5.1 correspond for a classical square-well 2D fluid, i.e., $\Lambda = 0.0$. On the other hand, for the case of quantum fluids in 2D, the VLE of five different values of the de Boer's quantumness parameter ($\Lambda = h/\sigma\sqrt{m\epsilon}$) are obtained in order to contabilized the effect of the quantum corrections in the classical theory in 2D. Results are shown in Fig. (5-2(d)) for the parameter of variable range of $\lambda = 1.5$, at five different de Boer's quantumness parameter $\Lambda = 0; 0.5991; 1.2249; 1.7378$ and 2.6783. The results are summarized in the Table 5.2. In this work, we studied quantum fluids characterized by a number of monomeric segment $m = 1$. In Table 5.2 are presented the results obtained by modifying the de Boer's quantumness parameter (Λ).

5.4 Quantitative expression of adsorption

Without any independent information concerning the structure of the adsorbed layer, we might suppose that the density of the adsorbable component decreases progressively by increasing, z coordinate, from the adsorbent surface area; at distance $z = \lambda_w\sigma$, this density reaches the constant value of the gas or bulk density ρ_b. This hypothetical variation of the density in the gas/solid interface is illustrated in Fig. 5-3(a), where we also identify three zones (I, II and III). We shall assume that there is no penetration of gas into the solid (*i.e.*, no *absorption*) so that zone I is occupied solely by the adsorbent. In zone II is the adsorbed layer, which is an intermediate region confined within the limits $0 < z < \lambda_w\sigma$, here the density $\rho(z)$ is higher than the concentration of the gas in zone III. In zone III, the adsorbable gas is at sufficient distance from the solid surface to have a uniform bulk density, ρ_b, and here $z > \lambda_w\sigma$. In this region, the concentration is dependent only on the equilibrium pressure and temperature. The concept of "*surface excess*" was introduced by Gibbs in 1877 in order to quantify the amount adsorbed. This concept introduce an imaginary surface placed parallel to the adsorbent surface and divide the system in two zones (I and II), as can be observed in Fig. 5-3(b). In this model, the *surface excess amount*, n, represented by the hatched area C_1, is defined as the difference between the total area A_T and the area C_2.

In Fig. 5-3(b), the surface excess amount n is represented by hatched area C_1.

The amount n is a extensive quantity, which depends on the extent of the interface and can be related with the "*surface excess concentration*", Γ [molecules/m^2], given by

$$\Gamma/N_A = n/A_s, \qquad [\text{mol/m}^2] \tag{5.42}$$

where N_A is the Avogadro's number and A_s is the surface area associated with the mass of the adsorbent solid m_s. The specific surface area a is therefore

$$a_s = A_s/m_s, \qquad [\text{m}^2/\text{g}_\text{s}] \tag{5.43}$$

where the specific surface area a_s can be obtained by different experimental methodologies.[41]

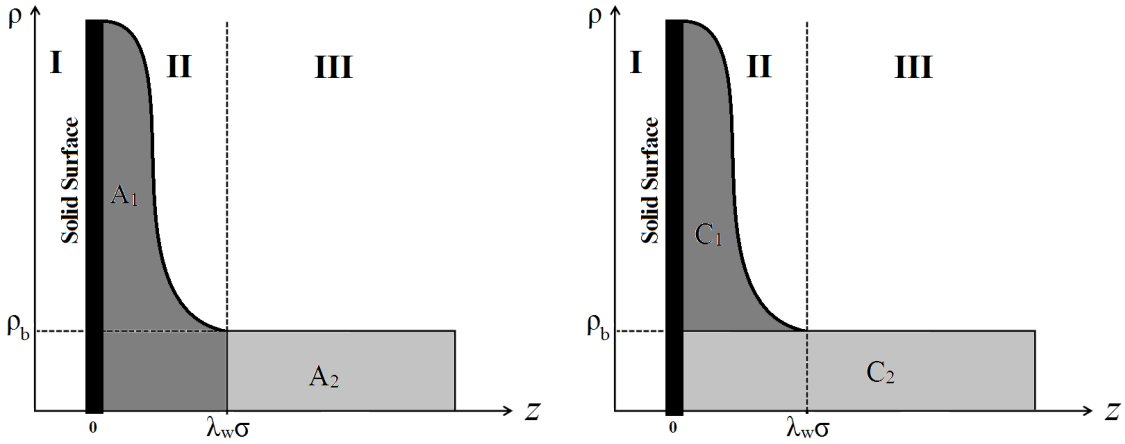

(a) (b)

Figure 5-3: Representation of the adsorption of a adsorbable gas into a solid surface area as a funtion of a z distance from the surface. a) The Layer model, b) The Gibbs surface excess amount.

In this work, we use the specific surface area values reported as the Brunnauer-Emmett-Teller area, S_{BET}, considered as a standard methodology to determine the specific surface area.[42,43] In many cases, the experimental adsorption data values are reported using the quantity (n/m_s) denominated "*specific surface excess amount*" and defined as a rate the surface excess amount over solid mass. From the Eqs.

(5.42-5.43) we can obtain a compacted expression for specific surface excess amount

$$n/m_s = \Gamma S_{BET}/N_A \qquad [\text{mol/g}_\text{s}] \tag{5.44}$$

where $a_s = S_{BET}$. For convenience, this quantity (n/m_s), will be often referred to as "*amount adsorbed*". According with the Eq. (5.49) the only undefined term is the surface excess concentration, Γ. In the following chapters we will try to explain, how the surface excess concentration can be obtained from statistical mechanics.

5.4.1 Surface excess concentration

The subtle task of quantifying the amount of adsorbed particles can be made by using the surface excess concentration, Γ, which is defined as

$$\Gamma = \int_0^\infty dz[\rho(z) - \rho_b], \tag{5.45}$$

where $\rho(z)$ is the density of the particles and ρ_b is the bulk density of particles, *i.e.*, $\rho(z \to \infty) = \rho_b$. The surface excess amount is commonly called Gibbs surface excess concentration, denoted as Γ_{Gibbs} (we are adopting this convention in all the document). In the specific case of a fluid interacting via a a square-well pair-potential with a wall surface the Eq. (5.45) can be written as

$$\Gamma_{Gibbs} = \int_0^{\lambda_w\sigma} dz\rho(z) - \rho_b\lambda_w\sigma, \qquad [\text{molecules/m}^2] \tag{5.46}$$

where $\lambda_w\sigma$ is a length scale of a adsorbed fluid. The related quantity Γ_{Gibbs}, is an intensive quantity which has units of [molecules/m^2]. Other amount, as may be considered attractive, is the absolute adsorption concentration, Γ_{abs}, defined by the total concentration of adsorptive molecules, given by

$$\Gamma_{abs} = \rho_{ads} = \int_0^{\lambda_w\sigma} dz\rho(z), \qquad [\text{molecules/m}^2] \tag{5.47}$$

where ρ_{ads} is the density of the adsorbed fluid, defined in last sections. On the SAFT-VR and SAFT-VRQ formalism a compacted expression can be obtained for the Eq. (5.46)

$$\Gamma_{Gibbs}\sigma^2 = \Gamma_{abs}\sigma^2 - 6\eta\lambda_w/\pi \qquad [\text{molecules}] \tag{5.48}$$

where $\Gamma_{abs}\sigma^2 = 4\gamma/\pi$. Finally, from the Eq.(5.48) the Gibbs surface excess concentration and the absolute adsorption concentration values can be calculated when the equilibrium conditions are satisfied.

Therefore, the connexion with the experimental data values is accomplished by the calculation of the adsorbed amount, given by

$$n/m_s = \frac{(\Gamma_{Gibbs}\sigma^2)S_{BET}}{N_A\sigma^2} \qquad [\text{mol/g}_\text{s}] \tag{5.49}$$

According with Eq. (5.49), the adsorbed amount is dependent on the equilibrium pressure, P, and the adsorbent temperature, T. Also, is common to find the adsorbed amount expressed as a weight percent $wt.\%$, where

$$wt.\% = \frac{m_{exc}}{m_s + m_{exc}} \times 100 = \frac{0.1(n/m_s)\text{MM}}{[100 + 0.1(n/m_s)\text{MM}]} \times 100 \tag{5.50}$$

or

$$n/m_s = \left(\frac{wt.\%}{100 - wt.\%}\right)\left(\frac{1}{\text{MM}}\right) \qquad [\text{mol/g}_\text{s}] \tag{5.51}$$

where m_{exc} is the excess absorbed mass, m_s is the mass of the solid and MM is the molecular mass of the component. Eqs. 5.50 and 5.51 are a useful tool in order to change the units from [mmol/g] to $[wt.\%]$ and vice versa.

5.5 Semiclassical Adsorption Isotherms

The prediction of the adsorption isotherms using classical SAFT-VR, is established by using the thermodynamic equilibrium conditions. In this case, the chemical potential of the adsorbed and bulk phases must be equal for a given temperature T and bulk pressure, P. Therefore, the density of the adsorbed fluid ρ_{ads} can be obtained by solving the equation

$$\mu_{ads} = \mu_b \tag{5.52}$$

where μ is the chemical potential and the subscripts ads and b correspond to adsorbed and bulk respectively. The chemical potential for a pure component can be obtained from the Helmholtz free energy using the following thermodynamic relation

$$\beta\mu_b = a_{3D} + \eta\left(\frac{\partial a_{3D}}{\partial \eta}\right)_{V,T}. \tag{5.53}$$

and

$$\beta\mu_{ads} = a_{ads} + \gamma \left(\frac{\partial a_{ads}}{\partial \gamma}\right)_{V,T}, \tag{5.54}$$

where η and γ are the molar packing fraction of a three and two dimensional fluid, respectively. Therefore, substituting the expressions for μ_b and μ_{ads} into the Eq. (5.52), we obtain

$$a_{3D} + \eta \left(\frac{\partial a_{3D}}{\partial \eta}\right)_{V,T} = a_{ads} + \gamma \left(\frac{\partial a_{ads}}{\partial \gamma}\right)_{V,T}, \tag{5.55}$$

The Eq. (5.55) is the "equilibrium" equation used in the prediction of the adsorption curves. On the other hand, obtaining the chemical potentials μ_{ads} and μ_b from Eqs (5.16)-(5.23), we can rewrite the Eq. (5.52) in the following way

$$\beta\mu_b = \beta\mu_{2D} + \beta\mu_w, \tag{5.56}$$

where μ_{3D} and μ_{2D} are the chemical potentials for 3D and 2D fluids, and μ_w is the contribution to the chemical potential due to the wall. These chemical potentials are redefined as

$$\beta\mu_w = \ln(2/3) - \ln(\lambda_w) - \beta m\epsilon_w \tag{5.57}$$

where

$$\beta\mu_{2D} = \ln(\gamma) + m\left(a_{HD} + \beta(a_1^{2D} + a_1^{Q2D}) + \beta^2 a_2^{2D}\right) + a_{2D}^{chain} + Z_{2D}, \tag{5.58}$$

$$\beta\mu_b = \ln(\eta) + m\left(a_{HS} + \beta(a_1^{3D} + a_1^{Q3D}) + \beta^2 a_2^{3D}\right) + a_{3D}^{chain} + Z_{3D} \tag{5.59}$$

The adsorption isotherms can be determined solving Eqs. (5.57)-(5.58) by using a Newton-Rhapson algorithm.[40] As can be seen from the above equations, we need the molecular parameters for the 2D, 3D fluids and the specific parameters of the interaction between the wall and the particles. In the case of the 3D-fluids, molecular parameters (m, σ, ϵ/k and λ) have been reported for many classical and quantum fluids in the literature.[28,33]

Also, there are some considerations that must be taken into account when the adsorption isotherms are calculated:

a. The adsorbed particles have the same size as the particles in the bulk, i.e,

$\sigma_{ads} = \sigma$. In the particular case of $\sigma_{ads} \neq \sigma$, the wall modifies the particle size, this effect is not considered in the adsorption model.

b. Sinanoglu and Pitzer[44] obtained theoretical results for Lennard-Jones pair potential interaction, where they show that the energy well depth of the particle-particle potential in an adsorbed monolayer changes in a range of $0.6\epsilon \leq \epsilon_{ads} \leq 0.8\epsilon$ from its bulk phase value. Recent theoretical studies of adsorption have shown that a criterion of $\epsilon_{ads} = 0.8\epsilon$, really works for a square-well fluids compared with experimental data.[24,45]

c. The critical temperature in the adsorbed fluid is related with the bulk temperature as ($T_c^{bulk} < T_c^{ads}$), i.e, there are a critical relation ($R_c = T_c^{ads}/T_c^{bulk}$.) between the two temperatures. This ratio is known for the case of noble gases and methane adsorbed onto graphite surface, $R_c \approx 0.4$. In this work, experimental adsorption data are obtained using $R_c = 0.4$.

d. F. del Rio and Gil-Villegas[46] reported the upper and lower limit for the wall-particle potential ($0.1305 \leq \lambda_w \leq 0.8165$) that can be used to describe monolayer adsorption for square-well according to mean-field criteria. In all cases, we use the upper limit, i.e, $\lambda_w = 0.8165$.

e. The only free parameter is the wall-energy parameter ϵ_w. Recently, experimental studies have shown results for energetic values of binding energy for monolayer adsorption of different fluids onto different materials. These energetic parameters are used to establish a energetic range of possible values of ϵ_w. We fitted the energetic parameter ϵ_w in order to reproduce the adsorption isotherm data.

5.6 Isosteric heat of adsorption

The heat released when a gas is adsorbed on a solid surface, can be quantified by using the enthalpy change per molecule adsorbed. This quantity is defined as isosteric heat of adsorption (q_{st}). The isosteric heat of adsorption of the pure components and their mixtures has a relevant importance for the design of gas separation pressure such as: pressure swing and thermal swing adsorption.[47] Although there are many

different definitions of the isosteric heat of adsorption,[48] in this section we explain the difference between the corresponding multiple approaches.

In order to obtain the isosteric heat of adsorption, we use the following conventions and simplifying assumptions:

- Only the case of a single fluid adsorbed on a solid adsorbent is considered.
- The adsorbent is assumed to remain inert and therefore to undergo no change in its surface area, internal energy or entropy at any stage of physisorption.
- The model assumes two different phases of equilibrium. Both are 3D but a quasi 2D approximation is used to model the adsorbed fluid.
- We consider the free Helmholtz energy as the primary thermodynamic potential since this is most suitable for experiments carried out at constant temperature and surface area.
- We assume that there is no penetration of gas into the solid, i.e., no absorption.

There are two definitions of the isosteric heat of adsorption (q_{st}), denoted by molar integral quantities and differential quantities, both are explained in the following sections.[41,49]

5.6.1 Integral enthalpy of adsorption

The integral enthalpy of adsorption (q_{st}), is the difference between the enthalpy of the adsorbed fluid and bulk fluid,[41]

$$q_{st} = h_b - h_{ads}, \qquad [\text{kJ/mol}] \tag{5.60}$$

or

$$\beta q_{st} = \left(\frac{U_b}{NkT} + Z_b\right) - \left(\frac{U_{ads}}{NkT} + Z_{ads}\right) \tag{5.61}$$

where N is the number of particles, h is the enthalpy, U is the internal energy, Z is the compressibility factor and the subscripts b and ads refers to bulk and adsorbed phases. The Eqs. (5.60)-(5.61) describe the thermodynamic relation between the enthalpy of

the bulk fluid and the adsorbed fluid. The internal energy U, is calculated from the thermodynamic relation given by

$$\frac{U_b}{NkT} = \beta \left(\frac{\partial a}{\partial \beta} \right)_p \qquad \frac{U_{ads}}{NkT} = \beta \left(\frac{\partial a_{ads}}{\partial \beta} \right)_p \tag{5.62}$$

where a is the Helmholtz free energy $a = A/NkT$ and $\beta = 1/kT$. By replacing Eqs. (5.62) into (5.61):

$$\beta q_{st} = \left(\beta \left(\frac{\partial a_b}{\partial \beta} \right)_p + Z_b \right) - \left(\beta \left(\frac{\partial a_{ads}}{\partial \beta} \right)_p + Z_{ads} \right) \tag{5.63}$$

Therefore, the integral enthalpy of adsorption defined by the Eq. (5.60) can be calculated using the Eq. (5.63) as follows

$$\begin{aligned} q_{st} =& \epsilon_w + kT(Z^{HS} - Z^{HD}) + a_1^{3D} - a_1^{2D} + \eta \frac{\partial}{\partial \eta}(a_1^{3D} + a_1^{3DQ}) - \gamma \frac{\partial}{\partial \gamma}(a_1^{2D} + a_1^{2DQ}) \\ &+ 2\beta(a_2^{3D} - a_2^{2D}) + \beta \left(\eta \frac{\partial a_2^{3D}}{\partial \eta} - \gamma \frac{\partial a_2^{2D}}{\partial \gamma} \right) + \beta \frac{\partial}{\partial \beta}(a_1^{3DQ} - a_1^{2DQ}) \end{aligned} \tag{5.64}$$

where Z^{HD} and Z^{HS} denote the compressibility factor for hard disks and hard spheres fluids, respectively. In the low-density limit value, $q_{st} = \epsilon_w$, and this is an important feature of the present theory, since experimental values of q_{st} can be used to determine the parameter ϵ_w.

5.6.2 Differential heat of adsorption

As a gas is adsorbed on the surface, heat is involved and there is enthalpy change per molecule adsorbed. This quantity is denoted by differential enthalpy of adsorption (q_{st}), given by[49]

$$q_{st} = \dot{H}_b - \dot{H}_{ads}, \qquad [\text{kJ}] \tag{5.65}$$

or

$$q_{st} = \left(\dot{U}_b + \frac{P_b}{\rho_b} \right) - \left(\dot{U}_{ads} + \frac{P_{ads}}{\rho_{ads}} \right) \tag{5.66}$$

where H is the enthalpy, $\dot{U}$ is the internal energy, P is the pressure, ρ is the density and the subscripts b and ads refers to bulk and adsorbed phases. In many cases, $\dot{U}$ is named differential surface excess internal energy and this quantity is calculated from

the canonical partition function (Q) as

$$\dot{U_b} = -k\frac{\partial^2 \ln(Q_b)}{\partial N_b \partial(1/T)} \qquad \dot{U_{ads}} = -k\frac{\partial^2 \ln(Q_{ads})}{\partial N_{ads} \partial(1/T)} \tag{5.67}$$

where N is the number of particles. The Eq. (5.67) can be rewritten using two thermodynamic relations $A = -kT\ln(Q)$ and $\beta\mu = a + Z$, as follows

$$\dot{U_b} = \frac{\partial a_b}{\partial \beta} + \frac{\partial Z_b}{\partial \beta} \qquad \dot{U_{ads}} = \frac{\partial a_{ads}}{\partial \beta} + \frac{\partial Z_{ads}}{\partial \beta} \tag{5.68}$$

where a is the Helmholtz free energy and Z is the compressibility factor. Therefore, the isosteric heat adsorption defined by the Eq. (5.65) can be calculated using Eq. (5.68) as follows

$$\beta q_{st} = \left(\frac{\partial a_b}{\partial \beta} + \frac{\partial Z_b}{\partial \beta} + Z_b\right) - \left(\frac{\partial a_{ads}}{\partial \beta} + \frac{\partial Z_{ads}}{\partial \beta} + Z_{ads}\right) \tag{5.69}$$

The differential heat of adsorption given by Eq. (5.69) is not commonly reported in the concerning adsorption literature.

5.7 Results for classical and quantum fluids

In Figures 5-4(a)-5-4(b) predictions are given for the adsorbed 2D packing-fraction γ as a function of the bulk 3D packing-fraction η, for a monomeric SW fluid with range $\lambda = 1.5$ adsorbed onto a structureless planar wall at $T^* = kT/\epsilon = 1.5$. The wall-particle interaction has a fixed range $\lambda_w = 0.2453$, the values of the energy well depth are related as $\epsilon_{ads} = \epsilon$ and $\epsilon_{ads} = 0.8\epsilon$ in the adsorbed phase. The results are given for several values for the energy ratio $\epsilon^* = \epsilon_w/\epsilon$, that measures the relative strength between the particle-wall and bulk particle-particle interactions. Classical and quantum adsorption are presented for each value of ϵ^*, indicated by the values of the de Boer's quantumness parameter, $\Lambda = 0$ and $\Lambda = 1.7378$, respectively. In Fig. 5-4(a), good agreement between theoretical predictions and simulations data are observed at low packing fractions and low values of wall-particle parameter ϵ^*. In Fig. 5-4(b), a remarkable effect of the decrement of the adsorbed 2D packing fraction γ from the classical ($\Lambda = 0$) to quantum ($\Lambda = 1.7378$) model is observed. Quantum effects increase at high values of the de Boer's parameter.

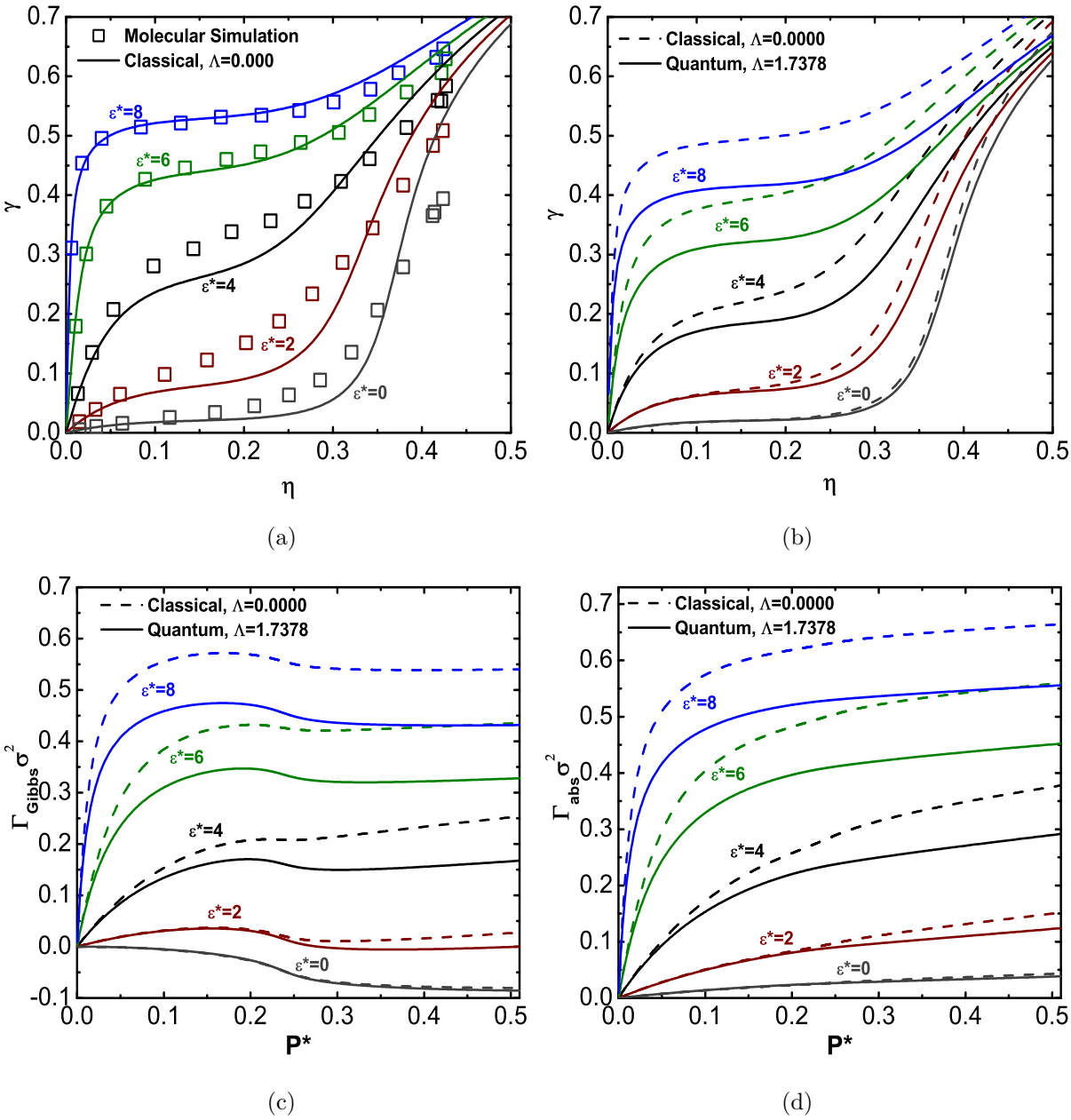

Figure 5-4: (a)-(b) Predictions for the adsorbed two-dimensional packing-fraction γ as a function of the bulk three-dimensional packing-fraction η, for a monomeric SW fluid with range $\lambda = 1.5$ adsorbed onto a planar wall at $T^* = 1.5$. The wall-particle interaction is described by a SW potential with a fixed range $\lambda_w = 0.2453$ and several values for the energy ratio $\epsilon^* = \epsilon_w/\epsilon$. Solid and dashed lines correspond to the theoretical predictions obtained from SAFT-VRQ ($\Lambda = 1.7378$) and SAFT-VR ($\Lambda = 0$), respectively, where Λ is the de Boer's quantumness parameter. Squares (□) correspond to 2D packing fractions obtained obtained from density profiles simulated with the Gibbs ensemble Monte Carlo technique for inhomogenous fluids. (c)-(d). Predictions for the absolute and Gibbs adsorption isotherms, Γ_{abs} and Γ_{Gibbs}, respectively. Solid and dashed lines correspond to the theoretical predictions obtained from SAFT-VRQ and SAFT-VR, respectively.

A more complete summary of predictions for the absolute and Gibbs adsorption isotherms are presented on Ref. [50].

In a previous work,[24] we have shown that Monte Carlo (MC) computer simulations for the same classical system agrees very accurately with the theoretical predictions. For the quantum case, special methods are required to simulate this system, like the MC method using path integrals. As it results clear from this figure, the introduction of quantum corrections modifies the adsorption pattern observed for classical fluids, and there is an effective decrement on γ, particularly at high values of η and ϵ^*.

This effect is explained as a consequence of a higher effective diameter σ introduced when the interparticle potential is modified by a quantum correction, as in the case of the Lennard-Jones potential $u_{LJ}(r)$ in the Wigner-Kirkwood theory,[51,52]

$$u_{eff}(r) = u_{LJ} + \frac{\Lambda^2}{48\pi^2 T^*}\nabla^2 u_{LJ} \tag{5.70}$$

where the second term gives a repulsive contribution that increase the interparticle distance σ_{eff} where $u_{eff}(\sigma_{eff}) = 0$, and also reduces the energy depth of the potential.[53] For the case of a hard-spheres system, the effective hard-core diameter is approximately given by $\sigma_{eff} = \sigma_{HS} + \frac{\lambda_B}{2\sqrt{2}}$.[54] In this way, quantum particles have a bigger size than the corresponding classical ones, and the amount of surface area available is reduced with respect to the classical prediction, for the same value of the bulk packing fraction η, i.e., $\gamma_Q(\eta) > \gamma_C(\eta)$.

The behavior of Γ_{abs} and Γ_{Gibbs} in terms of the adimensional bulk pressure $P^* = P_b\sigma^3/\epsilon$ is presented in Figs. 5-4(c) and 5-4(d), where the effect of the reduction in the amount of adsorbed fluid is evident. An apparent kink seems to be present for the Gibbs adsorption isotherms, although from Eq. (5.48) and Fig. 5-4(a) we can see that γ is a continuous function in η, and Γ_{Gibbs} depends linearly on these two packing fractions. Moreover, its first derivative is continuous, since

$$\frac{\partial \Gamma_{Gibbs}\sigma^2}{\partial P^*} = \left[\frac{2}{3}\frac{\partial \gamma}{\partial \eta} - \lambda_w\right]\frac{K_T}{T^*} \tag{5.71}$$

where K_T is the isothermal compressibility of the bulk fluid, given by $K_T = kT(\partial\rho_b/\partial P_b)_T$. Since $K_T > 0$ for stable phases, the sign of the derivative is determined by the factor between brackets. From Fig. 5-4(a) is clear that $\partial\gamma/\partial\eta \geq 0$. For all the values of ϵ^* shown in Fig. 5-4(a), $\partial\gamma/\partial\eta \approx 0$ when $0.05 \leq \eta \leq 0.25$, and $\Gamma_{Gibbs} < 0$, whereas for

$\eta < 0.05$ or $\eta > 0.25$ $\Gamma_{Gibbs} > 0$. These tendencies explain the shape of the curves as observed in Fig. 5-4(b). The very fast change around the pressure $P^* = 0.25$ is mainly due to the damping effect that K_T has when η (and then P^*) increases, since the isothermal compressibility decreases strongly for dense fluids.

5.7.1 Classical Fluids: Methane, Ethane, Propane, Butane, Nitrogen and Propylene

The adsorption curves obtained by using the classical model are in concordance with the simulation results, now, we can apply the developed theory above in the description of the adsorption phenomena of real fluids with a classical or semiclassical description. The molecular parameters values of 3D-fluids (m, σ, ϵ/k and λ), 2D-fluids (λ_{ads} and ϵ_{ads}) and wall-particle interaction (λ_w and ϵ_w) for methane, ethane, propane, butane, nitrogen, and propylene on different porous surfaces are reported in references [24, 28, 45]. The adsorbed amounts were compared with experimental data values reported by different types of adsorbents. In all cases the energy parameter of the wall, ϵ_w was fitted in order to reproduce the experimental adsorption isotherms.

In Figs. (5-5) and (5-6), we present the results obtained for the adsorption isotherms of *n*-alkanes,nitrogen and propylene on different materials. Gibbs and absolute isotherms were obtained according to Eqs. 5.46 and 5.47, respectively, and compared with experimental data. Adsorption isotherms results on BDH-activated carbon, NSG silica gel and Na-Y zeolite are shown in Fig. (5-5) for chains-alkanes (methane, ethane, propane and butane). In all cases, the temperature range was between [303 - 423]K, and the adsorption isotherms results were in concordance with the experimental data.

In Fig. (5-6) are shown results for methane, nitrogen and propylene at different temperatures and pressures. The predicted isotherm adsorption data values for all the fluids, were in agreement with the experimental data. In all cases, we present different adsorbate/adsorbent pairs at two different values of the temperature $[303 - 423]$K and relative high pressures $[0 - 1]$MPa. The continuous line and circle symbols correspond to SAFT-VR approach and experimental data, respectively. Good agreement between SAFT-VR results and experimental can be observed in all cases.

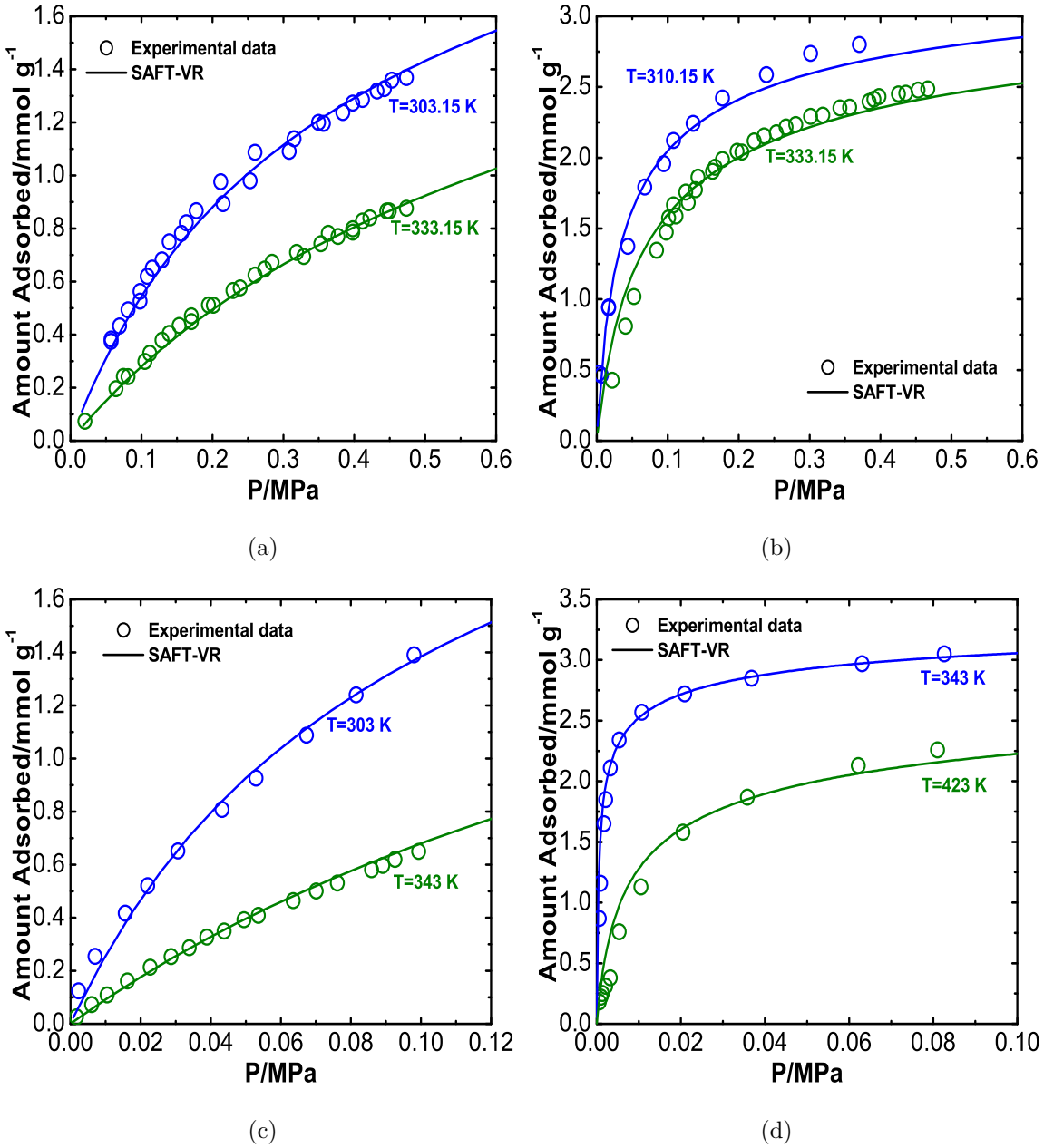

Figure 5-5: Adsorption isotherms for methane, ethane, propane and butane on different porous materials. Solid and dashed lines correspond to the SAFT-VRQ and SAFT-VR results, respectively. Symbols correspond to experimental data. (a) methane adsorption on BDH-activated carbon at 303.15, and 333.15 K,[57] (b) ethane adsorption on BDH-activated carbon at 310.15, and 333.15 K,[57] (c) propane on NSG silica gel at 303, and 343 K,[58] (d) butane adsorption on Na-Y zeolite at 343, and 423 K.[59]

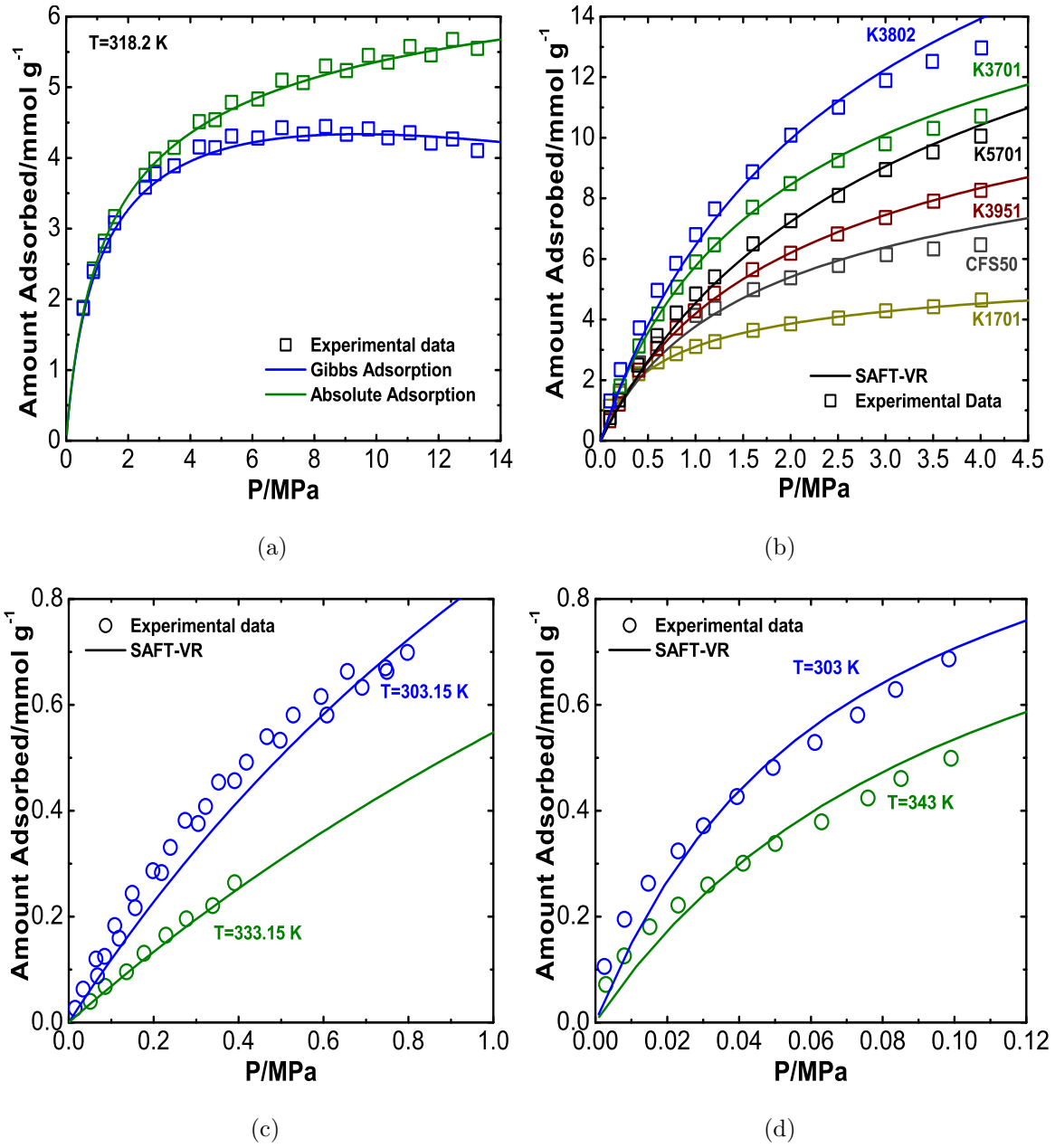

Figure 5-6: Adsorption isotherms for methane, nitrogen and propylene on different porous materials. Solid and dashed lines correspond to the SAFT-VRQ and SAFT-VR results, respectively. Symbols correspond to experimental data. (a) methane adsorption on dry activated carbon at 318.2 K,[55] (b) methane adsorption on microporous carbons at 298 K,[56] (c) nitrogen adsorption on BDH-activated carbon,[57] (d) propylene adsorption on WSG silica gel at 303, and 343 K[58]

5.7.2 Quantum Fluids: Hydrogen

Predictions of adsorption isotherms for classical systems have been detailed in previous work for molecular fluids and their mixtures[24,25,30] as well as for asphaltenes in porous materials.[31] The molecular parameters required to be determined for non-associating systems are seven, assuming that the diameter of the particles is not modified by being adsorbed onto a surface. The parameters are related to the three types of SW interactions required by the theory, i.e., a) particle-particle interaction for the bulk phase: σ, λ, ϵ; b) particle-particle interaction for the adsorbed phase: σ, λ_{ads}, ϵ_{ads}; c) particle-wall interaction: λ_w, ϵ_w.

Bulk parameters are obtained from experimental data for saturated liquid densities and vapor pressures, and their values are independent of the adsorption process; the values reported in Table 5.3 for bulk molecular hydrogen were determined with this procedure, as reported in Ref. [33]. In this way, there is complete transferability and it is not necessary to obtain new fitted values to describe the bulk phase in an adsorption isotherm. The parameters to obtain are then reduced to four: λ_{ads}, ϵ_{ads}, λ_w, ϵ_w. From the pioneering work by Sinanoglu and Pitzer,[44] it is known that the pair interaction between molecules is modified by the presence of a surface and that the energy depth for adsorbed particles is reduced with respect to its bulk phase.

Table 5.3: Molecular parameters used to describe the adsorption of classical and quantum hydrogen on different surfaces. Parameters λ, σ and ϵ, corresponding to the bulk phase, were taken from reference [33]. Particles adsorbed have the same diameter σ, whereas the SW attractive parameters (λ_{ads}, ϵ_{ads}) were obtained following the same procedure used in our previous work.[24,25,30] The particle-wall SW attractive range is given by λ_w.

Substance	λ	σ/Å	(ϵ/k)/K	λ_{ads}	(ϵ_{ads}/k)/K	λ_w
Classical H_2	1.7184	3.0232	18.0805	1.7122	14.4644	0.8165
Quantum H_2	1.7114	2.8983	19.9291	1.7009	15.9433	0.8165

Theoretical estimations of the range of reduction allowed us to select as a fixed value for all the systems $\epsilon_w = 0.8\epsilon$, as done in previous work for classical adsorption.[23–25,30,31] On the other hand, critical temperatures for adsorbed monolayers of different substances follow approximately the relationship $T_c^{ads} \approx 0.4T_c^b$,[16,18] where T_c^{ads} and T_c^b are the adsorbed and bulk critical temperatures, respectively. This result

is exact for the ratio of the critical temperatures for the two- and three-dimensional Ising models for closed packed lattices[60] and agrees very well with results for 2D and 3D Lennard-Jones fluids.[21] The range λ_{ads} as a function of λ is then obtained from the theoretical expressions for T_c^{ads} and T_c^b and its ratio. In this way, the parameters required to be adjusted to reproduce experimental adsorption isotherms are restricted only to λ_w and ϵ_w. From physical considerations about the formation of a monolayer, $0.1305 \leq \lambda_w \leq 0.8165$,[23] we have selected the highest value, $\lambda_w = 0.8165$. In this way, the only parameter required to be fitted to experimental data is ϵ_w. The standard value used for S is the Brunnauer-Emmett-Teller area,[42,43] S_{BET}, that is given in Table 5.4 as reported by different experimental studies for several materials.

Table 5.4: Optimized values for the particle-wall energy parameter ϵ_w for hydrogen adsorption onto different substrates. Results are given for the classical (C) and quantum (Q) adsorption SAFT-VR methods used in this work. Experimental values of the BET specific surface area (S_{BET}) and isosteric heats q_{st} are reported. The different substrates correspond to metal organic frameworks (MOF), activated carbon (DAC AX-21) and graphene.

Adsorbent	$S_{BET}/\mathrm{m^2g^{-1}}$	T/K	q_{st}/kJ mol^{-1}	ϵ_w(C)/kJ mol^{-1}	ϵ_w(Q)/kJ mol^{-1}
MOF-5	3800[61]	77	–	2.45	2.24
MOF-205	4460[61]	77	–	2.60	2.25
MOF-210	6240[61]	77	–	2.12	2.34
DAC AX-21	2800[62]	35	6.00-7.60[62]	5.04	6.54
		40		5.04	6.54
		45		5.04	5.88
		77		3.23	3.16
		93		3.23	3.16
		113		3.23	3.16
Graphene	640[63]	77	5.14-6.37[64]	3.64	3.46
		123		4.19	4.03
		173		4.21	4.23

Adsorption isotherms of hydrogen adsorbed onto different materials are presented in Fig. 5-7, using the set of parameters given in Tables 5.4 and 5.5. Following the procedure outlined previously, results were obtained comparing with experimental data published for several adsorbents with high porosity and high specific area such as metal-organic frameworks (MOF), graphene and dry activated carbon.

Classical and quantum approximations are compared with experimental data for adsorption of hydrogen onto dry activated carbon (AX-21) in Figures 5-7(a) and 5-7(b). At low temperatures (T = 35 K, 40 K and 45 K) quantum predictions improve the classical results in all the cases, as observed in Figure 5-7(a), whereas in Figure 5-7(b) the results correspond to higher temperatures (T = 77 K, 93 K and 113 K), where SAFT-VRQ gives a better prediction for T = 77 K.

Table 5.5: Experimental values of the BET specific surface area (S_{BET}) use to obtain the adsorption isotherms of hydrogen at different temperatures.

Adsorbent	$S_{BET}/\mathrm{m^2g^{-1}}$	Ref.	Adsorbent	$S_{BET}/\mathrm{m^2g^{-1}}$	Ref.
DAC AX-21	2800	[62]	IRMOF-1	4180	[68]
MOF-5	3800	[61]	IRMOF-6	3300	[68]
MOF-205	4460	[61]	IRMOF-11	2350	[68]
MOF-210	6240	[61]	HKUST-1	2260	[68]
Graphene	640	[63]	MSC-30	3244	[66]
ZTC-1	1691	[66]	ZTC-2	2964	[66]
MSC-30	3244	[66]	CNS-201	1440	[66]
PCN-11	2442	[67]	ZTC-3	3591	[66]

A similar pattern is observed when other substrates are considered, like Metal Organic Frameworks (Fig. 5-7(c)) and graphene nanosheets (Fig. 5-7(d)). In the first case all the isotherms correspond to the same temperature T = 77 K), and the differences between the classical and quantum predictions is noticeable and in overall SAFT-VRQ gives a slight better prediction. The case of graphene behaves similarly, since for T = 77K the quantum approach gives better agreement with experimental data, and at higher temperatures there is not a significant difference between theories.

On the other hand, adsorption isotherms of hydrogen adsorbed onto isoreticular metal organic frameworks (IRMOF), microporous metal organic frameworks (PCN-11), zeolite-templated carbon (ZTC) and superactivated carbon (MSC-30) are shown in Fig. 5-8, using the set of parameters reported in Table 5.6. In this table, fitted values of the scaled particle-wall energy parameter, ϵ_w/ϵ, are reported for the corresponding adsorption isotherm temperature.

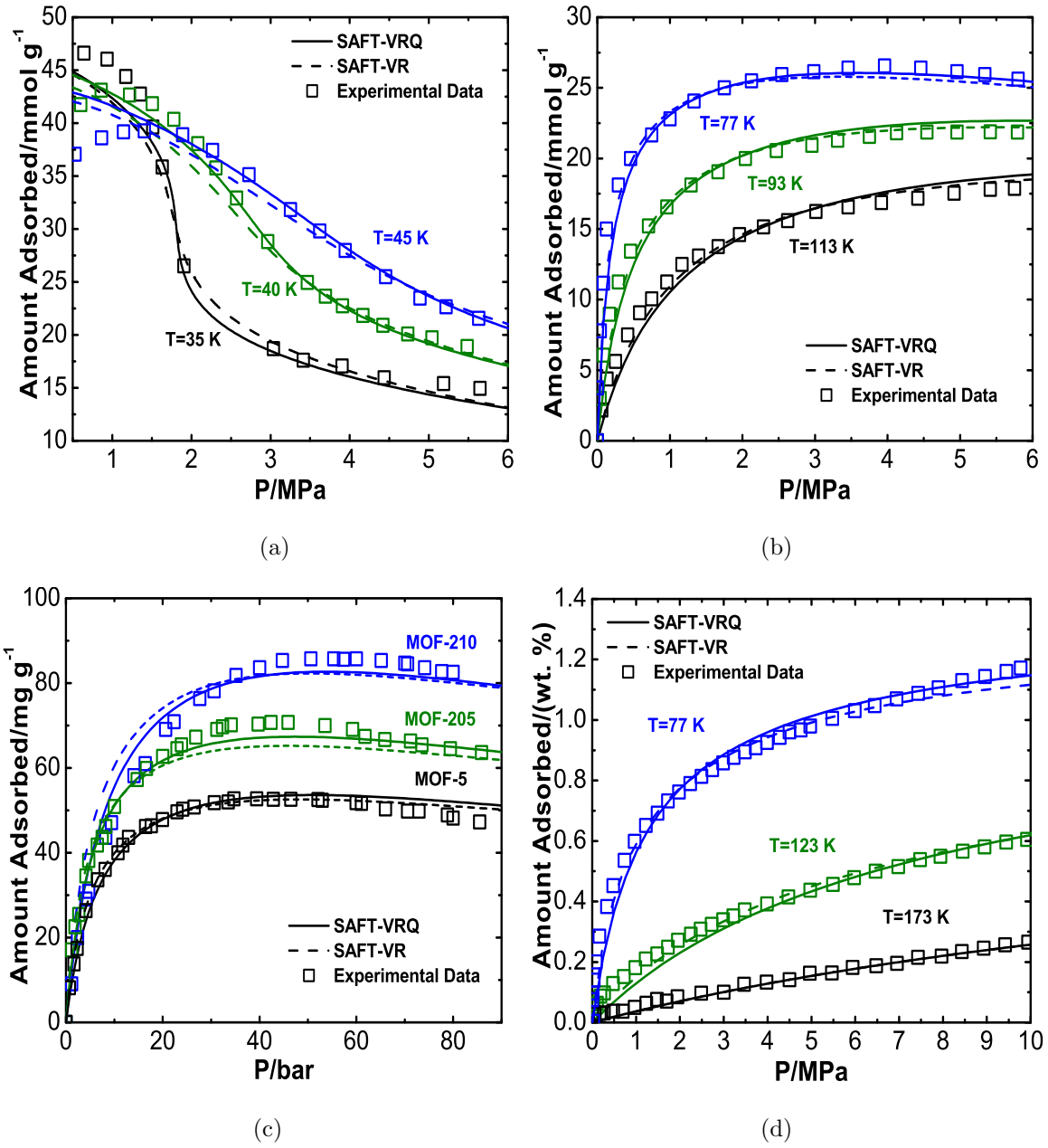

Figure 5-7: Adsorption isotherms of hydrogen on differents porous materials. Solid and dashed lines correspond to the SAFT-VRQ and SAFT-VR prediction respectively. The symbols correspond to experimental data. Porous surface materials presented are: (a) hydrogen on dry activated carbon AX-21 at 35, 40, and 45 K,[62,69,70] (b) hydrogen on dry activated carbon AX-21 at 77, 93, and 113 K,[62,69,70] (c) hydrogen on metal-organic frameworks (MOF) at 77K,[61] (d) hydrogen on graphene nanosheets at 77, 123 and 173K.[63]

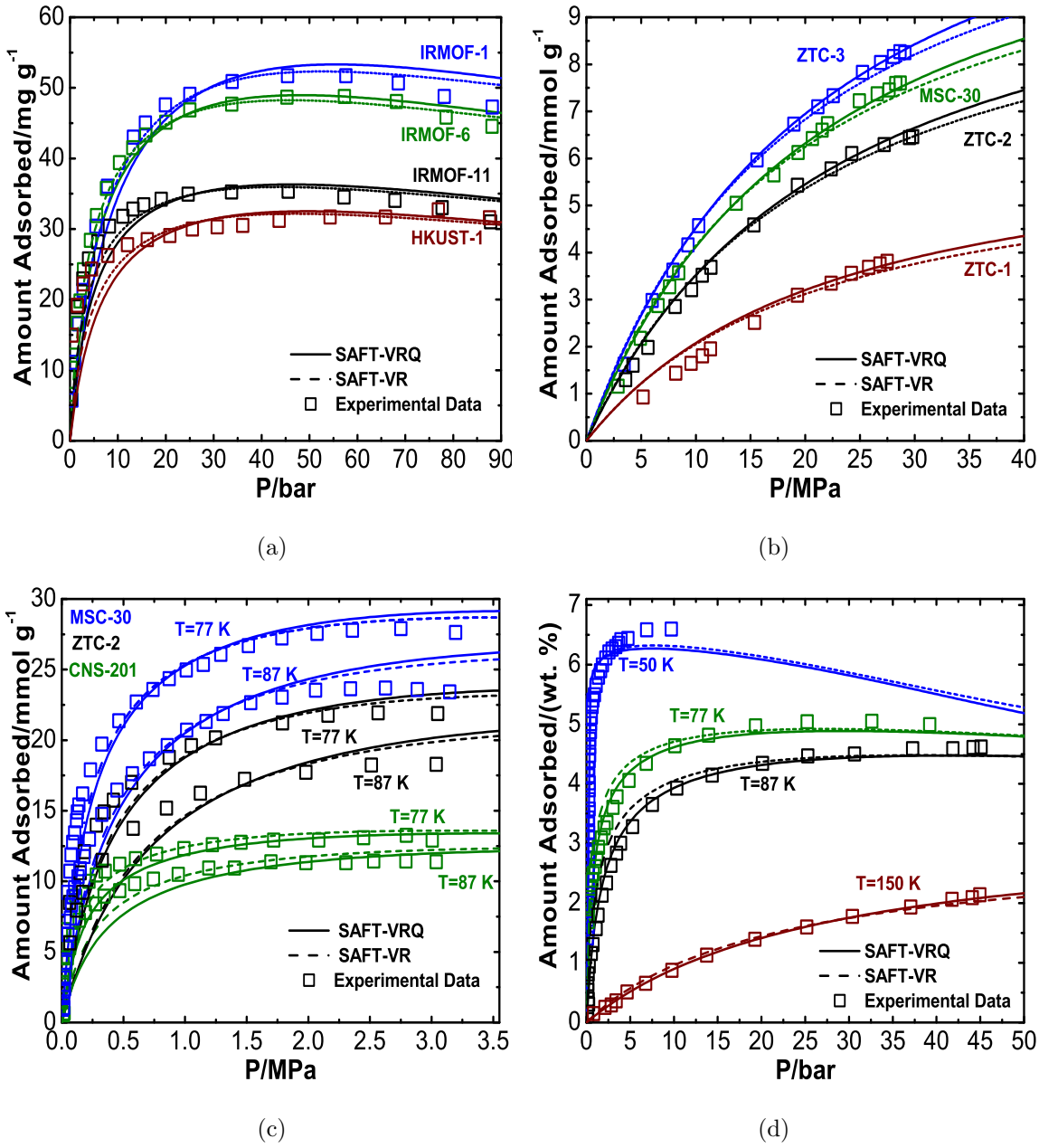

Figure 5-8: Adsorption isotherms of hydrogen on differents porous materials. Solid and dashed lines correspond to the SAFT-VRQ and SAFT-VR prediction respectively. The symbols correspond to experimental data. Porous surface materials presented are: (a) hydrogen on microporous metal-organic framework IRMOF-1, IRMOF-6, IRMOF-11 and HKUST-1 materials at 77 K,[65] (b) hydrogen on zeolite-templated ZTC-1, ZTC-2, ZTC-3 and superactivated carbon MSC-30 at 298 K,[66] (c) hydrogen on superactivated carbon MSC-30, zeolite-templated ZTC-2, and activated carbon CNS-201 at 77 and 87 K,[66] (d) hydrogen on PCN-11 at 50, 77, 87 and 150 K.[67]

Table 5.6: Optimized values for the scaled particle-wall energy parameter ϵ_w for hydrogen adsorption onto different substrates. Results are given for the classical (C) and quantum (Q) adsorption SAFT-VR methods used in this work. The different substrates correspond to isoreticular metal organic frameworks (IRMOF), microporous metal organic frameworks (PCN-11), zeolite-templated carbon (ZTC) and superactivated carbon (MSC-30).

Adsorbent	T/K	ϵ_w/ϵ (C)	ϵ_w/ϵ (Q)	Adsorbent	T/K	ϵ_w/ϵ (C)	ϵ_w/ϵ (Q)
IRMOF-1[65]	77	14.7	12.1	ZTC-1[66]	298	16.8	15.5
IRMOF-6[65]	77	17.3	14.3	ZTC-2[66]	298	16.5	15.1
IRMOF-11[65]	77	18.2	15.0	ZTC-3[66]	298	17.3	15.8
HKUST-1[65]	77	16.8	13.8	MSC-30[66]	298	17.5	15.9
PCN-11[67]	50	29.0	26.5	PCN-11[67]	87	27.5	22.5
PCN-11[67]	77	28.0	23.0	PCN-11[67]	150	23.0	20.0

Fig. 5-8 shows classical and quantum adsorption isotherms predictions using SAFT-VRQ approach compared with experimental data at high pressures. In Fig. 5-8(a), adsorption isotherms of hydrogen on microporous metal-organic framework materials denoted by IRMOF-1, IRMOF-6, IRMOF-11 and HKUST-1 at $T = 77K$,[65] are presented. Hydrogen adsorption predictions at room temperature onto zeolite-templated denoted by ZTC-1, ZTC-2, ZTC-3 and superactivated carbon MSC-30 are shown in Fig. 5-8(b). This figure shows that quantum effects are not remarkable at low pressures but becomes to be significant at high pressures ($P > 20MPa$).

Fig. 5-8(c) shows the experimental and predicted adsorption isotherms for hydrogen at $T = 77$ and $87K$. Here, superactivated carbon MSC-30, zeolite-templated ZTC-2, and activated carbon CNS-201 adsorbents are compared. In all the cases, the amount adsorbed representation are reasonably very accurate taking into account the range of experimental data. Adsorption isotherms for hydrogen onto microporous metal organic frameworks denoted by PCN-11 at T=50, 77, 87 and 150 K are shown in Fig. 5-8(d). Here, the correponding lower BET surface area value reported by the authors in reference [67] was not taken into account in this work. Therefore, the adsorption isotherms were obtained using an especific Langmuir surface area value of $S_{BET} = 2442$, with good results in all cases.

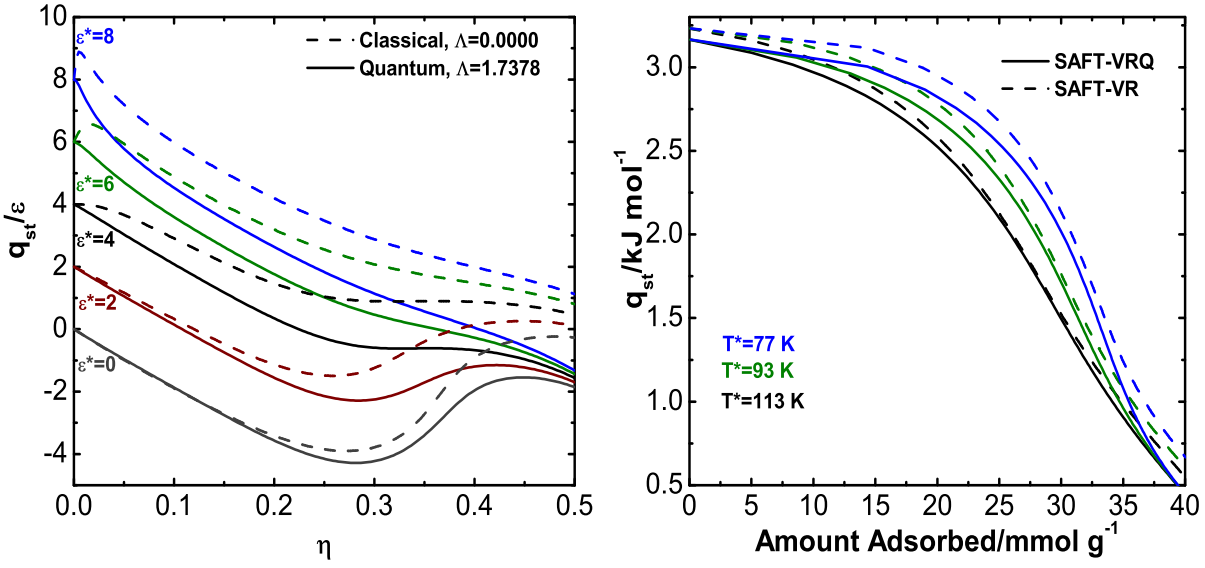

(a) (b)

Figure 5-9: (a) Predictions for the isosteric heat of adsorption, q_{st}, as a function of the three-dimensional packing fraction η, for a monomeric SW fluid with a range of $\lambda = 1.5$ adsorbed onto a planar wall at $T* = 1.5$. The wall-particle interaction is described by a SW potential with a fixed range $\lambda_w = 0.2453$ and several values for the energy ratio $\epsilon^* = \epsilon_w/\epsilon$. Solid and dashed lines correspond to the theoretical predictions obtained from SAFT-VRQ ($\Lambda = 1.7378$) and SAFT-VR ($\Lambda = 0$), respectively, where Λ is the de Boer's quantumness parameter. (b) Isosteric heat of hydrogen on dry activated carbon AX-21 at 77, 93, and 113 K.[62,69,70] Solid and dashed lines correspond to the theoretical predictions obtained from SAFT-VRQ and SAFT-VR, respectively, as indicated by the value of the de Boer's quantumness parameter Λ.

In Fig. 5-9(a), predictions are presented for the isoteric heat of adsoption, q_{st}, as a function of the bulk 3D packing-fraction η, for a monomeric SW with range $\lambda = 1.5$ adsorbed onto a planar wall at $T^* = kT/\epsilon = 1.5$. Results are given for several values of the energy ratio $\epsilon^* = \epsilon_w/\epsilon$. Classical and quantum isosteric heat predictions are presented for each value of ϵ^*, indicated by the values of the de Boer's quantumness parameter, $\Lambda = 0$ and 1.7378, respectively. As can be observed in this figure in the limit of low densities, $q_{st}/\epsilon = \epsilon^*$, classical and quantum predictions are presented for isosteric heat of hydrogen onto dry activated carbon (AX-21) in Fig. 5-9(b). In all the cases, in the limit of low adsorption amount, the results are in concordance with the isosteric heat values reported in Table 5.4 for hydrogen on dry activated carbon AX-21 at 77, 93 and 113 K.

Finally, it is important to stress that the values obtained for the energy ϵ_w are very

close to the experimental values derived from the isosteric adsorption heat, as given in Table 5.4. The isosteric heat gives information of the strength of the interaction between an adsorbate and a solid adsorbent.[71] This feature remarks that the present approach uses parameters with a clear molecular basis, and can be very useful to give accurate estimations of the binding energies in adsorption process where experimental data is not available.

Conclusions

In this chapter, we have presented an extension of the SAFT-VR theory for confined fluids introducing quantum corrections to describe adsorption of hydrogen onto several substrates. The theory relies on the determination of seven parameters, assuming that the size σ of the particles is the same for bulk and adsorbed fluids. These parameters are related to the SW interactions used to model the particle-particle potential in the bulk and adsorbed phases, and the particle-wall potential. The diameter σ and the SW bulk parameters ϵ and λ can be determined by phase equilibria properties of the bulk phase and can be transfered to the adsorption model. The SW parameters for the adsorbed phase, ϵ_{ads} and λ_{ads}, can be determined from knowing the modification of the well potential by the substrate and the ratio of the critical temperatures of the adsorbed and bulk phases. These quantities have been determined for a wide range of systems and allows us to use the relations $\epsilon_{ads} = 0.8\epsilon$ and $R_c = 0.4$. The range of the SW particle-wall interaction can also be fixed as $\lambda_w = 0.8165$, corresponding to the theoretical maximum value that allows the formation of an adsorbed monolayer. In this way, the remaining parameter is the energy depth ϵ_w, that is obtained by fitting to experimental data. As discussed in this chapter, ϵ_w is also related to the isosteric heat capacity in its low density value. We have found that quantum corrections have a noticeable effect for hydrogen adsorbed onto different substrates for temperatures $T \leq 77K$, according to the systems studied here: graphene, activated carbon and metallic organic frameworks. In the model developed in this chapter we have not considered the possibility of having adsorption of reacting hydrogen; however, in the literature there are two remarkable cases: the first case is the adsorption of associating classical fluids[30] and the second case is the SAFT-VR model for reacting systems in bulk fluids.[72] These developments could be used together to predict the thermodynamics of reacting adsorbed systems.

BIBLIOGRAPHY

[1] V. A. Goltsov, T. N. Veziroglu, *Int. J. Hydrogen Energy* **26**, 909 (2001).

[2] J. Yang, A. Sudik, C. Wolverthon, D. J. Siegel, *Chem. Soc. Rev.* **39**, 656 (2010).

[3] V. Tozzini, V. Pellegrini, *Phys. Chem. Chem. Phys.* **15**, 80 (2013).

[4] J. J. Breenakker, V. D. Borman, S. Y. Krylov, *Chem. Phys. Lett.* **232**, 379 (1995).

[5] J. Teufel, H. Oh, M. Hirscher, M. Wahiduzzaman, L. Zhechkov, A. Kuc, T. Heine, D. Denysenko, D. Volkmer, *Adv. Mater.* **25**, 635 (2013).

[6] P. Kowalczyk, P. A. Gauden, A. P. Terzyk, *J. Phys. Chem. B* **114**, 5047 (2010).

[7] M.Felderhoff, C. Weidenthaler,R. von Helmolt, U. Eberle, *Phys. Chem. Chem. Phys.* **9**, 2643 (2007).

[8] A. W. C. Van den Berg, C. Otero, *Chem. Commun.*, 668 (2008).

[9] S. Figueroa-Gerstenmaier, C. Daniel, G. Milano, G. Guerra, O. Zavorotynska, J. G. Vitillo, A. Zecchina, G. Spotto, *Phys. Chem. Chem. Phys.* **12**, 5369 (2010).

[10] J. Landers, G. Yu, A. Neimark, *Colloids and Surfaces A*, **437**, 3 (2013).

[11] K. E. Gubbins, Y-C. Liu, J. D. Moore, J. C. Palmer,*Phys. Chem. Chem. Phys.* **13**, 58 (2011).

[12] C. Avendaño, T. Lafitte, A. Galindo, C. S. Adjiman, G. Jackson, E. Müller, *J. Phys. Chem. B* **115**, 11154, (2011).

[13] T. Lafitte, A. Apostolakou, C. Avendaño, A. Galindo, C. S. Adjiman, E. Müller, G. Jackson *J. Chem. Phys.* **139**, 154504 (2013).

[14] T. L. Hill, *J. Chem. Phys.*,**14**, 441 (1946).

[15] J. H. de Boer, *The dynamical character of adsorption*, Clarendon Press, Oxford (1953).

[16] W. D. Machin, S. Ross, *Proc. R. Soc. Lond. A***265**, 455 (1962).

[17] S. E. Hoory, J. M. Prausnitz, *Chem. Eng. Sci.***22**, 1025 (1967).

[18] J. G. Dash, *Films on Solid Surfaces*, Academic Press, New York, (1975).

[19] S. Ross, J. P. Olivier, *On Physical Adsorption*, Interscience, New York, (1964).

[20] Ch. Zhou, F. Hall, K. A. M. Gasem, R. L. Robinson, Jr., *Ind. Eng. Chem. Res.* **33**, 1280 (1994).

[21] D. Henderson, *Mol. Phys.* **34**, 301 (1977).

[22] B. M. Mishra, S. K. Sinha, *Pramana* **23**, 79 (1984).

[23] Fernando del Río, A. Gil-Villegas, *J. Phys. Chem.***95**, 788 (1991)

[24] A. Martínez, M. Castro, C. McCabe, A. Gil-Villegas, *J. Chem. Phys.* **126**, 074707 (2007).

[25] M. Castro, A. Martínez, A. Gil-Villegas, *AST* **29**, 59 (2011).

[26] S. J. Mejía-Rosales, A. Gil-Villegas, B. I. Ivlev, J. Ruíz-García, *J. Phys.: Condens. Matter* **14**, 4795 (2002).

[27] C. E. Campbell, *Helium liquids in confined geometries*, in *Microscopic approaches to quantum liquids in confined geometries*, E. Krostcheck, J. Navarro editors, Series on Advances in Quantum Many-Body Theory **4**, World Scientific, Singapore (2002).

[28] A. Gil-Villegas, A. Galindo, P. J. Whitehead, S. J. Mills, G. Jackson, A. N. Burgess, *J. Chem. Phys.* **106**, 4168 (1997).

[29] A. Galindo, L. A. Davies, A. Gil-Villegas, G. Jackson,*Mol. Phys.***93**, 241 (1998).

[30] G. Jiménez-Serratos, S. Santillán, C. Avendaño, M. Castro, A. Gil-Villegas, *Oil & Gas Sci. Tech.* **63**, 329 (2008).

[31] M. Castro, J.L Mendoza de la Cruz, E. Buenrostro-González, S. Lopéz-Ramírez, A. Gil-Villegas,*Fluid Phase Equilib.* **87**, 113 (2009).

[32] E. Buenrostro-González, C. Lira, A. Gil-Villegas, J. Wu, *AICheJ* **50**, 2552 (2004).

[33] V. M. Trejos, A. Gil-Villegas, *J. Chem. Phys.* **136**, 184506 (2012).

[34] Y. Singh, *Mol. Phys.* **27**, 1687 (1974).

[35] B. P. Singh, S. K. Sinha, *J. Chem. Phys.* **67**, 3645 (1977).

[36] B. P. Singh, S. K. Sinha, *J. Chem. Phys.* **68**, 562 (1978).

[37] N. Singh, S. K. Sinha, *J. Chem. Phys.* **69**, 2709 (1978).

[38] P. Dagaut, G. Dayma, *Int. J. Hydrogen Energy* **31**, 505 (2006).

[39] D. Henderson, *Mol. Phys.* **30**, 71 (1975).

[40] W. H. Press, S. A. Teukolsky, W. T. Vetterling, B. P. Flannery, *Numerical Recipes:The art of the scientific computing* (Cambridge University Press, 3rd ed., New York, 2007).

[41] F. Rouquerol, J. Rouquerol, K. Sing, *Adsorption by powders and porous solids*, Academic Press, London, (1999)

[42] S. Brunauer, P. H. Emmett, E. Teller, *J. Am. Chem. Soc.* **60**, 309 (1938).

[43] S. J. Gregg, K. S. W. Sing, *Adsorption, surface area and porosity*, Academic Press, 2nd edition, London, (1982)

[44] O. Sinanoglu, K. S. Pitzer, *J. Chem. Phys.* **32**, 1279 (1960).

[45] M. Castro and A. Martínez, *Adsorption* **19**, 63 (2013).

[46] F. del Río and Gil-Villegas, *J. Chem. Phys.* **95**, 788 (1991).

[47] S. Sircar, R. Mohr, C. Ristic, and M. B. Rao, *J. Phys. Chem. B* **103**, 6539 (1999).

[48] D. M. Young, A. D. Crowell, *Physical Adsorption of Gases* (Washington, Butterworths, DC, 1962).)

[49] L. L. Lee, *Molecular Thermodynamics of Nonideal Fluids*, Butherworths, United States of America (1988).

[50] M. F. Becerra Esparza, *Termodinámica molecular semiclasica de adsorción de fluidos cuánticos*, Master Degree Thesis, University of Guanajuato, 2013.

[51] E.Wigner, *Phys. Rev.* **40**, 749 (1932).

[52] J. G. Kirkwood, *Phys. Rev.* **44**, 31 (1933).

[53] V. M. Trejos, A. Gil-Villegas, A. Martínez, *J. Chem. Phys.* **139**, 184505 (2013).

[54] B.-J. Yoon, H. A. Scheraga, *J. Chem. Phys.* **88**, 3923 (1988).

[55] M. Sudibandriyo, Z. Pan, J. E. Fitzgerald, R. L. Robinson, Jr. and A. M. Gaasem, *Langmuir* **19**, 5323 (2003).

[56] D. A.-Monje, D. L.-Castelló, D. C.-Amorós, A. L.-Solano, *Microporous and Mesoporous Materials* **124**, 110 (2009).

[57] S. A. Al-Muhtaseb, F. A. Abu Al-Rub, M. A. Zarooni, *J. Chem. Eng. Data* **52**, 60 (2007).

[58] C. A. Grande, A. E. Rodrigues, *Ind. Eng. Chem. Res.* **40**, 1686 (2001).

[59] L. Wender, A. Barreau, C. Lefebvre, A. Di Lella, A. Boutin, P. Ungerer, A. H. Fuchs, *Adsorption* **13**, 439 (2007).

[60] C. Domb, *Adv. Phys.* **9**, 149; 245 (1960).

[61] H. Furukawa, N. Ko, Y. B. Go, N. Aratani, S. B. Choi, E. Choi, A. O. Yazaydin, R. Q. Snurr, M. O'Keeffe, J. Kim, O. M. Yaghi, *Science* **329**, 424 (2010).

[62] P. Bénard and R. Chahine, *Langmuir* **17**, 1950 (2001).

[63] G. Srinivas, Y. Zhu, R. Piner, N. Skipper, M. Ellerby, R. Ruoff, *Carbon* **48**, 630 (2010)

[64] Q. Zheng, X. Ji, S. Gao, X. Wang, *Int. J. Hydrogen Energy*, **38**, 10896 (2013).

[65] A. G. Wong-Foy, A. J. Matzger, O. M. Yaghi, *J. Am. Chem. Soc.* **128**, 3494 (2006).

[66] N. P. Stadie, J. J. Vajo, R. W. Cumberland, A. A. Wilson, C. C. Ahn, B. Fultz *Langmuir* **28**, 10057 (2012).

[67] X-S. Wang, S. Ma, K. Rauch, J. M. Simmons, D. Yuan, X. Wang, T. Yildirim, W. C. Cole, J. J. López, A. de Meijere, H-C. Zhou, *Chem. Mater.* **20**, 3145 (2008).

[68] S. S. Kaye, A. Dailly, O. M. Yaghi, J. R. Long, *J. Am. Chem. Soc.* **129**, 14176 (2007).

[69] P. Bénard, R. Chahine, P.A. Chandonia, D. Cossement, G. Dorval-Douville, L. Lafia, P. Lachance, R. Paggiaro, E. Poirier, *J. of Alloys and Compounds* **446**, 380 (2007).

[70] P. Bénard and Richard Chahine, *Scripta Materialia* **56**, 803 (2007).

[71] S. Builes, S. I. Sandler, R. Xiong, *Langmuir* **29**, 10416 (2013).

[72] F. A. Perdomo, B. M. Millán-Malo, G. Mendoza-Díaz, A. Gil-Villegas, *J. Mol. Liq.* **185**,8 (2013)

CHAPTER 6

SEMICLASSICAL THEORY FOR ADSORPTION OF MIXTURES

Adsorption of binary mixtures containing hydrogen onto different nanoporous materials become to be a particular interest in potential applications for adsorption-separation of gas mixtures. One of them is when the methane and carbon dioxide must be removed from the synthetic gas before hydrogen can be used effectively. We present a semiclassical theoretical framework to model isotherms adsorption of mixtures based on the statistical associating fluid theory approach for classical and quantum bulk fluids (SAFT-VRQ), and its extension to describe adsorbed systems (SAFT-VR-2D). The application of the theory relies on the use of eight molecular parameters, seven of them are obtained from the bulk vapor-liquid equilibrium, the ratio of the critical temperatures of the adsorbed and bulk phases and finally the energy depth of the surface-particle potential, ϵ_w, is obtained by fitting to experimental data from adsorption isotherms prediction of pure components. Additionally, the expression for the calculations of vapor-liquid equilibrium of binary mixtures are presented. The results were found to be in concordance with the experimental data.

6.1 Introduction

Nowadays hydrogen is a good candidate as a replacement for fossil fuels in mobile applications as fueling vehicles to protect the environment. Burning hydrogen in fuel cells is the most clean way of releasing energy, but there are other important

ways to use the hydrogen. For example, liquid hydrogen is used to fuel vehicles equipped with an inner combustion engine. Therefore, hydrogen storage is the key in the technology of clean vehicles. The storage techniques available commercially cannot afford a hydrogen vehicle potential of competition with vehicles fueled by petroleum products.[1] Additionally, conventional storage of large amounts of hydrogen is difficult and expensive because it requires employing either extremely high pressures as a gas or very low temperatures as a liquid.[2] Then practical materials with higher capacity when the weight of the tank and associated cooling or regeneration system is considered. The size and weight of these components will vary substantially depending on whether the material operates by a chemisorption or physisorption mechanism.[3] In the case of physisorption, promising adsorbent materials such as on carbon activated,[1] Metal-Organic Frameworks (MOFs),[3,4] graphene nanosheets,[5] among others, have received continuous interest as potential hydrogen storage media. In all of them, different features as surface area, porosity, size and shape are tuneable and allow further improvements.[6]

On the other hand, the design of adsorption-based processes requires two properties, the adsorption isotherm and the heat of adsorption. The adsorption of gases on solids is commonly used for the characterization of surface properties and also for the separation and capture of gases and vapors.[7] The adsorption of gases, as hydrogen, is based on the characterization of adsorption isotherms over a wide range of pressures and temperatures above the critical point of the adsorbate materials. Recently, more suitable models in order to predict adsorption isotherms are being reported in the literature. Additionally, accurate predictions of thermodynamic properties and adsorption isotherms over a wide range of temperatures and pressures would reduce the number of lengthy experiments required for performance evaluation.[8]

In this way, Statistical Associating Fluid Theory of Variable Range (SAFT-VR) has been used to study classical single-component fluids,[9] adapted for two-dimensional (2D) fluids interacting via square-well pair potential.[10–14] This approach has been applied to predict the adsorption of classical pure molecular fluids as carbon dioxide, nitrogen, propylene, methane among others, onto different adsorbed surface materials.[10–14] Recently, a semiclassical version of the SAFT-VR theory for classical and quantum bulk fluids was developed in order to predict thermodynamic properties and adsorption isotherms of quantum fluids, such as hydrogen.[15]

In this work, the semiclassical SAFT-VR approach to model quantum fluids has

been used to model the adsorption isotherms of binary mixtures of classical and quantum fluids at high pressures. The experimental data were correctly correlated with the fitted parameters from pure components, presented in previous works. Expressions for chemical potential of quantum terms in 2D and 3D were obtained and discussed widely. The adsorption isotherms were studied onto different adsorbed materials.

6.2 Mathematical Model

In this chapter, we present the theory used to describe the adsorption of a mixture of fluids onto a uniform wall, using a semiclassical approximation of 2D and 3D fluids within the SAFT-VR approach. We considered a fluid composed of a binary mixture of M-components, each i-species being formed by N_i-spherical particles of diameter σ_{ii}. The particle-particle and particle-wall interactions are modeled by square-well potentials (SW). The particle-particle SW u_{pp} interaction is given by

$$u_{pp}(r_{ij}, \sigma_{ij}, \lambda_{ij}) = \begin{cases} \infty & \text{if } \ r_{ij} \leq 0 \\ -\epsilon_{ij} & \text{if } \ 0 < r_{ij} \leq \lambda_{ij}\sigma_{ij} \\ 0 & \text{if } \ r_{ij} > \lambda_{ij}\sigma_{ij} \end{cases} \tag{6.1}$$

where r_{ij} is the interparticle distance between particles of species i and j, ϵ_{ij} and $\lambda_{ij}\sigma_{ij}$ are the energy-depth well and attractive-potential range, respectively, and σ_{ij} is the mixture diameter. On the other hand, the particle-wall is denoted as u_{pw}, and we can assume the potential as a function of the perpendicular distance of the wall. In this case, the particle-wall potential u_{pw} is given by

$$u_{pw}(z, \sigma_{ii}, \lambda_w) = \begin{cases} \infty & \text{if } \ z \leq 0 \\ -\epsilon_w & \text{if } \ 0 < z \leq \lambda_w\sigma_{ii} \\ 0 & \text{if } \ z > \lambda_w\sigma_{ii} \end{cases} \tag{6.2}$$

where z is the perpendicular distance of the particles from the wall, ϵ_w is the depth, and $\lambda_w\sigma_{ii}$ is the range of the attractive potential. In our approximation, we describe the system as being composed of two subsystems: a fluid whose particles are near to the wall, i.e., when $z \leq \lambda_w\sigma_{ii}$, which we shall refer to as the "adsorbed fluid", and a fluid whose particles are far from the wall, i.e, when $z > \lambda_w\sigma_{ii}$, i.e., the "bulk fluid".

The pair potential of the adsorbed particles u_{pp}^{ads}, only depends of the coordinates in parallel directions to the wall. Therefore, the adsorbed fluid can be approximated by a quasi-two dimensional system.

To describe the amount of particles adsorbed onto the wall, we use an analogous expression for the surface excces concentration, Γ, defined in Chapter 5, as

$$\Gamma_i = \int_0^\infty dz_i[\rho_i(z_i) - \rho_i^b] \tag{6.3}$$

where ρ_i is the density particles of species i, and ρ_i^b, is the bulk density, *i.e.*, $\rho_i(z_i \to \infty) = \rho_b$. Since the length scale of the adsorbed phase for species is defined by $\lambda_w\sigma_{ii}$, as follows

$$\Gamma_i = \int_0^{\lambda_w\sigma_{ii}} dz_i\rho_i(z_i) - \rho_i^b\lambda_w\sigma_{ii} \tag{6.4}$$

In order to obtain the density ρ_i, the thermodynamic equilibrium must be satisfied in adsorbed and bulk phases. The chemical potential of the adsorbed phase, μ_i^{ads}, and bulk phase, μ_i^{bulk} must be equal, *i.e.*,

$$\mu^b = \sum_i x_i\mu_i^b = \sum_i x_i\mu_i^{ads} = \mu^{ads} \tag{6.5}$$

where

$$\mu_i^{ads} = \left(\frac{\partial A_{ads}}{\partial N_{ads}}\right) \tag{6.6}$$

and

$$\mu_i^b = \left(\frac{\partial A_b}{\partial N_b}\right) \tag{6.7}$$

where A_b and A_{ads} are the Helmholtz free energies for the bulk and adsorbed systems formed by N_b and N_{ads} particles. The adsorbed phase, A_{ads}, can be obtained from a 2D approximation. Therefore, we need to calculate the canonical partition function of the mixture of fluids adsorbed onto a surface as

$$Q_{ads}(N_i, V_i, T) = \prod_{i=1} \frac{V_i^{N_i}}{N_i!\lambda_{Bi}^{3N_i}} Z_{ads}, \tag{6.8}$$

where V_i is the adsorbed volume, λ_B, is the de Broglie wavelength, and Z_{ads} is the

configurational partition function defined by

$$Z_{ads} = \frac{1}{V_i^{N_i}} \int d^{N_i}\vec{r} e^{-\beta U}, \tag{6.9}$$

where $\beta = 1/kT$, and U is the total interaction potential, expressed as the sum of two terms as

$$U(x^N, y^N, z^N) = \frac{1}{2} \sum_k \sum_j \sum_{S_k} \sum_{S_j} U_{pp}^{ads}(r_{s_k,s_j}) + \sum_k \sum_{S_k} U_{pw}(z_{s_k}) \tag{6.10}$$

where r_{s_k,s_j} is the distance between particles S_k and S_j corresponding to species k and j, respectively. In the case of the adsorbed fluid, the pair potential $U_{pp}^{ads}(r_{s_k,s_j})$, can described as a decoupling z-coordinate direction, and then justify a 2D approximation to describe the particle-particle potential,

$$U_{pp}^{ads}(r_{s_k,s_j}) = U_{pp}^{ads}(x_{s_k,s_j}, y_{s_k,s_j}) \tag{6.11}$$

In this way, Eq. (6.9) can be rewritten as

$$Z_{ads} = \frac{1}{V_i^{N_i}} \int d^{N_i} z e^{-\beta \sum_k \sum_{S_k} U_{pw}(z_{s_k})} \int d^{N_i} x_i d^{N_i} y_i e^{-\beta \sum_k \sum_j \sum_{S_k} \sum_{S_j} U_{pp}^{ads}(r_{s_k,s_j})/2}. \tag{6.12}$$

The adsorbed fluid can be characterized by a volume V_i, that corresponds to an adsorption area (S), and perpendicular distance between the wall and the fluid affected by the wall (z_o). Therefore, the Eq. (6.12) can be rewritten as

$$Z_{ads} = Z_{1D} Z_{2D}, \tag{6.13}$$

where

$$Z_{1D} = \frac{1}{z_0^{N_i}} \int_0^{z_0} d^{N_i} z e^{-\beta \sum_k \sum_{S_k} U_{pw}(z_{s_k})} \tag{6.14}$$

$$Z_{2D} = \frac{1}{S^{N_i}} \int d^{N_i} x_i d^{N_i} y_i e^{-\beta \sum_k \sum_j \sum_{S_k} \sum_{S_j} U_{pp}^{ads}(r_{s_k,s_j})/2}, \tag{6.15}$$

where Z_{1D} and Z_{2D} are the one and two-dimensional configurational partition functions, respectively. The distance z_o can be written as a function of the range of the attractive potential of the wall and the diameter of the particles ($z_o = \lambda_w \sigma_{ii}$). In this

way, the Eq. (6.14) can be expressed as

$$Z_{1D} = \frac{1}{(\lambda_w \sigma_{ii})^{N_i}} \int_0^{\lambda_w \sigma_{ii}} d^{N_i} z e^{-\beta \sum_k \sum_{S_k} U_{pw}(z_{s_k})} = \left[\frac{1}{\lambda_w \sigma_{ii}} \int_0^{\lambda_w \sigma_{ii}} dz e^{-\beta \sum_k \sum_{S_k} u_{pw}(z_{s_k})} \right]^{N_i}, \tag{6.16}$$

The configurational partition function Z_{1D} in Eq. (6.16) can be evaluated using the mean-value theorem, *i.e.*,

$$Z_{1D} = e^{-\beta N_i \sum_i \sum_{S_i} u_{pw}(z^*_{s_i})}. \tag{6.17}$$

where $z^*_{s_k}$ is the value of the coordinate z that guarantees the mean value of the Boltzmann factor. The canonical partition function of the adsorbed fluid is given by

$$Q_{ads} = Q^{1D}_{ads} Q^{2D}_{ads} \tag{6.18}$$

where

$$Q^{1D}_{ads} = \prod_{i=1} \frac{z_o^{N_i}}{\lambda_B^{N_i}} e^{-\beta N_i \sum_i \sum_{S_i} u_{pw}(z^*_{s_i})} \tag{6.19}$$

$$Q^{2D}_{ads} = \prod_{i=1} \frac{S^{N_i}}{N_i! \lambda_B^{2N_i}} \int d^{N_i} x_i d^{N_i} y_i e^{-\beta \sum_k \sum_j \sum_{S_k} \sum_{S_j} U^{ads}_{pp}(r_{s_k, s_j})/2}, \tag{6.20}$$

Rearranging the Eqs. (6.18-6.20) we can obtain

$$Q_{ads} = Q^{2D}_{ads} \prod_{i=1} \left(\frac{\lambda_w \sigma_{ii}}{\lambda_{Bi}} \right)^{N_i} e^{-\beta N_i \sum_i \sum_{S_i} u_{pw}(z^*_{s_i})}, \tag{6.21}$$

Applying the standard relation $A_{ads} = -kT \ln(Q_{ads})$, the Helmholtz free energy of the absorbed fluid is given by

$$\frac{A_{ads}}{NkT} = \frac{A_{2D}}{NkT} - \sum_i x_i \left[\ln \left(\frac{\lambda_w \sigma_{ii}}{\lambda_B} \right) + \beta m_i \epsilon_{wi} \right]. \tag{6.22}$$

where $x_i = N_i/N$ is the molar fraction of species i, and A_{2D} is the Helmholtz free energy of a two-dimensional fluid interacting via the potential U^{ads}_{pp}, that is given in terms of classical and quantum contributions,

$$\frac{A_{2D}}{NkT} = \frac{A^C_{2D}}{NkT} + \frac{A^Q_{2D}}{NkT} \tag{6.23}$$

where the superindexes C and Q denote classical and quantum contributions, respectively. The classical A_{2D} contribution can be described by using perturbation theory of hard-disks as a reference fluid,

$$\frac{A_{2D}^{\mathrm{C}}}{NKT} = \frac{A_{2D}^{\mathrm{ideal}}}{NkT} + \frac{A_{2D}^{\mathrm{mono}}}{NkT} + \frac{A_{2D}^{\mathrm{chain}}}{NkT} \tag{6.24}$$

where A^{ideal} is the ideal free energy, A^{mono} is the excess free energy due to monomer segments, and A^{chain} is the contribution due to the formation of the chains of monomers. Following the high-temperature expansion theory of Barker and Henderson,[16,17]

$$\frac{A_{2D}^{C}}{NKT} = \sum_i x_i \ln(\rho_i^{2D}\lambda_{Bi}^2) - 1 + S\left(a^{\mathrm{HD}} + \beta a_1^{2D} + \beta^2 a_2^{2D}\right) + a_{2D}^{\mathrm{chain}} \tag{6.25}$$

where $S = \sum_k x_k m_k$, a^{HD} is the free energy for a mixture of hard disks, a_1^{2D}, a_2^{2D} are the first and second-order perturbation terms, respectively, and a_{2D}^{chain} is the Helmholtz free energy contribution due to formation of chains. The quantum contribution for the 2D-mixture system is given by

$$\frac{A_{2D}^{Q}}{NkT} = \gamma_x \left(\frac{\beta\epsilon_x}{\pi}\right)^{1/2} \sum_k \sum_j x_{s,k} x_{s,j} \Lambda_{kj} \mathrm{g}_{\mathrm{2D}}^{\mathrm{SW}}(\sigma_x; \lambda_x) \tag{6.26}$$

The properties of the bulk fluid may also be obtained as

$$\frac{A_b}{NkT} = \frac{A_{3D}^{C}}{NkT} + \frac{A_{3D}^{Q}}{NkT} \tag{6.27}$$

where the superidices C and Q denote classical and quantum contributions respectively. The classical A_{3D} contribution can be described by using perturbation theory of hard-disks as a reference fluid,

$$\frac{A_{3D}^{C}}{NKT} = \frac{A_{3D}^{\mathrm{ideal}}}{NkT} + \frac{A_{3D}^{\mathrm{mono}}}{NkT} + \frac{A_{3D}^{\mathrm{chain}}}{NkT} \tag{6.28}$$

where A^{ideal} is the ideal free energy, A^{mono} is the excess free energy due to monomer segments, and A^{chain} is the contribution due to the formation of the chains of monomers. The properties of the bulk 3D-fluid may also be obtained by perturbation theory at

the same expansion order in β,[18]

$$\frac{A_{3D}^{C}}{NKT} = \sum_{i} x_i \ln(\rho_i^{3D}\lambda_{Bi}^{3}) - 1 + S\left(a^{\mathrm{HS}} + \beta a_1^{3D} + \beta^2 a_2^{3D}\right) + a_{3D}^{\mathrm{chain}} \tag{6.29}$$

where a^{HS} is the free energy for a mixture of hard-sphere, a_1^{3D}, a_2^{3D} are the first and second-order perturbation terms, respectively; and a_{3D}^{chain} is the Helmholtz free energy contribution due to the formation of chains. The quantum contribution for the 3D-mixture system is given by

$$\begin{aligned}\frac{A_{3D}^{Q}}{NkT} =& \frac{1}{(2\pi)^2} t_x \left[\sum_{k}\sum_{j} x_{s,k}x_{s,j}\Lambda_{k,j}^{2}\left(\frac{\partial a_1^{3D}}{\partial \lambda_x}\right)\right] \times \left[(t_x - \frac{2}{\lambda_x} - \mu_1(\zeta_x)\right. \\ & \left. -2\mu_2(\zeta_x)\lambda_x - 3\mu_3(\zeta_x)\lambda_x^2)\right]\end{aligned} \tag{6.30}$$

where $t_x = \left(1 - e^{-\beta\epsilon_x}\right)$. The mathematical expressions for the Helmholtz free energy contributions of bulk and 2D-mixtures are presented on Appendix A and B, respectively. The methodology described in this section can be described by discontinuous potentials.[11]

6.3 Results

6.3.1 Adsorption of classical fluids

In this section, we presented the semiclassical version of the SAFT-VRQ theory applied in the prediction of the binary adsorption isotherms of classical fluids. We study the case of the adsorption of chain molecule fluids, assuming that the monomer-monomer and monomer-wall interactions can be described via square-well potentials. The theory presented in this section was applied to two different systems adsorbed onto activaded carbon.[19] The adsorption isotherms were obtained for two system: methane/carbon dioxide and nitrogen/methane onto activated carbon at $T = 318.2$ K. The molecular parameters for the pure components are reported in Table 6.3.1. The pure parameters are the number of segments, m, the variable range parameter, λ, the diameter of monomer segments, σ, the energy depth, ϵ, the adsorption variable range parameter, λ_{ads}, the adsorption energy parameter, ϵ_{ads}, the particle-wall attractive range, λ_w, and the particle-wall potential parameter, ϵ_w.

Table 6.1: Molecular parameters used to describe the adsorption of classical fluids on different surfaces. Parameters λ, σ and ϵ, corresponding to the bulk phase, were taken from references [13,14]. Particles adsorbed have the same diameter σ, whereas the SW attractive parameters (λ_{ads}, ϵ_{ads}) were obtained following the same procedure used in our previous work.[10,11,13] λ_w is the particle-wall SW attractive range and ϵ_w is the particle-wall potential parameter.

Substance	m	λ	σ/Å	(ϵ/k)/K	λ_{ads}	(ϵ_{ads}/k)/K	λ_w	(ϵ_w/ϵ)
CH_4	1.00	1.444	3.6700	168.800	1.200	135.040	0.8165	7.60
CO_2	2.00	1.5257	2.7864	179.270	1.262	143.416	0.8165	3.95
N_2	1.33	1.5500	3.1590	81.485	1.474	65.188	0.8165	9.10

The theory requires eight molecular parameters for each pure compound; four of these (m, σ, ϵ, and λ), were obtained from previous studies.[10–14] The relations for the SW attractive parameters (λ_{ads}, ϵ_{ads}), particle-wall parameter (λ_w) and particle-wall potential parameter (ϵ_w), were explained in Chapter 5. To follow up, it is convenient to summarize the way to translate between theoretical and experimental variables. If we denote by n_i the number of moles of the adsorbed fluid, then it is related either to Γ_{abs} through the equation,

$$(n/m_s)_i = \frac{(\Gamma_{abs}\sigma_{ii}^2)m_i S_i}{N_A \sigma_x^2} \tag{6.31}$$

where $\Gamma_{abs}\sigma_{ii}^2 = 4\gamma/\pi$, with $\gamma_i = x_i\gamma$, and $\sigma_x^2 = \sum_i x_i m_i \sigma_i^2$. Expressions for η and γ of the mixture are obtained in Appendix A and B, respectively. The relation n/m_s is known as *amount of adsorbed* fluid. The standard value used for S is the Brunnauer-Emmett-Teller area,[20,21] S_{BET}, that is reported by different experimental studies for several materials.

Theoretical results and experimental data for pure carbon dioxide, methane and nitrogen onto dry activated carbon are compared in Fig. 6-1. Here the adsorption isotherms are reported as absolute adsorption recently explained in Chapter 5.

The BET area value was taken from Sudibarandiyo *et al.*,[19] which has value of 850 m^2/g, for the reported isotherms we found two values of 580 m^2/g for nitrogen and 850 m^2/g for methane and carbon dioxide. In the limit case of $x_i \to 1$, the results converge to the behavior of pure component i. As can be observed the Fig. 6-2(a) in the limit of $x_{CH_4} \to 1$ the results converge to the pure methane experimental data.

Similar results are observed for CO_2 and N_2 in Figs. 6-2(b) and 6-2(d).

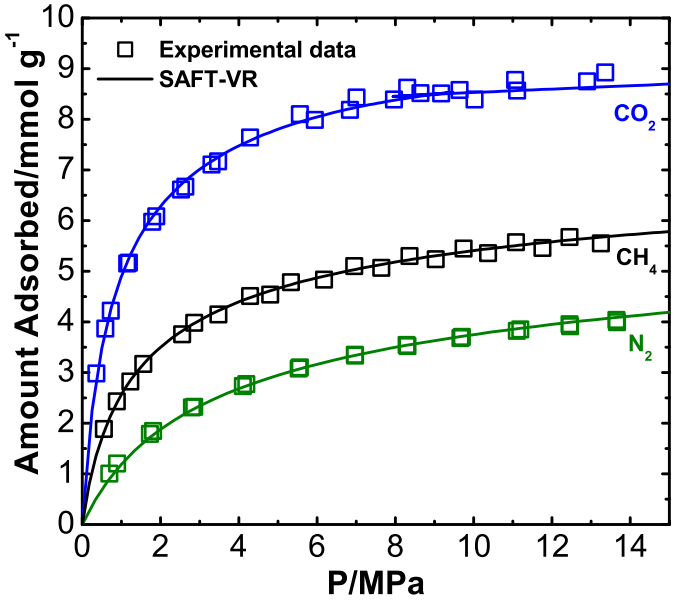

Figure 6-1: Absolute amount adsorbed for the adsorption of carbon dioxide (CO_2), methane (CH_4) and nitrogen (N_2) onto dry activated carbon at T=318.2 K. The solid lines and symbols correspond to the SAFT-VR prediction and experimental data,[19] respectively.

Experimental and predicted adsorption isotherms for CH_4 + CO_2 binary system is shown in Figs. 6-2(a) and 6-2(b). Predictions with optimal particle-wall parameters, ϵ_w obtained from experimental data of pure components are compared. It can be appreciated that predictions corresponding to molar fraction of CH_4 are slightly better than those corresponding to molar fraction of CO_2.

Figs. 6-2(c) and 6-2(d) shows experimental and predicted adsorption isotherms for CH_4 + N_2 binary mixture. In these two figures, the predictions with the optimal particle-wall parameters, ϵ_w are accurate related to the experimental data. Mereover, deviations between predictions and experimental data for the adsorption isotherms of N_2 (Fig. 6-2(d)) are better than those corresponding Fig. 6-2(c).

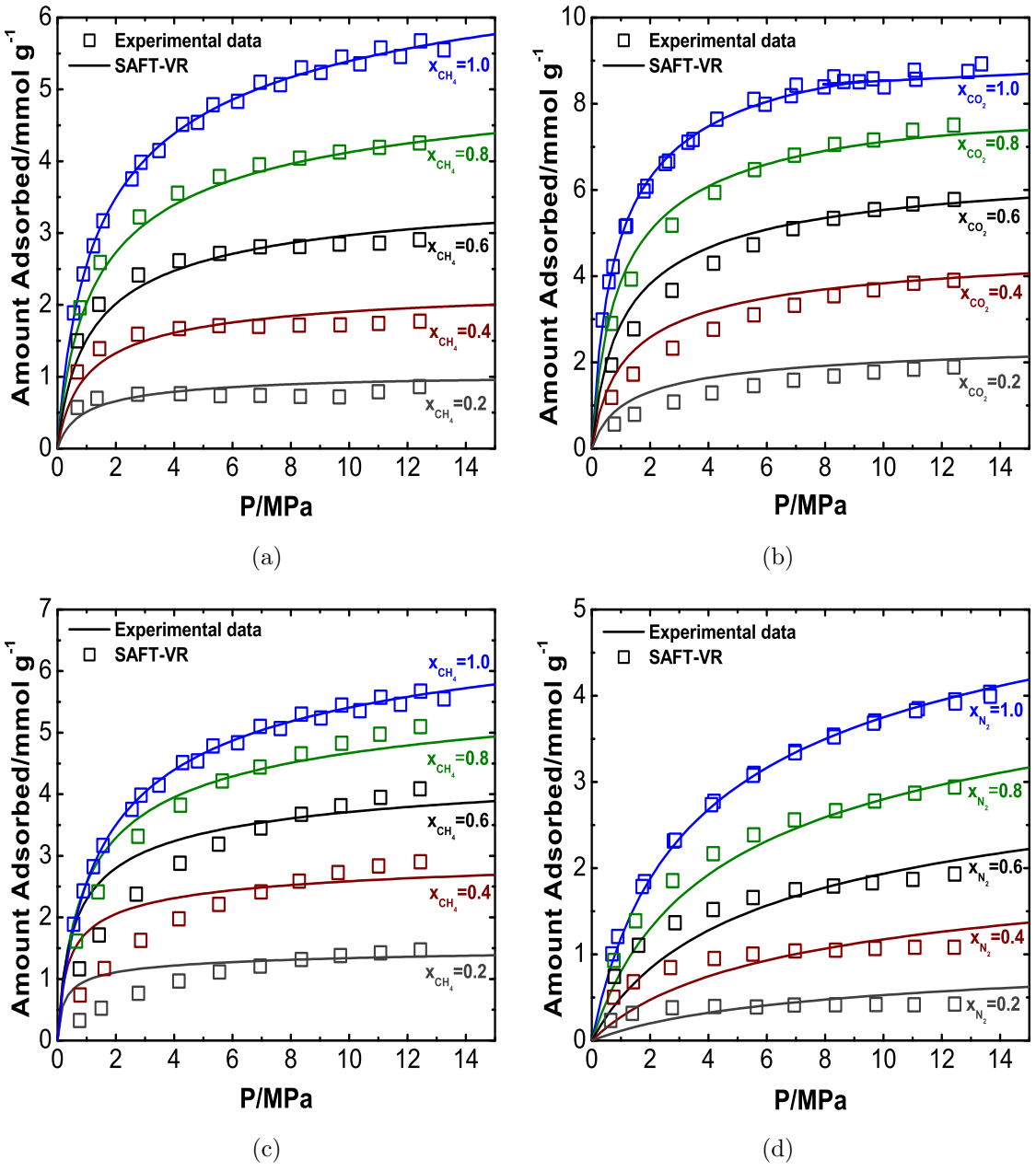

Figure 6-2: Absolute amount adsorbed for the adsorption of of CH_4/CO_2 and CO_2/N_2 mixtures. In all cases, the adsorption isotherms were obtained using dry activaded carbon at T=318.2 K. Solid lines and symbols correspond to the SAFT-VR prediction and the experimental data,[19] respectively. Adsorption isotherms presented are: (a) Adsorption of CH_4 on the mixture CH_4/CO_2 (b) Adsorption of CO_2 on the mixture CO_2/CH_4 (c) Adsorption of CH_4 on the mixture CH_4/N_2 (d) Adsorption of N_2 on the mixture CH_4/N_2

6.3.2 Adsorption of Quantum fluids

In this section, the theory presented in this chapter was applied to two different systems adsorbed onto dry activated carbon AX-21. The systems studied were hydrogen + neon and hydrogen + helium-4. The molecular parameters for the pure components are reported in Table 6.3.2. The eight molecular parameters required for each pure compound were explained in detail in Chapter 5. Fig. 6-3 presents a predictive comparison between the theoretical and experimental adsorption isotherms at T=77 K. The results are reported as Gibbs amount adsorbed of the component i at different values of molar concentration. In all cases, the surface area, S_{BET} value of 2800 m^2/g was taken from the experimental value reported by Bénard *et. al.*,.[22–24] In Table 6.3.2, the de Boer's quantumness parameter $\Lambda = h/\sigma\sqrt{m\epsilon}$, take values from classical fluids ($\Lambda = 0$) to quantum fluids as helium ($\Lambda = 4.2409$).

Table 6.2: Molecular parameters used to describe the adsorption of classical and quantum fluids on different surfaces. Parameters λ, σ and ϵ, corresponding to the bulk phase, were taken from reference [33]. Particles adsorbed have the same diameter σ, whereas the SW attractive parameters (λ_{ads}, ϵ_{ads}) were obtained following the same procedure used in our previous work.[24,25,30] λ_w is the particle-wall SW attractive range, ϵ_w is the particle-wall potential parameter and $\Lambda = h/\sigma\sqrt{m\epsilon}$ is the de Boer's quantumness parameter.

Substance	λ	σ/Å	(ϵ/k)/K	λ_{ads}	(ϵ_{ads}/k)/K	λ_w	(ϵ_w/ϵ)	Λ
H_2	1.7184	3.0232	18.0805	1.7122	14.4644	0.8165	21.5	0
	1.7114	2.8983	19.9291	1.7009	15.9433	0.8165	19.1	2.3921
Ne	1.5442	2.6914	32.8449	1.4506	26.2760	0.8165	18.0	0
	1.5328	2.6949	33.4450	1.4304	15.9433	0.8165	19.0	0.6264
He	1.7260	2.9860	2.6943	1.7248	2.1554	0.8165	28.0	0
	1.6799	2.7595	3.4973	1.6531	15.9433	0.8165	22.0	4.2409

Adsorption isotherms of pure neon (Ne), hydrogen (H_2) and helium-4 (He) onto dry activated carbon AX-21 at high pressures are presented in Fig. 6-3. Here, classical and semiclassical approximation using SAFT-VRQ were obtained; in the case of hydrogen, the results were compared with experimental data reported by Bennard *et. al.*,.[22–24] For the case of neon and helium-4, the experimental data for adsorption isotherms are not available in the literature. Figs. 6-3 and 6-4 were obtained estimating the particle-wall potential parameter, ϵ_w, from the isosteric heat reported by

several authors.[25–27] From experimental isosteric heat values, q_{st}, we could obtain a range of acceptable values of the wall parameter ϵ_w for neon and helium-4. The parameter values used in order to obtained the adsorption isotherms are given in Table 6.3.2.

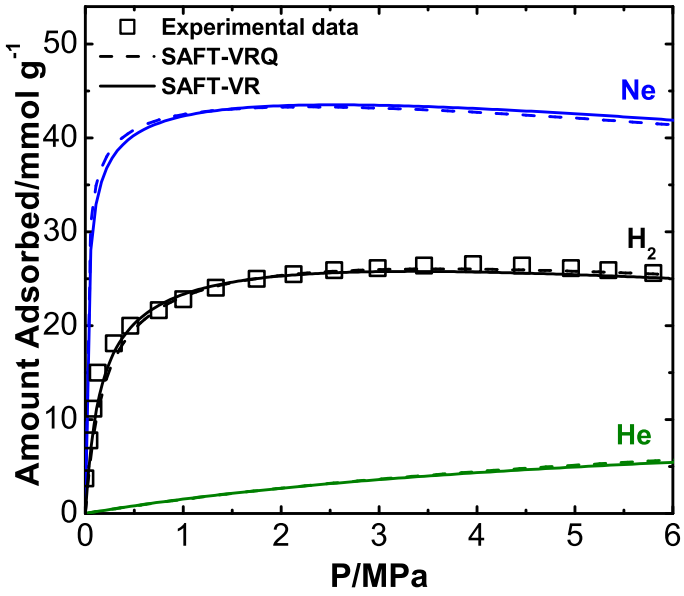

Figure 6-3: Gibbs isotherms for the adsorption of neon (Ne), hydrogen (H_2) and helium (He) onto dry activated carbon AX-21 at T=77 K. The solid lines, dashed lines and symbols correspond to the SAFT-VR, SAFT-VRQ prediction and experimental data,[19] respectively.

Adsorption isotherms for the adsorption of hydrogen + neon and hydrogen + helium-4 are presented in Fig. 6-4 as a function of pressure and molar fraction composition. Results are reported as Gibbs amount adsorption isotherms. In the case of the neon adsorption, values near to 43 mmol/g are obtained when molar fraction of neon approaches to 1 ($x_{Ne} \to 1$), this behavior is contrary to the case of helium-4 were the amount of adsorption is near to 8 mmol/g when ($x_{He} \to 1$).

In this chapter, we developed a systematic procedure to describe and predict the adsorption isotherms of mixtures containing hydrogen. Semiclassical theory taking into account quantum corrections using pure-molecular parameters and only one fitted parameter was developed. In general, we show the adsorption curves tendency for quantum fluids as hydrogen, neon and helium-4. This tendency curves of adsorption is a valuable information for the experimental research, because the SAFT-VRQ is a predictive approach and these results give a particular range of values in order to

obtain experimental adsorption data.

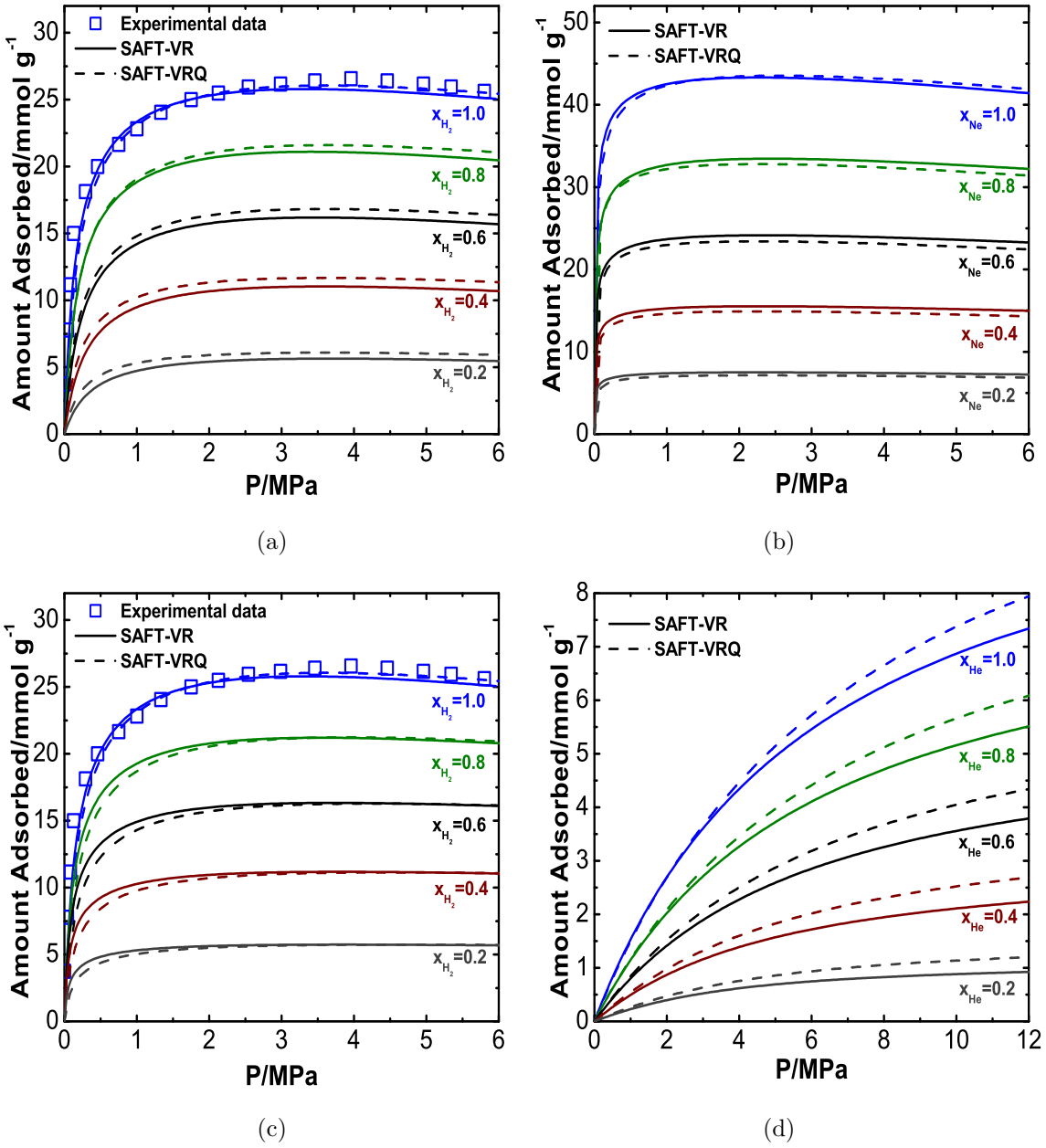

Figure 6-4: Adsorption isotherms for the adsorption of the systyems H_2/Ne and H_2/He mixture. For both systems, the adsorption isotherms are studied onto dry activaded carbon AX-21 at T=77 K. Solid lines and symbols correspond to the SAFT-VR prediction and the experimental data,[19] respectively. Adsorption isotherms presented are: (a) Adsorption of H_2 on the mixture H_2/Ne (b) Adsorption of Ne on the mixture H_2/Ne (c) Adsorption of H_2 on the mixture H_2/He (d) Adsorption of He on the mixture H_2/He.

Conclusions

An extension of the semiclassical SAFT-VRQ approach to modeling mixtures is described and used for two classical systems (methane + nitrogen/methane + carbon dioxide) and two quantum systems (hydrogen + neon/hydrogen + helium-4). For classical systems, adsorption isotherm predictions were compared with experimental data and a good concordance was obtained in all cases. Pure compound parameters were previously presented by many authors.[10–14] Quantum fluids predictions were obtained using pure compound parameters reported by Trejos *et. al,*.[28] Theory was found to be capable of predicting the overall phase diagram for real mixtures. Adsorption of reactive systems and vapor-liquid calculations of asymmetric mixtures containing quantum fluids is an expectative to be studied in a future work.

BIBLIOGRAPHY

[1] L. Zhou, Y. Zhou, Y. Sun, *Int. J. of Hydrogen Energy* **29**, 475 (2004).

[2] A. Z uttel, *Materials Today* **6**, 24 (2003).

[3] A. G. Wong-Foy, A. J. Matzger, O. M. Yaghi, *J. Am. Chem. Soc.* **128**, 3494 (2006).

[4] H. Furukawa, N. Ko, Y. B. Go, N. Aratani, S. B. Choi, E. Choi, A. O. Yazaydin, R. Q. Snurr, M. O'Keeffe, J. Kim, O. M. Yaghi, *Science* **329**, 424 (2010).

[5] G. Srinivas, Y. Zhu, R. Piner, N. Skipper, M. Ellerby, R. Ruoff, *Carbon* **48**, 630 (2010).

[6] J. P. Marco-Lozar, J. Juan-Juan, F. Suárez-García, D. Cazorla-Amorós, A. Linares-Solano, *Int. J. of Hydrogen Energy* **37**, 2370 (2012).

[7] S. Builes, S. I. Sandler, R. Xiong, *Langmuir* **29**, 10416 (2013).

[8] P. Bénard and R. Chahine, *Langmuir* **17**, 1950 (2001).

[9] A. Gil-Villegas, A. Galindo, P. J. Whitehead, S. J. Mills, G. Jackson, A. N. Burgess, *J. Chem. Phys.* **106**, 4168 (1997).

[10] A. Martínez, M. Castro, C. McCabe, A. Gil-Villegas, *J. Chem. Phys.* **126**, 074707 (2007).

[11] G. Jiménez-Serratos, S. Santillán, C. Avendaño, M. Castro, A. Gil-Villegas, *Oil & Gas Sci. Tech.* **63**, 329 (2008).

[12] M. Castro, J.L Mendoza de la Cruz, E. Buenrostro-González, S. Lopéz-Ramírez, A. Gil-Villegas,*Fluid Phase Equilib.* **87**, 113 (2009).

[13] M. Castro, A. Martínez, A. Gil-Villegas, *AST* **29**, 59 (2011).

[14] M. Castro and A. Martínez, *Adsorption* **19**, 63 (2013).

[15] V. M. Trejos, M. Becerra,S. Figueroa-Gerstenmaier, and A. Gil-Villegas, *Mol. Phys.* **1**, 1, (2014).

[16] J. A. Barker, D. Henderson, *J. Chem. Phys.* **47**, 2856, (1967).

[17] J. A. Barker, D. Henderson, *J. Chem. Phys.* **47**, 4714, (1967).

[18] A. Galindo, L. A. Davies, A. Gil-Villegas, G. Jackson,*Mol. Phys.***93**, 241 (1998).

[19] M. Sudibandriyo, Z. Pan, J. E. Fitzgerald, R. L. Robinson, Jr. and A. M. Gaasem, *Langmuir* **19**, 5323 (2003).

[20] S. Brunauer, P. H. Emmett, E. Teller, *J. Am. Chem. Soc.* **60**, 309 (1938).

[21] S. J. Gregg, K. S. W. Sing, *Adsorption, surface area and porosity*, Academic Press, 2nd edition, London, (1982)

[22] P. Bénard and R. Chahine, *Langmuir* **17**, 1950 (2001).

[23] P. Bénard, R. Chahine, P.A. Chandonia, D. Cossement, G. Dorval-Douville, L. Lafia, P. Lachance, R. Paggiaro, E. Poirier, *J. of Alloys and Compounds* **446**, 380 (2007).

[24] P. Bénard and Richard Chahine, *Scripta Materialia* **56**, 803 (2007).

[25] T. Wilson, O. E. Vilches, *Physica B* **329**, 278, (2003).

[26] H. Tanaka, M. El-Merraoui, T. Kodaira, K. Kaneko, *Chemical Physics Letters* **351** 417 (2002).

[27] R. Yanlk, *Vacuum* **205** 207 (1996).

[28] Víctor M. Trejos, Mario Becerra,Susana Figueroa-Gerstenmaier, and Alejandro Gil-Villegas,*Mol. Phys.*, **1** 1 (2014).

CHAPTER 7

CONCLUSIONS AND PERSPECTIVES

As summarizy of the sections of the present thesis, recent developments in molecular simulations and theoretical approaches of adsorption have enhanced the applicability of these methodologies in order to predict quantum contributions in the adsorption of quantum fluids. This thesis presents multiple aspects of molecular statistical physics, where theoretical results are compared with simulation and experimental data. Particular conclusions have been exposed and presented in previous chapters and summarized throughout the document. In this chapter, future perspectives are given:

- On Chapter 3, a semiclassical theory to model quantum fluids within the framework of SAFT-VR approach was developed. There, the thermodynamic properties were obtained using a square-well pair potential. It would be interesting to obtain thermodynamic properties of quantum fluids, such as second virial coefficient, inversion curves, Joule-Thomson coefficients and heat capacities using a continuous Mie-pair potentials in the framework of the SAFT-γ. These methodology have been not used in the study of complex fluids such as hydrogen or helium. In this way, further work would be in order to reply all the mentioned thermodynamic properties using SAFT-γ and discrete pair potentials.

- On Chapter 4, computer simulations of liquid-vapor coexistence of confined quantum fluids were studied by Monte Carlo computer simulation for particles interacting via a semiclassical effective pair potential. Other extensions and

further analysis of this approach is considering quantum methodologies such as path-integral. This methodology is a powerful tool in order to study quantum fluids. It would be interesting to obtain the vapor-liquid coexistence of confined quantum fluids and structure properties; such as radial distribution function by using path integrals. Our research group is being developing this work.

– On Chapter 5, adsorption of molecular hydrogen onto different substrates are described using a semiclassical theoretical framework based on the SAFT-VRQ. In this way, it would be interesting to measure experimentally the differential heats of adsorption of quantum fluids at low temperatures onto different materials. On the other hand, further analysis and research are required in the study of reactive systems. This study is very promising, as it provides the opportunity to analyze simulation results obtained from reactive Monte Carlo Gibbs ensemble and compared this results with SAFT-VR for square-well pair potentials. Molecular simulations, together with theoretical studies using SAFT-VR, will thus be helpful in the study of adsorption-reaction onto catalytic surfaces.

– On Chapter 6, adsorption of binary mixtures containing hydrogen were studied in the framework of SAFT-VRQ approach. There, adsorption isotherm results were obtained for mixtures of hydrogen + classic fluids, using fitted molecular parameters from pure fluids. Further studies should be made in order to obtain the vapor-liquid equilibrium of asymmetric binary mixtures containing hydrogen + n-alkanes and n-alkanols. The major problem with adsorption of mixtures, such as hydrogen + quantum fluid, is due to the poor experimental data reported in the literature. This difficulty is also present in mixtures with lower complexity, such as classic fluids.

APPENDIX A

APPENDIX A

Expression for the chemical potential

We discuss the chemical potential terms from the corresponding Helmholtz free energy terms. The expressions are as follows

$$\frac{\mu_i}{kT} = \frac{\mu_i^{\text{ideal}}}{kT} + \frac{\mu_i^{\text{mono}}}{kT} + \frac{\mu_i^{\text{chain}}}{kT} \tag{A.1}$$

where μ_i is the chemical potential of the i-component, T is the temperature and k is the Boltzmann constant. Using standard thermodynamic relationships the chemical potentials for the i-component can be obtained as

$$\mu_i = \left(\frac{\partial A}{\partial N_i}\right)_{T,V,N_{i\neq j}} \tag{A.2}$$

or

$$\frac{\mu_i}{kT} = a + N\left(\frac{\partial a}{\partial N_i}\right)_{T,V,N_{i\neq j}} \tag{A.3}$$

where N is the total number of molecules, V is the volume of the system, A is the Helmholtz free energy and $a = A/NkT$. The Helmholtz free energy for an n-component mixture of chain molecules can be separated into the various contributions as

$$a = a^{\text{ideal}} + a^{\text{mono}} + a^{\text{chain}} \tag{A.4}$$

There is no need to include the association term since we are dealing with a nonassociating system.

1. Ideal Contribution: The ideal contribution to the chemical potential, μ_i^{ideal}, can be expressed as

$$\frac{\mu_i^{\text{ideal}}}{kT} = a^{\text{ideal}} + N\left(\frac{\partial a^{\text{ideal}}}{\partial N_i}\right)_{T,V,N_{i\neq j}} = \ln\left(\rho_i \lambda_{Bi}^3\right) \tag{A.5}$$

with

$$a^{\text{ideal}} = \sum_{i=1}^{n} x_i \ln\left(\rho_i \lambda_{Bi}^3\right) - 1 \tag{A.6}$$

where $x_i = N_i/N$ is the mole fraction, $\rho_i = N_i/V$ the molecular number of density, N_i the number of molecules, λ_{Bi} the thermal Broglie wavelength of species i.

2. Monomer contribution: The monomer contribution to the chemical potential, μ_i^{mono}, can be expressed as

$$\frac{\mu_i^{\text{mono}}}{kT} = a^{\text{mono}} + N\left(\frac{\partial a^{\text{mono}}}{\partial N_i}\right)_{T,V,N_{i\neq j}} \tag{A.7}$$

where a^{mono} is the monomer Helmholtz free energy,

$$a^{\text{mono}} = \left(\sum_k x_k m_k\right) a^{\text{M}} = S a^{\text{M}} = S\left[a^{\text{HS}} + \beta a_1 + \beta^2 a_2\right] \tag{A.8}$$

where m_k is the number of spherical segments of chain i, S is the average of m_i, $(S = \sum_k x_k m_k)$, $\beta = 1/kT$, and a^{M} is the monomer free energy per segment of the mixture, a^{HS} is the Helmholtz free energy of the a mixture of hard-sphere, and $a_{1,2}$ are the first and the second order perturbation terms respectively, obtained from the Barker Henderson expansion. From the Eqs. (A.7)-(A.8), the monomer contribution to the chemical potential, μ_i^{mono}, can be written as

$$\begin{aligned}\frac{\mu_i^{\text{mono}}}{kT} &= S\left[a^{\text{M}} + N\left(\frac{\partial a^{\text{M}}}{\partial N_i}\right)\right] + a^{\text{M}}(m_i - S) \\ &= S\left[\frac{\mu_i^{\text{HS}}}{kT} + \beta\frac{\mu_{1i}}{kT} + \beta^2\frac{\mu_{2i}}{kT}\right] + a^{\text{M}}(m_i - S)\end{aligned} \tag{A.9}$$

2.1 Hard-Sphere contribution: The hard-sphere contribution to the chemical potential, μ^{HS}, is given by

$$\frac{\mu_i^{\mathrm{HS}}}{NkT} = a^{\mathrm{HS}} + N\left(\frac{\partial a^{\mathrm{HS}}}{\partial N_i}\right)_{T,V,N_{i\neq j}} \tag{A.10}$$

The hard-sphere contribution a^{HS} is determined from the expression of Boublik[2] and Mansoori and co-workers[3] for multicomponent hard sphere systems

$$a^{\mathrm{HS}} = \frac{6}{\pi\rho_s}\left[\left(\frac{\zeta_2^3}{\zeta_3^2} - \zeta_0\right)\ln(1-\zeta_3) + \frac{3\zeta_1\zeta_2}{1-\zeta_3} + \frac{\zeta_2^3}{\zeta_3(1-\zeta_3)^2}\right] \tag{A.11}$$

where $\rho_s = N_s/V$ is the number density of segments, which is defined as the total number of segments N_s, divided by the total volume V. Note that $\rho_s = \rho S$ where ρ is the total number density of the mixture. The reduced densities ζ_l are defined as

$$\zeta_l = \frac{\pi}{6}\rho_s\left[\sum_{i=1}^{n} x_{s,i}\sigma_i^l\right] \tag{A.12}$$

where σ_i is diameter of spherical segments of chain i, and $x_{s,i}$ is the mole fraction of segments in the mixtures ($x_{s,i} = m_i x_i/S$).The overall packing fraction of the mixture is thus given by ζ_3, which is equivalent to η in the pure component case. The differential expression of the Eq. (A.10), can be written as

$$N\left(\frac{\partial a^{\mathrm{HS}}}{\partial N_i}\right)_{T,V,N_{i\neq j}} = \frac{m_i}{S}\left(\delta\Psi - a^{\mathrm{HS}}\right) \tag{A.13}$$

$$\begin{aligned}\delta\Psi = &\left(\frac{3\zeta_2^2\sigma_i^2}{\zeta_3^2} - \frac{2\zeta_2^3\sigma_i^3}{\zeta_3^3} - 1\right)\ln(1-\zeta_3) + \frac{3\zeta_1\zeta_2\sigma_i^3}{(1-\zeta_3)^2} - \left(\frac{\zeta_2^3}{\zeta_3^2} - \zeta_0\right)\frac{\sigma_i^3}{(1-\zeta_3)} \\ &+ \frac{3\zeta_1\sigma_i^2}{(1-\zeta_3)} + \frac{2\zeta_2^3\sigma_i^3}{\zeta_3(1-\zeta_3)^3} + \frac{3\zeta_2\sigma_i}{(1-\zeta_3)} + \frac{3\zeta_2^2\sigma_i^2}{\zeta_3(1-\zeta_3)^2} - \frac{\zeta_2^3\sigma_i^3}{\zeta_3^2(1-\zeta_3)^2}\end{aligned} \tag{A.14}$$

where $\zeta_{0,1,2,3}$ are acalculated using Eq. (A.12).

2.2 First-order perturbation term: The first-order perturbation term contri-

bution to the chemical potential, μ_{1i}, is expressed as

$$\frac{\mu_{1i}}{kT} = a_1 + N\left(\frac{\partial a_1}{\partial N_i}\right)_{T,V,N_{i\neq j}} \tag{A.15}$$

The mean-attractive energy represented by the a_1 term is obtained from the sum of the partial terms corresponding to each type of pair interaction,

$$a_1 = -2\pi\rho_s \sum_k \sum_j x_{s,k} x_{s,j} \epsilon_{kj} \int_{\sigma_{kj}}^{\infty} r_{kj}^2 \mathrm{g}_{kj}^{\mathrm{HS}}(r_{kj};\zeta_3) dr_{kj} \tag{A.16}$$

and $\mathrm{g}_{kj}^{\mathrm{HS}}$ is the radial distribution function for a mixture of hard spheres. Using the mean value theorem,[4,5] we obtain an expression for a_1 in terms of the contact value of $\mathrm{g}_{kj}^{\mathrm{HS}}$

$$a_1 = -\rho_s \sum_k \sum_j x_{s,k} x_{s,j} \alpha_{kj}^{\mathrm{VDW}} \mathrm{g}_{kj}^{\mathrm{HS}}(\sigma_{kj};\zeta_3^{\mathrm{eff}}) \tag{A.17}$$

where

$$\alpha_{kj}^{\mathrm{VDW}} = 2\pi\epsilon_{kj}\sigma_{kj}^3(\lambda_{kj}^3 - 1)/3 \tag{A.18}$$

In the van der Waals one-fluid theory (VDW-1) $\mathrm{g}_{kj}^{\mathrm{HS}}$ is approximated by the radial distribution function for a single fluid such as

$$a_1 = -\rho_s \sum_k \sum_j x_{s,k} x_{s,j} \alpha_{kj}^{\mathrm{VDW}} \mathrm{g}_o^{\mathrm{HS}}(\sigma_x;\zeta_x^{\mathrm{eff}}) = -\rho_s \alpha_x^{\mathrm{VDW}} \mathrm{g}_o^{\mathrm{HS}}(\sigma_x;\zeta_x^{\mathrm{eff}}) \tag{A.19}$$

where

$$\alpha_x^{\mathrm{VDW}} = \sum_k \sum_j x_{s,k} x_{s,j} \alpha_{kj}^{\mathrm{VDW}} \tag{A.20}$$

where $\mathrm{g}_o^{\mathrm{HS}}$ is the contact value of the hard-sphere pair radial distribution function obtained from the Carnahan and Starling equation,[3]

$$\mathrm{g}_o^{\mathrm{HS}}(\sigma_x;\zeta_x^{\mathrm{eff}}) = \frac{1 - \zeta_x^{\mathrm{eff}}/2}{(1-\zeta_x^{\mathrm{eff}})^3} \tag{A.21}$$

where ζ_x^{eff} is the effective packing fraction obtained within the VDW-1 from the corresponding packing fraction of the mixture ζ_x given by,

$$\zeta_x^{\mathrm{eff}}(\zeta_x,\lambda_x) = C_1(\lambda_x)\zeta_x + C_2(\lambda_x)\zeta_x^2 + C_3(\lambda_x)\zeta_x^3 \tag{A.22}$$

where

$$\zeta_x = \frac{\pi}{6}\rho_s \sum_k \sum_j x_{s,k} x_{s,j} \sigma_{kj}^3 = \frac{\pi}{6}\rho_s \sigma_x^3 \tag{A.23}$$

with

$$\sigma_x^3 = \sum_k \sum_j x_{s,k} x_{s,j} \sigma_{kj}^3 \tag{A.24}$$

The coefficients C_1, C_2 and C_3 are approximated by those of the pure fluid,

$$\begin{pmatrix} C_1 \\ C_2 \\ C_3 \end{pmatrix} = \begin{pmatrix} 2.25855 & -1.50349 & 0.249434 \\ -0.669270 & 1.40049 & -0.827739 \\ 10.1576 & -15.0427 & 5.30827 \end{pmatrix} \begin{pmatrix} 1 \\ \lambda_x \\ \lambda_x^2 \end{pmatrix} \tag{A.25}$$

The unlike range parameter is obtained from the weighted mean of the pure components values used in a previous works[7]

$$\lambda_x^3 = \frac{\sum_k \sum_j x_{s,k} x_{s,j} \epsilon_{kj} \lambda_{kj}^3 \sigma_{kj}^3}{\sum_k \sum_j x_{s,k} x_{s,j} \epsilon_{kj} \sigma_{kj}^3} \tag{A.26}$$

According with the Eq. (A.19), the differential expression in the Eq. (A.15) can be calculated as

$$\begin{aligned} N\left(\frac{\partial a_1}{\partial N_i}\right)_{T,V,N_{i\neq j}} = &- \alpha_x^{\mathrm{VDW}} \mathrm{g}_o^{\mathrm{HS}}(\sigma_x; \zeta_x^{\mathrm{eff}}) N\left(\frac{\partial \rho_s}{\partial N_i}\right) - \rho_s \mathrm{g}_o^{\mathrm{HS}}(\sigma_x; \zeta_x^{\mathrm{eff}}) N\left(\frac{\partial \alpha_x^{\mathrm{VDW}}}{\partial N_i}\right) \\ &- \rho_s \alpha_x^{\mathrm{VDW}} N\left(\frac{\partial \mathrm{g}_o^{\mathrm{HS}}(\sigma_x; \zeta_x^{\mathrm{eff}})}{\partial N_i}\right) \end{aligned} \tag{A.27}$$

with

$$N\left(\frac{\partial \rho_s}{\partial N_i}\right) = \rho m_i \tag{A.28}$$

$$N\left(\frac{\partial \alpha_x^{\mathrm{VDW}}}{\partial N_i}\right) = \frac{2}{S} \sum_k \sum_j m_i x_{s,j} \alpha_{kj}^{\mathrm{VDW}} (\delta_{ik} - x_{s,k}) \tag{A.29}$$

The last differential expression in Eq.(B.26), can be development as

$$N\left(\frac{\partial \mathrm{g}_o^{\mathrm{HS}}(\sigma_x; \zeta_x^{\mathrm{eff}})}{\partial N_i}\right) = \left(\frac{\partial \mathrm{g}_o^{\mathrm{HS}}(\sigma_x; \zeta_x^{\mathrm{eff}})}{\partial \zeta_x^{\mathrm{eff}}}\right) N\left(\frac{\partial \zeta_x^{\mathrm{eff}}}{\partial N_i}\right) \tag{A.30}$$

where

$$\left(\frac{\partial \mathrm{g}_o^{\mathrm{HS}}(\sigma_x;\zeta_x^{\mathrm{eff}})}{\partial \zeta_x^{\mathrm{eff}}}\right) = \left(\frac{5/2-\zeta_x^{\mathrm{eff}}}{(1-\zeta_x^{\mathrm{eff}})^4}\right) \tag{A.31}$$

$$N\left(\frac{\partial \zeta_x^{\mathrm{eff}}}{\partial N_i}\right) = \left(\frac{\partial \zeta_x^{\mathrm{eff}}}{\partial \zeta_x}\right) N\left(\frac{\partial \zeta_x}{\partial N_i}\right) + \left(\frac{\partial \zeta_x^{\mathrm{eff}}}{\partial \lambda_x}\right) N\left(\frac{\partial \lambda_x}{\partial N_i}\right) \tag{A.32}$$

The differential terms in Eq. (B.31) are given by

$$\left(\frac{\partial \zeta_x^{\mathrm{eff}}}{\partial \zeta_x}\right) = C_1 + 2C_2\zeta_x + 3C_3\zeta_x^2 \tag{A.33}$$

$$N\left(\frac{\partial \zeta_x}{\partial N_i}\right) = \frac{\pi}{6}\rho \sum_k \sum_j m_i x_{s,j} \sigma_{kj}^3 (2\delta_{ki} - x_{s,k}) \tag{A.34}$$

where δ_{ki} is the Kronecker's delta.

$$\left(\frac{\partial \zeta_x^{\mathrm{eff}}}{\partial \lambda_x}\right) = \sum_{l=1}^{3} \zeta_x^l \left(\frac{\partial C_l}{\partial \lambda_x}\right) \tag{A.35}$$

$$N\left(\frac{\partial \lambda_x}{\partial N_i}\right) = \frac{2}{3S\lambda_x^2}\left(\frac{D_1\sigma_{2x}^3 - E_1\lambda_{2x}^3}{(\sigma_{2x}^3)^2}\right) \tag{A.36}$$

with

$$D_1 = \sum_j m_i x_{s,j} \epsilon_{ij} \lambda_{ij}^3 \sigma_{ij}^3 \tag{A.37}$$

$$E_1 = \sum_j m_i x_{s,j} \epsilon_{ij} \sigma_{ij}^3 \tag{A.38}$$

$$\sigma_{2x}^3 = \sum_k \sum_j x_{s,k} x_{s,j} \epsilon_{kj} \sigma_{kj}^3 \tag{A.39}$$

$$\lambda_{2x}^3 = \sum_k \sum_j x_{s,k} x_{s,j} \epsilon_{kj} \lambda_{kj}^3 \sigma_{kj}^3 \tag{A.40}$$

2.3 Second-order perturbation term: The second-order perturbation term contribution to the chemical potential, μ_{2i}, is given by

$$\frac{\mu_{2i}}{kT} = a_2 + N\left(\frac{\partial a_2}{\partial N_i}\right)_{T,V,N_{i\neq j}} \tag{A.41}$$

The second-order perturbation term for the monomer excess free energy a_2, is obtained through the local compresibility approximation as

$$a_2 = \frac{1}{2}\rho_s \sum_k \sum_j x_{s,k} x_{s,j} \epsilon_{kj} K^{\mathrm{HS}} \left(\frac{\partial a_1^{kj}}{\partial \rho_s} \right) \tag{A.42}$$

within the VdW-1 fluid theory the term a_1^{kj} is approximated by that for a pure fluid

$$a_1^{kj} = -\rho_s \alpha_{kj}^{\mathrm{VDW}} \mathrm{g}_o^{\mathrm{HS}}(\sigma_x; \zeta_x^{\mathrm{eff}}) \tag{A.43}$$

In Eq. (A.42) the differential expression on ρ_s, can be written as

$$\left(\frac{\partial a_1^{kj}}{\partial \rho_s} \right) = -\alpha_{kj}^{\mathrm{VDW}} \left[\mathrm{g}_o^{\mathrm{HS}}(\sigma_x; \zeta_x^{\mathrm{eff}}) + \rho_s \left(\frac{\partial \mathrm{g}_o^{\mathrm{HS}}(\sigma_x; \zeta_x^{\mathrm{eff}})}{\partial \rho_s} \right) \right] \tag{A.44}$$

According with the Eqs. (A.42)-(A.44), the second-order perturbation term a_2 can be reorganized as follows

$$a_2 = -\frac{1}{2}\rho_s K^{\mathrm{HS}} \alpha_{2x}^{\mathrm{VDW}} g_{ox}^{\mathrm{HS}} \tag{A.45}$$

where g_{ox}^{HS} is given by

$$g_{ox}^{\mathrm{HS}} = \mathrm{g}_o^{\mathrm{HS}}(\sigma_x; \zeta_x^{\mathrm{eff}}) + \rho_s \left(\frac{\partial \mathrm{g}_o^{\mathrm{HS}}(\sigma_x; \zeta_x^{\mathrm{eff}})}{\partial \rho_s} \right) \tag{A.46}$$

with

$$\rho_s \left(\frac{\partial \mathrm{g}_o^{\mathrm{HS}}(\sigma_x; \zeta_x^{\mathrm{eff}})}{\partial \rho_s} \right) = \left(\frac{\partial \mathrm{g}_o^{\mathrm{HS}}(\sigma_x; \zeta_x^{\mathrm{eff}})}{\partial \zeta_x^{\mathrm{eff}}} \right) \left(\frac{\partial \zeta_x^{\mathrm{eff}}}{\partial \zeta_x} \right) \zeta_x \tag{A.47}$$

and

$$\alpha_{2x}^{\mathrm{VDW}} = \sum_k \sum_j x_{s,k} x_{s,j} \epsilon_{kj} \alpha_{kj}^{\mathrm{VDW}} \tag{A.48}$$

where K^{HS} is the Perkus-Yevik expression for the hard-sphere isothermal compresibility,

$$K^{\mathrm{HS}} = \frac{\zeta_0 (1-\zeta_3)^4}{\zeta_0 (1-\zeta_3)^2 + 6\zeta_1 \zeta_2 (1-\zeta_3) + 9\zeta_2^3} \tag{A.49}$$

For the particular case of $x_i \to 1$, Eq. A.49 is reduced to

$$\lim_{x_i \to 1} K^{\mathrm{HS}} = \frac{(1-\zeta_3)^4}{1 + 4\zeta_3 + 4\zeta_3^2} \tag{A.50}$$

Here the K^{HS} of mixtures is reduced to the expression of pure components, with $\zeta_3 = \eta$. In order to calculate the contribution to the chemical potential, μ_{2i}, the partial derivative expression for a_2 can be written as

$$N\left(\frac{\partial a_2}{\partial N_i}\right)_{T,V,N_{i\neq j}} = -\frac{1}{2}K^{\mathrm{HS}}\alpha_{2x}^{\mathrm{VDW}}\left[g_{ox}^{\mathrm{HS}}\rho m_i + \rho_s N\left(\frac{\partial g_{ox}^{\mathrm{HS}}}{\partial N_i}\right)\right] - \frac{1}{2}\rho_s g_{ox}^{\mathrm{HS}}\left[\alpha_{2x}^{\mathrm{VDW}}N\left(\frac{\partial K^{\mathrm{HS}}}{\partial N_i}\right) + K^{\mathrm{HS}}N\left(\frac{\partial \alpha_{2x}^{\mathrm{VDW}}}{\partial N_i}\right)\right] \tag{A.51}$$

The three partial derivative expressions are now

$$N\left(\frac{\partial K^{\mathrm{HS}}}{\partial N_i}\right) = \frac{\pi}{6}m_i\rho\left[-(f_1/f_2^2)\zeta_0(1-\zeta_3)^4 + \left((1-\zeta_3)^4 - 4\zeta_0(1-\zeta_3)^3\sigma_i^3\right)/f_2\right] \tag{A.52}$$

with

$$f_1 = \zeta_2\sigma_i^2(27\zeta_2 - 6\zeta_1\sigma_i) + (1-\zeta_3)[(1-\zeta_3) - 2\zeta_0\sigma_i^3 + 6\zeta_2\sigma_i + 6\zeta_1\sigma_i^2] \tag{A.53}$$

$$f_2 = \zeta_0(1-\zeta_3)^2 + 6\zeta_1\zeta_2(1-\zeta_3) + 9\zeta_2^3 \tag{A.54}$$

$$N\left(\frac{\partial \alpha_{2x}^{\mathrm{VDW}}}{\partial N_i}\right) = \frac{2}{S}\sum_k\sum_j m_i x_{s,j}\epsilon_{kj}\alpha_{kj}^{\mathrm{VDW}}(\delta_{ik} - x_{s,k}) \tag{A.55}$$

and

$$N\left(\frac{\partial \mathrm{g}_{ox}^{\mathrm{HS}}}{\partial N_i}\right) = \left(\frac{\partial \mathrm{g}_o^{\mathrm{HS}}(\sigma_x;\zeta_x^{\mathrm{eff}})}{\partial \zeta_x^{\mathrm{eff}}}\right)\left[\zeta_x N\frac{\partial}{\partial N_i}\left(\frac{\partial \zeta_x^{\mathrm{eff}}}{\partial \zeta_x}\right) + \left(\frac{\partial \zeta_x^{\mathrm{eff}}}{\partial \zeta_x}\right)N\left(\frac{\partial \zeta_x}{\partial N_i}\right)\right] + N\left(\frac{\partial \mathrm{g}_o^{\mathrm{HS}}(\sigma_x;\zeta_x^{\mathrm{eff}})}{\partial N_i}\right) + \zeta_x\left(\frac{\partial \zeta_x^{\mathrm{eff}}}{\partial \zeta_x}\right)N\frac{\partial}{\partial N_i}\left(\frac{\partial \mathrm{g}_o^{\mathrm{HS}}(\sigma_x;\zeta_x^{\mathrm{eff}})}{\partial \zeta_x^{\mathrm{eff}}}\right) \tag{A.56}$$

In Eq. (A.56) the first order differential terms were calculated using the Eqs. (A.30)-(A.40). We only need calculate the following expressions

$$N\frac{\partial}{\partial N_i}\left(\frac{\partial \mathrm{g}_o^{\mathrm{HS}}(\sigma_x;\zeta_x^{\mathrm{eff}})}{\partial \zeta_x^{\mathrm{eff}}}\right) = \left[\frac{9 - 3\zeta_x^{\mathrm{eff}}}{(1-\zeta_x^{\mathrm{eff}})^5}\right]N\left(\frac{\partial \zeta_x^{\mathrm{eff}}}{\partial N_i}\right) \tag{A.57}$$

and

$$N\frac{\partial}{\partial N_i}\left(\frac{\partial\zeta_x^{\text{eff}}}{\partial\zeta_x}\right) =(2C_2+6C_3\zeta_x)N\left(\frac{\partial\zeta_x}{\partial N_i}\right)+N\left(\frac{\partial C_1}{\partial N_i}\right)+2\zeta_x N\left(\frac{\partial C_2}{\partial N_i}\right) + 3\zeta_x N\left(\frac{\partial C_3}{\partial N_i}\right) \tag{A.58}$$

with

$$N\left(\frac{\partial C_l}{\partial N_i}\right)=\left(\frac{\partial C_l}{\partial\lambda_x}\right)N\left(\frac{\partial\lambda_x}{\partial N_i}\right) \tag{A.59}$$

where $l=1,2,3$.

3. Chain Contribution: The chain contribution to the chemical potential, μ_i^{chain}, is expressed as

$$\frac{\mu_i^{\text{chain}}}{kT}=a^{\text{chain}}+N\left(\frac{\partial a^{\text{chain}}}{\partial N_i}\right)_{T,V,N_{i\neq j}} \tag{A.60}$$

The contribution to the free energy due to chain formation is expressed in terms of the contact value of the background correlation function[4,5]

$$a^{\text{chain}}=-\sum_k x_k(m_k-1)\ln(y_{kk}^{\text{SW}}(\sigma_{kk})) \tag{A.61}$$

where $y_{kk}^{\text{SW}}(\sigma_{kk})=\text{g}_{kk}^{\text{SW}}(\sigma_{kk})\exp(-\beta\epsilon_{kk})$. According with the Eq. (A.61) the chemical potential of chains, μ_i^{chain}, can be rewritten

$$\frac{\mu_i^{\text{chain}}}{kT}=-(m_i-1)\ln(y_{ii}^{\text{SW}})-\sum_k x_k(m_k-1)\left(\frac{1}{\text{g}_{kk}^{\text{SW}}}\right)N\left(\frac{\partial\text{g}_{kk}^{\text{SW}}}{\partial N_i}\right) \tag{A.62}$$

where the $g_{kk}^{\text{SW}}(\sigma_{kk})$ can be expressed as a expansion at high temperature, as

$$\text{g}_{kk}^{\text{SW}}(\sigma_{kk})=\text{g}_{kk}^{\text{HS}}(\sigma_{kk})+\beta\epsilon_{kk}\text{g}_1(\sigma_{kk}) \tag{A.63}$$

The hard-sphere term $\text{g}_{kk}^{\text{HS}}$ is given by the expression of Boublik,[2]

$$\text{g}_{kj}^{\text{HS}}(\sigma_{kj};\zeta_3)=\frac{1}{1-\zeta_3}+3\frac{D_{kj}\zeta_3}{(1-\zeta_3)^2}+2\frac{(D_{kj}\zeta_3)^2}{(1-\zeta_3)^3} \tag{A.64}$$

with the parameter D_{kj} defined by

$$D_{kj} = \frac{\sigma_{kk}\sigma_{jj}}{\sigma_{kk}+\sigma_{jj}} \frac{\sum_{k=1} x_{s,k}\sigma_{kk}^2}{\sum_{k=1} x_{s,k}\sigma_{kk}^3} \tag{A.65}$$

The term $g_1(\sigma_{kk})$ is obtained from a self-consistent representation of the pressure P from the Clausius virial theorem and from the density derivative of the Helmholtz free energy,[4,5]

$$\mathrm{g}_1(\sigma_{kk}) = \mathrm{g}_o^{\mathrm{HS}}(\sigma_x;\zeta_x^{\mathrm{eff}}) + (\lambda_{kk}^3-1)\frac{\partial \mathrm{g}_o^{\mathrm{HS}}(\sigma_x;\zeta_x^{\mathrm{eff}})}{\partial \zeta_x^{\mathrm{eff}}}\left(\frac{\lambda_{kk}}{3}\frac{\partial \zeta_x^{\mathrm{eff}}}{\partial \lambda_{kk}} - \zeta_3 \frac{\partial \zeta_x^{\mathrm{eff}}}{\partial \zeta_3}\right) \tag{A.66}$$

In the above equation the partial differential expressions of ζ_x^{eff} are given by

$$\left(\frac{\partial \zeta_x^{\mathrm{eff}}}{\partial \lambda_{kk}}\right) = \sum_{l=1}^{3} \zeta_x^l \left(\frac{\partial C_l}{\partial \lambda_x}\right)\left(\frac{\partial \lambda_x}{\partial \lambda_{kk}}\right) \tag{A.67}$$

where the last derivative expression can be written as

$$\left(\frac{\partial \lambda_x}{\partial \lambda_{kj}}\right) = \left(\frac{x_{s,j}\sigma_{jj}^{3/2}\lambda_{kk}^2}{\lambda_x^2\sigma_{2x}^3(\lambda_{jj}^3-1)^{1/2}}\right)\sum_l x_{s,l}\epsilon_{jl}\sigma_{ll}^{3/2}(\lambda_{ll}^3-1)^{1/2} \tag{A.68}$$

with

$$\left(\frac{\partial \zeta_x^{\mathrm{eff}}}{\partial \zeta_3}\right) = \left(\frac{\partial \zeta_x^{\mathrm{eff}}}{\partial \zeta_x}\right)\left(\frac{\partial \zeta_x}{\partial \zeta_3}\right) \tag{A.69}$$

and

$$\left(\frac{\partial \zeta_x}{\partial \zeta_3}\right) = \sigma_x^3 \Big/ \left(\sum_k x_{s,k}\sigma_{kk}^3\right) \tag{A.70}$$

where σ_x^3 is given by Eq. (A.24). In order to calculate the chemical potentials of chains, μ_i^{chain}, from the Eq. (A.62), we need to calculate the following expression

$$N\left(\frac{\partial \mathrm{g}_{kk}^{\mathrm{SW}}}{\partial N_i}\right) = N\left(\frac{\partial \mathrm{g}_{kk}^{\mathrm{HS}}}{\partial N_i}\right) + (\beta\epsilon_{kk})N\left(\frac{\partial \mathrm{g}_1}{\partial N_i}\right) \tag{A.71}$$

where the first differential expression is given by

$$N\left(\frac{\partial \mathrm{g}_{kk}^{\mathrm{HS}}}{\partial N_i}\right)=\left[\frac{1+3D_{kk}}{(1-\zeta_3)^2}+\frac{2D_{kk}\zeta_3(3+2D_{kk})}{(1-\zeta_3)^3}+\frac{6(D_{kk}\zeta_3)^2}{(1-\zeta_3)^4}\right]N\left(\frac{\partial\zeta_3}{\partial N_i}\right)+\left[\frac{3\zeta_3}{(1-\zeta_3)^2}+\frac{4D_{kk}\zeta_3^2}{(1-\zeta_3)^3}\right]N\left(\frac{\partial D_{kk}}{\partial N_i}\right) \tag{A.72}$$

with

$$N\left(\frac{\partial D_{kk}}{\partial N_i}\right)=\left(\frac{\sigma_{kk}\sigma_{kk}}{\sigma_{kk}+\sigma_{kk}}\right)\left(\frac{mi\sigma_{ii}^2}{S}\right)\left[\frac{\sum_k x_{s,k}\sigma_{kk}^3-\sigma_{ii}\sum_k x_{s,k}\sigma_{kk}^2}{\left(\sum_k x_{s,k}\sigma_{kk}^3\right)^2}\right] \tag{A.73}$$

and

$$N\left(\frac{\partial\zeta_3}{\partial N_i}\right)=\frac{\pi}{6}\rho m_i\sigma_i^3 \tag{A.74}$$

In the Eq. (A.71) the second differential expression is given by

$$N\left(\frac{\partial \mathrm{g}_1}{\partial N_i}\right)=N\left(\frac{\partial \mathrm{g}_o^{\mathrm{HS}}(\sigma_x;\zeta_x^{\mathrm{eff}})}{\partial N_i}\right)+(\lambda_{kk}^3-1)\times\left[N\frac{\partial}{\partial N_i}\left(\frac{\partial \mathrm{g}_o^{\mathrm{HS}}(\sigma_x;\zeta_x^{\mathrm{eff}})}{\partial\zeta_x^{\mathrm{eff}}}\right)\varphi_{kk}+\left(\frac{\partial \mathrm{g}_o^{\mathrm{HS}}(\sigma_x;\zeta_x^{\mathrm{eff}})}{\partial\zeta_x^{\mathrm{eff}}}\right)N\left(\frac{\partial\varphi_{kk}}{\partial N_i}\right)\right] \tag{A.75}$$

where

$$\varphi_{kk}=\frac{\lambda_{kk}}{3}\left(\frac{\partial\zeta_x^{\mathrm{eff}}}{\partial\lambda_{kk}}\right)-\zeta_3\left(\frac{\partial\zeta_x^{\mathrm{eff}}}{\partial\zeta_3}\right) \tag{A.76}$$

In Eq. (A.76) the two differential expressions are calculated using Eqs. (A.67)-(A.69). In Eq. (A.75) the first differential expression are calculated using Eqs. (A.30)-(A.31) and (A.57), the remaining expression related with φ_{kk} is given by

$$N\left(\frac{\partial\varphi_{kk}}{\partial N_i}\right)=\frac{\lambda_{kk}}{3}N\frac{\partial}{\partial N_i}\left(\frac{\partial\zeta_x^{\mathrm{eff}}}{\partial\lambda_{kk}}\right)-\zeta_3 N\frac{\partial}{\partial N_i}\left(\frac{\partial\zeta_x^{\mathrm{eff}}}{\partial\zeta_3}\right)-N\left(\frac{\partial\zeta_3}{\partial N_i}\right)\left(\frac{\partial\zeta_x^{\mathrm{eff}}}{\partial\zeta_3}\right) \tag{A.77}$$

where the first order derivative expressions of ζ_3 and ζ_x^{eff} are obtained from the Eqs. (A.69) and (A.74), respectively. The second derivative expressions are given by

$$N\frac{\partial}{\partial N_i}\left(\frac{\partial\zeta_x^{\mathrm{eff}}}{\partial\zeta_3}\right)=\left(\frac{\partial\zeta_x}{\partial\zeta_3}\right)N\frac{\partial}{\partial N_i}\left(\frac{\partial\zeta_x^{\mathrm{eff}}}{\partial\zeta_x}\right)+\left(\frac{\partial\zeta_x^{\mathrm{eff}}}{\partial\zeta_x}\right)N\frac{\partial}{\partial N_i}\left(\frac{\partial\zeta_x}{\partial\zeta_3}\right) \tag{A.78}$$

where

$$N\frac{\partial}{\partial N_i}\left(\frac{\partial \zeta_x}{\partial \zeta_3}\right) = -\frac{1}{S_{\sigma_x}^2} S\sigma_x^3 N\left(\frac{\partial S_{\sigma_x}}{\partial N_i}\right) + \frac{1}{S_{\sigma_x}}\left[\sigma_x^3 N\left(\frac{\partial S}{\partial N_i}\right) + SN\left(\frac{\partial \sigma_x^3}{\partial N_i}\right)\right] \quad \text{(A.79)}$$

with the following derivative expresions

$$S_{\sigma_x} = \sum_k x_k m_k \sigma_{kk}^3 \quad \text{(A.80)}$$

$$N\left(\frac{\partial S_{\sigma_x}}{\partial N_i}\right) = m_i\sigma_{ii}^3 - S_{\sigma_x} \quad \text{(A.81)}$$

$$N\left(\frac{\partial S}{\partial N_i}\right) = m_i - S \quad \text{(A.82)}$$

$$N\left(\frac{\partial \sigma_x^3}{\partial N_i}\right) = \frac{2}{S}\sum_k \sum_j m_i x_{s,j}\sigma_{kj}^3(\delta_{ik} - x_{s,k}) \quad \text{(A.83)}$$

and the remaining second order expresion is given by

$$N\frac{\partial}{\partial N_i}\left(\frac{\partial \zeta_x^{\text{eff}}}{\partial \lambda_{kk}}\right) = N\frac{\partial}{\partial N_i}\left(\frac{\partial \zeta_x^{\text{eff}}}{\partial \lambda_x}\right)\left(\frac{\partial \lambda_x}{\partial \lambda_{kk}}\right) + N\frac{\partial}{\partial N_i}\left(\frac{\partial \lambda_x}{\partial \lambda_{kk}}\right)\left(\frac{\partial \zeta_x^{\text{eff}}}{\partial \lambda_x}\right) \quad \text{(A.84)}$$

with

$$N\frac{\partial}{\partial N_i}\left(\frac{\partial \zeta_x^{\text{eff}}}{\partial \lambda_x}\right) = \sum_l^3 l\zeta_x^{(l-1)}\left(\frac{\partial C_l}{\partial \lambda_x}\right) N\left(\frac{\partial \zeta_x}{\partial N_i}\right) + \sum_l^3 \zeta_x^l N\frac{\partial}{\partial N_i}\left(\frac{\partial C_l}{\partial \lambda_x}\right) \quad \text{(A.85)}$$

and

$$\begin{aligned} N\frac{\partial}{\partial N_i}\left(\frac{\partial \lambda_x}{\partial \lambda_{kj}}\right) =& \frac{1}{\lambda_x^2\sigma_{2x}^3}\left[\chi_j N\left(\frac{\partial \psi_{kj}}{\partial N_i}\right) + \psi_{kj} N\left(\frac{\partial \chi_j}{\partial N_i}\right)\right] \\ & - \frac{\chi_j\psi_{kj}}{(\lambda_x^2\sigma_{2x}^3)^2}\left[\sigma_{2x}^3 N\left(\frac{\partial \lambda_x^2}{\partial N_i}\right) + \lambda_x^2 N\left(\frac{\partial \sigma_{2x}^3}{\partial N_i}\right)\right] \end{aligned} \quad \text{(A.86)}$$

where σ_{2x}^3 is given by the Eq. (A.39). The other derivative expressions in Eq. (A.86) are

$$\chi_j = \sum_l x_{s,l}\epsilon_{jl}\sigma_{ll}^{3/2}(\lambda_{ll}^3 - 1)^{1/2} \quad \text{(A.87)}$$

and

$$\psi_{kj} = x_{s,j}\sigma_{jj}^{3/2}\lambda_{kk}^2/(\lambda_{jj}^3 - 1)^{1/2} \quad \text{(A.88)}$$

The first order derivative expressions in Eq. (A.86) are given by

$$N\left(\frac{\partial\psi_{kj}}{\partial N_i}\right)=\left(\frac{m_i}{S}\right)\left[\sigma_{jj}^{3/2}\lambda_{kk}^2\delta_{ij}/(\lambda_{jj}^3-1)^{1/2}-\psi_{kj}\right] \tag{A.89}$$

where δ_{ij} is the kronecker's delta.

$$N\left(\frac{\partial\chi_j}{\partial N_i}\right)=\left(\frac{m_i}{S}\right)\left[\epsilon_{ji}\sigma_{ii}^{3/2}(\lambda_{ii}^3-1)^{1/2}-\chi_j\right] \tag{A.90}$$

and

$$N\left(\frac{\partial\sigma_{2x}^3}{\partial N_i}\right)=\left(\frac{2m_i}{S}\right)\left[\sum_j x_{s,j}\epsilon_{ij}\sigma_{ij}^3-\sigma_{2x}^3\right] \tag{A.91}$$

The others derivative expressions are easy to calculate.

4. Quantum Contribution: The quantum contribution to the chemical potential, μ_i^Q, is expressed as

$$\frac{\mu_i^{\mathrm{Q}}}{kT}=a_1^{\mathrm{Q}}+N\left(\frac{\partial a1^{\mathrm{Q}}}{\partial N_i}\right)_{T,V,N_{i\neq j}} \tag{A.92}$$

The first order quantum contribution term a_1^Q is given by

$$a_1^Q=\frac{1}{(2\pi)^2}\tau_x\Gamma_x \tag{A.93}$$

with

$$\Gamma_x=\left(\frac{\partial a_1}{\partial\lambda_x}\right)\Lambda_x^2=\left(\frac{\partial a_1}{\partial\lambda_x}\right)\sum_k\sum_j x_{s,k}x_{s,j}\Lambda_{k,j}^2 \tag{A.94}$$

$$\tau_x(\zeta_x;t_x;\lambda_x)=t_x\left[t_x-\frac{2}{\lambda_x}-\vartheta_1(\zeta_x)-2\vartheta_2(\zeta_x)\lambda_x-3\vartheta_3(\zeta_x)\lambda_x^2\right] \tag{A.95}$$

where $t_x=\left(1-e^{-\beta\epsilon_x}\right)$ and ϵ_x is given by

$$\epsilon_x=\sum_k\sum_j x_{s,k}x_{s,j}\epsilon_{kj} \tag{A.96}$$

The ϑ_i functions can be written as,

$$\vartheta_1(\zeta_x) = \frac{\zeta_x^4 + 6\zeta_x^2 - 12\zeta_x}{2(1-\zeta_x)^3} \tag{A.97}$$

$$\vartheta_2(\zeta_x) = -\frac{3\zeta_x^2}{8(1-\zeta_x)^2} \tag{A.98}$$

$$\vartheta_3(\zeta_x) = \frac{-\zeta_x^4 + 3\zeta_x^2 + 3\zeta_x}{6(1-\zeta_x)^3} \tag{A.99}$$

In the VdW-1 fluid theory the classical term a_1 is approximated as a single fluid, therefore

$$\left(\frac{\partial a_1}{\partial \lambda_x}\right) = -\rho_s \left[\alpha_x^{\mathrm{VDW}} \left(\frac{\partial \mathrm{g}_o^{\mathrm{HS}}(\sigma_x;\zeta_x^{\mathrm{eff}})}{\partial \lambda_x}\right) + \mathrm{g}_o^{\mathrm{HS}}(\sigma_x;\zeta_x^{\mathrm{eff}}) \left(\frac{\partial \alpha_x^{\mathrm{VDW}}}{\partial \lambda_x}\right)\right] \tag{A.100}$$

In order to determine the Eq. (A.100), we may proceed by write the following expressions

$$\alpha_x^{\mathrm{VDW}} = \frac{2}{3}\pi\sigma_{2x}^3(\lambda_x^3 - 1) \tag{A.101}$$

$$\left(\frac{\partial \alpha_x^{\mathrm{VDW}}}{\partial \lambda_x}\right) = 2\pi\lambda_x^2\sigma_{2x}^3\lambda_x^2 \tag{A.102}$$

and

$$\left(\frac{\partial \mathrm{g}_o^{\mathrm{HS}}(\sigma_x;\zeta_x^{\mathrm{eff}})}{\partial \lambda_x}\right) = \left(\frac{\partial \mathrm{g}_o^{\mathrm{HS}}(\sigma_x;\zeta_x^{\mathrm{eff}})}{\partial \zeta_x^{\mathrm{eff}}}\right)\left(\frac{\partial \zeta_x^{\mathrm{eff}}}{\partial \lambda_x}\right) \tag{A.103}$$

In Eqs. (A.102)- (A.103) the differential expressions were defined by Eqs. (A.31)-(A.35) and (A.68). In order to calculate the quantum contribution to the chemical potential, μ_i^Q, the partial derivative expression for a_1^Q can be written as

$$N\left(\frac{\partial a_1^{\mathrm{Q}}}{\partial N_i}\right)_{T,V,N_{i\neq j}} = \left(\frac{a_1^{\mathrm{Q}}}{\tau_x}\right) N\left(\frac{\partial \tau_x}{\partial N_i}\right) + \frac{\tau_x}{(2\pi)^2} N\left(\frac{\partial \Gamma_x}{\partial N_i}\right) \tag{A.104}$$

In order to evaluate the Eq. A.104, we need the Eq. A.36 and the expresions for the

following two terms:

$$N\left(\frac{\partial \tau_x}{\partial N_i}\right) = \frac{\tau_x}{t_x} N\left(\frac{\partial t_x}{\partial N_i}\right) + t_x\left\{-N\left(\frac{\partial \vartheta_1}{\partial N_i}\right) - 2\lambda_x N\left(\frac{\partial \vartheta_2}{\partial N_i}\right) - 3\lambda_x^2 N\left(\frac{\partial \vartheta_3}{\partial N_i}\right) + N\left(\frac{\partial t_x}{\partial N_i}\right) + \left[\left(\frac{2}{\lambda_x^2}\right) - 2\vartheta_2 - 6\lambda_x\vartheta_3\right] N\left(\frac{\partial \lambda_x}{\partial N_i}\right)\right\} \tag{A.105}$$

From the Eq. A.105 we need the following expresions

$$N\left(\frac{\partial t_x}{\partial N_i}\right) = \left(\frac{2m_i}{S}\right)\beta e^{-\beta\epsilon_x}\left[\sum_j x_{s,j}\epsilon_{ij} - \epsilon_x\right] \tag{A.106}$$

$$N\left(\frac{\partial \vartheta_k}{\partial N_i}\right) = \left(\frac{\partial \vartheta_k}{\partial \zeta_x}\right) N\left(\frac{\partial \zeta_x}{\partial N_i}\right) \tag{A.107}$$

where $k = 1, 2, 3$.

$$\begin{aligned} N\left(\frac{\partial \vartheta_1}{\partial \zeta_x}\right) &= \frac{1}{2}\left[\frac{-12 - 12\zeta_x + 6\zeta_x^2 + 4\zeta_x^3 - \zeta_x^4}{(1-\zeta_x)^4}\right] \\ N\left(\frac{\partial \vartheta_2}{\partial \zeta_x}\right) &= \frac{-3\zeta_x}{4(1-\zeta_x)^3} \\ N\left(\frac{\partial \vartheta_3}{\partial \zeta_x}\right) &= \frac{1}{6}\left[\frac{3 + 12\zeta_x + 3\zeta_x^2 - 4\zeta_x^3 + \zeta_x^4}{(1-\zeta_x)^4}\right] \end{aligned} \tag{A.108}$$

In Eq. A.104 the second term is given by

$$N\left(\frac{\partial \Gamma_x}{\partial N_i}\right) = \left(\frac{2m_i}{S}\right)\left(\frac{\partial a_1}{\partial \lambda_x}\right)\left[\sum_j x_{s,j}\Lambda_{ij}^2 - \Lambda_x^2\right] + N\frac{\partial}{\partial N_i}\left(\frac{\partial a_1}{\partial \lambda_x}\right)\Lambda_x^2 \tag{A.109}$$

where

$$\begin{aligned} N\frac{\partial}{\partial N_i}\left(\frac{\partial a_1}{\partial \lambda_x}\right) =& N\frac{\partial}{\partial N_i}\left\{-\rho_s\left[\left(\frac{\partial \alpha_x^{\mathrm{VDW}}}{\partial \lambda_x}\right)\mathrm{g}_o^{\mathrm{HS}}(\sigma_x;\zeta_x^{\mathrm{eff}}) + \alpha_x^{\mathrm{VDW}}\left(\frac{\partial \mathrm{g}_o^{\mathrm{HS}}(\sigma_x;\zeta_x^{\mathrm{eff}})}{\partial \lambda_x}\right)\right]\right\} \\ =& -\rho m_i\left[\alpha_x^{\mathrm{VDW}}\left(\frac{\partial \mathrm{g}_o^{\mathrm{HS}}}{\partial \lambda_x}\right) + \mathrm{g}_o^{\mathrm{HS}}(\sigma_x;\zeta_x^{\mathrm{eff}})\left(\frac{\partial \alpha_x^{\mathrm{VDW}}}{\partial \lambda_x}\right)\right] \\ & -\rho_s\left[\alpha_x^{\mathrm{VDW}} N\frac{\partial}{\partial N_i}\left(\frac{\partial \mathrm{g}_o^{\mathrm{HS}}}{\partial \lambda_x}\right) + \left(\frac{\partial \mathrm{g}_o^{\mathrm{HS}}}{\partial \lambda_x}\right) N\left(\frac{\partial \alpha_x^{\mathrm{VDW}}}{\partial N_i}\right)\right. \\ & \left. + \left(\frac{\partial \alpha_x^{\mathrm{VDW}}}{\partial \lambda_x}\right) N\left(\frac{\partial \mathrm{g}_o^{\mathrm{HS}}}{\partial N_i}\right) + \mathrm{g}_o^{\mathrm{HS}}(\sigma_x;\zeta_x^{\mathrm{eff}}) N\frac{\partial}{\partial N_i}\left(\frac{\partial \alpha_x^{\mathrm{VDW}}}{\partial \lambda_x}\right)\right] \end{aligned} \tag{A.110}$$

with

$$N\frac{\partial}{\partial N_i}\left(\frac{\partial \alpha_x^{\mathrm{VDW}}}{\partial \lambda_x}\right) = 2\pi\lambda_x\left[\lambda_x N\left(\frac{\partial \sigma_{2x}^3}{\partial N_i}\right) + 2\sigma_{2x}^3 N\left(\frac{\partial \lambda_x}{\partial N_i}\right)\right] \tag{A.111}$$

and

$$\begin{aligned} N\frac{\partial}{\partial N_i}\left(\frac{\partial \mathrm{g}_o^{\mathrm{HS}}(\sigma_x;\zeta_x^{\mathrm{eff}})}{\partial \lambda_x}\right) = &\left(\frac{\partial \zeta_x^{\mathrm{eff}}}{\partial \lambda_x}\right) N\frac{\partial}{\partial N_i}\left(\frac{\partial \mathrm{g}_o^{\mathrm{HS}}(\sigma_x;\zeta_x^{\mathrm{eff}})}{\partial \zeta_x^{\mathrm{eff}}}\right) \\ &+ \left(\frac{\partial \mathrm{g}_o^{\mathrm{HS}}(\sigma_x;\zeta_x^{\mathrm{eff}})}{\partial \zeta_x^{\mathrm{eff}}}\right) N\frac{\partial}{\partial N_i}\left(\frac{\partial \zeta_x^{\mathrm{eff}}}{\partial \lambda_x}\right) \end{aligned} \tag{A.112}$$

Combining rules: In this work, we use the standard Lorentz-Berthelot[8] in three cases: i) diameter of the molecules σ_{ij}, and ii) depth enregy parameter ϵ_{ij} and iii) the de Boer's parameter, as follows

$$\sigma_{ij} = \frac{\sigma_{ii} + \sigma_{jj}}{2}, \qquad \epsilon_{ij} = (\epsilon_{ii}\epsilon_{jj})^{1/2} \tag{A.113}$$

$$\Lambda_{ij} = \frac{\Lambda_{ii}\sigma_{ii} + \Lambda_{jj}\sigma_{jj}}{2\sigma_{ij}} \tag{A.114}$$

The cross parameter of variable range λ_{ij} was derived from the van der Waals energy constant according to the Berthelot rule.[5]

$$\lambda_{ij}^3 = 1 + \frac{1}{\sigma_{ij}^3}\left[(\lambda_{ii}^3 - 1)(\lambda_{jj}^3 - 1)\sigma_{ii}^3\sigma_{jj}^3\right]^{1/2} \tag{A.115}$$

Other useful differential expression from the Eq. A.115, is given by

$$\left(\frac{\partial \lambda_{ij}}{\partial \lambda_{kl}}\right) = \frac{\sigma_{ii}^{3/2}\sigma_{jj}^{3/2}\lambda_{kk}^2\delta_{il}(\lambda_{jj}^3 - 1)}{\sigma_{ij}^3\lambda_{ij}^2\left[(\lambda_{ii}^3 - 1)(\lambda_{jj}^3 - 1)\right]^{1/2}} \tag{A.116}$$

where δ_{il} is the Kronecker delta. As can be observed in Eq. A.116, when the subscripts have the following form $i = j = k = l$, the expression $(\partial\lambda_{ij}/\partial\lambda_{kl}) = (\partial\lambda_{ii}/\partial\lambda_{kk}) = 1$.

BIBLIOGRAPHY

[1] T. J. Boublik, *J. Chem. Phys.* **53**, 471 (1971).

[2] G. A. Mansoori, N. F. Carnahan, K. E. Starling, T. W. Leland, **54**, 1523 (1971).

[3] A. Gil-Villegas, A. Galindo, P. J. Whitehead, S. J. Mills, G. Jackson, A. N. Burgess, *J. Chem. Phys.* **106**, 4168 (1997).

[4] A. Galindo, L. A. Davies, A. Gil-Villegas, *Mol. Phys.* **93**, 241 (1998).

[5] M. Castro, A. Martínez, A. Gil-Villegas, *Ads. Sc. and Tech.* **29**, 59 (2011).

[6] L. L. Lee, *Molecular Thermodynamics of Nonideal Fluids*, Butherworths, United States of America (1988).

APPENDIX B

APPENDIX B

Expression for the chemical potentials

We discuss the chemical potential terms from the corresponding Helmholtz free energy terms. The expressions are as follows

$$\frac{\mu_i^{2D}}{kT} = \frac{\mu_i^{\text{ideal}}}{kT} + \frac{\mu_i^{\text{mono}}}{kT} + \frac{\mu_i^{\text{chain}}}{kT} \tag{B.1}$$

where μ_i is the chemical potential of the i-component, T is the temperature and k is the Boltzmann constant. There is no need to include the association term since we are dealing with a nonassociating system.

1. Ideal Contribution: The ideal contribution to the chemical potential, μ_i^{ideal}, can be expressed as

$$\frac{\mu_i^{\text{ideal}}}{kT} = a^{\text{ideal}} + N\left(\frac{\partial a^{\text{ideal}}}{\partial N_i}\right)_{T,V,N_{i\neq j}} = \ln\left(\rho_i^{2D}\lambda_{Bi}^2\right) \tag{B.2}$$

with

$$a^{\text{ideal}} = \sum_{i=1}^{n} x_i \ln\left(\rho_i^{2D}\lambda_{Bi}^2\right) - 1 \tag{B.3}$$

where $x_i = N_i/N$ is the mole fraction, $\rho_i^{2D} = N_i/A$ the molecular number of density, N_i the number of molecules, λ_{Bi} the thermal Broglie wavelength of species i.

2. Monomer contribution: The monomer contribution to the chemical potential, μ_i^{mono}, can be expressed as

$$\frac{\mu_i^{\text{mono}}}{kT} = a^{\text{mono}} + N\left(\frac{\partial a^{\text{mono}}}{\partial N_i}\right)_{T,V,N_{i\neq j}} \tag{B.4}$$

where

$$\begin{aligned}\frac{\mu_i^{\text{mono}}}{kT} &= S\left[a^{\text{M}} + N\left(\frac{\partial a^{\text{M}}}{\partial N_i}\right)\right] + a^{\text{M}}(m_i - S) \\ &= S\left[\frac{\mu_i^{\text{HD}}}{kT} + \beta\frac{\mu_{1i}}{kT} + \beta^2\frac{\mu_{2i}}{kT}\right] + a^{\text{M}}(m_i - S)\end{aligned} \tag{B.5}$$

where a^{mono} is the monomer Helmholtz free energy, given by

$$a^{\text{mono}} = \left(\sum_k x_k m_k\right) a^{\text{M}} = S a^{\text{M}} = S\left[a^{\text{HD}} + \beta a_1 + \beta^2 a_2\right] \tag{B.6}$$

where m_k is the number of spherical segments of chain i, S is the average of m_i, $(S = \sum_k x_k m_k)$, $\beta = 1/kT$.

2.1 Hard-Disk contribution: The hard-disk contribution to the chemical potential, μ^{HD}, is given by

$$\frac{\mu_i^{\text{HD}}}{NkT} = a^{\text{HD}} + N\left(\frac{\partial a^{\text{HD}}}{\partial N_i}\right)_{T,V,N_{i\neq j}} \tag{B.7}$$

In this work the hard-disk propeties were obtained by using the equation of state proposed by Santos *et al.* (1999)[1]

$$a^{\text{HD}} = -w + \ln(1-\gamma)\left((B_3 - 3)w - 1\right) + \frac{w\left(1 + (B_3 - 3)\gamma\right)}{(1-\gamma)} \tag{B.8}$$

where B_3 is the third virial coefficient of the system $(B_3 = (16/3) - (4/\pi)\sqrt{3})$ and diameter average $w = (\sum_k x_{s,k}\sigma_k)^2 / \sum_k x_{s,k}\sigma_k^2$. The packing fraction for a hard-disk mixture γ is given by

$$\gamma = \frac{\pi}{4}\rho_s^{2D}\left[\sum_{i=1}^{n} x_{s,i}\sigma_i^2\right] \tag{B.9}$$

where σ_i is diameter of segments of type i and $x_{s,i}$ is the mole fraction of segments in the mixtures $(x_{s,i} = m_i x_i / S)$. In Eq. (B.7), the differential expression can be written

as

$$N\left(\frac{\partial a^{\mathrm{HD}}}{\partial N_i}\right)_{T,V,N_{i\neq j}} = -\frac{(B_3-1)w-1}{(1-\gamma)}N\left(\frac{\partial \gamma}{\partial N_i}\right) - N\left(\frac{\partial w}{\partial N_i}\right) + \frac{1}{(1-\gamma)}\left[(1+(B_3-3)\gamma)N\left(\frac{\partial w}{\partial N_i}\right) + w(B_3-3)N\left(\frac{\partial \gamma}{\partial N_i}\right)\right] + \ln(1-\gamma)(B_3-3)N\left(\frac{\partial w}{\partial N_i}\right) + \frac{w(1+(B_3-3)\gamma)}{(1-\gamma)^2}N\left(\frac{\partial \gamma}{\partial N_i}\right) \quad \text{(B.10)}$$

where

$$N\left(\frac{\partial \gamma}{\partial N_i}\right) = \frac{\pi}{4}\rho^{2D} m_i \sigma_i^2 \quad \text{(B.11)}$$

and

$$N\left(\frac{\partial w}{\partial N_i}\right) = \left(\frac{w_1}{w_2}\right)\left[2N\left(\frac{\partial w_1}{\partial N_i}\right) - \left(\frac{w_1}{w_2}\right)N\left(\frac{\partial w_2}{\partial N_i}\right)\right] \quad \text{(B.12)}$$

with

$$w_l = \sum_k x_{s,k}\sigma_k^l \quad \text{(B.13)}$$

$$N\left(\frac{\partial w_l}{\partial N_i}\right) = m_i(\sigma_i^l - w_l)/S \quad \text{(B.14)}$$

where $l = 1, 2$.

2.2 First-order perturbation term: The first-order perturbation term contribution to the chemical potential, μ_{1i}, is expressed as

$$\frac{\mu_{1i}}{kT} = a_1 + N\left(\frac{\partial a_1}{\partial N_i}\right)_{T,V,N_{i\neq j}} \quad \text{(B.15)}$$

Using the mean value theorem,[4,5] we obtain an expression for a_1 in terms of the contact value of g_{kj}^{HD}

$$a_1 = -\rho_s^{2D}\sum_k\sum_j x_{s,k}x_{s,j}\alpha_{kj}^{\mathrm{VDW}}\mathrm{g}_{kj}^{\mathrm{HD}}(\sigma_{kj};\gamma) \quad \text{(B.16)}$$

where

$$\alpha_{kj}^{\mathrm{VDW}} = \pi\epsilon_{kj}\sigma_{kj}^2(\lambda_{kj}^2 - 1)/2 \quad \text{(B.17)}$$

In the van der Waals one-fluid theory (VDW-1) $\mathrm{g}_{kj}^{\mathrm{HD}}$ is approximated by the radial

distribution function for a single fluid such as

$$a_1 = -\rho_s^{2D} \sum_k \sum_j x_{s,k} x_{s,j} \alpha_{kj}^{\mathrm{VDW}} \mathrm{g}_o^{\mathrm{HD}}(\sigma_x; \gamma_x^{\mathrm{eff}})$$
$$= -\rho_s^{2D} \alpha_x^{\mathrm{VDW}} \mathrm{g}_o^{\mathrm{HD}}(\sigma_x; \gamma_x^{\mathrm{eff}}) \tag{B.18}$$

where

$$\alpha_x^{\mathrm{VDW}} = \sum_k \sum_j x_{s,k} x_{s,j} \alpha_{kj}^{\mathrm{VDW}} \tag{B.19}$$

where $\mathrm{g}_o^{\mathrm{HD}}$ is the contact value of the hard-sphere pair radial distribution function obtained from the Henderson equation,[6]

$$\mathrm{g}_o^{\mathrm{HD}}(\sigma_x; \gamma_x^{\mathrm{eff}}) = \frac{1 - 7\gamma_x^{\mathrm{eff}}/16}{(1 - \gamma_x^{\mathrm{eff}})^2} \tag{B.20}$$

where γ_x^{eff} is the effective packing fraction obtained within the VDW-1 from the corresponding packing fraction of the mixture γ_x given by,

$$\gamma_x^{\mathrm{eff}}(\gamma_x, \lambda_x) = d_1(\lambda_x)\gamma_x + d_2(\lambda_x)\gamma_x^2 \tag{B.21}$$

where

$$\gamma_x = \frac{\pi}{4} \rho_s^{2D} \sum_k \sum_j x_{s,k} x_{s,j} \sigma_{kj}^2 = \frac{\pi}{4} \rho_s^{2D} \sigma_x^2 \tag{B.22}$$

with

$$\sigma_x^2 = \sum_k \sum_j x_{s,k} x_{s,j} \sigma_{kj}^2 \tag{B.23}$$

The coefficients d_1 and d_2 are approximated by those of the pure fluid,

$$\begin{pmatrix} d_1 \\ d_2 \end{pmatrix} = \begin{pmatrix} 1.4215 & -0.405625 & -0.0386998 \\ 1.5582 & -1.89768 & 0.405215 \end{pmatrix} \begin{pmatrix} 1 \\ \lambda_x \\ \lambda_x^2 \end{pmatrix} \tag{B.24}$$

In the case of 2D-fluid the unlike range parameter is obtained from the weighted mean of the pure components values used in a previous works[7]

$$\lambda_x^2 = \frac{\sum_k \sum_j x_{s,k} x_{s,j} \epsilon_{kj} \lambda_{kj}^2 \sigma_{kj}^2}{\sum_k \sum_j x_{s,k} x_{s,j} \epsilon_{kj} \sigma_{kj}^2} \tag{B.25}$$

The differential expression in the Eq. (B.15) can be calculated as

$$N\left(\frac{\partial a_1}{\partial N_i}\right)_{T,V,N_{i\neq j}} = -\alpha_x^{\mathrm{VDW}} \mathrm{g}_o^{\mathrm{HD}}(\sigma_x;\gamma_x^{\mathrm{eff}}) N\left(\frac{\partial \rho_s^{2D}}{\partial N_i}\right) - \rho_s^{2D} \mathrm{g}_o^{\mathrm{HD}}(\sigma_x;\gamma_x^{\mathrm{eff}}) N\left(\frac{\partial \alpha_x^{\mathrm{VDW}}}{\partial N_i}\right) - \rho_s^{2D}\alpha_x^{\mathrm{VDW}} N\left(\frac{\partial \mathrm{g}_o^{\mathrm{HD}}(\sigma_x;\gamma_x^{\mathrm{eff}})}{\partial N_i}\right) \quad \text{(B.26)}$$

where

$$N\left(\frac{\partial \rho_s^{2D}}{\partial N_i}\right) = \rho^{2D} m_i \quad \text{(B.27)}$$

end

$$N\left(\frac{\partial \alpha_x^{\mathrm{VDW}}}{\partial N_i}\right) = \frac{2}{S}\sum_k \sum_j m_i x_{s,j} \alpha_{kj}^{\mathrm{VDW}} (\delta_{ik} - x_{s,k}) \quad \text{(B.28)}$$

The last differential expression in Eq.(B.26), can be development as

$$N\left(\frac{\partial \mathrm{g}_o^{\mathrm{HD}}(\sigma_x;\gamma_x^{\mathrm{eff}})}{\partial N_i}\right) = \left(\frac{\partial \mathrm{g}_o^{\mathrm{HD}}(\sigma_x;\gamma_x^{\mathrm{eff}})}{\partial \gamma_x^{\mathrm{eff}}}\right) N\left(\frac{\partial \gamma_x^{\mathrm{eff}}}{\partial N_i}\right) \quad \text{(B.29)}$$

where

$$\left(\frac{\partial \mathrm{g}_o^{\mathrm{HD}}(\sigma_x;\gamma_x^{\mathrm{eff}})}{\partial \gamma_x^{\mathrm{eff}}}\right) = \frac{(25 - 7\gamma_x^{\mathrm{eff}})/16}{(1-\gamma_x^{\mathrm{eff}})^3} \quad \text{(B.30)}$$

$$N\left(\frac{\partial \gamma_x^{\mathrm{eff}}}{\partial N_i}\right) = \left(\frac{\partial \gamma_x^{\mathrm{eff}}}{\partial \gamma_x}\right) N\left(\frac{\partial \gamma_x}{\partial N_i}\right) + \left(\frac{\partial \gamma_x^{\mathrm{eff}}}{\partial \lambda_x}\right) N\left(\frac{\partial \lambda_x}{\partial N_i}\right) \quad \text{(B.31)}$$

The differential terms in Eq. (B.31) are given by

$$\left(\frac{\partial \gamma_x^{\mathrm{eff}}}{\partial \gamma_x}\right) = d_1 + 2d_2\gamma_x \quad \text{(B.32)}$$

$$N\left(\frac{\partial \gamma_x}{\partial N_i}\right) = \frac{\pi}{4}\rho^{2D}\sum_k \sum_j m_i x_{s,j} \sigma_{kj}^2 (2\delta_{ki} - x_{s,k}) \quad \text{(B.33)}$$

where δ_{ki} is the Kronecker's delta.

$$\left(\frac{\partial \gamma_x^{\mathrm{eff}}}{\partial \lambda_x}\right) = \gamma_x\left(\frac{\partial d_1}{\partial \lambda_x}\right) + \gamma_x^2\left(\frac{\partial d_2}{\partial \lambda_x}\right) \quad \text{(B.34)}$$

$$N\left(\frac{\partial \lambda_x}{\partial N_i}\right) = \frac{1}{S\lambda_x}\left(\frac{D_1\sigma_{2x}^2 - E_1\lambda_{2x}^2}{(\sigma_{2x}^2)^2}\right) \quad \text{(B.35)}$$

with

$$D_1 = \sum_j m_i x_{s,j} \epsilon_{ij} \lambda_{ij}^2 \sigma_{ij}^2 \tag{B.36}$$

$$E_1 = \sum_j m_i x_{s,j} \epsilon_{ij} \sigma_{ij}^2 \tag{B.37}$$

$$\sigma_{2x}^2 = \sum_k \sum_j x_{s,k} x_{s,j} \epsilon_{kj} \sigma_{kj}^2 \tag{B.38}$$

$$\lambda_{2x}^2 = \sum_k \sum_j x_{s,k} x_{s,j} \epsilon_{kj} \lambda_{kj}^2 \sigma_{kj}^2 \tag{B.39}$$

2.3 Second-order perturbation term: The second-order perturbation term contribution to the chemical potential, μ_{2i}, is given by

$$\frac{\mu_{2i}}{kT} = a_2 + N \left(\frac{\partial a_2}{\partial N_i} \right)_{T,V,N_{i \neq j}} \tag{B.40}$$

The second-order perturbation term for the monomer excess free energy a_2, is obtained through the local compresibility approximation as

$$a_2 = \frac{1}{2} \rho_s^{2D} \sum_k \sum_j x_{s,k} x_{s,j} \epsilon_{kj} K^{\mathrm{HD}} \left(\frac{\partial a_1^{kj}}{\partial \rho_s^{2D}} \right) \tag{B.41}$$

with

$$\left(\frac{\partial a_1^{kj}}{\partial \rho_s^{2D}} \right) = -\alpha_{kj}^{VDW} \left[\mathrm{g}_o^{\mathrm{HD}}(\sigma_x; \gamma_x^{\mathrm{eff}}) + \rho_s^{2D} \left(\frac{\partial \mathrm{g}_o^{\mathrm{HD}}(\sigma_x; \gamma_x^{\mathrm{eff}})}{\partial \rho_s^{2D}} \right) \right] \tag{B.42}$$

According with the Eqs. (B.41-B.42), the second-order perturbation term a_2 can be reorganized as follows

$$a_2 = -\frac{1}{2} \rho_s^{2D} K^{\mathrm{HD}} \alpha_{2x}^{\mathrm{VDW}} \mathrm{g}_{ox}^{\mathrm{HD}} \tag{B.43}$$

where $\mathrm{g}_{ox}^{\mathrm{HD}}$ is given by

$$\mathrm{g}_{ox}^{\mathrm{HD}} = \mathrm{g}_o^{\mathrm{HD}}(\sigma_x; \gamma_x^{\mathrm{eff}}) + \rho_s^{2D} \left(\frac{\partial \mathrm{g}_o^{\mathrm{HD}}(\sigma_x; \gamma_x^{\mathrm{eff}})}{\partial \rho_s^{2D}} \right) \tag{B.44}$$

with

$$\rho_s^{2D}\left(\frac{\partial \mathrm{g}_o^{\mathrm{HD}}(\sigma_x;\gamma_x^{\mathrm{eff}})}{\partial \rho_s^{2D}}\right)=\left(\frac{\partial \mathrm{g}_o^{\mathrm{HD}}(\sigma_x;\gamma_x^{\mathrm{eff}})}{\partial \gamma_x^{\mathrm{eff}}}\right)\left(\frac{\partial \gamma_x^{\mathrm{eff}}}{\partial \gamma_x}\right)\gamma_x \tag{B.45}$$

and

$$\alpha_{2x}^{\mathrm{VDW}}=\sum_k\sum_j x_{s,k}x_{s,j}\epsilon_{kj}\alpha_{kj}^{\mathrm{VDW}} \tag{B.46}$$

where K^{HD} is the expression for the hard-disk isothermal compresibility,

$$K^{\mathrm{HD}}=\frac{(1-\gamma)^3}{1+(2w-1)\gamma+3w(B_3-3)\gamma^2-w(B_3-3)\gamma^3} \tag{B.47}$$

For the particular case of $x_i\to 1$, Eq. B.47 is reduced to

$$\lim_{x_i\to 1}K^{\mathrm{HD}}=\frac{(1-\gamma)^3}{1+\gamma+\frac{3}{8}\gamma^2+\frac{1}{8}\gamma^3} \tag{B.48}$$

Here the K^{HD} of mixtures is reduced to the expression of pure components, with $w=1$ and $(B_3-3)\approx 1/8$. In order to calculate the contribution to the chemical potential, μ_{2i}, the partial derivative expression for a_2 can be written as

$$\begin{aligned}N\left(\frac{\partial a_2}{\partial N_i}\right)_{T,V,N_{i\neq j}}=&-\frac{1}{2}\rho_s^{2D}\mathrm{g}_{ox}^{\mathrm{HD}}\left[\alpha_{2x}^{\mathrm{VDW}}N\left(\frac{\partial K^{\mathrm{HD}}}{\partial N_i}\right)+K^{\mathrm{HD}}N\left(\frac{\partial \alpha_{2x}^{\mathrm{VDW}}}{\partial N_i}\right)\right]\\&-\frac{1}{2}K^{\mathrm{HD}}\alpha_{2x}^{\mathrm{VDW}}\left[\mathrm{g}_{ox}^{\mathrm{HD}}\rho^{2D}m_i+\rho_s^{2D}N\left(\frac{\partial \mathrm{g}_{ox}^{\mathrm{HD}}}{\partial N_i}\right)\right]\end{aligned} \tag{B.49}$$

The three partial derivative expressions are now

$$N\left(\frac{\partial K^{\mathrm{HD}}}{\partial N_i}\right)=\left(\frac{1-\gamma}{\psi_\gamma}\right)^2\left[-3N\left(\frac{\partial \gamma}{\partial N_i}\right)\psi_\gamma-(1-\gamma)N\left(\frac{\partial \psi_\gamma}{\partial N_i}\right)\right] \tag{B.50}$$

with

$$\psi_\gamma=1-(2w-1)\gamma+3w(B_3-3)\gamma^2-w(B_3-3)\gamma^3 \tag{B.51}$$

$$\begin{aligned}N\left(\frac{\partial \psi_\gamma}{\partial N_i}\right)=&\left[2\gamma+(3-\gamma)(B_3-3)\gamma^2\right]N\left(\frac{\partial w}{\partial N_i}\right)\\&+\left[(2w-1)+3w(3-\gamma)(B_3-3)\gamma\right]N\left(\frac{\partial \gamma}{\partial N_i}\right)\end{aligned} \tag{B.52}$$

The last two derivative expressions in Eq. (B.49) can be written as

$$N\left(\frac{\partial\alpha_{2x}^{\mathrm{VDW}}}{\partial N_i}\right)=\frac{2}{S}\sum_k\sum_j m_i x_{s,j}\epsilon_{kj}\alpha_{kj}^{\mathrm{VDW}}(\delta_{ik}-x_{s,k}) \tag{B.53}$$

and

$$\begin{aligned}N\left(\frac{\partial \mathrm{g}_{ox}^{\mathrm{HD}}}{\partial N_i}\right)=&\left(\frac{\partial \mathrm{g}_o^{\mathrm{HD}}(\sigma_x;\gamma_x^{\mathrm{eff}})}{\partial\gamma_x^{\mathrm{eff}}}\right)\left[\gamma_x N\frac{\partial}{\partial N_i}\left(\frac{\partial\gamma_x^{\mathrm{eff}}}{\partial\gamma_x}\right)+\left(\frac{\partial\gamma_x^{\mathrm{eff}}}{\partial\gamma_x}\right)N\left(\frac{\partial\gamma_x}{\partial N_i}\right)\right]\\&+N\left(\frac{\partial \mathrm{g}_o^{\mathrm{HD}}(\sigma_x;\gamma_x^{\mathrm{eff}})}{\partial N_i}\right)+\gamma_x\left(\frac{\partial\gamma_x^{\mathrm{eff}}}{\partial\gamma_x}\right)N\frac{\partial}{\partial N_i}\left(\frac{\partial \mathrm{g}_o^{\mathrm{HD}}(\sigma_x;\gamma_x^{\mathrm{eff}})}{\partial\gamma_x^{\mathrm{eff}}}\right)\end{aligned} \tag{B.54}$$

In Eq. (B.54) the first order differential terms were calculated using the Eqs. (B.29-B.39). We only need calculate the following expressions

$$N\frac{\partial}{\partial N_i}\left(\frac{\partial \mathrm{g}_o^{\mathrm{HD}}(\sigma_x;\gamma_x^{\mathrm{eff}})}{\partial\gamma_x^{\mathrm{eff}}}\right)=\left[\frac{(34-7\gamma_x^{\mathrm{eff}})/8}{(1-\gamma_x^{\mathrm{eff}})^4}\right]N\left(\frac{\partial\gamma_x^{\mathrm{eff}}}{\partial N_i}\right) \tag{B.55}$$

and

$$N\frac{\partial}{\partial N_i}\left(\frac{\partial\gamma_x^{\mathrm{eff}}}{\partial\gamma_x}\right)=2d_2N\left(\frac{\partial\gamma_x}{\partial N_i}\right)+N\left(\frac{\partial d_1}{\partial N_i}\right)+2\gamma_x N\left(\frac{\partial d_2}{\partial N_i}\right) \tag{B.56}$$

with

$$N\left(\frac{\partial d_l}{\partial N_i}\right)=\left(\frac{\partial d_l}{\partial\lambda_x}\right)N\left(\frac{\partial\lambda_x}{\partial N_i}\right) \tag{B.57}$$

where $l=1,2$.

3. Chain Contribution: The chain contribution to the chemical potential, μ_i^{chain}, is expressed as

$$\frac{\mu_i^{\mathrm{chain}}}{kT}=a^{\mathrm{chain}}+N\left(\frac{\partial a^{\mathrm{chain}}}{\partial N_i}\right)_{T,V,N_{i\neq j}} \tag{B.58}$$

The contribution to the free energy due to chain formation is expressed in terms of the contact value of the background correlation function[4,5]

$$a^{\mathrm{chain}}=-\sum_k x_k(m_k-1)\ln(y_{kk}^{\mathrm{SW}}(\sigma_{kk})) \tag{B.59}$$

where $y_{kk}^{\mathrm{SW}}(\sigma_{kk})=\mathrm{g}_{kk}^{\mathrm{SW}}(\sigma_{kk})\exp(-\beta\epsilon_{kk})$. According with the Eq. (B.59) the chemical

potential of chains, μ_i^{chain}, can be rewritten

$$\frac{\mu_i^{\text{chain}}}{kT} = -(m_i - 1)\ln(y_{ii}^{\text{SW}}) - \sum_k x_k(m_k - 1)\left(\frac{1}{\mathrm{g}_{kk}^{\text{SW}}}\right) N\left(\frac{\partial \mathrm{g}_{kk}^{\text{SW}}}{\partial N_i}\right) \tag{B.60}$$

where the $g_{kk}^{\text{SW}}(\sigma_{kk})$ can be expressed as a expansion at high temperature, as

$$\mathrm{g}_{kk}^{\text{SW}}(\sigma_{kk}) = \mathrm{g}_{kk}^{\text{HD}}(\sigma_{kk}) + \beta\epsilon_{kk}\mathrm{g}_1(\sigma_{kk}) \tag{B.61}$$

where $\mathrm{g}_{kk}^{\text{HD}}$ is the contact value of the Hard-Disk radial distribution function given by

$$\mathrm{g}_{kj}^{\text{HD}}(\gamma) = \frac{1}{2(1-\gamma)} + \frac{(1 + (B_3 - 3)\gamma)\sigma_k\sigma_j}{2w_2(1-\gamma)^2} \tag{B.62}$$

Using the VdW-1 fluid approximation we have

$$\mathrm{g}_1(\lambda_{kj}) = \mathrm{g}_o^{\text{HD}}(\sigma_x; \gamma_x^{\text{eff}}) + (\lambda_{kj}^2 - 1)\frac{\partial \mathrm{g}_o^{\text{HD}}(\sigma_x; \gamma_x^{\text{eff}})}{\partial \gamma_x^{\text{eff}}}\left(\frac{\lambda_{kj}}{2}\frac{\partial \gamma_x^{\text{eff}}}{\partial \lambda_{kj}} - \gamma\frac{\partial \gamma_x^{\text{eff}}}{\partial \gamma}\right) \tag{B.63}$$

In the above equation the partial differential expressions of γ_x^{eff} are given by

$$\left(\frac{\partial \gamma_x^{\text{eff}}}{\partial \lambda_{kj}}\right) = \left[\gamma_x\left(\frac{\partial d_1}{\partial \lambda_x}\right) + \gamma_x^2\left(\frac{\partial d_2}{\partial \lambda_x}\right)\right]\left(\frac{\partial \lambda_x}{\partial \lambda_{kj}}\right) \tag{B.64}$$

where the last derivative expression can be writtten as

$$\left(\frac{\partial \lambda_x}{\partial \lambda_{kj}}\right) = \left(\frac{x_{s,j}\sigma_{jj}\lambda_{kk}}{\lambda_x\sigma_{2x}^2(\lambda_{jj}^2 - 1)^{1/2}}\right)\sum_l x_{s,l}\epsilon_{jl}\sigma_{ll}(\lambda_{ll}^2 - 1)^{1/2} \tag{B.65}$$

with

$$\left(\frac{\partial \gamma_x^{\text{eff}}}{\partial \gamma}\right) = \left(\frac{\partial \gamma_x^{\text{eff}}}{\partial \gamma_x}\right)\left(\frac{\partial \gamma_x}{\partial \gamma}\right) \tag{B.66}$$

and

$$\left(\frac{\partial \gamma_x}{\partial \gamma}\right) = \sigma_x^2 / \left(\sum_k x_{s,k}\sigma_{kk}^2\right) \tag{B.67}$$

where σ_x^2 is given by Eq. (B.23). In order to calculate the chemical potentials of chains, μ_i^{chain}, from the Eq. (B.60), we need to calculate the following expression

$$N\left(\frac{\partial \mathrm{g}_{kk}^{\text{SW}}}{\partial N_i}\right) = N\left(\frac{\partial \mathrm{g}_{kk}^{\text{HD}}}{\partial N_i}\right) + (\beta\epsilon_{kk})N\left(\frac{\partial \mathrm{g}_1(\sigma_{kk})}{\partial N_i}\right) \tag{B.68}$$

where the first differential expression is given by

$$N\left(\frac{\partial \mathrm{g}_{kj}^{\mathrm{HD}}}{\partial N_i}\right) = \frac{\zeta_i \sigma_{kk}\sigma_{jj}}{2(1-\gamma)^3 w_2^2} + \frac{1}{2(1-\gamma)^2} N\left(\frac{\partial \gamma}{\partial N_i}\right) \tag{B.69}$$

with

$$\begin{aligned}\zeta_i =& w_2(1-\gamma)(B_3-3)N\left(\frac{\partial \gamma}{\partial N_i}\right) - (1+(B_3-3)\gamma)\left[(1-\gamma)N\left(\frac{\partial w_2}{\partial N_i}\right)\right. \\ & \left. -2w_2 N\left(\frac{\partial \gamma}{\partial N_i}\right)\right]\end{aligned} \tag{B.70}$$

The differential expressions for γ and w_2 are given in Eqs. (B.11)-(B.14). In the Eq. (B.68) the second differential expression is given by

$$\begin{aligned}N\left(\frac{\partial \mathrm{g}_1(\sigma_{kj})}{\partial N_i}\right) =& N\left(\frac{\partial \mathrm{g}_o^{\mathrm{HD}}(\sigma_x;\gamma_x^{\mathrm{eff}})}{\partial N_i}\right) + (\lambda_{kj}^2-1)\left[N\frac{\partial}{\partial N_i}\left(\frac{\partial \mathrm{g}_o^{\mathrm{HD}}(\sigma_x;\gamma_x^{\mathrm{eff}})}{\partial \gamma_x^{\mathrm{eff}}}\right)\varphi_{kj}\right. \\ & \left. + \left(\frac{\partial \mathrm{g}_o^{\mathrm{HD}}(\sigma_x;\gamma_x^{\mathrm{eff}})}{\partial \gamma_x^{\mathrm{eff}}}\right) N\left(\frac{\partial \varphi_{kj}}{\partial N_i}\right)\right]\end{aligned} \tag{B.71}$$

where

$$\varphi_{kj} = \frac{\lambda_{kj}}{2}\left(\frac{\partial \gamma_x^{\mathrm{eff}}}{\partial \lambda_{kj}}\right) - \gamma\left(\frac{\partial \gamma_x^{\mathrm{eff}}}{\partial \gamma}\right) \tag{B.72}$$

In Eq. (B.72) the two differential expressions for γ_x^{eff} are calculated using Eqs. (B.64)-(B.66). In Eq. (B.71) the first differential expressions for $\mathrm{g}_o^{\mathrm{HD}}$ are calculated using Eqs. (B.29)-(B.30) and (B.55). On the other hand, the remaining expression for φ_{kk} are given by

$$N\left(\frac{\partial \varphi_{kj}}{\partial N_i}\right) = \frac{\lambda_{kj}}{2} N\frac{\partial}{\partial N_i}\left(\frac{\partial \gamma_x^{\mathrm{eff}}}{\partial \lambda_{kj}}\right) - \gamma N\frac{\partial}{\partial N_i}\left(\frac{\partial \gamma_x^{\mathrm{eff}}}{\partial \gamma}\right) - N\left(\frac{\partial \gamma}{\partial N_i}\right)\left(\frac{\partial \gamma_x^{\mathrm{eff}}}{\partial \gamma}\right) \tag{B.73}$$

where the first order derivative expressions of γ and γ_x^{eff} are obtained from the Eqs. (B.11) and (B.66). The second derivative expressions are given by

$$N\frac{\partial}{\partial N_i}\left(\frac{\partial \gamma_x^{\mathrm{eff}}}{\partial \gamma}\right) = \left(\frac{\partial \gamma_x}{\partial \gamma}\right) N\frac{\partial}{\partial N_i}\left(\frac{\partial \gamma_x^{\mathrm{eff}}}{\partial \gamma_x}\right) + \left(\frac{\partial \gamma_x^{\mathrm{eff}}}{\partial \gamma_x}\right) N\frac{\partial}{\partial N_i}\left(\frac{\partial \gamma_x}{\partial \gamma}\right) \tag{B.74}$$

where first order derivative expresions are given by Eqs. (B.32) and (B.67). The

second order derivative expresions on the above equation, can written as

$$N\frac{\partial}{\partial N_i}\left(\frac{\partial \gamma_x}{\partial \gamma}\right) = -\frac{1}{S_{\sigma_x}^2} S\sigma_x^2 N\left(\frac{\partial S_{\sigma_x}}{\partial N_i}\right) + \frac{1}{S_{\sigma_x}}\left[\sigma_x^2 N\left(\frac{\partial S}{\partial N_i}\right) + SN\left(\frac{\partial \sigma_x^2}{\partial N_i}\right)\right] \quad \text{(B.75)}$$

with the following derivative expresions

$$S_{\sigma_x} = \sum_k x_k m_k \sigma_{kk}^2 \quad \text{(B.76)}$$

$$N\left(\frac{\partial S_{\sigma_x}}{\partial N_i}\right) = m_i\sigma_{ii}^2 - S_{\sigma_x} \quad \text{(B.77)}$$

$$N\left(\frac{\partial S}{\partial N_i}\right) = m_i - S \quad \text{(B.78)}$$

$$N\left(\frac{\partial \sigma_x^2}{\partial N_i}\right) = \frac{2}{S}\sum_k \sum_j m_i x_{s,j}\sigma_{kj}^2(\delta_{ik} - x_{s,k}) \quad \text{(B.79)}$$

and the remaining second order expresion is given by

$$N\frac{\partial}{\partial N_i}\left(\frac{\partial \gamma_x^{\text{eff}}}{\partial \lambda_{kj}}\right) = N\frac{\partial}{\partial N_i}\left\{\left[\gamma_x\left(\frac{\partial d_1}{\partial \lambda_x}\right) + \gamma_x^2\left(\frac{\partial d_2}{\partial \lambda_x}\right)\right]\left(\frac{\partial \lambda_x}{\partial \lambda_{kj}}\right)\right\} \quad \text{(B.80)}$$

with

$$\begin{aligned} N\frac{\partial}{\partial N_i}\left(\frac{\partial \lambda_x}{\partial \lambda_{kj}}\right) =& \frac{1}{\lambda_x\sigma_{2x}^2}\left[\chi_j N\left(\frac{\partial \psi_{kj}}{\partial N_i}\right) + \psi_{kj}N\left(\frac{\partial \chi_j}{\partial N_i}\right)\right] \\ & - \frac{\chi_j\psi_{kj}}{(\lambda_x\sigma_{2x}^2)^2}\left[\sigma_{2x}^2 N\left(\frac{\partial \lambda_x}{\partial N_i}\right) + \lambda_x N\left(\frac{\partial \sigma_{2x}^2}{\partial N_i}\right)\right] \end{aligned} \quad \text{(B.81)}$$

where σ_{2x}^3 is given by the Eq. (B.38). The other derivative expressions in Eq. (B.81) are

$$\chi_j = \sum_j x_{s,l}\epsilon_{jl}\sigma_{ll}(\lambda_{ll}^2 - 1)^{1/2} \quad \text{(B.82)}$$

and

$$\psi_{kj} = x_{s,j}\sigma_{jj}\lambda_{kk}/(\lambda_{jj}^2 - 1)^{1/2} \quad \text{(B.83)}$$

The first order derivative expressions in Eq. (B.81) are given by

$$N\left(\frac{\partial \psi_{kj}}{\partial N_i}\right) = \left(\frac{m_i}{S}\right)\left[\sigma_{jj}\lambda_{kk}\delta_{ij}/(\lambda_{jj}^2 - 1)^{1/2} - \psi_{kj}\right] \quad \text{(B.84)}$$

where δ_{ik} is the kronecker's delta.

$$N\left(\frac{\partial\chi_j}{\partial N_i}\right) = \left(\frac{m_i}{S}\right)\left[\epsilon_{ji}\sigma_{ii}(\lambda_{ii}^2-1)^{1/2}-\chi_j\right] \tag{B.85}$$

and

$$N\left(\frac{\partial\sigma_{2x}^2}{\partial N_i}\right) = \left(\frac{2m_i}{S}\right)\left[\sum_j x_{s,j}\epsilon_{ij}\sigma_{ij}^2-\sigma_{2x}^2\right] \tag{B.86}$$

The others derivative expressions are easy to calculate.

3. Quantum Contribution: The quantum contribution to the chemical potential, μ_i^{Q}, is expressed as

$$\frac{\mu_i^{\mathrm{Q}}}{kT} = a_1^{\mathrm{Q}} + N\left(\frac{\partial a_1^{\mathrm{Q}}}{\partial N_i}\right)_{T,V,N_{i\neq j}} \tag{B.87}$$

The contribution to the Helmholtz free energy due to the quatum corrections, a_1^{Q}, is given as

$$a_1^{\mathrm{Q}} = \gamma_x\left(\frac{\beta\epsilon_x}{\pi}\right)^{1/2}\Gamma_x \tag{B.88}$$

$$\Gamma_x = \mathrm{g}_x^{\mathrm{SW}}(\sigma_x;\lambda_x)\Lambda_x = \mathrm{g}_x^{\mathrm{SW}}(\sigma_x;\lambda_x)\sum_k\sum_j x_{s,k}x_{s,j}\Lambda_{kj} \tag{B.89}$$

where

$$\epsilon_x = \sum_k\sum_j x_{s,k}x_{s,j}\epsilon_{kj} \tag{B.90}$$

where γ_x is given by the Eq. B.22. The partial differential equation in Eq. B.87 can be calculated as

$$N\left(\frac{\partial a_1^Q}{\partial N_i}\right) = a_1^Q\left[\frac{1}{\gamma_x}N\left(\frac{\partial\gamma_x}{\partial N_i}\right)+\frac{1}{2\epsilon_x}N\left(\frac{\partial\epsilon_x}{\partial N_i}\right)+\frac{1}{\Gamma_x}N\left(\frac{\partial\Gamma_x}{\partial N_i}\right)\right] \tag{B.91}$$

The differential expresion for γ_x with respect to N_i is given by Eq. (B.33). The thers correponding differential expresions are given by

$$N\left(\frac{\partial\epsilon_x}{\partial N_i}\right) = \frac{2m_i}{S}\left[\sum_j x_{s,j}\epsilon_{ij}-\epsilon_x\right] \tag{B.92}$$

$$N\left(\frac{\partial\Gamma_x}{\partial N_i}\right)=\left(\frac{2m_i}{S}\right)\mathrm{g}_x^{\mathrm{SW}}(\sigma_x;\lambda_x)\left[\sum_j x_{s,j}\Lambda_{ij}-\Lambda_x\right]+\Lambda_x N\left(\frac{\partial \mathrm{g}_x^{\mathrm{SW}}(\sigma_x;\lambda_x)}{\partial N_i}\right) \tag{B.93}$$

In the last equation, the first differential expresion can be writtten as

$$\mathrm{g}_x^{\mathrm{SW}}(\sigma_x;\lambda_x)=\mathrm{g}_x^{\mathrm{HD}}(\sigma_x;\gamma_x)+(\beta\epsilon_x)\mathrm{g}_1(\lambda_x) \tag{B.94}$$

and

$$N\left(\frac{\mathrm{g}_x^{\mathrm{SW}}(\sigma_x;\lambda_x)}{\partial N_i}\right)=N\left(\frac{\mathrm{g}_x^{\mathrm{HD}}(\sigma_x;\gamma_x^{\mathrm{eff}})}{\partial N_i}\right)+\mathrm{g}_1(\lambda_x)\beta N\left(\frac{\partial\epsilon_x}{\partial N_i}\right)+(\beta\epsilon_x)N\left(\frac{\partial \mathrm{g}_1(\lambda_x)}{\partial N_i}\right) \tag{B.95}$$

where

$$\mathrm{g}_1(\lambda_x)=\mathrm{g}_o^{\mathrm{HD}}(\sigma_x;\gamma_x^{\mathrm{eff}})+(\lambda_x^2-1)\frac{\partial \mathrm{g}_o^{\mathrm{HD}}(\sigma_x;\gamma_x^{\mathrm{eff}})}{\partial\gamma_x^{\mathrm{eff}}}\left(\frac{\lambda_x}{2}\frac{\partial\gamma_x^{\mathrm{eff}}}{\partial\lambda_x}-\gamma\frac{\partial\gamma_x^{\mathrm{eff}}}{\partial\gamma}\right) \tag{B.96}$$

The differential expression $N(\partial \mathrm{g}_1(\lambda_x)/\partial N_i)$ only need the following expresion

$$N\frac{\partial}{\partial N_i}\left(\frac{\partial\gamma_x^{\mathrm{eff}}}{\partial\lambda_x}\right)=N\frac{\partial}{\partial N_i}\left\{\gamma_x\left(\frac{\partial d_1}{\partial\lambda_x}\right)+\gamma_x^2\left(\frac{\partial d_2}{\partial\lambda_x}\right)\right\} \tag{B.97}$$

Combining rules: In this work, we use the standard Lorentz-Berthelot[8] in two cases: i) diameter of the molecules σ_{ij}, and ii) depth enregy parameter ϵ_{ij} and iii) the de Boer's parameter, as follows

$$\sigma_{ij}=\frac{\sigma_{ii}+\sigma_{jj}}{2},\qquad \epsilon_{ij}=(\epsilon_{ii}\epsilon_{jj})^{1/2} \tag{B.98}$$

$$\Lambda_{ij}=\frac{\Lambda_{ii}\sigma_{ii}+\Lambda_{jj}\sigma_{jj}}{2\sigma_{ij}} \tag{B.99}$$

The cross parameter of variable range λ_{ij} was derived from the van der Waals energy constant according to the Berthelot rule.[5]

$$\lambda_{ij}^2=1+\frac{\sigma_{ii}\sigma_{jj}}{\sigma_{ij}^2}\left[(\lambda_{ii}^2-1)(\lambda_{jj}^2-1)\right]^{1/2} \tag{B.100}$$

Other useful differential expression from the Eq. B.100, is given by

$$\left(\frac{\partial \lambda_{ij}}{\partial \lambda_{kl}}\right) = \frac{\sigma_{ii}\sigma_{jj}\lambda_{kk}\delta_{il}(\lambda_{jj}^2 - 1)}{\sigma_{ij}^2\lambda_{ij}\left[(\lambda_{ii}^2 - 1)(\lambda_{jj}^2 - 1)\right]^{1/2}} \tag{B.101}$$

where δ_{il} is the Kronecker delta. As can be observed in Eq. B.101, when the subscripts have the following form $i = j = k = l$, the expression $(\partial\lambda_{ij}/\partial\lambda_{kl}) = (\partial\lambda_{ii}/\partial\lambda_{kk}) = 1$.

BIBLIOGRAPHY

[1] A. Santos, S. B. Yuste, M. L. Haro, *Mol. Phys.*, **96**, 1 (1999).

[2] T. J. Boublik, *J. Chem. Phys.* **53**, 471 (1971).

[3] G. A. Mansoori, N. F. Carnahan, K. E. Starling, T. W. Leland, **54**, 1523 (1971).

[4] A. Gil-Villegas, A. Galindo, P. J. Whitehead, S. J. Mills, G. Jackson, A. N. Burgess, *J. Chem. Phys.* **106**, 4168 (1997).

[5] A. Galindo, L. A. Davies, A. Gil-Villegas, *Mol. Phys.* **93**, 241 (1998).

[6] D. Henderson, *Mol. Phys.* **30**, 971 (1975).

[7] M. Castro, A. Martínez, A. Gil-Villegas, *Ads. Sc. and Tech.* **29**, 59 (2011).

[8] L. L. Lee, *Molecular Thermodynamics of Nonideal Fluids*, Butherworths, United States of America (1988).

AGRADECIMIENTOS

Concluyendo mi trabajo de tesis doctoral, me gustaría agradecer de la manera más cordial a todas las personas que de una u otra manera han contribuido positivamente en este proceso de estudios. Inicialmente quiero agradecer al CONACYT, a la Universidad de Guanajuato y al gobierno Mexicano por brindarme la oportunidad de realizar mis estudios de posgrado en tan excelente país y grandiosa universidad. Agradezco enormemente la valiosa oportunidad que me dieron y espero haberlos retribuido de la mejor manera.

En el ámbito académico agradezco al Dr. Alejandro Gil-Villegas Montiel. Ha sido un gran privilegio trabajar al lado de tan excelente investigador, siempre me impresionaron sus ideas, la forma de concebir la ciencia, su interés por la física y ese deseo interminable de motivar a los demás en el entendimiento de la naturaleza. Mil gracias por sus enseñanzas. Mi más sincero respeto y admiración!!!

Agradezco también de la manera más atenta al grupo de sinodales que hicieron parte de la revisión de este trabajo, con sus comentarios y aportes mejoraron ostensiblemente la calidad de esta tesis: Dr. Eduardo Buenrostro, Dr. Carlos Ariel Cardona, Dr. Leonardo Alvarez, Dr. José Socorro.

Quiero también agradecer a aquellos profesores e investigadores que siempre estuvieron a mi lado para apoyarme y brindarme su amistad a lo largo de este proceso, en particular: Dr. Ramón Castañeda, Dr. José Torres Arenas, Dr. Juan Barranco, Dr. Gerardo Gutíerrez, Dr. Miguel Sabido y Dr. Mauro Napsuciale. Espero algún día poder transmitir ese amor por la ciencia, tal como ustedes lo hacen!!!

Agradezco a la Dra. Susana Figueroa, Dr. Jorge Delgado, Dr. Arturo Vega y Dra. Iraís Quintero por sus interminables tertulias y variedades gastronómicas, mil gracias por el tiempo compartido, hicieron de momentos díficiles gratas experiencias. Adicionalmente, expreso mis más sinceros agradecimientos al Dr. Ramón Castañeda y al Dr. William Smith por sus fructíferas discusiones, apoyo y entusiasmo, la Mecánica Estadística no sería la misma, sin su particular punto de vista. Al viejo "Super", Dr. Alejandro Martínez, un gran amigo y por supuesto un investigador de una altura mayor a su estatura..jaja !!!. Mil gracias por tus aportes, tu trabajo y por ese café que siempre nos acompaño en días interminables de programación; creo sin lugar a dudas, que mis códigos nunca hubieran estado a la altura de no ser por tu permanente

ayuda y paciencia. Mil gracias!!.

También tengo que agradecer a los integrantes del grupo de investigación del Dr. Gil, desafortunadamente algunos ya no están como es el caso de: Lupita, Libertad, El Parce, el Pepe, la Dra. Perla y Claudia; otros más recientes: Mario Becerra, César Serna, mil gracias por los gratos momentos y por su apoyo en el desarrollo de este trabajo, estoy seguro que sin sus discusiones, chistes y especialmente sin su compañia, las reuniones de grupo nunca hubieran sido igual.

Quiero extender también mis agradecimientos a todos los trabajadores de la división, por aguantar mis malos chistes, mis malos ratos, mil gracias!!. Agradezco también a las eficientes Lílian Quintero, Laura Durón, Alma Rosario y Yanet Hernández, sin sus esfuerzos y ardua labor mis trámites y dudas nunca hubieran quedado resueltas.

Tengo que agradecer a cada uno de los amigos que hicieron parte de este proceso. Por sus tardes de asados y sus noches de fiestas, mil gracias. En México, por mencionar algunos: el Tachi, Selim, Leonel Toledo, el Efra, el "señor enojado" don Alexis, el Lenin, el Nes, Salomón, Wichin, Selene, Susanita, Xóchilt Judith, Lorena Velázquez, Marianita, Carlos Wiechers, Slim, Xareni, Jorge el árbitro, Leo el "Guapo", Moshky Lemoto, Dr. Alberto Diez, Tete, Dalia, Pau, Luis Medina y el Carlitos. De mis amigos en Colombia resalto a Jorge H. Ramírez, Juan A. Díez, Rojas, Juan Muelitas, Cubillitos, Jimmy López y en particular a tres grupos de amigos: JOY's group: Jorge Iván, Monkis, Mao, Alexa, el Negro, Osquillar y Posadita. Valery's group: Guevara, Raúl, Dianita, La Flaca, Diego y PateTabla. UTP's group: Pao, Marce, Moni, Nata, Diana, Anchico, Ariel y Leo. Gracias porque siempre estuvieron pendientes de mí en todo instante, mil gracias!!. También agradezco de todo corazón a mis dos buenas amigas Ana Isabel Ramos y Angélica Alzate mil gracias, por sus gratas palabras de aliento cuando más lo necesitaba.

Por último y no por eso menos importante, agradezco de todo corazón a mi familia en Colombia, a mi hermano Cristian y a mis padres Víctor Manuel y Dolly Montoya por su inalcanzable paciencia y apoyo en todas las etapas de mi vida. Siempre les amaré con todo mi corazón y solo espero que el tiempo y el destino nos permita compartir más momentos felices juntos. De mi familia en particular quiero agradecer a mi prima Isabel, Mary, Lili, y a mi tía Sandra Montoya por estar siempre pendientes de mí, gracias!!. También agradezco de corazón a la que considero mi segunda familia en México, doña Alice mil gracias por prestarme su familia y hacerme sentir como en

casa, Jafet, la Güera, el Güero, Camila y Aranza, mil gracias!!. A la “negrita” Lizbeth Montesinos, agradezco su inmenso amor, paciencia y apoyo durante todo este tiempo. Gracias por hacerme tan feliz y alentarme todo el tiempo a culminar mis estudios de la mejor manera. De no ser por tu compañía difícilmente esto hubiera sido posible, me siento muy afortunado de tenerte a mi lado, mil gracias!!!. Finalmente, agradezco a todos aquellas personas que de una u otra forma hicieron posible la realización de este trabajo. Mil gracias!!.